entropy

Special Issue Reprint

Statistical Physics and Its Applications in Economics and Social Sciences

Edited by
José Roberto Iglesias

mdpi.com/journal/entropy

MDPI

Statistical Physics and Its Applications in Economics and Social Sciences

Statistical Physics and Its Applications in Economics and Social Sciences

Editor

José Roberto Iglesias

MDPI

Basel • Beijing • Wuhan • Barcelona • Belgrade • Novi Sad • Cluj • Manchester

Editor
José Roberto Iglesias
Instituto de Física
Universidade Federal do Rio
Grande do Sul
Porto Alegre
Brazil

Editorial Office
MDPI
St. Alban-Anlage 66
4052 Basel, Switzerland

This is a reprint of articles from the Special Issue published online in the open access journal *Entropy* (ISSN 1099-4300) (available at: www.mdpi.com/journal/entropy/special_issues/L43APK4F3D).

For citation purposes, cite each article independently as indicated on the article page online and as indicated below:

Lastname, A.A.; Lastname, B.B. Article Title. *Journal Name* **Year**, *Volume Number*, Page Range.

ISBN 978-3-7258-1256-1 (Hbk)
ISBN 978-3-7258-1255-4 (PDF)
doi.org/10.3390/books978-3-7258-1255-4

Contents

About the Editor

José Roberto Iglesias

Prof. Dr. José Roberto Iglesias is an Emeritus Professor at The Federal University of Rio Grande do Sul (UFRGS), located in Porto Alegre, Brazil. He was born in Argentina and studied physics at the Instituto Balseiro, in Bariloche, Argentina. He obtained his Ph. D. (Doctorat ès Sciences) at the Laboratoire de Physique des Solides, Université Paris-Sud, Orsay, France.

Following his thesis, he become first Associate Professor and later Full Professor at the Instituto de Física of UFRGS. In 2019, he was granted the title of an Emeritus Professor. He is also a research fellow of the Brazilian National Research Council (CNPq) and member of the National Institute of Science and Technology on Complex Systems (INCT-SC).

He has worked on the Solid State Theory, particularly on strongly correlated electron systems such as Kondo systems. Over the last three decades, he has been working in the study of neural networks, cellular systems, fractal aggregation and, more recently, in the fields of econophysics and sociophysics. He has been an invited professor at several universities in South America, Europe and US, and has managed financial grants and international cooperation agreements with different countries of Europe, North and South America. He has guided several theses in physics and economics, and published more than 160 articles.

entropy

MDPI

Article

Kinetic Models of Wealth Distribution with Extreme Inequality: Numerical Study of Their Stability against Random Exchanges

Asim Ghosh [1,*], Suchismita Banerjee [2], Sanchari Goswami [3], Manipushpak Mitra [2] and Bikas K. Chakrabarti [2,4]

[1] Department of Physics, Raghunathpur College, Raghunathpur, Purulia 723133, India
[2] Economic Research Unit, Indian Statistical Institute, Kolkata 700108, India; suchib.1993@gmail.com (S.B.); manipushpak.mitra@gmail.com (M.M.); bikask.chakrabarti.retd@saha.ac.in (B.K.C.)
[3] Department of Physics, Vidyasagar College, Kolkata 700006, India; sg.phys.caluniv@gmail.com
[4] Saha Institute of Nuclear Physics, Kolkata 700064, India
* Correspondence: asimghosh066@gmail.com

Abstract: In view of some recent reports on global wealth inequality, where a small number (often a handful) of people own more wealth than 50% of the world's population, we explored if kinetic exchange models of markets could ever capture features where a significant fraction of wealth can concentrate in the hands of a few as the market size N approaches infinity. One existing example of such a kinetic exchange model is the Chakraborti or Yard-Sale model; in the absence of tax redistribution, etc., all wealth ultimately condenses into the hands of a single individual (for any value of N), and the market dynamics stop. With tax redistribution, etc., steady-state dynamics are shown to have remarkable applicability in many cases in our extremely unequal world. We show that another kinetic exchange model (called the Banerjee model) has intriguing intrinsic dynamics, where only ten rich traders or agents possess about 99.98% of the total wealth in the steady state (without any tax, etc., like external manipulation) for any large N value. We will discuss the statistical features of this model using Monte Carlo simulations. We will also demonstrate that if each trader has a non-zero probability f of engaging in random exchanges, then these condensations of wealth (e.g., 100% in the hand of one agent in the Chakraborti model, or about 99.98% in the hands of ten agents in the Banerjee model) disappear in the large N limit. Moreover, due to the built-in possibility of random exchange dynamics in the earlier proposed Goswami–Sen model, where the exchange probability decreases with the inverse power of the wealth difference between trading pairs, one does not see any wealth condensation phenomena. In this paper, we explore these aspects of statistics of these intriguing models.

Keywords: wealth inequality; kinetic exchange models; Yard-Sale model; Monte Carlo simulations

Citation: Ghosh, A.; Banerjee, S.; Goswami, S.; Mitra, M.; Chakrabarti, B.K. Kinetic Models of Wealth Distribution with Extreme Inequality: Numerical Study of Their Stability against Random Exchanges. *Entropy* **2023**, *25*, 1105. https://doi.org/10.3390/e25071105

Academic Editor: José Roberto Iglesias

Received: 5 June 2023
Revised: 19 July 2023
Accepted: 22 July 2023
Published: 24 July 2023

1. Introduction

The first successful theory involving classical many-body physics or classical condensed matter systems, the kinetic theory of the (classical) ideal gas, is about one-and-a-quarter centuries old. It consists of Avogadro's number (about 10^{23}) of constituent atoms or molecules (each following Newtonian dynamics). It is a robust, versatile, and extremely successful foundation of classical many-body physics. Social systems, economic markets in particular, are many-body dynamical systems composed of fewer constituents (ranging from the order of 10^{10} for a global market). A lone Robinson Crusoe on an island cannot develop a market or a society for that matter, as markets are intrinsically many-body systems. It is no wonder that kinetic exchange models of money or wealth have been conjectured early on (e.g., by Saha and Srivastava [1] in 1931, Mandelbrot [2] in 1960) and resurrected recently (e.g., by Chakrabarti and Marjit [3] in 1995, Dragulecu and Yakovenko [4] in 2000, Chakraborti and Chakrabarti [5] in 2000, Chatterjee, Chakrabarti, and Manna [6] in 2004).

Kinetic exchange models of trades and their statistics have been quite successful in capturing several realistic features of wealth distributions among agents in societies

(see, e.g., [7,8]). The beneficial effects of an agent's saving propensity in reducing social inequality have been extensively studied [5,6,8]. The choice of the poorest trader in each trade (with the other trade partner being randomly chosen) leads to a remarkable self-organized poverty line, beneath which, no one remains in a steady state (see, e.g., [9–12]). This model was inspired by some crucial observations by economists (see, e.g., [10]) and suggests built-in (self-organized) remedies for reducing social inequality. However, it must be admitted that such intriguing self-organizing properties of the kinetic exchange models have not yet been thoroughly investigated.

Contrarily, recent focus has shifted to the unusual growth rate of social inequality in the post world war II period (see, e.g., [13–16]), which in some countries seems to have significantly crossed the 80-20 Pareto limit, reaching a steady state, with 87% of the wealth accumulated by 13% of the population. This has been argued, following an analogy with the inequality index values for the avalanche burst statistics in self-organized sand-pile models near their critical points, to be the natural limit in all social competitive situations, where welfare mechanisms (helping those who fail to participate properly in such self-organizing dynamics) are either absent or removed (see, e.g., a recent review [16]).

Although the Pareto-like inequality mentioned above—where a small fraction of people (say 13%) possess a large fraction (say 87%) of wealth—can already be devastating, more disturbing types of inequalities are being reported. For example, the Oxfam Report [17] of January 2020 stated "The world's 2153 billionaires have more wealth than the 4.6 billion people who makeup 60 percent of the planet's population". In other words, a handful number (about 10^3) of rich people possess more than about 60% (or 10^9 order) of poor people's wealth on this planet. This dangerous trend in the world, as a whole, has repeatedly been mentioned in various recent reports.

The Pareto-type inequality mentioned above has long been investigated (see, e.g., [6,18]) using the kinetic exchange models with non-uniform saving propensities of traders (see, e.g., [8,19] for reviews). One may naturally wonder if the kinetic exchange theory allows for possible models, where only a handful of traders (say, about 10) possess a significant fraction (say, above 50%) of the total wealth considered in the model, even when its population N tends to infinity.

The answer is yes. The Chakraborti model [20], widely known today as the Yard-Sale model, as in [21], has attracted a lot of attention (see, e.g., [22–24]). In its barest form [20], in the Chakraborti model (denoted here as the C-model), two randomly chosen traders at any point in time participate in an exchange trade when the richer one saves the excess over the poorer one's wealth and goes for a random exchange of the total available wealth (double that of the poorer one). The slow but inevitable attractor fixed point of the trade dynamics arrives when all wealth ends up in the hand of just one trader, no matter how large the population (N) is. Because of the particular form of savings during a trade, whenever one becomes a pauper, nobody trades with him, and all gradually condense to the state where one trader acquires the entire wealth and the trade dynamics stop (see [22]). External perturbations, like regular redistribution of tax collections by the central government (or any non-playing agent), can help relieve [23,24] the condensation phenomenon, and this seems to fit well with many observed situations [23]. We will show here that if each trader has a finite probability (f) of playing Dragulecu and Yakovenko (DY)-type [4] random exchanges, then for any $f > 0$, the condensation of wealth in the hands of one trader disappears and the steady-state distribution of wealth exponentially decreases, as in the DY model.

In the Goswami–Sen (or GS) model [25], one considers a kinetic exchange mechanism, where the interaction (trade) probabilities among the trade partners (i and j) decrease with the wealth differences ($|m_i - m_j|$) at that instant of trading (time), following a power law ($|m_i - m_j|^{-\alpha}$). Of course, for $\alpha = 0$, the model reduces to that of DY. The numerical results showed that, for α values of less than about 2.0, the steady-state wealth distribution among the traders was still DY-like (it exponentially decayed with increasing wealth). For higher values (beyond 2.0) of α, power law (Pareto-law) decays occurred. No condensation

of wealth in the hands of a finite number of traders or agents was observed due to the inherent DY-like exchange probability in the dynamics of the model. This was confirmed by extrapolating the fraction of total wealth held in the steady state by the ten richest traders, with respect to N.

We finally consider a seemingly natural version of the kinetic exchange model, denoted here as the Banerjee (B) model [26], where the intrinsic dynamics of the model lead to another extreme kind of inequality in the steady state, in the sense that precisely ten traders (out of the N traders in the market; $N \to \infty$) possess $(99.98 \pm 0.01)\%$ of the total wealth. These fortunate traders are not unique and their fortune does not last for long (the residence time, on average, is about 66 time units, with the most probable value around 25 time units, counted in units of N trades or exchanges, for any value of N) and it decreases continuously with the increasing fraction (f) of random trades or interactions. Unlike in the Chakraborti or Yard-Sale model [20,21], where the dynamics stop after the entire wealth goes to one (unless perturbed externally), the trade dynamics continue here with the total wealth circulating only with a handful of traders (about ten) in the steady state. In this model, after each trade, the traders are ordered from the lowest wealth to the highest, and each trader trades only with the nearest-in-wealth trader, richer or poorer, with equal probability. Even if, by chance, the entire wealth goes to one trader, the dynamics of random exchanges do not stop in this model as all the paupers become the nearest neighbors (wealth-wise) of this trader, and random exchanges among them occur. The process continues. Apart from the steady-state wealth distributions and the most probable wealth amounts of the top few rich traders, we will show that, in this model, the condensation of almost all the wealth (99.98%) occurs in the hands of 10 traders (no matter how big N is). We will show that this condensation disappears when a finite fraction f of the time traders engage in DY-type random exchanges. Eventually, a DY-type exponentially decaying wealth distribution emerges after a power law region for low values of f.

2. Models and Numerical Studies for Their Statistics

We numerically study the statistical features of the three kinetic exchange models introduced in the introduction. We begin with the B (Banerjee [26]) model. Next, we consider the C (Chakraborti, or Yard Sale) model [20,21], and then the GS (Goswami–Sen) model [25]. In order to explore the stability of the condensation of wealth in these models, we study the steady-state wealth distribution $P(m)$ in each model and the fraction of total wealth concentrated in the hands of a few (say ten) traders or agents (whenever meaningful), allowing each trader to have a nonvanishing probability f (the faction of tradings or times) to go for DY (Dragulecu and Yakovenko [4])-type random exchanges.

Most of the numerical (Monte Carlo) studies of the dynamics of these models are studied with four sets of numbers N of agents or traders: N = 100, 200, 400, and 800, and at each time step, t, the dynamics run over all the N order traders. We consider total money (M) to be distributed among the agents equal to N and we denote the money of any agent i at time t by $m_i(t)$ and, as such, $M = \sum_i m_i(t) = N$. When the steady state is reached after the respective relaxation times, when the average quantities do not change with time (with the relaxation time typically being much less than 10^5 trades/interactions for the N values considered here), the statistical quantities are evaluated from averages of over 10^5 post-relaxation time steps.

2.1. Banerjee Model Results

In this B-model, when the DY fraction (f) is set equal to zero, no wealth distribution $P(m)$ in the population is meaningful because of the wealth condensation in the hands of a few. We first study the distributions (see Figure 1) of the total wealth fraction in the hands of the richest three. Note that these three are not unique, and once they become so rich, their residence times (in units of N) are finite (about 66), and in case these positions are lost, the return times are also finite.

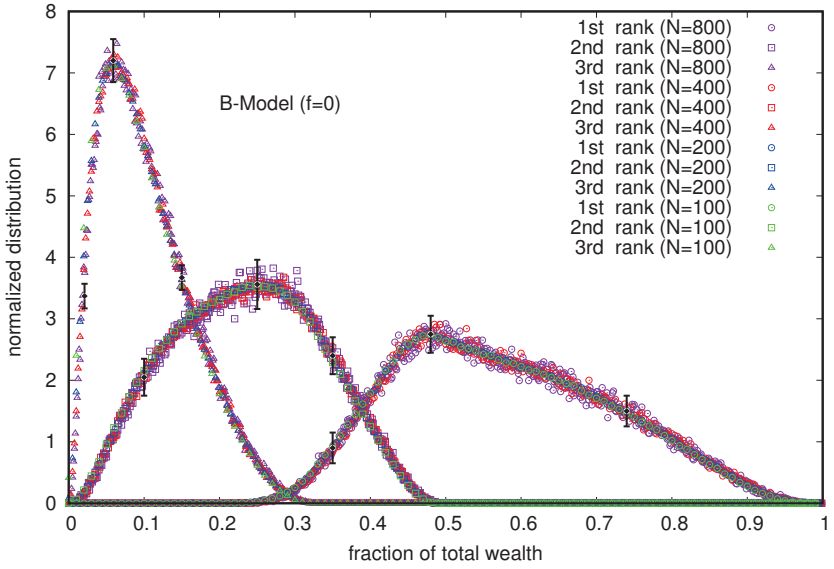

Figure 1. Distributions of the fraction of total wealth ($M = N$) ending up in the hands of the richest three traders. The error estimation is based on 10 runs. The typical errors in the distribution grow with N near the most probable value of the wealth fraction and are indicated for $N = 800$ for all three traders. Far away from the most probable values, the errors are less than the data point symbol sizes.

Although the distribution of the total wealth fraction in the hands of the richest few (shown in Figure 1) is rather wide (each one spread over more than 30% of the total wealth and not N), the distribution of the total wealth fraction possessed by the ten richest (at any time in the steady state) is extremely narrow and spreads over 0.1% only (see Figure 2). At any time in the steady state, its value is much more robust in this B model (with $f = 0$), and its value is less than unity, but very close to 0.9998.

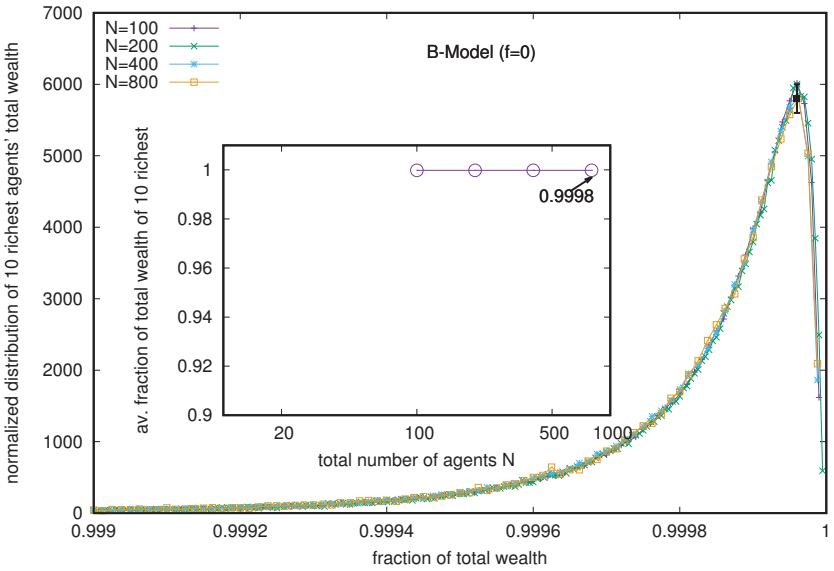

Figure 2. Distribution of the total wealth fraction possessed by the ten richest (at any time in the steady state and for different N values). The inset shows that the average of the total wealth fraction of the ten richest (for any time and any value of N) in the steady state is very close to 0.9998. Although the wealth share fractions of the richest ten traders have considerable fluctuations (see Figure 1), their wealth fraction totals hardly have any fluctuations (much less than the symbol size in the inset). The error estimation is based on 10 runs. The typical errors in the distribution of total wealth of the ten richest are more than the data point symbol sizes near the most probable values, where indicated.

Next, we consider the B model with a nonvanishing probability f of each trader to follow DY trades or exchanges. We see, immediately, that the wealth condensation disappears, and with increasing values of f, the wealth is Boltzmann (exponentially)-distributed among all the agents (see Figure 3), starting with the Pareto-like power law distribution for lower values of f (see the inset of Figure 3). Indeed, when we consider the limiting values (for large N) of the average fraction of total wealth ($M = N$) possessed by the ten richest traders in the steady state, they all seem to vanish (see Figure 4) for any non-zero value of f (there remains a constant of 0.9998 for $f = 0$, for the pure B model).

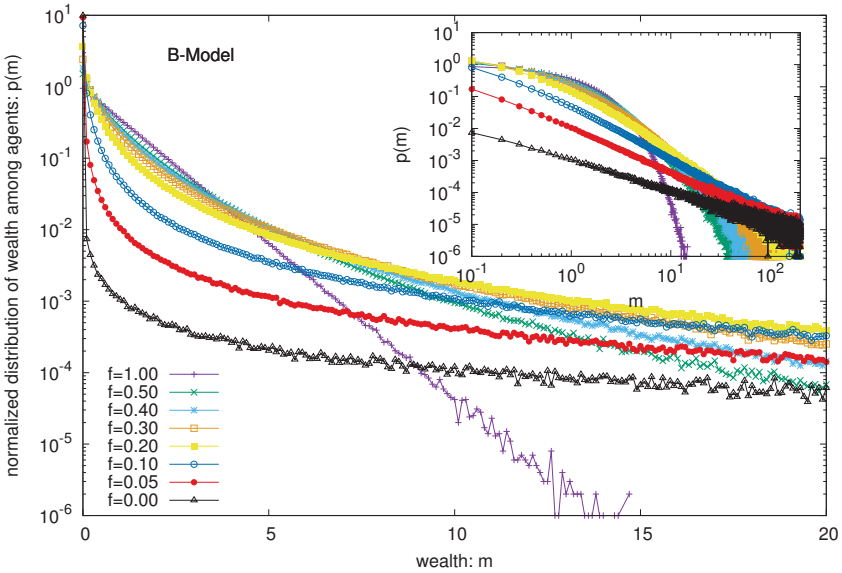

Figure 3. Wealth distribution $P(m)$ among all agents against the wealth m in the B model for different probabilities f of DY random exchanges. Note that the fluctuations appear to grow more for the lower values of the distribution of wealth due to the log scale used in the y-axis.

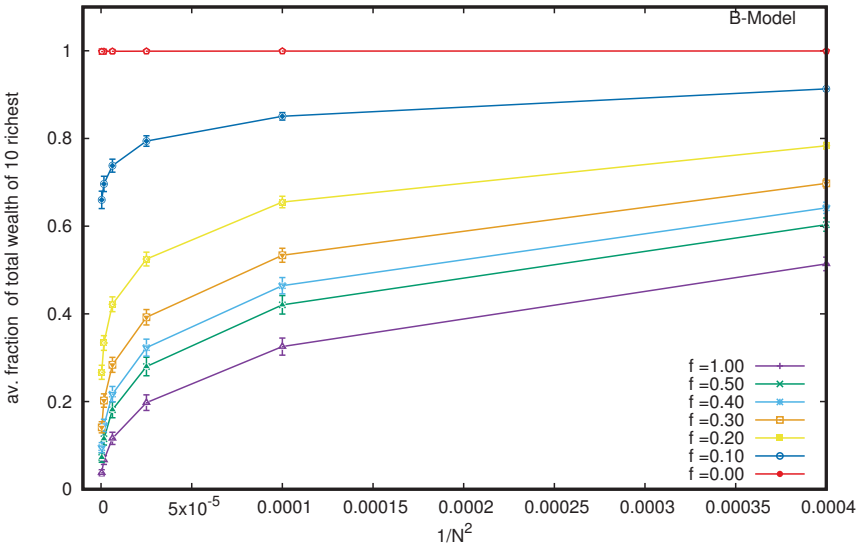

Figure 4. To obtain the limiting values (for large N) of the average fraction of total wealth ($M = N$) possessed by the ten richest traders in the steady state, we plot the fraction against $1/N^2$ (as with DY-type trades, each N trader interacts with the $N - 1$ other trader. The extrapolated values all seem to approach zero for any non-zero value of f (but there remains a constant 0.9998 for $f = 0$, as in the pure B model). The error estimation is based on 10 runs. Typical sizes of error bars are indicated.

For the wealth condensation in the B-model (with $f = 0$), Figure 5A shows the distribution of residence times (in units of N) of the 10 fortunate traders and, in the inset, the variation of the most probable and average values of residence times (τ, in the unit of N). For the same model with $f = 0$, Figure 5B shows the distribution of the return time to fortune (becoming one of the 10 richest starts from the 20th rank) and (in the inset) the variation of the most probable and average values of the residence times with market sizes N.

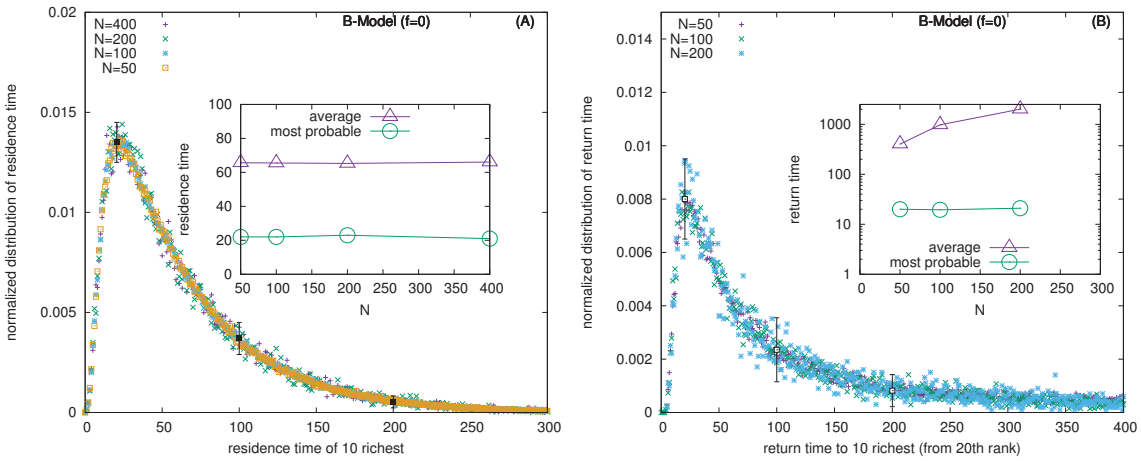

Figure 5. (**A**) The distribution of residence times (in units of N) of the 10 fortunate traders and (in the inset) the variation of the most probable and average values of the residence times. (**B**) The distribution of the return time to fortune (becoming one of the 10 richest, starting from the 20th rank) and (in the inset) the variation of the most probable and average values of the return times (in units of N). The error estimation is based on 10 runs. The typical errors in the distribution of both the residence and return times grow with N near the most probable values of the respective quantities, and are indicated for $N = 400$ here when they are bigger than the symbol sizes.

2.2. Chakraborti or Yard-Sale Model Results

The C model or Yard sale model is well-studied. However, in order to check the stability of the condensation of wealth (with the entire money $M = N$ going to the hands of one trader only, we added a nonvanishing probability f of each trader to follow DY trades or exchanges. We can immediately see that the wealth condensation disappears for any $f > 0$ (see Figure 6) and the wealth is distributed in the Boltzmann form (exponentially decaying with increasing wealth) among all the agents. The inset shows that for any nonzero value of f, the steady state wealth distribution is exponentially decaying (and there is a power law region) in this extended model C. When we consider the limiting values (for large N) of the average fraction of total wealth ($M = N$) possessed by the ten richest traders in the steady state (see Figure 7), they all seem to vanish from the unit value in the original C model (with $f = 0$) for any non-zero value of f.

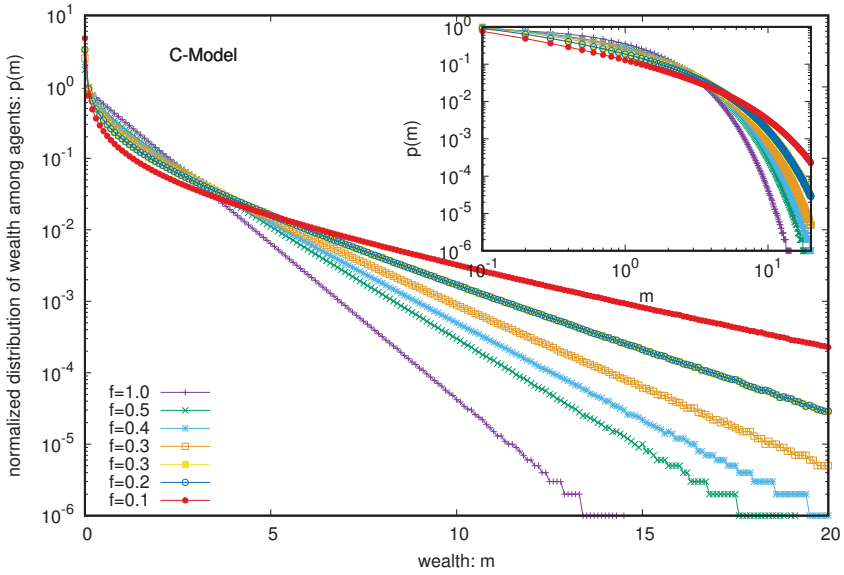

Figure 6. Wealth distribution $P(m)$ among all the agents against the wealth m in the C model for different probabilities f of DY random exchanges. Note that the fluctuations appear to grow more for the lower values of the distribution due to the log scale used in the y-axis.

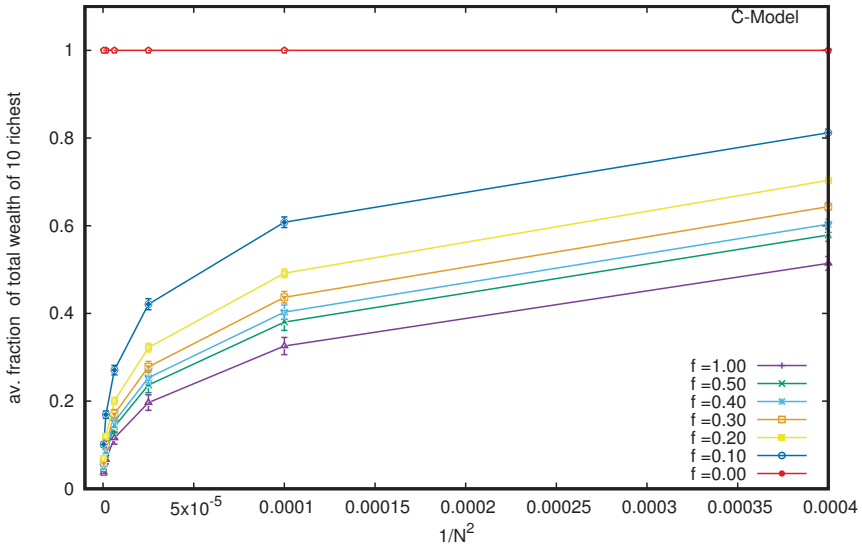

Figure 7. The limiting values (for large N) of the average fraction of total wealth ($M = N$) possessed by the ten richest traders in the steady state of the C model with the f fraction of DY-like trades. For $f = 0$, the money goes to one agent and the other nine agents contribute nothing. When we plot the fraction against $1/N^2$ (as with DY-type trades, each N trader interacts with $(N-1)$ other traders), the extrapolated values all seem to approach zero for any non-zero value of f. The error estimation is based on 10 runs. Typical sizes of error bars are indicated.

2.3. Goswami–Sen Model Results

Here, the interaction (trade) probability (i and j) decreases with the wealth difference ($|mi - mj|$) at the instance of trading (time), following a power law ($|mi - mj|^{-\alpha}$). As such, in the GS model, there is always a finite (but small) probability of random exchanges. We do not need to consider the additional fraction of the DY interaction in this model. Of course, for $\alpha = 0$, the model reduces to that of DY. Our numerical results confirm (see Figure 8) that for α values of less than about 2.0, the steady-state wealth distribution is still DY-like (exponentially decaying). For higher values (beyond 2.0) of α, power law (Pareto-like) decays occur (but no condensation of wealth). Although the model leads to

extreme inequality, there is no condensation of wealth in the hands of a few traders for any (larger) value of α. In order to check that, we studied the average fraction of total wealth ($M = N$) possessed by the ten richest traders in the steady state of the GS model with α. When we plot the fraction against $1/N^2$ (see Figure 9), the extrapolated values of the fraction all seem to approach zero for any non-zero value for any of the α values considered.

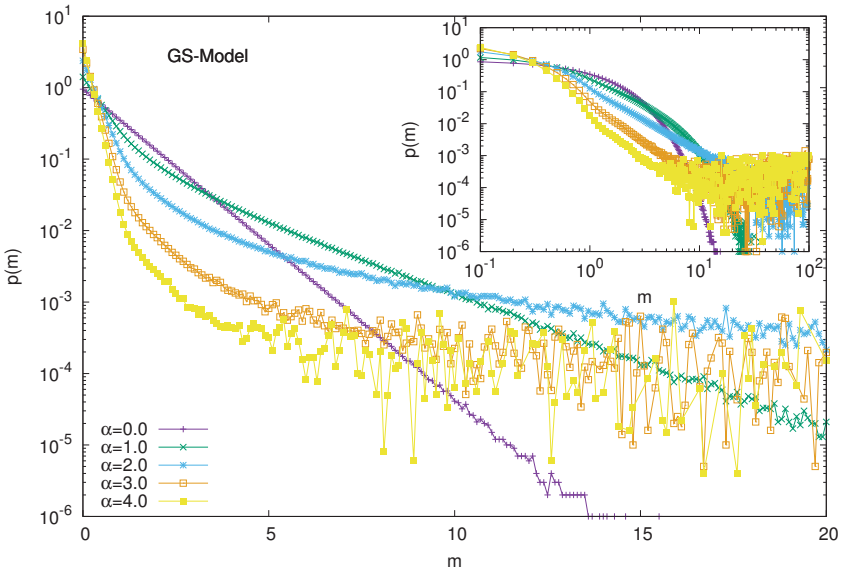

Figure 8. Wealth distribution $P(m)$ among all the agents against the wealth m in the GS model for different values of α. Note that the fluctuations appear to grow more for the lower values of the distribution due to the log scale used in the y-axis.

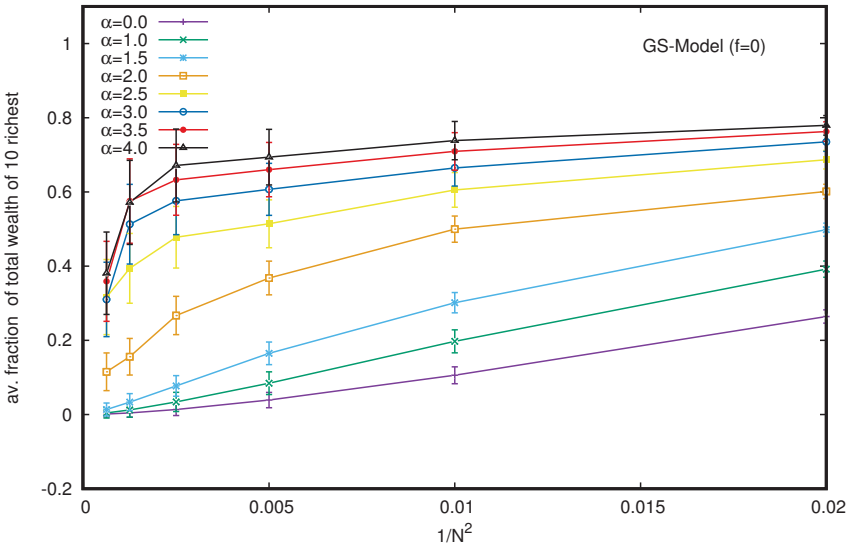

Figure 9. Plot of the fraction of total wealth ($M = N$) against $1/N^2$ for different values of α in the GS model. The extrapolated (with N) values of the fraction all seem to approach zero for any non-zero value of α. The error estimation is based on 10 runs. Typical sizes of error bars are indicated.

3. Summary and Discussion

In view of the observed extreme income or wealth inequalities in society, we investigated the suitability of capturing the kinetic exchange models [8], at least qualitatively. We distinguish between two types of such extreme inequalities: the (Pareto) type [16], where a small fraction (typically 13%) of the population possesses about 87% of the total wealth (following a power law distribution) of the respective country. The other more recently

observed type (as reported by Oxfam [17]) regards the truly extreme nature of income and wealth inequalities worldwide, where only a handful (say a few hundred to thousands) of super-rich people throughout the world own more wealth than 50 to 60% of poor people.

Several kinetic exchange models (see, e.g., [6,8]) have been developed to analyze Pareto-type inequalities. We investigated the statistics of some kinetic exchange models, where even with N going to the infinity limit, only one person can grab the entire wealth (as in the Yard-Sale, Chakraborti, or C models [20,21]), or only 10 people can accumulate about 99.98% of the total wealth (as in the Banerjee or B model [26], see Figure 2). We investigate how these extreme inequalities in the kinetic models are softened to the Dragulescu–Yakovenko (DY) [4] types of exponentially decaying wealth distributions among all traders or agents, when the traders each have non-vanishing probabilities f of DY-type random exchanges. These condensations of wealth (100% in the hands of one agent in the C model [20], or about 99.98% in the hands of ten agents in the B model) then disappear in the large N limit (this is clearly seen when extrapolating against $1/N^2$, as in DY-type random exchanges, where each N agent interacts or exchanges with all others; see Figures 4 and 7). We also show that due to the built-in possibility of DY-type random exchange dynamics in the Goswami–Sen or GS model [25], where the exchange probability decreases with the inverse power of the wealth difference of the pair of traders, one does not see any wealth condensation phenomena. In both GS and B models (with $f > 0$ fraction DY interactions or exchanges) no wealth condensation occurs, although a strong Pareto-type power law wealth distribution $P(m)$ or inequalities occur for large values of α, as well as smaller values of f in the GS and B models, respectively (see Figures 3 and 8). For the wealth condensation in the B model, for $f = 0$, we additionally find that the top ten fortunate traders are not unique and their fortunes do not last for long (the residence time τ of the fortune, on average, is about 66 time units, with the most probable value being around 25 time units, when counted in units of N trades or exchanges; see Figure 5A). The most probable 'return time' to such a fortune (of the 20th rank holder, coming within the group of fortunate 10), is found to be about 20 (in units of N; see Figure 5B). It should be noted that with $f = 0$, in the C-model, the residence time τ is infinity for the only fortunate one accumulating the entire wealth in the system. Indeed, with increasing values of DY fraction f, the values of τ in both cases decrease rapidly (see Figure 10), following inverse power laws with f. We further note that, for $f = 0$ in the B-model near the most probable values of the wealth fractions (Figures 1 and 2) and residence or return times (Figure 5), the fluctuations tend to grow with N, indicating the possible divergence there in the macroscopic limit of N. We plan to explore this significance later.

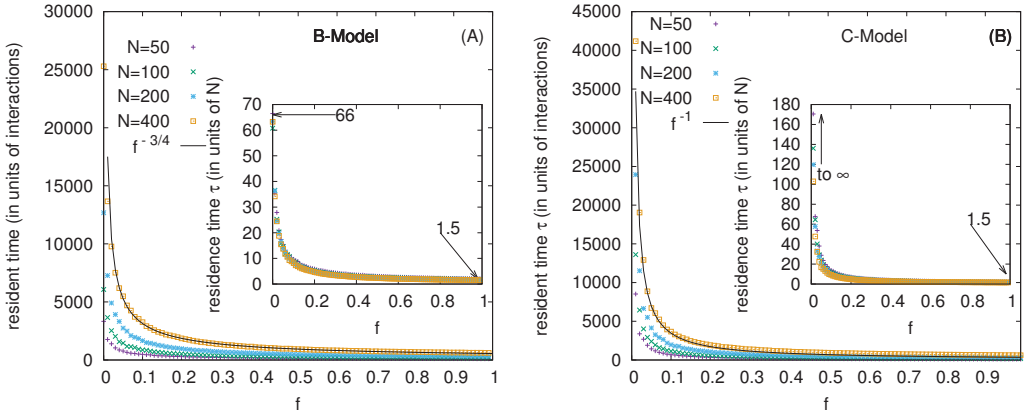

Figure 10. The DY fraction f dependence of the bare residence time (in units of interactions or exchanges) at different N values for the B-model (**A**) and for the C-model (**B**) are shown. Their power law fits with f for $N = 400$ are shown (for other N vales, the respective pre-factors change linearly with N). The insets show the f dependence of the residence times τ (in units of N). Note that the limiting values of τ at $f = 0$ are about 66 for the B-model, while they go to infinity for the C-model.

Our studies for the B, C, and GS kinetic exchange models using Monte Carlo techniques suggest that the potential condensation type of extreme inequality can disappear in all of them if a non-vanishing probability of random exchange is allowed, converging to the Pareto-type power law inequality (for the B and GS models), converging to the Gibbs-like (exponentially decaying) wealth distribution for larger values of f in the B model, smaller values of α in the GS model, or any values of $f > 0$ in the C model. These observations may help to formulate public welfare policies.

Author Contributions: Methodology, A.G., S.B., S.G., M.M. and B.K.C.; Formal analysis, A.G.; Writing—original draft, B.K.C.; Writing—review & editing, A.G., S.B., S.G. and M.M.; Visualization, A.G.; Supervision, B.K.C. All authors have read and agreed to the published version of the manuscript.

Funding: This research received no external funding.

Institutional Review Board Statement: Not applicable.

Data Availability Statement: Code will be available from the corresponding author upon request.

Acknowledgments: S.B. acknowledges the support from DST INSPIRE. B.K.C. is grateful to the Indian National Science Academy for their Senior Scientist Research grant.

Conflicts of Interest: The authors declare no conflict of interest.

References

1. Saha, M.N.; Srivastava, B.N. *A Treatise on Heat*; Indian Press: Allahabad, India, 1931; p. 105.
2. Mandelbrot, B.B. The Pareto-Levy law and the distribution of income. *Int. Econ. Rev.* **1960**, *1*, 79–106. [CrossRef]
3. Chakrabarti, B.K.; Marjit, S. Self-organisation and complexity in simple model systems: Game of life and economics. *Indian J. Phys.* **1995**, *69B*, 681–698.
4. XDragulescu, S.; Yakovenko, V.M. Statistical mechanics of money. *Eur. Phys. J. B–Condens. Matter Complex Syst.* **2000**, *17*, 723–729. [CrossRef]
5. Chakraborti, A.; Chakrabarti, B.K. Statistical mechanics of money: How saving propensity affects its distribution. *Eur. Phys. J. B–Condens. Matter And Complex Syst.* **2000**, *17*, 167–170. [CrossRef]
6. Chatterjee, A.; Chakrabarti, B.K.; Manna, S.S. Pareto law in a kinetic model of market with random saving propensity. *Phys. Stat. Mech. Its Appl.* **2004**, *335*, 155–163. [CrossRef]
7. Yakovenko, V.M.; Barkley, J. Rosser. Statistical mechanics of money, wealth, and income. *Rev. Mod. Phys.* **2009**, *81*, 1703. [CrossRef]
8. Chakrabarti, B.K.; Chakraborti, A. *Chakravarty and Chatterjee, Econophysics of Income and Wealth Distributions*; Cambridge University Press: Cambridge, UK, 2013.
9. Pianegonda, S.; Iglesias, J.R. Inequalities of wealth distribution in a conservative economy. *Phys. A* **2004**, *42*, 193–199. [CrossRef]
10. Iglesias, J.R. How simple regulations can greatly reduce inequalities. *Sci. Cult.* **2010**, *76*, 437–443.
11. Ghosh, A.; Basu, U.; Chakraborti, A.; Chakrabarti, B.K. Threshold-induced phase transition in kinetic exchange models. *Phys. Rev. E* **2011**, *83*, 061130. [CrossRef]
12. Paul, S.; Mukherjee, S.; Joseph, B.; Ghosh, A.; Chakrabarti, B.K. Kinetic exchange income distribution models with saving propensities: Inequality indices and self-organized poverty level. Philosophical Transactions of the Royal. *Soc. A* **2022**, *380*, 20210163.
13. Pickety, T. *Capital in Twenty First Century*; Harvard University Press: Harvard, MA, USA, 2014.
14. Iglesias, J.R.; Cardoso, B.-H.F.; Gonçalves, S. Inequality, a scourge of the XXI century. *Commun. Nonlinear Sci. Numer.* **2021**, *95*, 105646. [CrossRef]
15. Danial, L.; Yakovenko, V.M. Physics-inspired analysis of the two-class income distribution in the USA in 1983–2018. *Phil. Trans. R. Soc. A* **2022**, *380*, 20210162. [CrossRef]
16. Banerjee, S.; Biswas, S.; Chakrabarti, B.K.; Ghosh, A.; Mitra, M. Sandpile Universality in Social Inequality: Gini and Kolkata Measures. *Entropy* **2023**, *25*, 735. [CrossRef]
17. Oxfam International Report. 20th January 2020. Available online: https://www.oxfam.org/en/press-releases/worlds-billionaires-have-more-wealth-46-billion-people (accessed on 20 July 2023).
18. Chatterjee, A.; Chakrabarti, B.K. Kinetic exchange models for income and wealth distributions. *Eur. Phys. J. B* **2007**, *60*, 135–149. [CrossRef]
19. Pareschi, L.; Toscani, G. *Interacting Multiagent Systems*; Oxford University Press: Oxford, UK, 2014.
20. Chakraborti, A. Distributions of money in model markets of economy. *Int. J. Mod. C* **2002**, *13*, 1315–1321. [CrossRef]
21. Hayes, B. Follow the Money. *Am. Sci.* **2002**, *90*, 400–405. [CrossRef]
22. Cardoso, B.-H.F.; Gonçalves, S.; Iglesias, J.R. Why equal opportunities lead to maximum inequality? The wealth condensation paradox generally solved, Chaos. *Solitons Fractals* **2023**, *168*, 113181. [CrossRef]
23. Boghosian, B. Is Inequality Inevitable? *Sci. Am.* **2019**, *321*, 70–77.

24. Julian, N.; Cardoso, C.B.-H.F.; Fabiana, L.M.; Gonçalves, S.; Iglesias, J.R. Study of taxes, regulations and inequality using machine learning algorithms. *Philos. Trans. R. Soc. A* **2022**, *380*, 20210165.
25. Goswami, S.; Sen, P. Agent based models for wealth distribution with preference in interaction. *Phys. A Stat. Mech. Its Appl.* **2014**, *415*, 514–524. [CrossRef]
26. Banerjee, S. Role of Neighbouring Wealth Preference in Kinetic Exchange model of market. *arXiv* **2023**, arXiv:2305.16238.

entropy

MDPI

Article

Wealth Redistribution and Mutual Aid: Comparison Using Equivalent/Non-Equivalent Exchange Models of Econophysics

Takeshi Kato

Kyoto University Laboratory, Open Innovation Institute, Kyoto University, Kyoto 606-8501, Japan; kato.takeshi.3u@kyoto-u.ac.jp

Abstract: Given wealth inequality worldwide, there is an urgent need to identify the mode of wealth exchange through which it arises. To address the research gap regarding models that combine equivalent exchange and redistribution, this study compares an equivalent market exchange with redistribution based on power centers and a non-equivalent exchange with mutual aid using the Polanyi, Graeber, and Karatani modes of exchange. Two new exchange models based on multi-agent interactions are reconstructed following an econophysics-based approach for evaluating the Gini index (inequality) and total exchange (economic flow). Exchange simulations indicate that the evaluation parameter of the total exchange divided by the Gini index can be expressed by the same saturated curvilinear approximate equation using the wealth transfer rate and time period of redistribution, the surplus contribution rate of the wealthy, and the saving rate. However, considering the coercion of taxes and its associated costs and independence based on the morality of mutual aid, a non-equivalent exchange without return obligation is preferred. This is oriented toward Graeber's baseline communism and Karatani's mode of exchange D, with implications for alternatives to the capitalist economy.

Keywords: inequalities and wealth redistribution; taxes and redistribution; mutual aid; equivalent exchange; non-equivalent exchange; markets; economic flow; econophysics

Citation: Kato, T. Wealth Redistribution and Mutual Aid: Comparison Using Equivalent/Non-Equivalent Exchange Models of Econophysics. *Entropy* **2023**, *25*, 224. https://doi.org/10.3390/e25020224

Academic Editor: José Roberto Iglesias

Received: 3 January 2023
Revised: 19 January 2023
Accepted: 21 January 2023
Published: 24 January 2023

1. Introduction

Wealth inequality is a major social problem in various countries worldwide [1]. Survey results indicate that the global Gini index is approximately 0.7, indicating widespread inequality [2]. A Gini index of 0.4 represents a warning level for social unrest [3], and some countries far exceed this level, including South Africa, Namibia, and Suriname [4]. Higher social unrest leads to lower production and further inequality, which in turn leads to social unrest again, creating a vicious cycle [5].

The United Nations Sustainable Development Goals has prioritized Goal 10—which aims to "reduce income inequalities", "promote universal social, economic and political inclusion", and "adopt fiscal and social policies that promote equality", among other targets—along with Goals 1, 2, 8, and 16 (no poverty, zero hunger, inclusive economic growth, and justice and inclusive institutions, respectively) [6]. Moreover, the United Nations University studies the impact of inequality on economic growth, human development, and governance, with inequality as a core concern [7]. Thus, there is a need to identify which types of economic relations—that is, which modes of exchange of wealth—result in inequality. For this, different definitions of the modes of exchange must be considered.

The economist K. Polanyi has identified three modes of economic exchange: reciprocity, redistribution, and market exchange [8]. Reciprocity includes the transfer of goods through gifts with the obligation to provide returns in non-hierarchical relationships; redistribution indicates the transfer of goods through the collection and refund of taxes based on the centrality of power; and market exchange represents the equivalent transfer of goods based on money prices in the market. In other words, reciprocity is a non-equivalent exchange

with the obligation to return, market is an equivalent exchange, and redistribution is an equivalent exchange coordinated by a power center.

The anthropologist D. Graeber has presented baseline communism, exchange, and hierarchy as the three moral principles of economic relations [9]. Baseline communism is a mutual-aid human relationship wherein each person contributes based on their ability and is provided a return according to need; exchange is a process toward equivalence, an inhuman relationship that can be dissolved through profit and loss; and hierarchy represents a relationship bound and controlled by custom and precedent, with no tendency to operate through reciprocity. Therefore, baseline communism is a non-equivalent exchange without the obligation to return, exchange is an exactly equivalent exchange, and hierarchy is a specific form of redistribution with tribute imposed on proteges and alms imposed as the protection of a power center.

The philosopher K. Karatani has presented four modes of exchange as the various stages of the world system [10]. Modes of exchange A, B, C, and D represent reciprocity in civil society (gift and return), plunder and redistribution in the empire (domination and protection), commodity exchange in the capitalist economy (money and commodities), and restoration of the reciprocal-mutual aid relationship of A to a higher level in the world republic idealized by Kant, respectively. Mode of exchange A is thus a non-equivalent exchange with the obligation to return, B is a form of redistribution, C is an equivalent exchange, and D is a non-equivalent exchange without the obligation to return.

A comparison of the three typologies above show that the following definitions correspond with each other, as shown in Table 1: Polanyi's reciprocity and Karatani's mode of exchange A with non-equivalence and return; Polanyi's redistribution, Graeber's hierarchy, and Karatani's mode of exchange B with centrality of power; Polanyi's market exchange, Graeber's exchange, and Karatani's mode of exchange C with equivalence; and Graeber's baseline communism and Karatani's mode of exchange D with non-equivalence and without return.

Table 1. Comparison of economic typologies by Polanyi, Graeber, and Karatani.

Typology	Polanyi	Graeber	Karatani
Non-equivalent exchange with obligation to return	Reciprocity	—	Mode of exchange A
Redistribution by power center	Redistribution	Hierarchy	B
Equivalent exchange in the market	Market exchange	Exchange	C
Non-equivalent exchange without obligation to return	—	Baseline communism	D

The contemporary capitalist economy and social security protections comprise a hybrid of equivalent market exchange (C) and redistribution by power center (B). In contrast, alternatives to the capitalist economy can be considered as a mutual-aid baseline communism and mode of exchange D, which sublimates mode of exchange A. Therefore, it is necessary to identify whether a hybrid of equivalent exchange and redistribution (B and C) or that of a mutual-aid non-equivalent exchange without obligation to return (D) would be preferable to suppress wealth inequality. This is also to clarify whether progressive capital taxation (a hybrid of B and C), as proposed by economist T. Piketty based on the famous inequality r (the rate of return on capital) $> g$ (the growth rate of income) [11], or dynamic equality (similar to D), which forces the wealthy to have "skin in the game" themselves, as proposed by philosopher N.N. Taleb instead of a power-centered redistributive system [12], is preferable.

Econophysics uses a statistical, physics-based approach for examining wealth exchange and distribution and the mechanisms of redistribution (see, for example, the comprehensive reviews by Chakrabarti A. S. and Chakrabarti B. K., Rosser, and Ribeiro,

respectively [13–15]). Champernowne explained Pareto's law based on time series changes in income distribution through stochastic processes [16]. Angle, writing from a sociologist's standpoint, showed that the gamma distribution arises through economic agents' stochastic processes [17]. Furthermore, Dragulescu and Yakovenko illustrated that the monetary distribution follows an exponential Boltzmann–Gibbs distribution based on the analogy of energy conservation [18], and Chakraborti and Hayes demonstrated that a delta distribution arises when applying a model of random wealth transfer to a model of the poor and the wealthy, based on the analogy of kinetic energy exchange in collisions of ideal gas particles [19,20].

Chatterjee and Chakrabarti extended these models and showed that an exponential distribution can be obtained using a model in which wealth is randomly divided among agents [21]. Furthermore, Chakraborti and Chakrabarti indicated that gamma and power distributions can be obtained using a model in which agents follow a non-equivalent exchange, except for savings [22]. Kato et al. showed that a delta distribution can be obtained using a model in which wealth is exchanged equivalently according to the poor [23]. In addition, Guala used a non-equivalent exchange model combining exchange and tax redistribution for obtaining exponential and gamma distributions based on the tax rate [24], and Chakrabarti A. S. and Chakrabarti B. K. used a model combining non-equivalent exchange and redistribution by insurance to obtain insurance-rate-based exponential, gamma, and delta distributions [25].

Furthermore, Kato and Hiroi used a non-equivalent exchange model in which the wealthy contribute surplus stock to obtain delta- and gamma-like distributions based on the contribution rate; they showed that the contribution of surplus stock by the wealthy is necessary for activating economic flow and reducing inequality [26]. Kato further used an exchange model combining interest, profit and loss, and redistribution to obtain delta- and gamma-like distributions and demonstrated that the prohibition of interest, fair distribution of profit and loss, and redistribution based upon the quintile axiom in welfare economics are required for reducing inequality [27].

Elsewhere, Iglesias showed that inequality, as measured by the Gini index, is dramatically reduced by externally modeling the collection of a tax proportional to the wealth difference from local or global agents around the poorest agent and the redistribution of the tax to the poorest agent [28]. Moreover, Lima et al. showed that a combination of win/lose equivalent transactions based on the wealth of the poor, power-law taxes that are more burdensome on the wealthy, and tax exemptions for the poor can result in bimodal or flat wealth distributions, and that tax exemptions do not necessarily reduce inequality, as assessed using the Gini index [29]. These Iglesias and Lima models are effectively non-equivalent exchanges, since each exchange is taxed according to wealth.

The above-mentioned studies do not use models that combine an equivalent exchange with a redistribution separated from it by a certain time period, however. In this study, I aim to reconstruct an exchange model that represents a hybrid of equivalent exchange and redistribution (modes of exchange B and C) and a mutual-aid non-equivalent exchange without obligation to return (mode D) based on the above-mentioned exchange model of econophysics. I also compare redistribution and mutual aid in terms of wealth distribution, inequality, and economic flow to provide guidelines for alternative capitalism. This study is novel in that it compares redistribution with mutual-aid non-equivalent exchange. Furthermore, it describes new relationships between the following phenomena: economic flow and inequality; wealth transfer, time period, and redistribution; and surplus contribution of the wealthy, saving, and mutual aid. Based on the comparison, I provide new insights into alternatives to the capitalist economy.

In the present model (hybrid of equivalent exchange and redistribution), I use the equivalent exchange model of Kato et al. [23] to represent, in combination, Polanyi's market exchange, Graeber's exchange, and Karatani's mode of exchange C, and Kato's redistribution model [27] to represent, combinedly, Polanyi's redistribution, Graeber's hierarchy, and Karatani's mode of exchange B. To model mutual-aid non-equivalent exchange, I adopt

Kato and Hiroi's surplus stock contribution model [26] to represent Graeber's baseline communism and Karatani's mode of exchange D, repositioning the surplus stock contribution of the wealthy as a mutual aid without the obligation of return.

The remainder of this paper is organized as follows. Section 2 presents models of equivalent exchange and redistribution and mutual-aid non-equivalent exchange models, as well as the methods for calculating the Gini index and total exchange to assess wealth inequality and economic flow. Section 3 compares the simulation results of wealth distributions with the Gini index and total exchange calculations for the two models to illustrate their relationship. Section 4 examines the contemporary significance of mutual aid for redistribution considering these results and presents discussions on the nature of mutual aid for alternatives to the capitalist economy. Section 5 presents the key conclusions and future challenges.

2. Methods

2.1. Exchange Models

Figure 1 visualizes different exchange models that can be used to measure and understand inequality, to be explained in detail below.

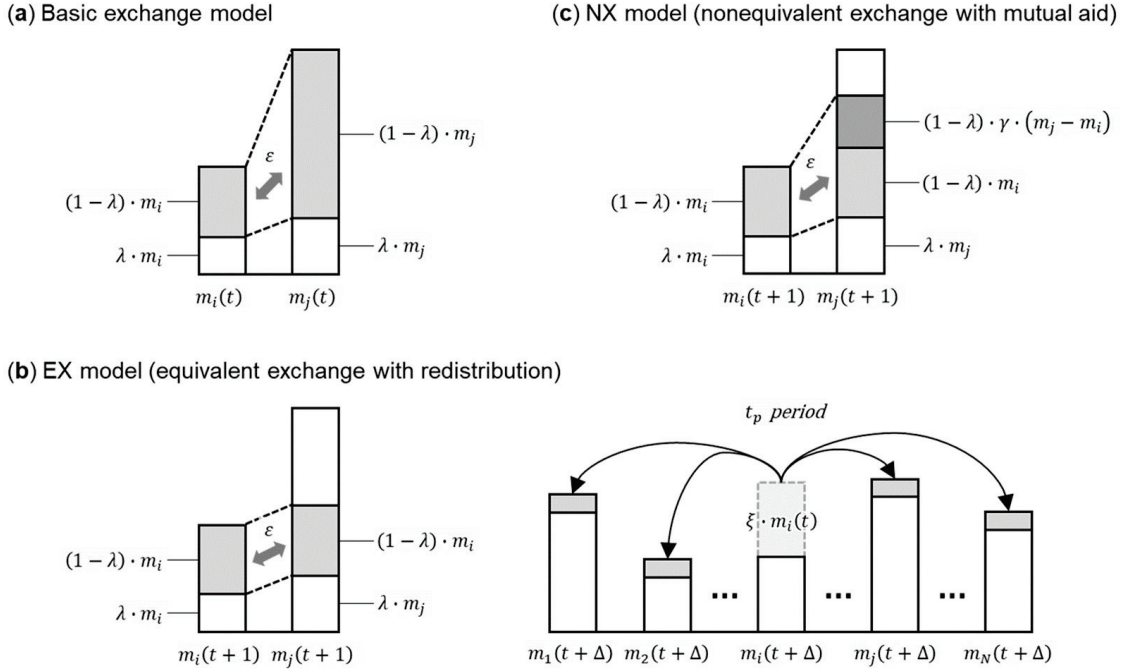

Figure 1. Exchange models: (**a**) basic exchange model; (**b**) equivalent exchange model (EX) with redistribution rate ξ and time period t_p; and (**c**) non-equivalent exchange model (NX) with surplus contribution rate γ. m_i and m_j represent the wealth of agents i and j, respectively, at times t, $t+1$ and $t+\Delta$. λ represents the common savings rate, and ε represents the random division probability.

2.1.1. Basic Exchange Model

First, I present the basic wealth exchange model proposed by Chakraborti and Chakrabarti [22]. Two agents i, j $(= 1, 2, \cdots, N)$ are selected randomly from among N economic agents. Let the wealth of agents i and j at time t be $m_i(t)$ and $m_j(t)$, respectively, with a common saving rate λ for both. Figure 1a shows that the two agents i and j save part of their wealth at time t with a savings rate λ and exchange the remaining wealth $(1-\lambda)\cdot\big(m_i(t)+m_j(t)\big)$, excluding savings, with a random division probability ε, which is a uniform random number defined in the range $0 \leq \varepsilon \leq 1$. This basic model is a non-equivalent exchange model wherein the poor and the wealthy offer all their wealth

(except their savings) in exchange. The wealth $m_i(t+1)$ and $m_j(t+1)$ of the two agents i and j, respectively, at time $t+1$ are expressed as

$$m_i(t+1) = \lambda \cdot m_i(t) + \varepsilon \cdot (1-\lambda) \cdot \big(m_i(t) + m_j(t)\big); \tag{1}$$

$$m_j(t+1) = \lambda \cdot m_j(t) + (1-\varepsilon) \cdot (1-\lambda) \cdot \big(m_i(t) + m_j(t)\big). \tag{2}$$

2.1.2. Equivalent Exchange Model

The equivalent exchange model that matches the wealth of the poor (hereinafter, the EX model) proposed by Kato et al. [23] is based on the non-equivalent exchange model, as presented in Equations (1) and (2). As indicated in Figure 1b, the EX model determines the amount of exchange based on the wealth $\mathrm{Min}\big(m_i(t),\ m_j(t)\big)$ of the poorer of the two agents, i and j. The exchange amount presented by the wealthy and the poor is exchanged with a random division probability ε, which is a uniform random number in the range $0 \leq \varepsilon \leq 1$. Wealth $m_i(t+1)$ and $m_j(t+1)$ at time $t+1$ are expressed as

$$min = \mathrm{Min}\big(m_i(t),\ m_j(t)\big), \tag{3}$$

$$m_i(t+1) = m_i(t) - (1-\lambda) \cdot min + 2 \cdot \varepsilon \cdot (1-\lambda) \cdot min; \tag{4}$$

$$m_j(t+1) = m_j(t) - (1-\lambda) \cdot min + 2 \cdot (1-\varepsilon) \cdot (1-\lambda) \cdot min. \tag{5}$$

Repeating the exchange process in the EX model yields a delta distribution in which all wealth is concentrated in one agent's hands, as shown in the literature [23]. Furthermore, in the EX model, redistribution is newly combined with the equivalent exchange shown in Equations (3)–(5). For the redistribution, I use the model proposed by Kato [27]. In this model, the wealth transfer rate ξ and the time period t_p for redistribution are set, and N agents simultaneously distribute the wealth $\xi \cdot m_i(t)$ corresponding to the transfer rate ξ to all others equally in every period t_p (Figure 1b). This is because establishing an average period and an average amount of redistribution when assessing the effectiveness of redistribution in reducing inequality is considered sufficient. The wealth $m_i(t+\Delta)$ of agent i at time $t+\Delta$ immediately after period t_p is expressed as

$$m_i(t+\Delta) = (1-\xi) \cdot m_i(t) + \xi \cdot \frac{\sum_{j \neq i} m_j(t)}{N-1}. \tag{6}$$

2.1.3. Non-Equivalent Exchange Model

I use the model proposed by Kato and Hiroi [26] as a mutual-aid non-equivalent exchange model without obligation to return (hereafter, the NX model). The NX model is a compromise between the non-equivalent and equivalent exchange models presented in Equations (1)–(5), respectively. In the first, the wealthy contribute all surplus wealth except savings, which is not realistic in exchange, that is, economic transactions. In the second, the wealthy only contribute wealth equivalent to that of the poor; in the absence of redistribution, extreme inequality, such as a delta distribution, is likely. Thus, Kato and Hiroi set up a model in which the wealthy contribute a portion of their surplus wealth over that of the poor to control inequality to a practical extent.

As shown in Figure 1c, in the NX model, the wealth of the poor and the wealth difference between the poor and wealthy are $min = \mathrm{Min}\big(m_i(t),\ m_j(t)\big)$ and $\delta = \big|m_i(t) - m_j(t)\big|$, respectively; the poor take the surplus wealth $(1-\lambda) \cdot min$ as the exchange amount. The wealthy's exchange amount is the wealth $(1-\lambda) \cdot (min + \gamma \cdot \delta)$; this is the sum of the poor's surplus wealth $(1-\lambda) \cdot min$ and the wealth $(1-\lambda) \cdot \gamma \cdot \delta$, which amounts to the wealthy's surplus wealth $(1-\lambda) \cdot max$ less $(1-\lambda) \cdot min$ multiplied by the surplus contribution rate γ.

The poor and wealthy then exchange the amounts mutually proposed with a random division probability ε, which is a uniform random number defined in the range $0 \leq \varepsilon \leq 1$. Graeber's baseline communism is a mutual-aid relationship in which each person contributes based on their ability and each person is given according to their need, without

obligation to return. Although the contribution of surplus wealth from the wealthy to the poor inherently varies based on need, the surplus contribution rate γ is set as a constant parameter to observe the general trends. The wealth $m_i(t+1)$ and $m_j(t+1)$ of two agents i and j, respectively, are expressed as

$$min = \mathrm{Min}\big(m_i(t),\ m_j(t)\big), \tag{7}$$

$$\delta = \big|m_i(t) - m_j(t)\big|, \tag{8}$$

$$\begin{aligned} if\quad & m_i(t+1) \le m_j(t+1), \\ & m_i(t+1) = m_i(t) - (1-\lambda)\cdot min + \varepsilon\cdot(1-\lambda)\cdot(2\cdot min + \gamma\cdot\delta); \end{aligned} \tag{9}$$

$$m_j(t+1) = m_j(t) - (1-\lambda)\cdot(min + \gamma\cdot\delta) + (1-\varepsilon)\cdot(1-\lambda)(2\cdot min + \gamma\cdot\delta). \tag{10}$$

$$\begin{aligned} if\quad & m_i(t+1) > m_j(t+1), \\ & m_i(t+1) = m_i(t) - (1-\lambda)\cdot(min + \gamma\cdot\delta) + \varepsilon\cdot(1-\lambda)\cdot(2\cdot min + \gamma\cdot\delta); \end{aligned} \tag{11}$$

$$m_j(t+1) = m_j(t) - (1-\lambda)\cdot min + (1-\varepsilon)\cdot(1-\lambda)\cdot(2\cdot min + \gamma\cdot\delta). \tag{12}$$

The NX model equals the non-equivalent exchange model shown in Equations (1) and (2) when the surplus contribution rate $\gamma = 1$ and the equivalent exchange model shown in Equations (3)–(5) when $\gamma = 0$.

2.2. Evaluation Indices

2.2.1. Gini Index

The Gini index g, used as a parameter for evaluating wealth inequality [30], is obtained by drawing the Lorenz curve and an equal distribution line [31]. Various proposed inequality indices are calculated from Lorenz curves [32], but the Gini index is used here because it is most common. Mathematically, the wealth $m_i(t)$ of the N agents at time t is ordered from the smallest to the largest; the k-th element in the ordered list $Sort(m_i(t))$ is denoted by $r_k(t)$, and the Gini index g is calculated as

$$r_k(t) \in \mathrm{Sort}(m_i(t)), \tag{13}$$

$$g = \frac{2\cdot\sum_{k=1}^{N} k\cdot r_k(t)}{N\cdot\sum_{k=1}^{N} r_k(t)} - \frac{N+1}{N}. \tag{14}$$

When the wealth of N agents is perfectly equal (uniform distribution), the Gini index $g = 0$; when all wealth is concentrated in a single agent's hands (delta distribution), $g = 1$. In other words, g ranges from 0 to 1. The greater the inequality, the larger the value of g.

2.2.2. Total Exchange

The total exchange amount f is used to evaluate economic flow [26]. The total exchange f is the sum of the exchanges of the wealthy and poor $(1-\lambda)\cdot(2\cdot min(t) + \gamma\cdot\delta(t))$ at time t from time $t = 1$ to $t = t_{max}$.

$$f = \frac{\sum_{t=1}^{t_{max}}(1-\lambda)\cdot(2\cdot min(t) + \gamma\cdot\delta(t))}{2\cdot t_{max}}. \tag{15}$$

Furthermore, Equation (15) applies to Equations (3)–(5) if $\gamma = 1$. The denominator in Equation (15), intended for normalization, is the total amount exchanged between the two agents from time $t = 1$ to $t = t_{max}$, when the two agents exchange one amount each. The larger the total exchange f, the more active the exchange of wealth, that is, the economic flows are large, and the market is active.

3. Results

I first examine wealth distributions for the EX model of equivalent exchange and redistribution represented by Equations (3)–(6) and the NX model of non-equivalent exchange represented by Equations (7)–(12). Figure 2 shows a representative example of the simulated wealth distribution results. I set a savings rate of $\lambda = 0.25$ because the average global savings rate relative to the gross domestic product (GDP) is approximately 0.25 [33], and a transfer rate of $\xi = 0.5$ in the EX model because the highest inheritance tax rate in the Organisation for Economic Co-operation and Development (OECD) countries is approximately 0.5 [34,35].

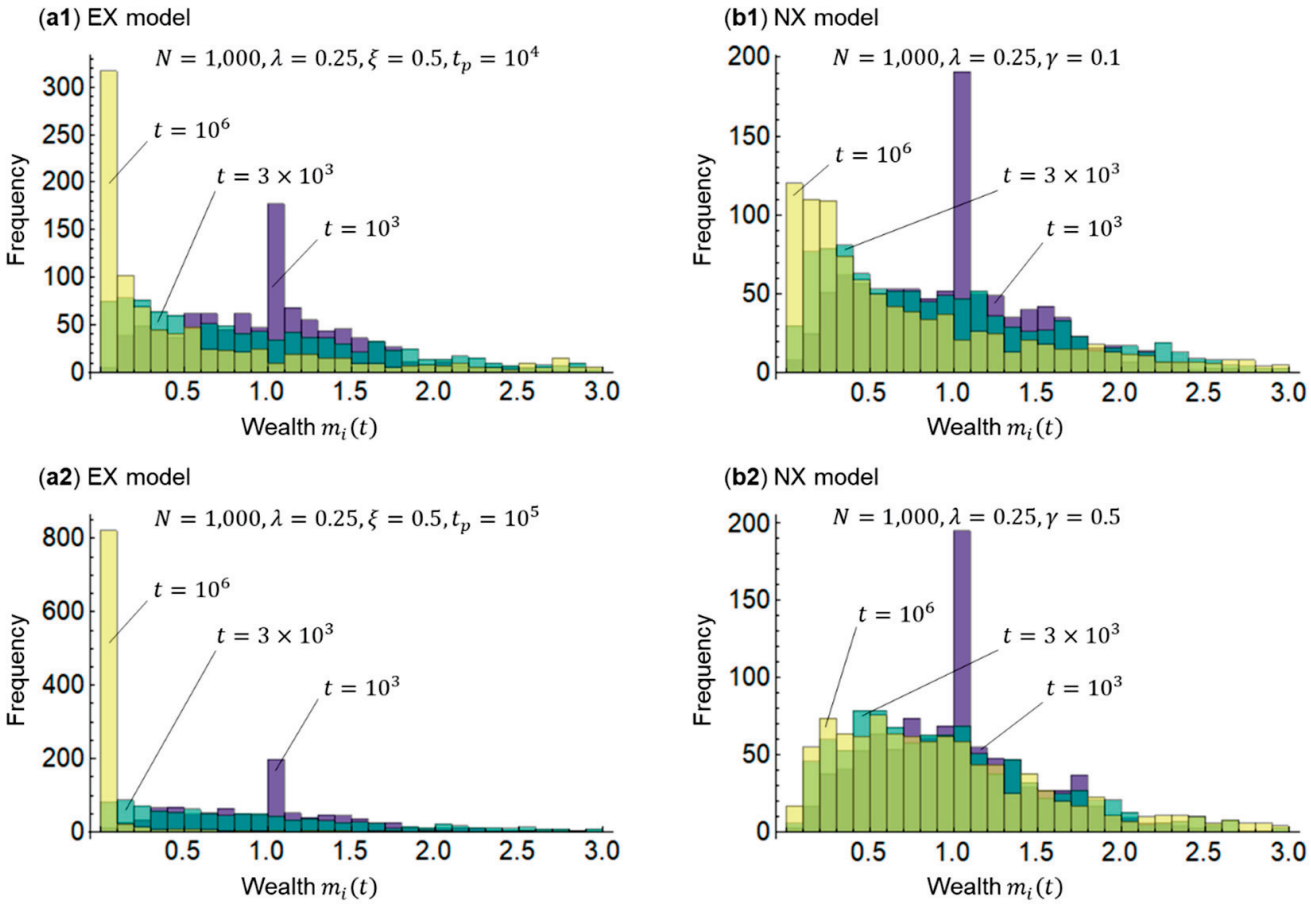

Figure 2. Wealth distribution. (**a1**) and (**a2**) represent EX models, and (**b1**) and (**b2**) represent NX models. In all models, the number of agents is $N = 1000$, the initial values of wealth at time $t = 0$ are $m_i(0) = 1$ $(i = 1, 2, \cdots, N)$, and the savings rate is $\lambda = 0.25$. In the EX model, the transfer rate is $\xi = 0.5$, and the time period is $t_p = 10^4,\ 10^5$. In the NX model, the surplus contribution rate is $\gamma = 0.1,\ 0.5$. To determine the changes in wealth distribution, the time (number of exchange repetitions) is $t = 10^3,\ 3 \times 10^3,\ 10^6$.

A consideration of Figure 2(a1,a2) reveals that as the wealth distribution in the EX model approaches a power distribution, a delta distribution with an increase in the redistribution period $t_p = 10^4$ to 10^5 occurs—that is, inequality increases. This implies that some form of redistribution must be conducted because only equivalent exchange leads to extreme inequality, as suggested by the literature [23] with respect to regional inequality. A consideration of Figure 2(b1,b2) shows that the wealth distribution approaches a gamma-like distribution from an exponential distribution in the NX model when the wealthy's surplus contribution rate increases from $\gamma = 0.1$ to 0.5, that is, the inequality narrows. This suggests that inequality can be controlled if considerable mutual aid is provided in a non-equivalent exchange.

Next, I examine the change in the Gini index (inequality) g over time (number of exchanges) t for the EX and NX models by Equations (13) and (14). Figure 3 shows the results of these simulations.

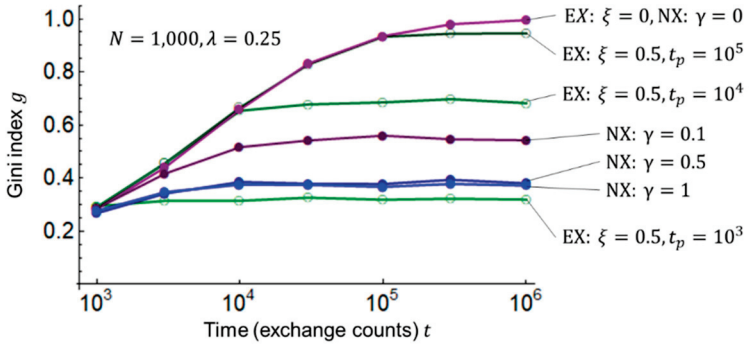

Figure 3. Gini index on time passage. The number of agents is $N = 1,000$, initial values of wealth at time $t = 0$ are $m_i(0) = 1$ $(i = 1, 2, \cdots, N)$, and the savings rate is $\lambda = 0.25$. In the EX model, the transfer rate is $\xi = 0$ and 0.5, and the time period is $t_p = 10^3, 10^4, 10^5$. In the NX model, the surplus contribution rate is $\gamma = 0, 0.1, 0.5, 1$.

In Figure 3, cases $\xi = 0$ (i.e., no redistribution in the EX model) and $\gamma = 0$ (i.e., no mutual aid in the NX model) are identical; as time t passes, the Gini index approaches $g = 1$, and all wealth is concentrated in one agent's hands. In other words, in an equivalent market exchange, inequality can only be maximized. In the EX model with $\xi = 0.5$, the redistribution period $t_p = 10^5$ to 10^3 is shortened. In the NX model, the Gini index g decreases and inequality is suppressed when the rate of surplus contribution from the rich to the poor increases from $\gamma = 0$ to $\gamma = 0.5$; however, $\gamma = 0.5$ and $\gamma = 1$ show little difference. The reason the Gini index saturates with respect to γ is presumably because the shape of the Lorenz curve itself, which calculates the Gini index g, does not change, although the wealthy and poor switch as γ increases, as discussed in the literature [26] regarding the rank correlation coefficient.

In Figures 2 and 3, the savings rate $\lambda = 0.25$ is held constant. Subsequently, I examine the Gini index (inequality) g by Equations (13) and (14) and total exchange (economic flow) f by Equation (15) for the savings rate λ and the redistribution parameter $\xi/t_p \times 10^{-3}$ of the EX model, and for the savings rate λ and the surplus contribution rate (mutual aid) γ of the NX model. The redistribution parameter $\xi/t_p \times 10^{-3}$ is introduced because the same inequality suppression effect is expected for an increase in the transfer rate ξ and a decrease in the period t_p; the $\times 10^{-3}$ is used for adjusting the computational orders of magnitude. Figure 4 shows the results of these simulations. The time (number of exchanges) t is set to 10^6, at which the Gini index g is almost stable, as shown in Figure 3.

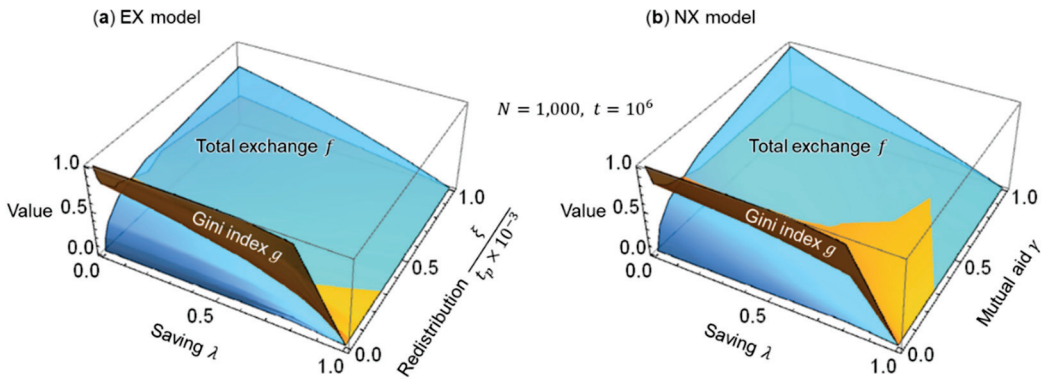

Figure 4. Three-dimensional graphs of Gini index g and total exchange f for saving rate λ and redistribution parameter $\xi/t_p \times 10^{-3}$ or mutual aid γ: (**a**) EX model and (**b**) NX model.

The consideration of Figure 4a,b reveals the same trend for both EX and NX models. In the EX model, the larger the savings rate λ, the smaller is the Gini index g (inequality is suppressed) and the smaller is the total exchange f (economic flow is reduced). Furthermore, the larger the redistribution parameter $\xi/t_p \times 10^{-3}$, the smaller is the g (inequality is suppressed) but the larger is the total exchange f (economic flow is activated). Figure 4b shows that in the NX model, the larger the savings rate λ, the smaller are the g (inequality is suppressed) and f (economic flow becomes stagnant). Moreover, the larger the mutual aid γ, the smaller is the g (inequality is suppressed) and the larger is the f (economic flow is activated). In other words, inequality g and economic flows f are inversely related with respect to the redistribution parameter $\xi/t_p \times 10^{-3}$ in the EX model and mutual aid γ in the NX model. As specific values are difficult to read in Figure 4, I examine the Gini index g for the redistribution parameter $\xi/t_p \times 10^{-3}$ of the EX model and the surplus contribution rate (mutual aid) γ of the NX model. Figure 5 shows the results of these simulations based on Figures 2–4.

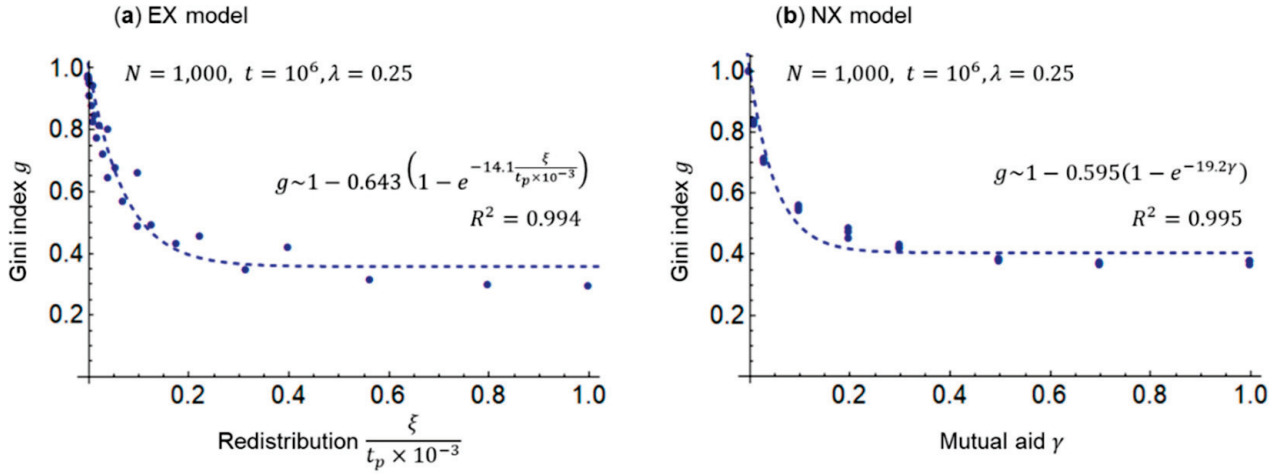

Figure 5. Relationship of Gini index g for the redistribution parameter $\xi/t_p \times 10^{-3}$ or mutual aid γ: (**a**) EX model and (**b**) NX model. In both models, dotted lines represent approximate curves.

Figure 5a,b shows that, as in Figure 4, the larger the redistribution parameter $\xi/t_p \times 10^{-3}$ in the EX model and the mutual aid γ in the NX model, the smaller is the Gini index g (inequality is reduced). In addition, both plots are accurately approximated by the saturation curve (dotted line in the figure) because the coefficient of determination R^2 is sufficiently large. At a global average savings rate $\lambda = 0.25$ [33], the redistribution parameter and the mutual aid must be as follows: $\xi/t_p \times 10^{-3} \geq 0.2$ in the EX model and $\gamma \geq 0.2$ in the NX model, respectively, to avoid exceeding the warning level $g = 0.4$ [3]. In other words, Figure 5 suggests that without a certain degree of redistribution or mutual aid, social unrest and disturbance will be triggered and Goal 10 of the Sustainable Development Goals to reduce wealth inequality [6] will not be achieved.

Finally, based on the inversely proportional relationship between the Gini index g and the total exchange f in Figure 4, I introduce the parameter f/g. Then, I examine the relationship of f/g to the redistribution parameter $\xi/t_p \times 10^{-3}$ in the EX model and to the parameter $(1-\lambda)\cdot\gamma$, comprising the savings rate λ and the surplus contribution rate (mutual aid) γ, in the NX model. I introduce the parameter $(1-\lambda)\cdot\gamma$ in the NX model because reducing the savings rate λ and increasing the surplus contribution rate γ are believed to increase the unitary exchange and mutual aid per exchange. In contrast, in the EX model, the transfer rate ξ is multiplied by the entire wealth, including savings, in every period t_p; thus, the effect of redistribution is considered independent of the savings rate λ. Figure 6 shows these simulation results.

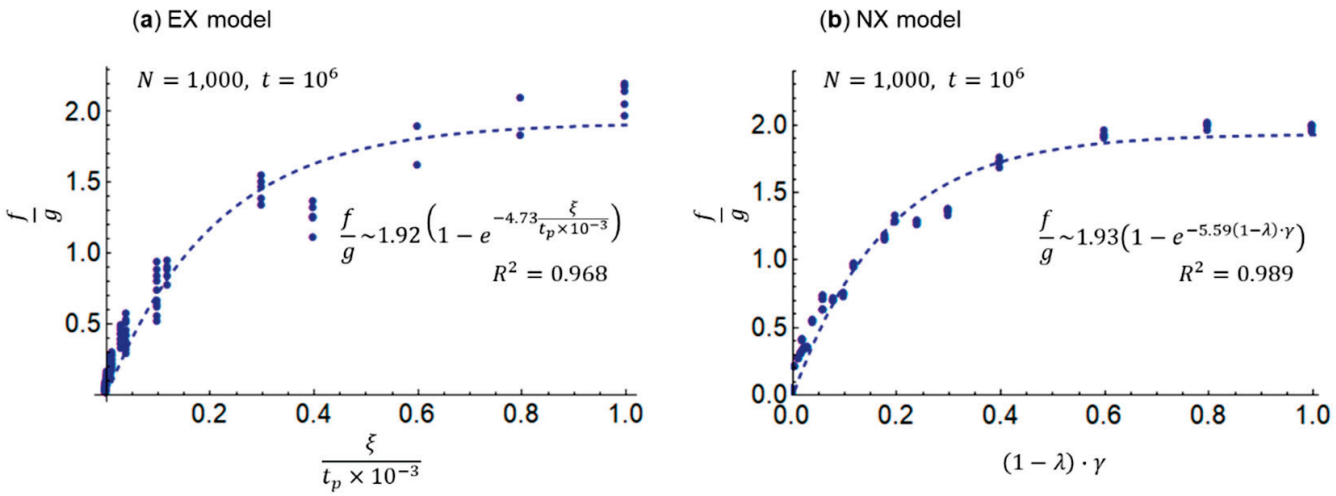

Figure 6. Relationship of the f/g parameter with the redistribution parameter $\xi/t_p \times 10^{-3}$, or mutual aid $(1-\lambda)\cdot\gamma$. (**a**) EX model and (**b**) NX model. In both models, dotted lines represent approximate curves.

Figure 6a,b show that the parameter f/g increases as $\xi/t_p \times 10^{-3}$ and $(1-\lambda)\cdot\gamma$ are increased for the EX and NX models, respectively. Furthermore, both plots are accurately approximated by the saturation curves (dotted lines in the figure) because the coefficients of determination R^2 are larger than 0.9. The EX and NX models yield $f/g \sim 0.241 \ln \xi/t_p \times 10^{-3} + 1.48$ ($R^2 = 0.779$) and $f/g \sim 0.403 \ln(1-\lambda)\cdot\gamma + 1.92$ ($R^2 = 0.937$), respectively, when approximated by logarithmic curves. The NX model results indicate that the logarithmic curves can be approximated with adequate accuracy, which is consistent with the view in the literature [26]. In Figure 6, I compare the EX and NX models using saturation curves that can be accurately approximated because both have sufficiently large R^2. It is safe to say that both approximations are isomorphic and that holds.

$$\frac{f}{g} \sim 2\left(1 - e^{-5x}\right), \tag{16}$$

$$x \sim \frac{\xi}{t_p \times 10^{-3}} \sim (1-\lambda)\cdot\gamma. \tag{17}$$

Therefore, the redistribution parameter $\xi/t_p \times 10^{-3}$ in an equivalent exchange and the mutual aid $(1-\lambda)\cdot\gamma$ that considers savings in a non-equivalent exchange yield roughly the same result with respect to the parameter f/g. The approximate equations shown in Figure 6 and Equations (16) and (17) imply that if the right side has a constant value, the Gini index (inequality) g and the total exchange (economic flow) f on the left side are inversely proportional, that is, activating economic flow will increase inequality. Additionally, it is necessary to increase $\xi/t_p \times 10^{-3}$ and $(1-\lambda)\cdot\gamma$ on the right side for the EX and NX models, respectively, to increase f/g on the left side (i.e., to increase the total exchange f while decreasing the Gini index g). Moreover, redistribution must either occur with a high transfer rate ξ and a short period t_p or with a low saving rate λ and considerable mutual aid γ to simultaneously reduce inequality and stimulate economic flow.

The numerical values presented in Figure 6a indicate that the redistribution parameters $\xi/t_p \times 10^{-3} \sim 1$ and $f/g \sim 2$ are at the saturation point of the EX model. At this point, the periods $t_p \sim 1000$, $t_p \sim 800$, and $t_p \sim 500$ should be set for transfer rates $\xi \sim 1$, $\xi \sim 0.8$, and $\xi \sim 0.5$, respectively. Given the results in Figure 3, this is tantamount to redistributing wealth before wealth distribution occurs, which is not realistic. If the target is $\xi/t_p \times 10^{-3} \sim 0.2$, where f/g does not drop considerably on the saturation curve, $t_p \sim 5000$ for $\xi \sim 1$, $t_p \sim 3000$ for $\xi \sim 0.6$, and $t_p \sim 2000$ for $\xi \sim 0.4$; this seems feasible within the range of the latter two, that is, $\xi \sim 0.5$ and $t_p \sim 2500$.

Based on the numerical values presented in Figure 6b, the saturation point of the NX model is $(1-\lambda)\cdot\gamma = 1$ and $f/g \sim 2$. The savings rate $\lambda = 0$ and the surplus contribution rate $\gamma = 1$ should be set at this point; however, it is unrealistic for the wealthy to always contribute the entirety of their surplus wealth, and for the poor and the wealthy to always save no wealth, respectively. The latter is because they must save to maintain long-term future reserves and meet contingent expenditures attributable to disasters. If the target is $(1-\lambda)\cdot\gamma \sim 0.2$, where f/g does not drop considerably on the saturation curve, $\gamma \sim 1$ for $\lambda \sim 0.8$, $\gamma \sim 0.33$ for $\lambda \sim 0.4$, and $\gamma \sim 0.25$ for $\lambda \sim 0.2$; it would be feasible to achieve $\lambda \sim 0.3$ and $\gamma \sim 0.28$ within the range of the last two considering the global average savings rate of 0.25 [33].

Figure 7 shows the relationship between redistribution and mutual aid based on Equations (16) and (17). The circle represents the tentative target. Lengthening the period of redistribution from $t_p = 2500$ to 5000 results in a transfer ratio $\xi \sim 1$, that is, transferring all assets and further lengthening the period would no longer maintain the same f/g as the mutual aid, and this would lead to economic stagnation or widening inequality. Conversely, if the redistribution period is shortened from $t_p = 2500$ to $1,250,\ 625$, the transfer rate decreases to $\xi \sim$0.25, 0.125, which necessitates frequent redistributions.

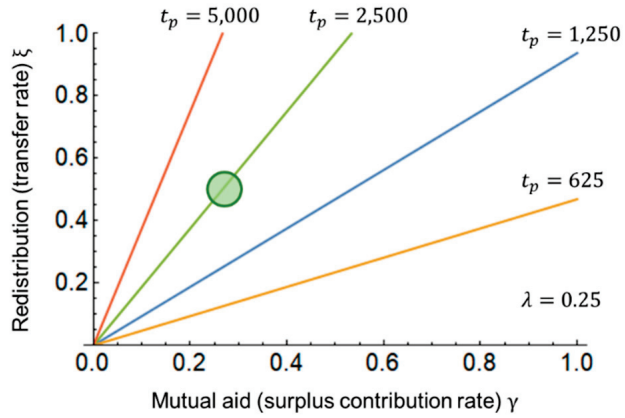

Figure 7. Relationship between redistribution parameter ξ and mutual aid γ. The savings rate is $\lambda = 0.25$, and the time period of redistribution is $t_p = 625,\ 1250,\ 2500,\ 5000$.

4. Discussion

This study compared a model combining equivalent exchange and redistribution (Polanyi's market exchange, Graeber's exchange, and Karatani's mode of exchange C combined with Polanyi's redistribution, Graeber's hierarchy, and Karatani's mode of exchange B) and a mutual-aid non-equivalent exchange model (Graeber's baseline communism and Karatani's mode of exchange D). This comparison reveals that both produce the same computational interpretation of the results for wealth inequality and economic flow. Reducing inequality and stimulating economic flow requires either power-centered collection and redistribution at a high tax rate and frequency in an equivalent market exchange or a mutual-aid non-equivalent exchange without obligation of return, in which savings are kept low and the wealthy's rate of surplus wealth contribution is high.

What does the computational similarity of authoritative redistribution and non-authoritative mutual aid imply? With respect to time t in these exchange models, a human lifetime would be considered equivalent to approximately 10^4 order of magnitude (~365 days $\times$ 100 years). Therefore, a redistribution target of $\xi/t_p \times 10^{-3} \sim 0.2$ would mean that a tax of ~50% is levied once every few decades on all assets and not the income. The maximum inheritance tax rate in OECD countries (i.e., once in a lifetime) is 50% [34,35], which means that collection and redistribution should be conducted more frequently. Expenses to the government are ~30% of GDP [36], and the collection and redistribution of taxes by the power center is extra costly; furthermore, the institutional design creates redistribution bias, that is, inequality.

In contrast, a mutual aid target of $(1-\lambda)\cdot\gamma \sim 0.2$ implies that the wealthy voluntarily give ~30% of their surplus stock to the poor in a single exchange, without obligation to return, assuming an average saving rate $\lambda = 0.25$ [33]. Although a prescribed surplus contribution rate γ is specified when modeling a mutual-aid non-equivalent exchange, the original baseline communism or mode of exchange D only requires that mutual aid be provided as required. In addition, even if redistribution and mutual aid are "computationally" similar, they are "qualitatively" different in that redistribution is coercion-based and driven by the centrality of power, whereas mutual aid is a voluntary choice based on non-centrism and morality. Extra-personal altruism and compassion, as opposed to coercion, are believed to result in wellbeing [37]. Therefore, it is evident that a mutual-aid non-equivalent exchange without obligation to return (the alternative human economy) is preferable to redistribution by power centers in an equivalent market exchange (capitalist economy and social security).

Here, examining the mechanism of the Islamic economy is instructive. As a legal system, the Islamic economy encompasses politics, economics, and society and prohibits interest (*riba*) and speculation (*gharar*), which lead to inequality. Furthermore, it also successfully balances selfishness as the pursuit of self-interest through joint ventures (*mudaraba*), consensual contracts (*murabaha*), and futures trading (*salam*) and altruism as mutual aid through donation (*waqf*), alms (*sadaqah*), and charity (*zakat*) in an equal and non-centered community (*ummah*) under God [38–40]. Redistribution through various institutions according to the Islamic legal system, rather than coercion by power centers, is more like a non-equivalent exchange of mutual aid.

According to Graeber, history over the past five millennia has alternated between cycles of bullion-based monetary economies and virtual money-based credit economies [9]. The monetary economic period is generally characterized by interest-bearing debt, war, and slavery, whereas the credit economic period has witnessed a morally peaceful society. In the Middle Ages, a credit economy era that predated the modern era, moral and financial innovations emerged from the Islamic world. As the modern era transitions from a monetary economy to a credit economy, the Islamic economy could, once again, provide an alternative to the capitalist economy [41–43].

Kato compares the Islamic and capitalist economies from the econophysics perspective; he proposes a return to a "real transaction-based economy" rooted in nature and local communities, the promotion of a "face-to-face association economy", and the revival of an "economy embedded in the morality of mutual aid" as guidelines for a credit economy as an alternative to capitalism [27]. He then states that the challenge in the non-Islamic world lies not in redistribution through taxes collected under centralized power but in mutual aid through one's free choice under the community's non-centrality and in the rebuilding of the morality of mutual aid, that is, without a specific religion.

These guidelines can be considered to be oriented toward anarchism. Anarchism is an ideology wherein individual freedom and communal solidarity are not contradictory. It seeks to build a free and equal society through mutual agreement. Graeber and Grubacic define anarchism in terms of four qualities: non-centrality, voluntary association, mutual aid, and the network model [44]. Graeber's baseline communism and Karatani's mode of exchange D, which are represented in this non-equivalent exchange model, are oriented toward anarchism as they both aim for a human economy in which free exchange occurs while incorporating the morality of mutual aid [45].

Deguchi, writing from the perspective of a philosopher, describes the East Asian view of the self, "Self-as-We", which is connected to the lineage of Laozhuang and Zen thought, as opposed to the Western view of self, "Self-as-I" [46–48]. According to Deguchi, human beings have a "fundamental incapability" to live alone, and "Self-as-We" is a network of multi-agents—including "I"—who entrust themselves to each other. The "mixed-life society" in which "we" live is one in which different self-nomadic people interact, mingle, and remain in contact, recognizing each other's "fundamental incapability" and sublimating it into solidarity. Deguchi's ideology also underlies Graeber's baseline

communism, Karatani's mode D of exchange, and the face-to-face association economy based on real transactions in the morality of mutual aid.

Another perspective is the triangle "state (public agencies)–community–market (private firms)" presented by Pestoff, writing as a political scientist [49]; the "public (state)–common (community)–private (market)" framework presented by policy scholar Y. Hiroi [50,51]; and the three pillars "state, community, market" presented by economist R. Rajan [52]. The state corresponds to Polanyi's redistribution, Graeber's hierarchy, and Karatani's mode of exchange B; the community corresponds to Polanyi's reciprocity and Karatani's mode of exchange A; and the market corresponds to Polanyi's market exchange, Graeber's exchange, and Karatani's mode of exchange C. Thus, Pestoff's association at the center of the triangle, Hiroi's synthesis of "public–community–private" and the departure from the local level, and the balance between Rajan's three pillars is oriented toward Graeber's baseline communism and Karatani's mode of exchange D.

In recent work, Karatani notes that the mode of exchange D has emerged repeatedly through the return of mode of exchange A (reciprocity and return) at a higher level, not as a world religion such as a monotheistic religion supporting the empire but as a universal religion emerging on the periphery in defiance of the empire. He also states that because of the crises of war and depression induced by modes of exchange B (imperial plunder and redistribution) and C (money and commodity exchange), mode of exchange D will arrive "from beyond" human will and planning [53].

Historian W. Sheidel states that human history has witnessed wars, revolutions, collapse of states, and epidemics, decreasing economic inequality [54]. Currently, the world is suffering from the COVID-19 pandemic, war in Ukraine, and natural disasters and conflicts caused by the effects of global warming. Although these crises are unfortunate, they may hasten the arrival of mode of exchange D and facilitate the transition from a capitalist economy to the alternatives suggested by Graeber and Karatani.

As an aside, economist T. Piketty proposes progressive capital taxation based on the famous inequality $r > g$ (the rate of return on capital > the growth rate of income) [11]. In terms of this study, this would correspond to imposing a progressive transfer rate on the wealthy in a combination of modes of exchange B and C. Furthermore, philosopher N.N. Taleb states that decentralization towards those who have "skin in the game" rather than a redistributive institution constituted by power centers will mitigate the inequality-generating asymmetry. He also formulates the idea that, to make society more equal, the wealthy should have "skin in the game" and risk falling out of the wealthy class (i.e., dynamic ergodicity should be restored) [12]. In this study's context, this would encourage the wealthy's surplus stock contribution, which may be said to be oriented toward the baseline communism and mode of exchange D.

This study is limited in that it compares general trends in redistribution and mutual aid, that the same transfer rate ξ and period t_p is set for all agents in the EX model, and that the same surplus contribution rate γ is set for all agents in the NX model. Future analytical studies should be conducted in more detail, for example, by setting the transfer rate ξ and period t_p in the EX model based on various social security programs and by choosing the surplus contribution rate γ in the NX model according to the ability of the wealthy and the needs of the poor. Moreover, empirical studies are needed that use real-world evidence to examine the relationship between economic flow and Gini index with respect to tax rate and frequency for the EX model, and with respect to stock and surplus contribution of the wealthy for the NX model.

In addition, this study uses a conservative model for aggregate wealth that deals only with exchange. Therefore, it does not deal with production and consumption, or interest and profit/loss in the real-world economy [15]. With respect to interest and profit/loss, there is a non-conservative model introduced by Kato in comparison of Islamic and capitalist economies [27]. In a future study, the redistribution or mutual aid of interest and profit/loss for the wealthy and the poor can be considered in such a non-conservative model.

It should be added that, although the present study used a model based on the kinetic energy exchange analogy, there is another model that uses potential function to compute probability distributions for income and expenditure [55], and a model that uses population dynamics to compute time developments for growth and inequality [56]. Future research could thus include such models that take into account the finiteness of earth's resources and the sustainability of economy. Such non-conservative models are subject to the constraint of resource limits, however, and eventually researchers may wish to revert to a conservative model that is primarily based on exchange.

5. Conclusions

In this study, I develop econophysics-based exchange models for a hybrid of a market-based equivalent exchange (EX) and power-centered redistribution and a mutual-aid non-equivalent exchange (NX). I also compare redistribution and mutual aid in terms of wealth inequality and economic flow.

Simulations conducted using these exchange models to evaluate the Gini index (inequality) g and total exchange (economic flow) f show that in both the EX and NX models, the larger the savings rate λ, the more the inequality is suppressed and economic flows stagnate. Furthermore, the larger the synthetic parameters $\xi/t_p \times 10^{-3}$ and $(1-\lambda)\cdot\gamma$ in the EX and NX models, respectively, the more the inequality is suppressed and economic flows are activated. I show that the EX and NX models have the same saturated curvilinear approximation equations $f/g \sim 2\cdot\left(1-e^{-5x}\right)$, $x \sim \xi/t_p \times 10^{-3} \sim (1-\lambda)\cdot\gamma$ for these relationships. This approximate expression indicates that inequality and economic flows are inversely proportional and that the parameter x must be large to achieve both.

Although the EX and NX models are "computationally" isomorphic approximations, the NX model of mutual-aid non-equivalent exchange, is "qualitatively" preferable to the EX model, a hybrid of market equivalence exchange and power redistribution. This is indicative of Graeber's baseline communism, Karatani's mode D of exchange, a face-to-face association economy based on real transactions as learned from the Islamic economy, and the ideals of anarchism.

Notwithstanding the fact that mutual aid is "qualitatively" preferable to redistribution, there remain issues that are beyond the scope of this study's econophysics-based approach: the reconstruction of a moral system in the non-Islamic world that is not based on any particular religion; the realization of a "mixed-life society" of "We" with "fundamental incapability"; and the incorporation of Graeber's stated capitalist economic alternative and Karatani's mode of exchange D. Future social practice activities based on philosophy, economics, and sociology should focus on addressing these issues.

Specifically, in order to shift steadily from redistribution toward mutual aid—that is, toward Pestoff's association and Hiroi's synthesis of "public-community-private" described in the Discussion section—mutual-aid communities could be built through cooperatives [57] and social enterprises [58,59] using environmental, social, and governance investing [60] as well as social impact bonds [61]. Such cooperatives and social enterprises will require governmental policies that provide them with preferential taxation and financial resources. They will also need to be administrated in a way that allows for the delegation of authority and lateral support. Still, though the progress toward social innovation will always be confronted by various social challenges [62], we must nevertheless reduce inequalities. This may be achieved in the future through the fusion of human society and information systems, such as in platform democracy [63], platform cooperatives [64], and cyber-human social cooperating systems [65].

Funding: This work was supported by the JSPS Topic-Setting Program to Advance Cutting-Edge Humanities and Social Sciences Research Grant Number JPJS00122679495.

Institutional Review Board Statement: Not applicable.

Data Availability Statement: Not applicable.

Acknowledgments: I am deeply grateful to Yasuo Deguchi of the Graduate School of Letters, Kyoto University, whose ideas of "Self-as-We", "fundamental incapability", and "mixed-life society" directly motivated this study. I would also like to express my deepest gratitude to Yoshinori Hiroi of the Institute for the Future of Human Society, Kyoto University, for his useful recommendations on post-capitalism, sustainable welfare society, and the economy of mutual aid. Furthermore, I would also like to thank my colleagues at the Hitachi Kyoto University Laboratory of the Kyoto University Open Innovation Institute for their ongoing cooperation and Bismark Addai.

Conflicts of Interest: The author declares no conflict of interest.

References

1. Peterson, E.W.F. Is economic inequality really a problem? A review of the arguments. *Soc. Sci.* **2017**, *6*, 147. [CrossRef]
2. Chancel, L.; Piketty, T.; Saez, E.; Zucman, G. World Inequality Report 2022. World Inequality Lab. Available online: https://wir2022.wid.world/www-site/uploads/2022/03/0098-21_WIL_RIM_RAPPORT_A4.pdf (accessed on 16 November 2022).
3. United Nations Habitat. *State of the World's Cities 2008/2009—Harmonious Cities*; Earthscan Publications: London, UK, 2008; Available online: https://unhabitat.org/state-of-the-worlds-cities-20082009-harmonious-cities-2 (accessed on 16 November 2022).
4. The World Bank. Gini Index. Available online: https://data.worldbank.org/indicator/SI.POV.GINI (accessed on 16 November 2022).
5. Saadi, T.; Xu, R. A Vicious Cycle: How Pandemics Lead to Economic Despair and Social Unrest. IMF Working Paper. 2020. Available online: https://www.imf.org/en/Publications/WP/Issues/2020/10/16/A-Vicious-Cycle-How-Pandemics-Lead-to-Economic-Despair-and-Social-Unrest-49806 (accessed on 11 December 2022).
6. United Nations. Department of Economic and Social Affairs, Sustainable Development. Available online: https://sdgs.un.org/ (accessed on 16 November 2022).
7. United Nations University. The Impact of Inequality on Growth, Human Development, and Governance. Available online: https://www.wider.unu.edu/project/impact-inequality-growth-human-development-and-governance-equal (accessed on 10 December 2022).
8. Polanyi, K. *The Livelihood of Man*; Academic Press: New York, NY, USA, 1977.
9. Graeber, D. *Debt: The First 5000 Years*; Melville House: New York, NY, USA, 2011.
10. Karatani, K. *The Structure of World History: From Modes of Production to Modes of Exchange*; Duke University Press: Durham, NC, USA, 2014.
11. Piketty, T. *Capital in the Twenty-First Century*; Harvard University Press: Cambridge, MA, USA, 2013.
12. Taleb, N.N. *Skin in the Game: Hidden Asymmetries in Daily Life*; Random House: New York, NY, USA, 2018.
13. Chakrabarti, A.S.; Chakrabarti, B.K. Statistical theories of income and wealth distribution. *Economics* **2010**, *4*, 1–31. [CrossRef]
14. Rosser, J.B., Jr. Econophysics and the entropic foundations of economics. *Entropy* **2021**, *23*, 1286. [CrossRef]
15. Ribeiro, M.B. *Income Distribution Dynamics of Economic Systems: An Econophysical Approach*; Cambridge University Press: Cambridge, UK, 2020.
16. Champernowne, D.G. A model of income distribution. *Econ. J.* **1953**, *63*, 318–351. [CrossRef]
17. Angle, J. The surplus theory of social stratification and the size distribution of personal wealth. *Soc. Forces.* **1986**, *65*, 293–326. [CrossRef]
18. Dragulescu, A.; Yakovenko, V.M. Statistical mechanics of money. *Eur. Phys. J. B* **2000**, *17*, 723–729. [CrossRef]
19. Chakraborti, A. Distributions of money in model markets of economy. *Int. J. Mod. Phys. C* **2002**, *13*, 1315–1321. [CrossRef]
20. Hayes, B. Follow the money. *Am. Sci.* **2002**, *90*, 400–405. Available online: http://bit-player.org/wp-content/extras/bph-publications/AmSci-2002-09-Hayes-money.pdf (accessed on 16 November 2022). [CrossRef]
21. Chatterjee, A.; Chakrabarti, B.K. Kinetic exchange models for income and wealth distributions. *Eur. Phys. J. B* **2007**, *60*, 135–149. [CrossRef]
22. Chakraborti, A.; Chakrabarti, B.K. Statistical mechanics of money: How saving propensity affects its distribution. *Eur. Phys. J. B* **2000**, *17*, 167–170. [CrossRef]
23. Kato, T.; Kudo, Y.; Mizuno, H.; Hiroi, Y. Regional inequality simulations based on asset exchange models with exchange range and local support bias. *Appl. Econ. Fin.* **2020**, *7*, 10–23. [CrossRef]
24. Guala, S. Taxes in a wealth distribution model by inelastically scattering of particles. *Interdiscip. Descript. Complex Syst.* **2009**, *7*, 1–7. Available online: https://www.indecs.eu/2009/indecs2009-pp1-7.pdf (accessed on 16 November 2022).
25. Chakrabarti, A.S.; Chakrabarti, B.K. Microeconomics of the ideal gas like market models. *Physica A* **2009**, *388*, 4151–4158. [CrossRef]
26. Kato, T.; Hiroi, Y. Wealth disparities and economic flow: Assessment using an asset exchange model with the surplus stock of the wealthy. *PLoS ONE* **2021**, *16*, e0259323. [CrossRef]
27. Kato, T. Islamic and capitalist economies: Comparison using econophysics models of wealth exchange and redistribution. *PLoS ONE* **2022**, *17*, e0275113. [CrossRef]
28. Iglesias, J.R. How simple regulations can greatly reduce inequality. *Sci. Cult.* **2010**, *76*, 437–443. Available online: https://arxiv.org/abs/1007.0461v2 (accessed on 11 December 2022).

29. Lima, H.; Vieira, A.R.; Anteneodo, C. Nonlinear redistribution of wealth from a stochastic approach. *Chaos Solit. Fractals* **2022**, *163*, 112578. [CrossRef]
30. Gini, C. Measurement of inequality of incomes. *Econ. J.* **1921**, *31*, 124–126. [CrossRef]
31. Xu, K. *How Has the Literature on Gini's Index Evolved in the Past 80 Years?* Economics Working Paper, Dalhousie University; SSRN: Rochester, NY, USA, 2003. [CrossRef]
32. Toscani, G. On Fourier-based inequality indices. *Entropy* **2022**, *24*, 1393. [CrossRef]
33. The World Bank. Gross Savings (% of GDP). Available online: https://data.worldbank.org/indicator/NY.GNS.ICTR.ZS (accessed on 19 November 2022).
34. OECD. *Inheritance Taxation in OECD Countries*; OECD Publishing: Paris, France, 2021. [CrossRef]
35. Cole, A. Estate and Inheritance Taxes Around the World. 2015. Available online: https://taxfoundation.org/estate-and-inheritance-taxes-around-world/ (accessed on 17 November 2022).
36. The World Bank. Expense (% of GDP). Available online: https://data.worldbank.org/indicator/GC.XPN.TOTL.GD.ZS (accessed on 17 November 2022).
37. Calvo, R.A.; Peters, D. *Positive Computing: Technology for Wellbeing and Human Potential*; The MIT Press: Cambridge, MA, USA, 2014.
38. Nagaoka, S. The future of capitalism and the Islamic economy. In *The Kyoto Manifesto for Global Economics: The Platform of Community, Humanity, and Spirituality*; Yamash'ta, S., Yagi, T., Hill, S., Eds.; Springer: Singapore, 2018; pp. 395–415. [CrossRef]
39. Nagaoka, S. *The Future of Capitalism and the Modern Islamic Economy*, Japanese ed.; Shisousha: Tokyo, Japan, 2020.
40. Kato, H. *Social Order in the Islamic World: Another "Market and Fairness"*, Japanese ed.; Shisousha: Tokyo, Japan, 2020.
41. Kamdzhalov, M. Islamic finance and the new technology challenges. *Eur. J. Islam. Financ.* **2020**, 1–6. [CrossRef]
42. Arfah, A.; Olilingo, F.Z.; Syaifuddin, S.; Dahliah, D.; Nurmiati, N.; Putra, A.H.P.K. Economics during global recession: Sharia-economics as a post COVID-19 agenda. *J. Asian Fin. Econ. Bus.* **2020**, *7*, 1077–1085. [CrossRef]
43. Yukti, R.H.; Supriadi, S.; Ariyadi, A. The Role of the Islamic Economic System in Tackling Global Economic Recession in the COVID-19 Era. In Proceedings of the 1st International Conference on Islamic Civilization (ICIC 2020), Semarang, Indonesia, 27 August 2020. [CrossRef]
44. Grubacic, A.; Graeber, D. Anarchism, or the Revolutionary Movement of the Twenty-First Century. 2004. Available online: https://theanarchistlibrary.org/library/andrej-grubacic-david-graeber-anarchism-or-the-revolutionary-movement-of-the-twenty-first-centu (accessed on 17 November 2022).
45. Yamada, H. *Possible Anarchism: Marcel Mauss and the Moral of Gift*, Japanese ed.; Inscript: Tokyo, Japan, 2020.
46. Deguchi, Y. After corona seen from "Self-as-We". In *Beyond Smart Life*, Japanese ed.; Hitachi Kyoto University Laboratory, Ed.; Nikkei Business Publications: Tokyo, Japan, 2020.
47. Deguchi, Y. Philosophy—What Is Self: "Self-as-We" and After Corona, Japanese ed. Available online: https://ukihss.cpier.kyoto-u.ac.jp/1783/ (accessed on 17 November 2022).
48. Deguchi, Y. Philosophy—From "Capability" to "Incapability": After Corona's View of Humanity, Japanese ed. Available online: https://ukihss.cpier.kyoto-u.ac.jp/2429/ (accessed on 17 November 2022).
49. Pestoff, V.A. Third sector and co-operative services—An alternative to privatization. *J. Consum. Policy* **1992**, *15*, 21–45. [CrossRef]
50. Hiroi, Y. *Rethinking on Community: Connection, Cities and Future of Japanese Society*, Japanese ed.; Chikumashobo: Tokyo, Japan, 2009.
51. Hiroi, Y. *The Design of Population-Declining Society*, Japanese ed.; Toyo Keizai: Tokyo, Japan, 2019.
52. Rajan, R. *The Third Pillar: How Markets and the State Leave the Community Behind*; Penguin Press: New York, NY, USA, 2019.
53. Karatani, K. *Power and Modes of Exchange*, Japanese ed.; Iwanami Shoten: Tokyo, Japan, 2020.
54. Sheidel, W. *The Great Leveler: Violence and the History of Inequality from the Stone Age to the Twenty-First Century*; Princeton University Press: Princeton, NJ, USA, 2017.
55. Aktaev, N.E.; Bannova, K.A. Mathematical modeling of probability distribution of money by means of potential formation. *Physica A* **2022**, *595*, 127089. [CrossRef]
56. Kemp, J.T.; Bettencourt, L.M. Statistical dynamics of wealth inequality in stochastic models of growth. *Physica A* **2022**, *607*, 128180. [CrossRef]
57. Nihon Nogyo Shinbun. *The Origins and Future of Cooperatives: Inheriting the Spirit of Mutual Aid*, Japanese ed.; Iwanami Shoten: Tokyo, Japan, 2017.
58. Fujii, A.; Harada, K.; Otaka, K. *Social Enterprise Tackling Social Exclusion*, Japanese ed.; Keisoshobo: Tokyo, Japan, 2013.
59. Yunus, M. *Building Social Business: The New Kind of Capitalism that Serves Humanity's Most Pressing Needs*; Public Affairs: New York, NY, USA, 2010.
60. Mizuguchi, T. *ESG Investment: The Shape of New Capitalism*, Japanese ed.; Nikkei Business Publications: Tokyo, Japan, 2017.
61. Epstein, M.J.; Buhovac, A.R. *Making Sustainability Work: Best Practices in Managing and Measuring Corporate Social, Environmental, and Economic Impacts*, 2nd ed.; Berrett-Koehler Publishers: San Francisco, CA, USA, 2014.
62. Takahashi, M.; Kimura, T.; Ishiguro, T. *Theorizing Social Innovation: To Discover New Practice of Social Entrepreneurship*, Japanese ed.; Bunshundo: Tokyo, Japan, 2018.
63. Newsom, G. *Citizenville: How to Take the Town Square Digital and Reinvent Government*; Penguin Books: London, UK, 2013.

64. Schneider, N. *Everything for Everyone: The Radical Tradition That Is Shaping the Next Economy*; Bold Type Books: New York, NY, USA, 2018.
65. Kato, T.; Kudo, Y.; Miyakoshi, J.; Owa, M.; Asa, Y.; Numata, T.; Mine, R.; Mizuno, H. Social Co-OS: Cyber-human social co-operating system. *IET Cyber Phys. Syst. Theor. Appl.* **2022**, *in press*. [CrossRef]

entropy

MDPI

Article

Productivity vs. Evenness in the U.S. Financial Market: A Business Ecosystem Perspective

Hugo Fort

Institute of Physics, Faculty of Science, Universidad de la República, Montevideo 11400, Uruguay; hugofortquijano@gmail.com or hugo@fisica.edu.uy

Abstract: This paper starts by presenting an empirical finding in the U.S. stock market: Between 2001 and 2021, high productivity was achieved when the Shannon evenness—measuring the inverse of concentration—dropped. Conversely, when the Shannon evenness soared, productivity plunged. The same inverse relationship between evenness and productivity has been observed in several ecosystems. This suggests explaining this result by adopting the business ecosystem perspective, i.e., regarding the tangle of interactions between companies as an ecological network, in which companies play the role of species. A useful strategy to model such ecological communities is through ensembles of synthetic communities of pairwise interacting species, whose dynamics is described by the Lotka–Volterra generalized equations. Each community is specified by a random interaction matrix whose elements are drawn from a uniform distribution centered around 0. It is shown that the inverse relationship between productivity and evenness can be generated by varying the strength of the interaction between companies. When the strength increases, productivity increases and simultaneously the market evenness decreases. Conversely, when the strength decreases, productivity decreases and evenness increases. This strength can be interpreted as reflecting the looseness of monetary policy, thus providing a link between interest rates and market structure.

Keywords: business ecosystem; population dynamics; Shannon evenness; co-evolution in markets

Citation: Fort, H. Productivity vs. Evenness in the U.S. Financial Market: A Business Ecosystem Perspective. *Entropy* **2023**, *25*, 1029. https://doi.org/10.3390/e25071029

Academic Editor: José Roberto Iglesias

Received: 5 June 2023
Revised: 30 June 2023
Accepted: 5 July 2023
Published: 7 July 2023

1. Introduction

Neoclassical economics, which assumes investors behave with rational expectations in order to maintain an efficient market, is frequently at odds to explain the dynamics of markets. Instead, the agents in markets are not perfectly rational, but rather they are boundedly rational satisfiers [1]. The idiosyncrasies in human behavior make financial markets depart from the assumption of informational efficiency leading for example to excess volatility, i.e., financial markets change more than rational measures of value would suggest [2].

An alternative viewpoint is to regard financial markets as ecosystems with a tangle of interactions between companies, investors, clients, etc. Indeed, according to [3,4], companies are engaged in "competition for differential advantage" which gives firms a position in the marketplace known as an "ecological niche" [3]. Companies survive and grow in the marketplace depending on the actions and reactions of agents permanently adjusting their behavior to match environmental opportunities. Such an ongoing process is similar to the one that operates in ecological systems competing for scarce resources [5–7]. That is, a process of *co-evolution*, shared by markets and ecosystems, in which interdependent species or companies evolve in an endless reciprocal cycle—such that changes in species A set the stage for the natural selection of changes in species B—and vice versa [8]. Co-evolution occurs in different forms, antagonistic, e.g., predators and their prey, mutually competitive, e.g., different species sharing the same trophic level, or cooperative co-evolution, e.g., flowering plants and their pollinators [9].

Moore [10] introduced biological ecology as a metaphor for strategic thinking about business co-evolution and radically new cooperative/competitive relationships. In a

similar vein, Farmer and Lo [11] regard markets as co-evolving ecologies of different strategies pursued by companies. These strategies are analogous to a biological species, and the amount of funds deployed by traders following a given strategy is analogous to the population of that species [11]. As the market evolves, the market shares of the inefficient companies decrease while the companies with greatest fitness capture market share. Therefore, companies often play the same role of selection units that species play in ecosystems.

The general goal in this paper is to use the above analogy between markets and ecosystems to better understand the forces that structure markets and determine their productivity. This includes the market responses to external shocks (analogous to environmental perturbations), such as expansive economic policies (analogous to nutrient enrichment), and the susceptibility of companies of being displaced by newcomer companies (species turnover in the case of ecosystems). Furthermore, the above analogy offers an opportunity to harness the potential of applying various powerful techniques from theoretical ecology to the fields of economics and finance. The specific primary objective of this study is to elucidate the inverse relationship detected between productivity and evenness within a set of firms encompassing the largest companies in the U.S. stock market. To accomplish this, we employ a combination of empirical evidence and theoretical modeling from ecology. Unraveling this relationship holds significant importance as it profoundly impacts the functioning of both markets and ecosystems. In fact, this ecological perspective allows us to use two central attributes which emerge from the co-evolution process of species in an ecological community, namely its productivity and its species diversity [12,13] to get insight into market dynamics. Both properties can be defined in several different ways in ecology. Productivity has been characterized by variables that range from direct estimates of energy flow to the ecosystem to accumulated biomass or biomass density (per area or volume) [14,15]. A common metric is the rate of generation of biomass in an ecosystem, usually expressed in units of mass per unit area per unit of time, such as grams per square meter per day [16]. In the case of agricultural crops, productivity is also commonly measured by the *total weight* per unit area [17], which is known as *crop yield* [18]. Diversity, in turn, involves concepts ranging from simplest concept of *species richness*, namely the number of species, to *evenness*, i.e., the measure of how similar species are in their abundance in an environment [19]. Indeed, species diversity is often intended as a combination of richness and evenness [20].

This study draws on and integrates elements of ecological science and economics, which is the scientific research program of ecological economics (EE), understood as "the relationship between ecosystems and economic systems in the broadest sense" [21]. In addition, it is transdisciplinary and uses methods and complex systems analysis [22].

2. The Business Ecosystem Perspective: Financial Markets as Ecosystems

The business ecosystem perspective refers to a framework or approach that views businesses and organizations as part of a larger interconnected system or ecosystem [10]. In the business ecosystem perspective, the focus is not solely on individual firms operating in isolation, but rather on understanding how they interact and mutually influence each other within the broader context of the ecosystem [23–25]. It recognizes that the success and sustainability of any given organization are influenced by the health and dynamics of the entire ecosystem in which it operates. Key features of the business ecosystem perspective include interconnectedness, collaborative relationships, and ecosystem dynamics. Interconnectedness recognizes that firms within the ecosystem are interconnected and depend on each other for resources, capabilities, and market opportunities. Actions and changes in one part of the ecosystem can have ripple effects on other entities within the system. Collaborative relationships refer for example to partnerships and alliances among different companies within the ecosystem. Through ecosystem dynamics, we understand that the perspective acknowledges that ecosystems are dynamic and subject to various forces and disruptions, rather than entities at equilibrium. New entrants, technological advancements,

market shifts, or changes in regulatory environments can shape the competitive landscape and the overall dynamics of the ecosystem [10,24].

Using the analogy between ecosystems and markets, companies can be regarded as species and the market value (In this paper 'market value' is taken as synonym of *market capitalization*, i.e., the number of a company's shares outstanding multiplied by the current price of a single share [26].) of a company as the abundance or biomass of a species [7,11,23–25]. Therefore, as in ecology, we consider as proxy for productivity a relative metric, corresponding to total returns—i.e., the rate of variation of the total market value. In addition, as it is carried out in agricultural sciences, we also consider an absolute metric, given by the total market value (analogous to crop yield). Likewise, as a measure of diversity, the *Shannon evenness* [27]—aka *Shannon equitability index* is used. This metric is widely used in ecology, for example, to measure the variation of the diversity of a community with a fixed number of species [28]. Notice that, in the same way as species evenness is highest when all species in a community have the same abundance, the market evenness is highest when all firms have the same market share. Market evenness is the opposite of concentration, which happens for example when a few disproportionately large firms dominate the returns of value weighted stock market indices such as the S&P500. The use of the concept of evenness and other diversity measures in economics was reviewed, for example, in [29]. Additionally, a comparison of ecological and economic measures of biodiversity was reviewed in [30]. Box 1 summarizes the correspondences between financial markets and community ecology.

Box 1. Correspondences between financial markets and community ecology.

	Financial market		Community ecology	Denoted by
•	company	↔	species	i
•	market value of a company	↔	species biomass	v_i
•	total market value	↔	total biomass (all species)	V
•	total market return	↔	rate of variation of the total biomass	R
•	market share of a company	↔	frequency of such species	x_i
•	evenness (inverse of concentration)	↔	evenness (species diversity)	E

Most natural ecological communities exist in a state of nonequilibrium where competitive equilibrium is prevented by several factors such as, for example, fluctuations in the physical and biotic environment [31]. The same happens in stock markets, where stock prices often do not settle down for long time but are driven by factors affecting supply and demand such as the economic environment, economic policies, market news, etc. In nonequilibrium ecological communities, although the number of coexisting competitors remains relatively stable, the level of diversity—measured by the evenness—varies. Indeed, a long-standing debate in ecology is that of how species diversity relates to the productivity of ecosystems (see for instance [32] or [33] and references therein).

Classical community ecology, developed by Lotka [34] and Volterra [35], has been the major descriptor of species interactions in the ecological literature for almost a century. The Lotka–Volterra generalized theory (LVGT) [36,37] rests on the assumption that species interactions play a major role in structuring an ecological community. The Lotka–Volterra generalized equations can be written in finite time as [37,38]:

$$v_i(t+1) - v_i(t) = r_i v_i(t)\left(1 + \sum_{j=1}^{S} \alpha_{ij} v_j(t)\right), \quad i = 1, 2, \cdots, S. \tag{1}$$

where i denotes the species number; $v_i(t)$ stands for its biomass at time t and r_i is the intrinsic growth rate of the species (dimension of time^{-1}). Thus, a central ingredient of LVGT is the *pairwise interaction matrix*, α_{ij}. whose element ij quantifies the effect of species j on the

growth of species i. The resulting variation in pairwise species interactions determines biodiversity in a community [39], and thus it is able to yield species abundance distributions and biodiversity as a function of species-specific interaction parameters. By analogy, one way to approach the relationship between productivity as a function of evenness in financial markets is through LVGT. The problem is that estimating the interaction matrix α_{ij} between companies is far from trivial. We will come back to this problem in Section 4.

3. Empirical Analysis

3.1. Dataset

The used dataset is based on the Fortune 100 list, i.e., a list of the top 100 public and privately held companies by revenues in the United States published by Fortune magazine [40]. From these 100 U.S. companies we selected those 78 *public* firms such that reported annual revenue and market cap from 1 January 2000 (see Table 1). Thus, the resulting dataset consists of time series for daily closing market values for each company, $v_i(t)$ (i =1, 2, . . . , 78), with t measured in days spanning 5536 days, from 1 January 2000 to 31 December 2021 [41]. The market value is a good firm size proxy; indeed, over the 27-year period of 1989–2015, it demonstrated providing high value relevance in predicting future returns [42].

Table 1. The 78 companies considered in this study ordered by their market value as of 31 December 2021 [41].

Company	Ticker	Market Val (USD Bill)	Rank	Sector	Industry
Apple	AAPL	2902	1	Technology	Consumer Electronics
Microsoft	MSFT	2522	2	Technology	Software–Infrastructure
Amazon	AMZN	1697	3	Consumer Cyclical	Internet Retail
Berkshire Hathaway	BRK	662.63	4	Financial Services	Insurance
JP Morgan	JPM	472.51	5	Financial Services	Banks
United Health Group	UNH	466.21	6	Healthcare	Healthcare Plans
Johnson & Johnson	JNJ	450.36	7	Healthcare	Drug Manufacturers
Home Depot	HD	433.37	8	Consumer Cyclical	Home Retail
Walmart	WMT	401.35	9	Consumer Defensive	Discount Stores
P&G	PG	392.11	10	Consumer Defensive	Household
Bank of America	BAC	359.38	11	Financial Services	Banks
Pfizer Inc.	PFE	331.86	12	Healthcare	Drug Manufacturers
The Walt Disney Company	DIS	281.54	13	Comm. Services	Entertainment
Cisco Systems, Inc.	CSCO	267.27	14	Technology	Comm. Equipment
Nike	NKE	263.55	15	Consumer Cyclical	Footwear and Access.
Thermo Fisher Scientific Inc.	TMO	263.18	16	Healthcare	Diagnosis and Research
Exxon Mobil	XOM	259.38	17	Energy	Oil and Gas
The Coca-Cola Company	KO	256.09	18	Consumer Defensive	Beverages
Costco	COST	251.74	19	Consumer Defensive	Discount Stores
Abbott Laboratories	ABT	248.28	20	Healthcare	Medical Devices
PepsiCo, Inc.	PEP	240.24	21	Consumer Defensive	Beverages
Oracle	ORCL	232.89	22	Technology	Software–Infrastructure
Comcast	CMCSA	228.16	23	Comm. Services	Telecom Services
Chevron	CVX	226.46	24	Energy	Oil and Gas
Verizon	VZ	218.12	25	Comm. Services	Telecom Services
Intel Corporation	INTC	209.6	26	Technology	Semiconductors
QUALCOMM Incorporated	QCOM	205.73	27	Technology	Semiconductors
Merck & Co., Inc.	MRK	193.72	28	Healthcare	Drug Manufacturers

Table 1. *Cont.*

Company	Ticker	Market Val (USD Bill)	Rank	Sector	Industry
Wells Fargo	WFC	186.44	29	Financial Services	Banks
Anthem	UPS	186.41	30	Industrials	Integrated Freight and Logistics
Lowe's	LOW	174.15	31	Consumer Cyclical	Home Retail
Morgan Stanley	MS	173.96	32	Financial Services	Banks
Honeywell International Inc.	HON	142.79	33	Industrials	Conglomerates
CVS Caremark	CVS	136.38	34	Healthcare	Healthcare Plans
Bristol-Myers Squibb Company	BMY	134.24	35	Healthcare	Drug Manufacturers
AT&T	T	132.58	36	Comm. Services	Telecom Services
Raytheon Technologies Corp.	RTX	128.51	37	Industrials	Aerospace and Defense
The Goldman Sachs Group, Inc.	GS	127.61	38	Financial Services	Banks
American Express Company	AXP	124.5	39	Financial Services	Credit Services
IBM	IBM	120.04	40	Technology	Information Tech. Serv.
Citigroup	C	119.84	41	Financial Services	Banks
Boeing	BA	118.56	42	Industrials	Aerospace and Defense
Target	TGT	110.89	43	Consumer Defensive	Discount Stores
Caterpillar Inc.	CAT	110.79	44	Industrials	Farm and Heavy Constr.
Deere & Company	DE	105.68	45	Industrials	Farm and Heavy Constr.
General electrics	GE	103.83	46	Industrials	Specialty Industr. Machinery
3M Company	MMM	101.58	47	Industrials	Conglomerates
Lockheed Martin Corporation	LMT	96.32	48	Industrials	Aerospace and Defense
ConocoPhillips	COP	94	49	Energy	Oil and Gas
Phillips 66	TJX	90.56	50	Energy	Oil and Gas
Ford Motors	F	85.59	51	Consumer Cyclical	Auto Manufacturers
Cigna Corporation	CI	74.16	52	Healthcare	Healthcare Plans
FedEx Corporation	FDX	68.53	53	Industrials	Integrated Freight and Logistics
Northrop Grumman Corp.	NOC	60.49	54	Industrials	Aerospace and Defense
Capital One Financial Corp.	COF	60.05	55	Financial Services	Credit Services
The Progressive Corporation	PGR	59.99	56	Financial Services	Insurance
Humana Inc.	HUM	59.75	57	Healthcare	Healthcare Plans
General Dynamics	GD	57.88	58	Industrials	Aerospace and Defense
Enterprise Products Partners L.P.	EPD	47.79	59	Energy	Oil and Gas
AIG	AIG	46.55	60	Financial Services	Insurance
Walgreens Boots Alliance	WBA	45.03	61	Healthcare	Pharmaceutical Retailers
HP Inc.	HPQ	40.79	62	Technology	Computer Hardware
Exelon Corporation	EXC	40.34	63	Utilities	Utilities-Regulated Electric
Sysco Corporation	SYY	40.27	64	Consumer Defensive	Food Distribution
Archer-Daniels-Midland Comp.	ADM	37.85	65	Consumer Defensive	Farm Products
The Travelers Companies, Inc.	TRV	37.73	66	Financial Services	Insurance
McKesson Corp.	MCK	37.24	67	Healthcare	Medical Distribution
The Kroger Co.	KR	33.28	68	Consumer Defensive	Grocery Stores

Table 1. *Cont.*

Company	Ticker	Market Val (USD Bill)	Rank	Sector	Industry
The Allstate Corporation	ALL	33.06	69	Financial Services	Insurance
Tyson Foods, Inc.	TSN	31.65	70	Consumer Defensive	Farm Products
Nucor Corporation	NUE	31.1	71	Basic Materials	Steel
Valero Energy	VLO	30.73	72	Energy	Oil and Gas
AmerisourceBergen	ABC	27.78	73	Healthcare	Medical Distribution
Best Buy Co., Inc.	BBY	24.44	74	Consumer Cyclical	Specialty Retail
Cardinal Health	CAH	14.26	75	Healthcare	Medical Distribution
Arrow Electronics, Inc.	ARW	9.14	76	Technology	Electronics Distribution
Fannie Mae	FNMA	0.95	77	Financial Services	Mortgage Finance
Chico's FAS, Inc.	CHS	0.66	78	Consumer Cyclical	Apparel Retail

According to the Federal Reserve [43], there were three recessions in this period:

- From the first to the third quarter of 2001, corresponding to the dot-com crash [44];
- From the fourth quarter of 2007 to the second quarter of 2009, associated with the "Subprime Mortgage Crisis" or the "Mortgage crisis" [45];
- Across the first and second quarters of 2020.

Hence, this sample covers two business cycles.

3.2. Variables

In this study, as mentioned, the three main global or aggregated variables considered are:
1. The total market value, $V(t)$, which depends on time t (measured in days), i.e.,

$$V(t) \equiv \sum_{i=1}^{78} v_i(t). \tag{2}$$

2. The total market return, $R(t)$, given by the annual variation of V, i.e.,

$$R(t) \equiv \sum_{j=1}^{S} (v_i(t+1) - v_i(t)). \tag{3}$$

In fact, I mainly consider the two abovementioned quantities adjusted by the annual consumer price index (CPI), respectively, denoted as $V_a(t)$ and $R_a(t)$, except as otherwise stated.

3. The Shannon evenness or Shannon equitability, $E(t)$, defined as:

$$E(t) \equiv \frac{-\sum_{i=1}^{78} x_i(t) \ln x_i(t)}{\ln 78}, \tag{4}$$

where $x_i(t)$ is the market share of company i at day t, i.e.,

$$x_i(t) = \frac{v_i(t)}{V(t)}. \tag{5}$$

This index is basically a normalized Shannon entropy, independent of the sample size ($N = 78$ in our particular study).

In addition, using daily data raises the problem of high-frequency variation of daily prices compared to the monthly, quarterly, or annual frequency which are much more relevant for the business ecosystem picture. To avoid this problem, the high frequency daily fluctuations were smoothed out by using moving averages over 252 stock trading days per year.

It is worth mentioning that the total (unadjusted) market value V of this set of companies at the end of the period was USD 18.9 trillion [40,41], and they represented at least 60% of the total New York Stock Exchange (NYSE) market cap in the period 2000–2021 [46]. Hence, as expected, V is strongly correlated with the S&P 500 index, as shown in Figure 1. This simply confirms that V for the selected set of companies serves as an aggregate measure of production to determine the business cycle chronology (working with the entire set of 2800 NYSE listed firms would be a daunting task).

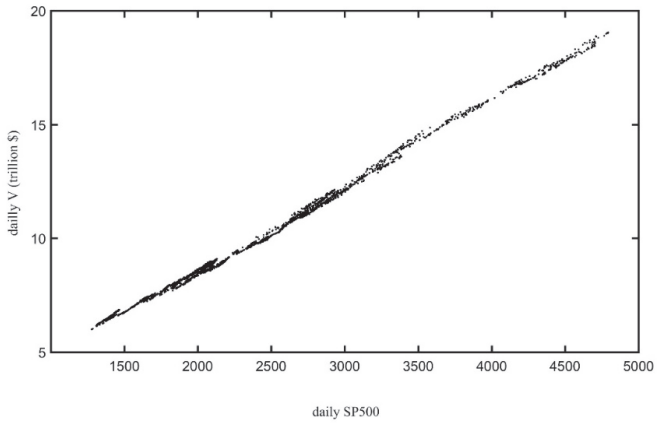

Figure 1. The total market value V vs. the S&P 500 index, for the period 2012–2021 [41].

As an additional check that that $E(t)$, given by Equation (4), correctly reflects the market evenness of the whole U.S. stock market the Shannon evenness was computed through Equation (3) but taking subsets of the whole set of 78 firms, i.e., the top 20 companies, the top 30, etc. (and replacing in Equation (3) 78 by N = 20, 30, etc.). Figure 2 shows that the corresponding succession of curves of E_N (t) converges towards the evenness $E(t)$ for the whole set; for $N \geq 50$ the curves are qualitatively very similar, while the curve E_{70} (t) only shows small departures from $E(t)$. This is because adding companies with very low shares does not change much E since $x_i \ln x_i \to 0$ when $x_i \to 0$.

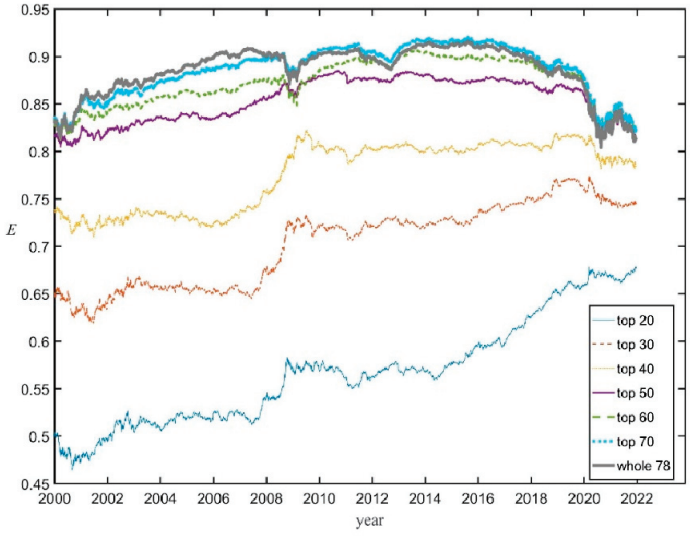

Figure 2. The Shannon evenness curves E_N (t) computed for the top N = 20 companies, the top N = 30, . . . , the whole set of 78 companies (thick gray curve).

It was checked that other different metrics used to quantify the evenness, like inverse Simpson and the Gini–Simpson indices, provide qualitatively identical curves to the Shannon evenness. (See Appendix A)

3.3. Productivity vs. Evenness in the U.S. Stock Market

The relationship between $R_a(t)$, the most widely used metric to measure market productivity, and $E(t)$ provides clear evidence of the inverse relationship between productivity vs. evenness. In Figure 3, the 21-year period is divided into three portions according to the behavior of the evenness E (full thick green curve). That is:

- A period of soaring $E(t)$, from January 2001 to December 2007, (almost exactly coinciding with the first business cycle);
- A period of relatively smooth oscillations of $E(t)$ around a high value, from January 2008 to December 2017;
- A period in which E plunged, from January 2018 to December 2021.

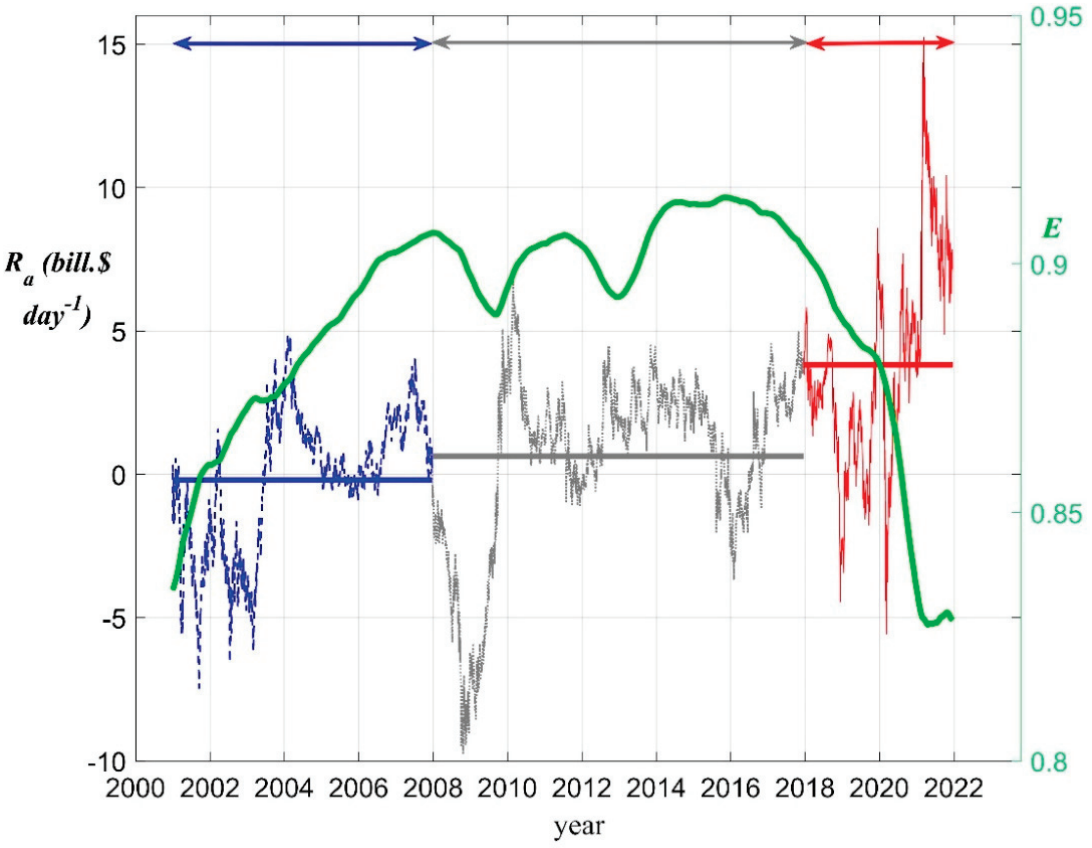

Figure 3. CPI adjusted total returns, R_a, and Shannon evenness, E, along the period 2001–2022 [41]. Right axis: Shannon evenness E (full tick green curve). Left axis: R_a plotted for three different periods depending on the behavior of E: 2001–2007 (dashed blue), characterized by soaring E and negative average R_a; 2008–2017 (dotted gray), of roughly constant E and low average R_a; January 2018 to December 2021, in which E plunged and the average R_a was high. The horizontal segments correspond to the mean of R_a along the respective period.

Notice that the R_a averaged over these periods, indicated in Figure 3 by horizontal segments, was slightly negative (blue), slightly positive (gray), and high (red), respectively. In other words, during periods in which $E(t)$ sharply decreased productivity was high, while in the other periods of soaring or high evenness, productivity was low.

The behavior of the absolute productivity metric, V_a, is also enlightening. Figure 4 shows the trajectory of V_a as a function of E from 2001 to 2021 together with some key financial events that occurred in this period. The three recessions divide the period in two business cycles, both characterized by E and V_a moving in opposite directions:

- From the beginning of 2001 until the end of 2007 (portion of the trajectory in blue in Figure 4), in which E steadily increased, while V_a ended in a slightly lower value.

- The 2009–2020 expansion (portion of the trajectory in red in Figure 4), which was the longest on record at 128 months—from July 2009 to February 2020—according to the Congressional Research Service (NBER 2022). This was a period in which, after some initial erratic movements, V_a grew strongly and E considerable declined.

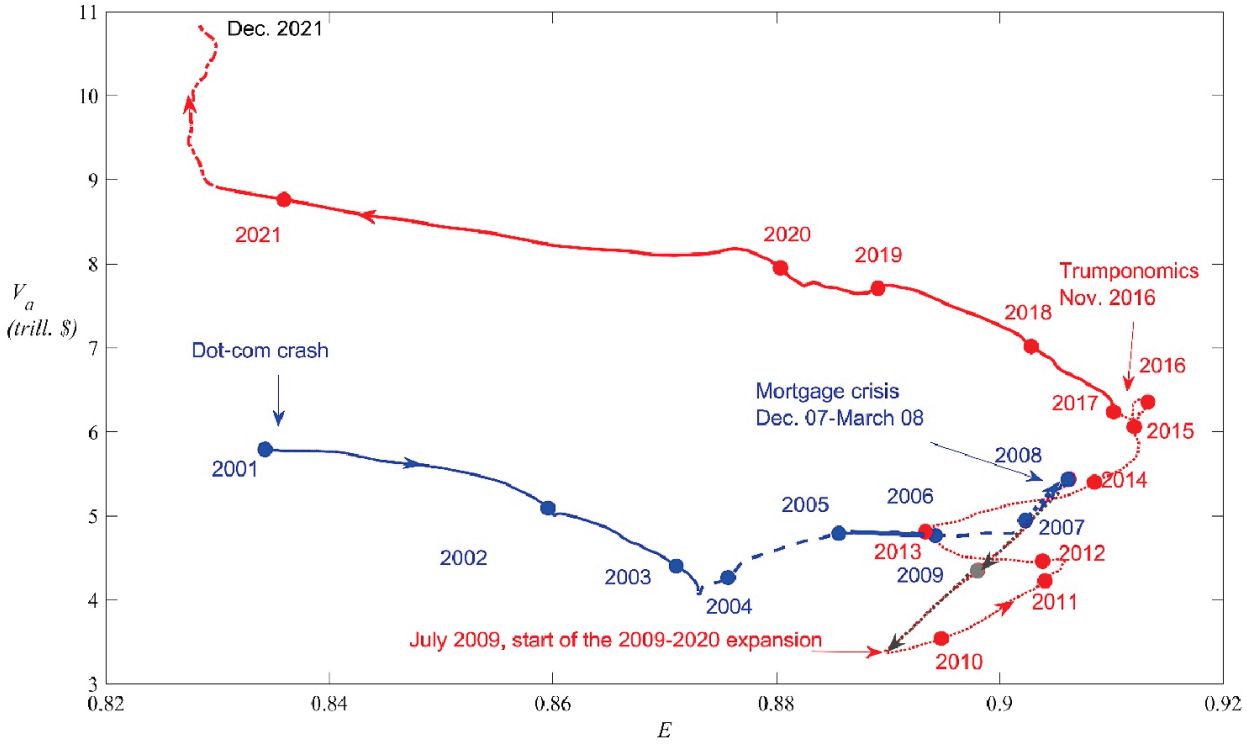

Figure 4. The trajectory of CPI adjusted total market value, V_a, as a function of E from 2001 to 2021 [41]. The portion in blue corresponds to the period between the dot-com crash and the Mortgage crisis (2001–2008). The red portion corresponds to the 2009–2020 expansion. Full lines correspond to entire periods in which V_a and E moved in opposite directions (see text). Dashed lines correspond to periods in which V_a and E moved in the same direction. The dotted section corresponds to the erratic period whose start coincided with the Mortgage crisis. The dot-dashed section in the upper left corresponds to the last three quarters of 2021 in which the market entered in a phase of almost vertical growth of V_a.

It is possible to identify some landmark events. For instance, the dot-com crash in 2001 seems to have triggered a process until 2003 in which V_a steadily decreased and E increased quickly. Conversely, from 2017 to 2021 V_a increased and E decreased fast and steadily. The start of this second period coincided with the advent of "Trumponomics". The term refers to the economic policies of U.S. President Donald Trump, who won the 8 November 2016 presidential election on the back of bold economic promises to cut personal and corporate taxes, restructure trade deals and introduce large fiscal stimulus measures [47]. The period 2008–2015 (dotted curve), whose start coincided with the "Subprime Mortgage Crisis" or the "Mortgage crisis", was quite erratic from the point of view of V_a vs. E.

In summary, after 21 years, the market evenness roughly returned to the value it had in 2001, but the total market value doubled in CPI-adjusted dollars. This growth occurred entirely in the second half of the period, characterized by a process of concentration in which the evenness lost everything it had gained in the first half.

The negative relationship between the two productivity metrics with the market evenness agrees to what is often observed in ecological communities across different taxa. For example, the analysis of data from a large multi-site grassland experiment revealed that for plots which started with the same and even species composition, but which diverged in evenness over time, those with lower evenness attained a significantly

greater biomass [48]. Moreover, the relationship between evenness and biomass across all plots in these experiments was also negative. The same was observed in other grassland experiments involving many plots of perennial grass species [49]. There are also examples of mixtures of species that converge with time towards a state of higher biomass and lower evenness for protozoa [50] and algae [51].

4. Explaining the Relationship between Productivity and Evenness in Stock Markets from a Community Ecology Perspective

Species interactions involve a complex balance of competition and facilitation in which indirect interactions occur if a third species (or more species) modifies the interaction between two other species [52]. It was argued that the success of species in a community is affected not only by direct interactions between species, but also by indirect interactions among groups of species [53,54]. The Lotka–Volterra generalized equations can naturally implement these indirect interactions through combinations of several pairwise interaction coefficients. That is, species i affects directly species k through the coefficient α_{ki}, but also indirectly through the combination of α_{ji} and α_{kj} (i.e., species i affects directly species j, which in turn affects directly species k).

Regarding markets as ecological communities enables us to use the general machinery of the theory of community ecology [9] to understand the observed negative relationship between productivity, measured by V_a and R_a, and evenness, E. We will focus in particular to the Lotka–Volterra generalized equations and the interaction matrix, α_{ij}, quantifying the strength of the effects between pairs of species.

To estimate the interaction matrix α_{ij} of an ecological community a far from trivial task. A straightforward procedure is through pairwise competition trials by comparing the species yields in biculture relative to monoculture [50,55]. However, these experiments, which are common in community ecology and agricultural science are feasible for a small number of coexisting species S [17,37,49,50]. This is because the number of required experiments grows as S^2. Furthermore, such experiments are not feasible in markets since one cannot isolate companies from the rest of the market to study their evolution under controlled conditions. Hence, we have to make use of theoretical analysis in terms of in silico synthetic communities.

4.1. Ensemble of Synthetic Communities

Therefore, let us use an approach based on Robert May's theoretical work in community ecology in terms of randomly assembled communities [38]. The idea is to consider an ensemble of pairwise interaction matrices whose diagonal elements, corresponding to intraspecific interactions of each species i, are set to -1, as it is customarily performed in community ecology [38]. The off-diagonal matrix elements, corresponding to interspecific interactions between different species i and j, are drawn from a uniform random distribution centered around 0 and with radius δ, which can thus be interpreted as the intensity of interspecific interactions. That, is:

$$\alpha_{ij} = \begin{cases} -1 & \text{if } i = j \\ \text{random in } [-\delta, +\delta] & \text{if } i \neq j \end{cases} \tag{6}$$

Notice that the mean of the interspecific interaction coefficients is $\mu = 0$, i.e., negative and positive interaction coefficients are equally likely. In fact, complex combinations of negative and positive interactions have been identified in a number of different ecological communities, like plant communities [49,56], freshwater communities [57], etc. The heterogeneity of interspecific interactions is controlled by δ since the variance of the interspecific interaction coefficients is given by $\delta^2 = \delta^2/3$, i.e., the greater δ, the greater the variance of interspecific interactions. To analyze the effect of varying the heterogeneity of interspecific interactions, we took into account that systems in which interspecific interactions are

stronger than intraspecific interactions are likely to be unstable [58], thus we kept $\delta < 1$. Thus, the parameter δ was varied from 0 to 0.9 in steps of 0.1.

To set the intrinsic growth rates, r_i, it was used that, by Equation (1), on average r_i is equal to the mean relative returns $(v_i(t+1) - v_i(t))/v_i(t)$. Therefore, let us take $r_i = 0.014$ for all i which is the mean of the empirically observed relative returns (This mean implies a double average, over companies and over time.). Next, to solve the Lotka–Volterra Equation (1) for each value of δ, 1000 simulations were run, each one starting from a random initial condition:

$$v_i(1) = \text{random in } [0,1\,],\ i = 1,2,\ldots,78. \tag{7}$$

The initial total market value, and the evenness are thus given, respectively, by: $V(1) \approx 78 \times 0.5 = 39$ (in arbitrary units) and $E(1) \approx 0.957$ (see Appendix B). Notice that these initial values are close to the equilibrium values for $\delta = 0$, $V_0{}^* = 39$ and $E_0{}^* = 1$(see Appendix C). From this initial arbitrary state, the transient dynamics towards equilibrium was studied. It is important to note that randomness only enters in the initial choice of the interspecific coefficients α_{ij}, which then define a particular community by Equation (6), and in the initial configuration (i.e., Equation (7)). For each simulation the subsequent dynamics is strictly deterministic, and the community specified by a random interaction matrix given by Equation (6), in general does not allow for the coexistence of all the 78 species. Instead, some species extinguish with time; the coexistence of the 78 species is in general unfeasible for random matrices [37]. Therefore, simulations were stopped for a time, T, for which the first species extinguished (A species is considered extinguished when its biomass drops below a cutoff $v_{\min} << 1$ (here I use $v_{\min} = 10^{-5}$)). For small values of δ, T can be quite large (thousands of time steps). However, as δ increases, T decreases, until $T \sim 30$ for $\delta = 0.9$. Hence, to use the same simulation cutoff time for all values of δ, $T = 30$ was fixed (qualitatively similar results were obtained for smaller values of T, as shown in Appendix C).

The results of simulations are shown in Figure 5. For $\delta = 0.1$, only slight deviations in V and E from their initial values, $V(1) = 39$ and $E(1) = 0.957$, occur (Figure 5a). As δ increases, the community moves towards higher values of V and lower values of E. Indeed, the curves $\overline{E}(\delta)$ and $\overline{V}[\delta]$ (the bars denote average over simulations) appear to be mirror images of each other.

These opposite trends for $\overline{E}(\delta)$ and $\overline{V}[\delta]$ can be understood as follows. It is immediate that the evenness will decline when δ is increased. This is because for $\delta = 0$ the interaction matrix α_{ij}, given by Equation (6), reduces to the identity matrix, and then all distinction among the companies disappears, Therefore, the evenness tends to its maximum possible value of $E_0{}^* = 1$ (see Appendix C). As the interactions between companies are "turned on" ($\delta > 0$), the equivalence between companies breaks down and the system departs from this state of maximum evenness. The larger the heterogeneity (variance) of these interactions the larger this departure. A derivation that $\overline{V}[\delta]$ is a monotonic increasing function of δ requires a little bit more of algebra. In a nutshell the idea is that, even though by Equation (6) positive and negative interspecific interactions are equally likely, the effect of positive interactions outweighs the effect of negative interactions, as it is shown in Appendix C. Moreover, it can also be derived that the time derivative of $\overline{V}[\delta]$, i.e., $\overline{R}[\delta]$, is a monotonic increasing function of δ.

Therefore, a way to generate the observed inverse relationship between productivity metrics and E, is by changing the interaction strength between companies: if δ increases (decreases) R and V tend to increase (decrease) and simultaneously E tends to do the opposite, i.e., to decline (rise).

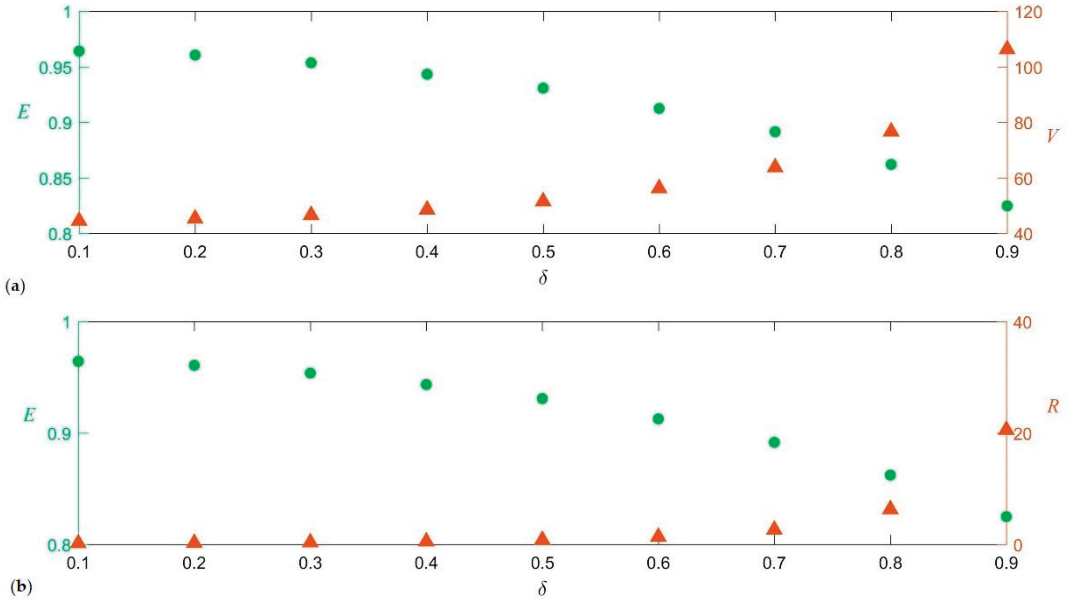

Figure 5. For each value of δ the corresponding E, R and V were obtained as averages $\overline{E}$, $\overline{R}$ and $\overline{V}$ over 1000 simulations of synthetic communities, defined by the interaction matrix of Equation (6), starting with the initial random configuration of Equation (7). (**a**): Curves of $\overline{E}$ vs. δ (circles, left axis) and $\overline{V}$ vs. δ (triangles, right axis). (**b**): Curves of $\overline{E}$ vs. δ (circles, left axis) and $\overline{R}$ vs. δ (triangles, right axis).

Regarding the mechanism promoting the growth of δ, and ultimately behind the negative relationship between productivity and evenness, monetary policy is a natural candidate. That is, when the monetary policy is loose and interest rates are low, capital flows to firms. This injection of money promotes the idea that firms address new business opportunities which multiply the interactions between them, either in the form of cooperation through new contracts, joint ventures, etc. or competition in new segments. Such an increase in the heterogeneity of interactions among companies is equivalent in our model to increase δ. Indeed, high productivity coincided with an expansion in money supply, M1 [59], and mainly with low effective interest rates (see Appendix D). The relationship between interest rates and evenness, or between money supply and evenness is less clear. Although at the beginning of the period the evenness soared with high interest rates, it persisted high during 2009–2015 when, in order to combat the Great Recession, the U.S. Federal Reserve ran a quantitative easing program and kept the effective interest rate at virtually zero [59] (see Appendix D). In a similar vein, it was observed that algal biovolume, a surrogate for biomass, increased, whereas evenness decreased with increasing total supply of resources in algal communities [60].

Two remarks are in order. Firstly, the monotonic curves $\overline{E}(\delta)$, $\overline{R}[\delta]$ and $\overline{V}[\delta]$ of Figure 5 were obtained as averages over 1000 simulations. Nevertheless, this does not imply that if $\delta_1 < \delta_2$ all simulations performed with δ_1 will produce a V smaller than the one produced by all simulation with δ_2 or an E larger than the one produced by all simulation with δ_2. Hence, this approach is also able to yield periods in which R and/or V move in the same direction as E (either both upward or downward), but they will be less likely than periods in which productivity metrics and E move in opposite directions. This is in agreement with what is shown in Figure 4 for the empirical trajectory of V vs. E: those sections in which both variables move in the same direction are rarer and shorter (e.g., during 2004).

Secondly, this approach, in terms of random matrices, produces only qualitative evidence for the observed V vs. E trend in the U.S. stock market. To obtain a better quantitative description, one has to consider more complicated structured interaction matrices. This issue is beyond the scope of this study, but some recent advances are briefly reviewed in the next subsection. Indeed, the random matrices approach, which is commonly used in various fields such as physics, mathematics, and finance, has certain limitations

and restrictions. A main restriction is its assumptions of randomness. The random matrices approach relies on the assumption that the matrix elements are independent and identically distributed random variables. However, in some real-world scenarios, this assumption may not hold true. Real-world data often exhibit correlations, dependencies, or non-random patterns that may not be accurately captured by random matrices.

4.2. Other Ecologically Based Approaches Supporting the Negative Relationship between Productivity and Evenness

The classical *Ecological Niche Theory* (ENT) states that an ecological community is made up of a limited number of niches, each occupied by a single species and that differences among species in their niches are important in determining the outcome of species interactions as might be revealed in their distributions and/or abundances in ecosystems [61]. Using ENT, the pattern of increasing biomass accompanied by decreasing evenness was firstly mathematically derived for the case of pure competition [62], which implies a restriction of the general interactions of LVGT only to mutually competitive interactions for resources. More recently, this result was extended to the more realistic case of generalized interactions. This was performed through the so-called Lotka–Volterra Niche Game Model (LVNGM) [63], resulting from the combination of ENT and Game Theory. Other recent works approaching financial markets as ecosystems have contributed to support the generality of the inverse relationship between productivity and evenness. Indeed, population dynamic models can be used in conjunction with time series of species abundances to infer the interaction coefficients between companies through indirect methods. One of such indirect methods is the so-called *Pairwise Maximum-Entropy* (PME) modeling [64]. PME modeling is a particular implementation of the of Maximum Entropy general approach proposed by Jaynes [65,66] which has been used in finance for different purposes, like ranking the performance of mutual funds [67], retrieving the risk neutral density of asset returns [68], investigating the effect of size differences on cost efficiency heterogeneity in U.S. commercial banks [69], etc. In the last two decades, PME models have been used to analyze ecological data associated with diverse problems, such as animal flocks [70], and community ecology [37,71–73]. In fact, PME modeling has been applied for a subset of the US companies I consider here in two recent studies, each one focused on a different subject, across different time lengths or training periods T_{tr}. The first one addressed the issue of inferring adjacency matrices defining the network that describe the interactions between firms in a fashion similar to how theoretical ecology pictures the interaction of species in an ecosystem [74]. A main finding of a community analysis on the resultant networks was that the network modules derived from a PME matrix, M_{ij}, coincide almost exactly with the industry groupings of the firms defined by the *Global Industry Classification Standard* (GICS) [75]. The second study tested the combination of this PME approach with evolutionary game theory for quantitative market forecasting by taking $\alpha_{ij} = M_{ij}$ [7]. It turns out that the resulting forecasting method does a decent job of predicting empirical shares of the companies along several choices of validation periods. Interestingly, these interaction matrices α_{ij} obtained by the PME method in [7,74] exhibit properties which are similar to the ones of the synthetic communities defined by Equation (6), namely that (a) most of its off-diagonal element are in the interval $(-1, +1)$ and (b) with a mean close to 0.

5. Conclusions

As we have seen, regarding markets as ecosystems can be traced back to the late 1950s [3]. Since then, different authors have contributed to building this analogy and used it to gain insight into market forces. However, there has been a lack of quantitative tools so far useful to the practitioners [76]. Indeed, the main novelties of this study are as follows:

Firstly, it raises the productivity vs. diversity issue, a fundamental question of community ecology, in the context of financial markets modeling. It is worth mentioning that a similar conclusion was drawn using a different diversity measure provided by the largest eigenvalue of the correlation matrix among stocks [77]. The productivity–diversity tradeoff is important because, as it happens in ecology, in economics, decision makers need to strike a

balance in resource allocation by considering both productivity-enhancing investments and maintaining a diverse to mitigate risks and promote long-term sustainability and resilience.

Secondly, it uses the Shannon evenness of market values to quantify the market diversity as opposed to market concentration. Being a normalized metric, the Shannon evenness is particularly useful when working with samples of companies of large markets such as NYSE. Additionally, it allows a quantitative comparison of the evenness among different markets or among different industrial sectors of the same market. The use of the Shannon evenness was instrumental to detect an important pattern of NYSE market dynamics between 2001 and 2021, namely the fact that high productivity was achieved when the evenness dropped; conversely when the evenness soared (during the business cycle 2001–2008) productivity plunged. Interestingly, such negatively correlated regime parallels the relationship between total biomass and species evenness observed in several ecosystems across distinct taxa (plants, algae, protozoa, etc.). In the case of economics and finance, balancing productivity and diversity is crucial for sustainable economic growth. High productivity can boost overall output and efficiency, leading to economic expansion. Diversity, on the other hand, can contribute to resilience and adaptability, allowing economies to better withstand disruptions. Diversity also plays a vital role in fostering innovation and creativity. When a system encompasses diverse perspectives, knowledge, and skill sets, it is more likely that it promotes the generation of new ideas and approaches. Recognizing the potential adverse effects of losing diversity, decision makers can implement policies that promote a more diverse economic landscape. This can involve supporting industries with growth potential, fostering entrepreneurship, encouraging small and medium-sized enterprises, and providing incentives for diverse business models and market entrants. Such policies can help maintain a resilient economy, reduce concentration risks, and encourage innovation and competition.

Thirdly, as far as the author knows, May's model [38] has not been previously used to analyze the relationship between evenness and productivity, neither in ecology nor in economics. Specifically, the model allows to explain how an inverse relationship between productivity and diversity can emerge when loosening or tightening the monetary policy. This has profound implications for decision makers, who need to carefully balance the short-term benefits of loosening monetary policy, such as increased liquidity and economic stimulus, with the potential long-term undesired effects on the economy. While monetary easing may provide immediate economic boosts, it can also discourage productivity improvements and hinder the development of a diverse and resilient economy. In that sense, the above finding serves to assess the trade-offs and evaluate the long-term consequences of monetary policy decisions.

Let us conclude with some research directions that seem worth investigating in future works. One important issue is the generality of negative correlation between market productivity and market evenness. For example, one may wonder whether this pattern is a particularity of the US stock market or if it is shared by other stock markets in different countries? Thus, analyzing financial markets from other countries is a natural next step. Another question is how the detected pattern is connected to long-term trends in demographics and the inter-industry reconfiguration of firms away from traditional manufacturing [78]. The business ecosystem perspective is also useful to develop quantitative methods to forecast future market values of firms [79], or to define fitnesses for firms and disentangle the effects of selection and the environment in the evolutionary dynamics of financial markets [80].

Funding: Partial financial support was received from PEDECIBA-Uruguay and SNI-ANII-Uruguay.

Institutional Review Board Statement: Not applicable.

Data Availability Statement: The data that support the findings of this study are available from the corresponding author upon request.

Acknowledgments: I thank R. Donangelo, E. Mordecki and A. Segura for useful discussions. Work supported in part by PEDECIBA & ANII-Uruguay for SNI support.

Conflicts of Interest: The author has no competing interest to declare that are relevant to the content of this article.

Abbreviations

EE	Ecological Economics
ENT	Ecological Niche Theory
GICS	Global Industry Classification Standard
LVGT	Lotka–Volterra generalized theory
NYSE	New York Stock Exchange
PME	Pairwise Maximum-Entropy

Appendix A. Other Metrics of Evenness

In addition to Shannon evenness there are other metrics to assess the equitability or evenness in a community. A couple of popular metrics are based on the Simpson index, which is given by:

$$\lambda \equiv \sum_{i=1}^{N} {x_i}^2, \tag{A1}$$

where N is the number of companies and x_i is the market share of company i, i.e.,

$$x_i = \frac{v_i}{V}. \tag{A2}$$

The first one is the inverse Simpson index, given by:

$$IS \equiv 1/\lambda. \tag{A3}$$

The second one is the *Gini–Simpson index*, given by:

$$GS \equiv 1 - \lambda. \tag{A4}$$

It turns out that both the above indices provide qualitatively identical curves to the Shannon evenness, as it can be seen in Figure A1 which shows the curves of $E(t)$ and $GS(t)$.

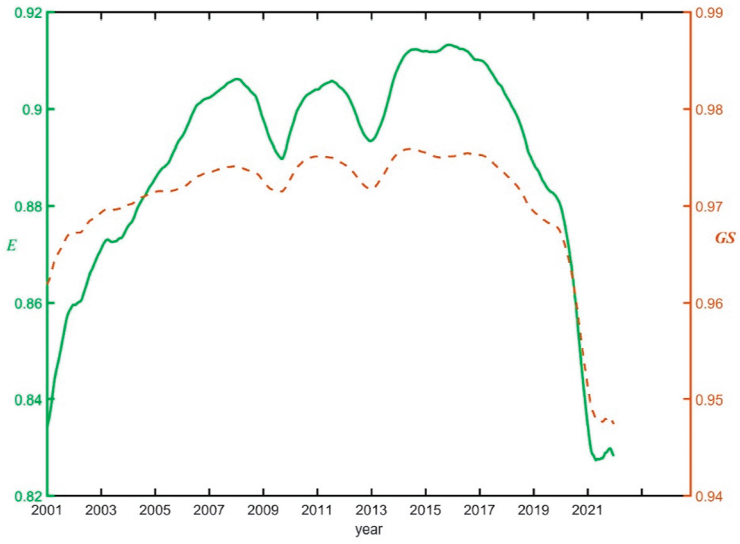

Figure A1. $E(t)$ (green, left axis) and $GS(t)$ (orange, right axis) for the set of the largest 78 companies. The curves were obtained by taking 252 days (i.e., 1 year) moving averages.

Appendix B. The Evenness of a Randomly Distributed Shares

Suppose that using a uniform distribution in the [0, 1] interval, we draw a set of S fractions y_i, which we assume that are proportional to the market values, v_i, of S firms. Therefore, the mean values $\overline{y}_i$ will be uniformly distributed in the [0, 1] interval:

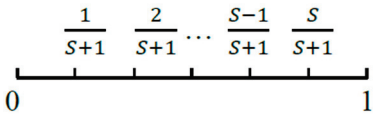

i.e.,

$$y_i = \frac{i}{S+1}, \text{ with } i = 1, 2, \cdots, S. \tag{A5}$$

To transform the fractions y_i into shares x_i we have to normalize them, i.e.,

$$x_i = \frac{\overline{y}_i}{\sum_{j=1}^{S} \overline{y}_j} = \frac{\overline{y}_i}{\frac{S}{2}(S+1)\frac{1}{S+1}} = \frac{2}{S}\overline{y}_i. \tag{A6}$$

Using Equation (4) we can write the evenness in terms of the fractions y_i as:

$$E = \frac{-\sum_{i=1}^{S} x_i \ln\left(\frac{2}{S} y_i\right)}{\ln S} = -\frac{2}{S}\frac{\sum_{i=1}^{S} y_i \ln y_i + \ln\left(\frac{2}{S}\right)}{\ln S}. \tag{A7}$$

Substituting Equation (A5) into (A7) we obtain:

$$E = \frac{2}{S(S+1)\ln S}\sum_{i=1}^{S}\left[i \ln \frac{S+1}{i}\right] + \frac{\ln \frac{S}{2}}{\ln S}. \tag{A8}$$

For example, Equation (A8) produces for S = 2 species, E = 0.9813, whereas for S = 78 companies, by performing the sum from 1 to 78, we obtain 0.11619 and then adding up ln19/ln38 (=0.84090), we finally obtain E = 0.95709.

The sum in the expression (A8) can be approximated as the integral (the larger S the larger the accuracy of this approximation):

$$\sum_{i=1}^{S}\left[i \ln \frac{S+1}{i}\right] \approx (S+1)^2 \int_0^1 y \ln y dy = \frac{(S+1)^2}{4}. \tag{A9}$$

Hence, substituting Equation (A9) into (A8), we obtain the following approximate expression of the evenness as a function of S:

$$E \approx \frac{S+1}{2S \ln S} + \frac{\ln \frac{S}{2}}{\ln S}. \tag{A10}$$

For S = 78, the evenness thus becomes $E \approx 0.11623 + 0.84090 = 0.95713$, which differs in 0.004% of the value we obtained performing the sum.

Appendix C. The Total Market Value as a Function of δ

The system of Equation (1) with an interaction matrix given by Equation (6) will converge towards an equilibrium total market value, $V^*(\delta)$. It is helpful to consider for a moment the effect of "switching off" the interspecific interactions, which corresponds to the trivial community of non-interacting species, so that as δ = 0, the interaction matrix α_{ij} given by Equation (6) reduces to the identity matrix. In this case, the Lotka–Volterra equations reduce to a set of uncoupled logistic equations:

$$v_i(t+1) - v_i(t) = r_i v_i(t)(1 - v_i(t)),\ i = 1, 2, \cdots, S. \tag{A11}$$

The solution of Equation (A11) converges for asymptotically large times towards the equilibrium v_i* = 1 for all species i. Then, by Equations (A11), (2) and (4), the corresponding total market value and evenness become V_0* = $\sum_{j=1}^{78} v_{0j}* = 78$ and E_0* = 1 (the sub index 0 are used to emphasize that these results hold for the trivial case $\delta = 0$).

If we now "switch on" the interspecific interactions, i.e., $\delta > 0$, from Equation (1), we have for the equilibrium in which the S companies coexist:

$$\sum_{j=1}^{S} \alpha_{ij} v_j* = -1,\ i = 1, 2, \cdots, S, \tag{A12}$$

Inverting Equation (A12), we can write the equilibrium total market value, to which the system eventually converges in terms of the inverse of the interaction matrix, ${\alpha^{-1}}_{ij}$, as:

$$V* = \sum_{i=1}^{S} v_i* = -\sum_{i}^{S}\sum_{j}^{S} {\alpha^{-1}}_{ij},\ i, j = 1, 2, \cdots, S. \tag{A13}$$

A general analytical expression of V* in terms of the coefficients $\alpha_{I\,ij}$ is very cumbersome and thus not very useful. In addition, we still have to perform the integrations in those $\alpha_{i\,ij}$ between $-\delta$ and δ to obtain the expected total market value at equilibrium for a given δ, V*(δ). However, for a given value of δ, such multiple integral of Equation (A13) can be computed numerically. To illustrate this calculation, let us consider the case of an ensemble for a community of just two companies. Hence, v_1* and v_2* can be written as [37]:

$$v_1* = \frac{1 + \alpha_{12}}{1 - \alpha_{12}.\alpha_{21}},\ v_2* = \frac{1 + \alpha_{21}}{1 - \alpha_{12}.\alpha_{21}} \tag{A14}$$

Therefore, Equation (A13) reduces to:

$$V*(\delta) = \int_{-\delta}^{+\delta}\int_{-\delta}^{+\delta} d\alpha_{12} d\alpha_{21} (v_1* + v_2*) = \int_{-\delta}^{+\delta}\int_{-\delta}^{+\delta} d\alpha_{12} d\alpha_{21} \frac{2 + \alpha_{12} + \alpha_{21}}{1 - \alpha_{12}.\alpha_{21}}. \tag{A15}$$

Performing the above double integral numerically, we obtain the total market value curve, V*(δ), at equilibrium towards this system, which is depicted in Figure A2. Notice that it is a monotonic function of δ. This implies that, even though positive and negative interactions are equally likely, the effect of positive interactions is not entirely erased by negative interactions.

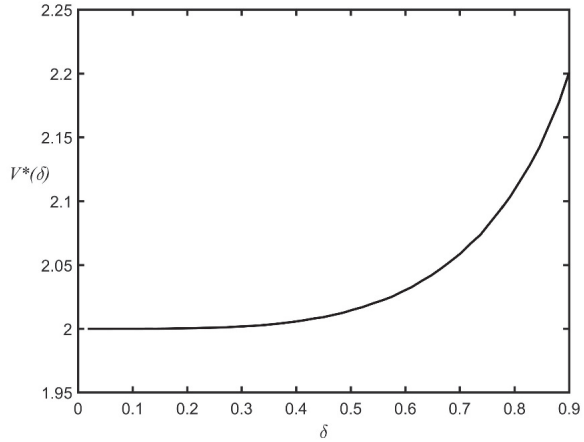

Figure A2. Total expected market value V* towards a community of two species or a market of two companies converges at equilibrium as a function of the intensity of interspecific interactions, δ.

The calculation shown above for two species can be generalized to any arbitrary $S > 2$ number of interacting companies.

The results of simulations of 78 species/companies governed by Equation (1), with random interaction matrices, given by Equation (6), and starting from the initial conditions given by Equation (7), are shown in Figure A3 for different values of δ, varying the simulation time cutoff, T, from 2 to 20. In panel (A), one can see that for $\delta = 0.1$, independently of the cutoff time T, only slight deviations in V and E from their initial values, $V(1) = 39$ and $E(1) = 0.957$, occur. As δ increases, the initial configuration moves further away from the equilibrium state. The community then moves towards higher values of V and lower values of E when increasing T, as shown in panel (A) for $\delta = 0.3$ and 0.5. Above $\delta = 0.5$, the tendency towards the upper left corner in the plane E-V becomes monotonic, as shown in panel (B) of Figure A3.

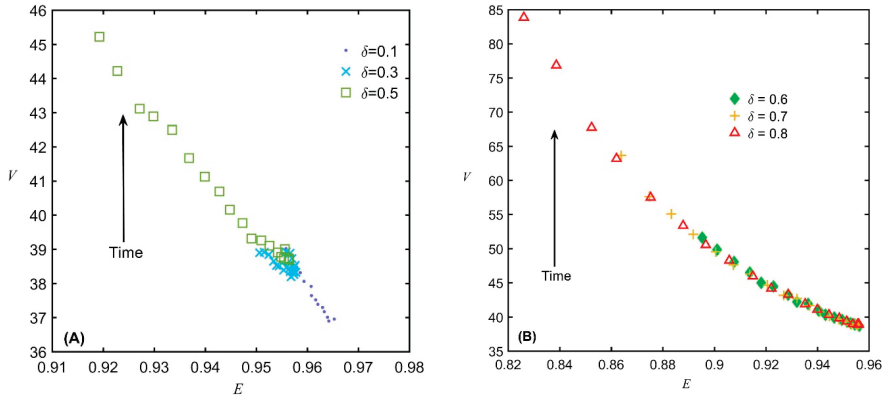

Figure A3. Curves of $V(T)$ vs. $E(T)$ for synthetic communities with different values of δ (see text). The simulation time runs upward as indicated by the black arrow; each symbol corresponds to a point $V(T)$, $E(T)$ with a cutoff simulation time $T = 2, 3, \ldots, 20$; the higher the symbol, the larger the simulation cutoff time T. (**A**): $\delta = 0.1$, 0.3 and 0.5. (**B**): $\delta = 0.6$, 0.7 and 0.8.

Appendix D. Effective U.S. FED Rates Compared with the Total Market Value and Evenness

In Figure A4, the curve of the U.S. Federal Reserve effective interest rate along 2000–2021 [59] is compared with E and V (in trillion USD) in panels (A) and (B), respectively.

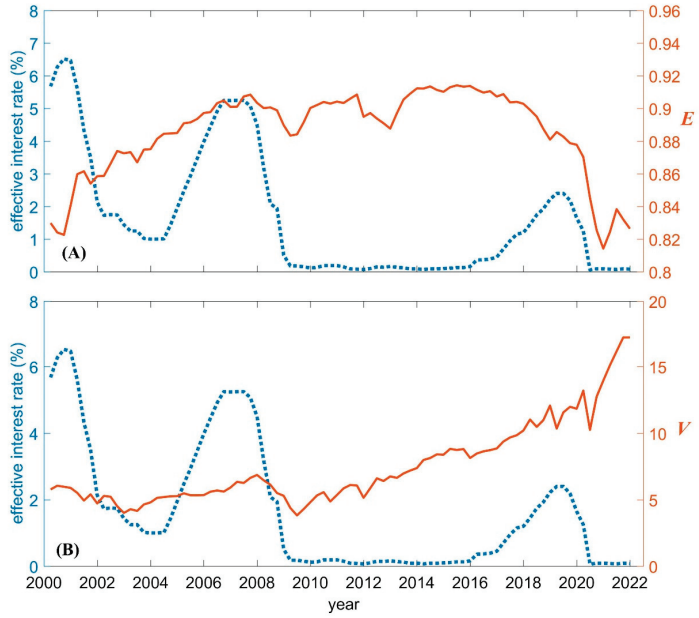

Figure A4. (**A**): Variation in the effective interest rate [59] and the total market value V. (**B**): Variation in the effective interest rate [59] and E.

For the evenness, no clear pattern emerges. As shown in panel (A), at the beginning of the period, E soared with high interest rates, but from 2009 to 2015, the effective interest remained virtually zero [59] and E remained high. On the other hand, high productivity occurred entirely during the period of very low to moderate interest rates. Conversely, the first business cycle 2001–2008 was characterized in general by high interest rates and low productivity (panel (B)).

References

1. Simon, H.A. A Behavioral Model of Rational Choice. *Q. J. Econ.* **1955**, *69*, 99–118. [CrossRef]
2. Shiller, R.J. *Market Volatility*; MIT Press: Cambridge, MA, USA, 1997.
3. Alderson, W. *Marketing Behavior and Executive Action: A Functionalist Approach to Marketing Theory*; Homewood: Irwin, IL, USA, 1957.
4. Alderson, W. *Dynamic Marketing Behavior: A Functionalist Theory of Marketing*; Homewood: Irwin, IL, USA, 1965.
5. Potters, M.; Cont, R.; Bouchaud, J.P. Financial Markets as Adaptive Ecosystems. *Europhys. Lett.* **2004**, *41*, 239. [CrossRef]
6. Manahov, V.; Hudson, R. A note on the relationship between market efficiency and adaptability. New evidence from artificial stock markets. *Expert Syst. Appl. Int. J.* **2014**, *41*, 7436–7454. [CrossRef]
7. Fort, H. *Forecasting with Maximum Entropy: The Interface between Physics, Biology, Economics and Information Theory*; Institute of Physics Publishing: Bristol, UK, 2022.
8. Moore, J.F. Predators and Prey: A new ecology of competition. *Harv. Bus. Rev.* **1993**, *71*, 75–86.
9. Morin, P. *Community Ecology*; Wiley-Blackwell: Chichester, UK, 2011.
10. Moore, J.F. *The Death of Competition: Leadership and Strategy in the Age of Business Ecosystems*; Harper Paperbacks: New York, NY, USA, 1993.
11. Farmer, D.J.; Lo, A.W. Frontiers of finance: Evolution and efficient markets. *Proc. Natl. Acad. Sci. USA* **1999**, *96*, 9991–9992. [CrossRef]
12. Krebs, C.J. *Ecology: The Experimental Analysis of Distribution and Abundance*, 2nd ed.; Harper & Row: New York, NY, USA, 1978.
13. Grime, J.P.; Pierce, S. *The Evolutionary Strategies That Shape Ecosystems*; Wiley: Chichester, UK, 2012.
14. Mittelbach, G.G.; Steiner, C.F.; Scheiner, S.M.; Gross, K.L.; Reynolds, H.L.; Waide, R.B.; Willig, M.R.; Dodson, S.I.; Gough, L. What is the observed relationship between species richness and productivity? *Ecology* **2001**, *82*, 2381–2396. [CrossRef]
15. Cardinale, B.J.; Hillebrand, H.; Harpole, W.S.; Gross, K.L.; Ptacnick, R. Separating the influence of resource 'availability' from resource 'imbalance' on productivity–diversity relationships. *Ecol. Lett.* **2009**, *12*, 475–487. [CrossRef]
16. Allaby, M. (Ed.) *A Dictionary of Ecology*, 3rd ed.; Oxford University Press: Oxford, UK, 2006.
17. Vandermeer, J.H. *The Ecology of Intercropping*; Cambridge University Press: Cambridge, UK, 1989.
18. Hayes, A. What Is Crop Yield? Investopedia. Available online: https://www.investopedia.com/terms/c/crop-yield.asp (accessed on 14 November 2022).
19. Magurran, A.E. *Measuring Biological Diversity*; Blackwell Science: Malden, MA, USA, 2004.
20. Chiarucci, A.; Bacaro, G.; Scheiner, S.M. Old and new challenges in using species diversity for assessing biodiversity. *Philos. Trans. R. Soc. B Biol. Sci.* **2011**, *366*, 2426–2437. [CrossRef]
21. Costanza, R. What is ecological economics? *Ecol. Econ.* **1989**, *1*, 1–7. [CrossRef]
22. Potts, J.; Foster, J.; Straton, A. An entrepreneurial model of economic and environmental co-evolution. *Ecol. Econ.* **2010**, *70*, 375–383. [CrossRef]
23. Farmer, D.J. Market Force, Ecology and Evolution. *Ind. Corp. Chang.* **2002**, *11*, 895–953. [CrossRef]
24. Moore, J.F. Business Ecosystems and the View from the Firm. *Antitrust Bull.* **2006**, *51*, 31–75. [CrossRef]
25. Hileman, J.; Kallstenius, I.; Häyhä, T.; Palm, C.; Cornell, S. Keystone actors do not act alone: A business ecosystem perspective on sustainability in the global clothing industry. *PLoS ONE* **2020**, *15*, e0241453. [CrossRef]
26. Pielou, E. *An Introduction to Mathematical Ecology*; Wiley: New York, NY, USA, 1969.
27. Van Dyke, F. *Conservation Biology: Foundations, Concepts, Applications*, 2nd ed.; Springer: New York, NY, USA, 2008.
28. Maignan, C.; Ottaviano, G.; Pinelli, D.; Rullani, F. Bio-Ecological Diversity vs. Socio-Economic Diversity: A Comparison of Existing Measures Nota di Lavoro. 2003. Available online: http://www.feem.it/web/activ/_wp.html (accessed on 15 March 2023).
29. Baumgärtner, S. Measuring the Diversity of What? And for What Purpose? A Conceptual Comparison of Ecological and Economic Biodiversity Indices. 2006. Available online: https://ssrn.com/abstract=894782 (accessed on 15 March 2023).
30. Boyte-White, C. Market Capitalization Versus Market Value: What's the Difference? Investopedia. Available online: https://www.investopedia.com/ask/answers/122314/what-difference-between-market-capitalization-and-market-value.asp (accessed on 9 November 2022).
31. Huston, M. A general hypothesis of species diversity. *Am. Nat.* **1979**, *113*, 81–101. [CrossRef]
32. Huston, M.A.; Aarssen, L.W.; Austin, M.P.; Cade, B.S.; Fridley, J.D.; Garnier, E.; Grime, J.P.; Hodgson, J.; Lauenroth, W.K.; Wardle, D.A. No consistent effect of plant diversity on productivity. *Science* **2000**, *289*, 1255. [CrossRef]
33. Schmid, B. The species richness-productivity controversy. *Trends Ecol. Evol.* **2002**, *17*, 113–114. [CrossRef]
34. Lotka, A.J. *Elements of Physical Biology*; Williams & Wilkins: New York, NY, USA, 1925.
35. Volterra, V. Fluctuations in the abundance of a species considered mathematically. *Nature* **1926**, *118*, 558–560. [CrossRef]
36. Hofbauer, M.; Sigmund, K. *Evolutionary Games and Population Dynamics*; Cambridge University Press: Cambridge, UK, 1998.

37. Fort, H. *Ecological Modelling and Ecophysics: Agricultural and Environmental Applications*; Institute of Physics Publishing: Bristol, UK, 2020.
38. May, R.M. Will a large complex system be stable? *Nature* **1972**, *238*, 413–414. [CrossRef]
39. Chesson, P. Mechanisms of maintenance of species diversity. *Ann. Rev. Ecol. Evol. Syst.* **2000**, *31*, 343–366. [CrossRef]
40. Fortune Magazine. Available online: https://fortune.com/rankings/ (accessed on 9 November 2022).
41. Core US Fundamentals Dataset. Available online: http://www.quandl.com/databases/SF1 (accessed on 15 March 2023).
42. Wakil, G. Firm size proxies and the value relevance of predictive stock return models. *J. Econ. Financ.* **2020**, *44*, 434–457. [CrossRef]
43. Hamilton, J. Dates of U.S. Recessions as Inferred by GDP-Based Recession Indicator JHDUSRGDPBR, Retrieved from FRED, Federal Reserve Bank of St. Louis. Available online: https://fred.stlouisfed.org/series/JHDUSRGDPBR (accessed on 12 October 2022).
44. Money Morning. The Dot-Com Crash of 2000–2002. Available online: https://moneymorning.com/2015/06/12/the-dot-com-crash-of-2000-2002/ (accessed on 23 November 2022).
45. NYT 2007. Bear Stearns Reports First Ever Quarterly Loss. Available online: https://archive.nytimes.com/dealbook.nytimes.com/2007/12/20/bear-reports-steep-but-expected-4th-quarter-loss/?_r=0 (accessed on 10 February 2023).
46. NYSE 2022. Available online: https://www.nyse.com/market-cap (accessed on 10 July 2022).
47. Kenton, W. What Is Trumponomics. Investopedia. Available online: https://www.investopedia.com.cach3.com/terms/t/trumponomics.asp.html (accessed on 14 November 2022).
48. Mulder, C.P.; Bazeley-White, E.; Dimitrakopoulos, P.G.; Hector, A.; Scherer-Lorenzen, M.; Schmid, B. Species Evenness and Productivity in Experimental Plant Communities. *Oikos* **2004**, *107*, 50–63. [CrossRef]
49. Halty, V.; Valdés, M.; Tejera, M.; Picasso, V.; Fort, H. Modelling plant interspecific interactions from experiments of perennial crop mixtures to predict optimal combinations. *Ecol. Appl.* **2017**, *27*, 2277–2289. [CrossRef]
50. Vandermeer, J.H. The competitive structure of communities: An experimental approach with protozoa. *Ecology* **1969**, *50*, 362–371. [CrossRef]
51. Huisman, J.; Jonker, R.R.; Zonneveld, C.; Weissing, F.J. Competition for light between phytoplankton species: Experimental tests of mechanistic theory. *Ecology* **1999**, *80*, 211–222. [CrossRef]
52. Connel, J.H. Apparent vs. "rea" competition in plants. In *Perspectives on Plant Competition*; Grace, J.B., Tilman, D., Eds.; Academic Press: New York, NY, USA, 1990; pp. 9–26.
53. Miller, T.E. Direct and indirect species interactions in an early old-field plant community. *Am. Nat.* **1994**, *143*, 1007–1025. [CrossRef]
54. Adler, F.R.; Morris, W.F. A general test for interaction modification. *Ecology* **1994**, *75*, 1552–1559. [CrossRef]
55. Fort, H. On predicting species yields in multispecies communities: Quantifying the accuracy of the linear Lotka-Volterra generalized model. *Ecol. Model.* **2018**, *387*, 154–162. [CrossRef]
56. Callaway, R.M.; Walker, L.R. Competition and facilitation: A synthetic approach to interactions in plant communities. *Ecology* **1997**, *78*, 1958–1965. [CrossRef]
57. Silknetter, S.; Creed, R.P.; Brown, B.L.; Frimpong, E.A.; Skelton, J.; Peoples, B.K. Positive biotic interactions in freshwaters: A review and research directive. *Freshw. Biol.* **2020**, *65*, 811–832. [CrossRef]
58. Yodzis, P. The stability of real ecosystems. *Nature* **1981**, *289*, 674–676. [CrossRef]
59. Federal Funds Effective Rate. Retrieved from FRED, Federal Reserve Bank of St. Louis. Available online: https://fred.stlouisfed.org/series/ (accessed on 2 December 2022).
60. Gamfeldt, L.; Hillebrand, H. Effects of Total Resources, Resource Ratios, and Species Richness on Algal Productivity and Evenness at Both Metacommunity and Local Scales. *PLoS ONE* **2011**, *6*, e21972. [CrossRef] [PubMed]
61. Chase, J.M.; Leibold, M.A. *Ecological Niches*; University of Chicago Press: Chicago, IL, USA, 2003.
62. Fort, H. Community diversity and total abundance: Quantitative predictions from competition niche theory. *Ecol. Complex.* **2015**, *21*, 120–127. [CrossRef]
63. Fort, H. Combining niche and game theories to address interspecific cooperation in ecological communities. *Community Ecol.* **2020**, *21*, 13–24. [CrossRef]
64. Roudi, Y.; Nirenberg, S.; Latham, P.E. Pairwise Maximum Entropy Models for Studying Large Biological Systems: When They Can Work and When They Can't. *PLoS Comput. Biol.* **2009**, *5*, e1000380. [CrossRef] [PubMed]
65. Jaynes, E.T. Information theory and statistical mechanics I. *Phys. Rev.* **1957**, *106*, 620–630. [CrossRef]
66. Jaynes, E.T. Information theory and statistical mechanics II. *Phys. Rev.* **1957**, *108*, 171–190. [CrossRef]
67. Vinod, H.D. Ranking mutual funds using unconventional utility theory and stochastic dominance. *J. Empir. Financ.* **2004**, *11*, 353–377. [CrossRef]
68. Rompolis, L. Retrieving risk neutral densities from European option prices based on the principle of maximum entropy. *J. Empir. Financ.* **2010**, *17*, 918–937. [CrossRef]
69. Balasubramanyan, L.; Stefanou, S.E.; Stokes, J.R. An entropy approach to size and variance heterogeneity in U.S. commercial banks. *J. Econ. Financ.* **2012**, *36*, 728–749. [CrossRef]
70. Bialek, W.; Cavagna, A.; Giardina, I.; Mora, T.; Silvestri, E.; Viale, M.; Walczak, A.M. Statistical mechanics for natural flocks of birds. *Proc. Natl. Acad. Sci. USA* **2012**, *109*, 4786–4791. [CrossRef]
71. Volkov, I.; Banavar, J.R.; Hubbell, S.P.; Maritan, A. Inferring species interactions in tropical forests. *Proc. Natl. Acad. Sci. USA* **2009**, *106*, 13854–13859. [CrossRef]

72. Fort, H.; Grigera, T. A method for predicting species trajectories tested with trees in Barro Colorado tropical forest. *Ecol. Model.* **2021**, *446*, 109504. [CrossRef]
73. Fort, H.; Grigera, T. A new early warning indicator of tree species crashes from effective intraspecific interactions in tropical forests. *Ecol. Indic.* **2021**, *125*, 107506. [CrossRef]
74. Emary, C.; Fort, H. Markets as ecological networks: Inferring interactions and identifying communities. *J. Complex Netw.* **2021**, *9*, cnab022. [CrossRef]
75. The Global Industry Classification Standard (GICS). Available online: https://www.msci.com/our-solutions/indexes/gics (accessed on 25 May 2023).
76. Adomavicius, G.; Bockstedt, J.C.; Gupta, A.; Kauffman, R.J. Technology roles and paths of influence in an ecosystem model of technology evolution. *Inf. Technol. Manag.* **2007**, *8*, 185–202. [CrossRef]
77. Drożdż, S.; Grümmer, F.; Górski, A.Z.; Ruf, F.; Speth, J. Dynamics of competition between collectivity and noise in the stock market. *Phys. A* **2000**, *287*, 440–449. [CrossRef]
78. Triplett, R.; Ozdemir, N.; Mason, P. Structural Change in the Investment Function. *J. Econ. Financ.* **2022**, *46*, 220–236. [CrossRef]
79. Fort, H. A quantitative assessment of the evolutionary dynamics of firms: Estimating the fitnesses from time series of their market caps and forecasting their shares. *J. Evol. Econ.* 2023; *submitted*.
80. Fort, H. Disentangling the effects of selection and the environment in the evolutionary dynamics of financial markets in terms of Malthusian fitness. Work in progress, to be published elsewhere.

entropy

MDPI

Article

Looking into the Market Behaviors through the Lens of Correlations and Eigenvalues: An Investigation on the Chinese and US Markets Using RMT

Yong Tang [1,2,*], Jason Xiong [3], Zhitao Cheng [4], Yan Zhuang [1], Kunqi Li [5], Jingcong Xie [6] and Yicheng Zhang [2]

1 School of Computer Science and Engineering, University of Electronic Science and Technology of China, Chengdu 610054, China; tukouacademic@gmail.com
2 Department of Physics, University of Fribourg, Chemin du Musée 3, 1700 Fribourg, Switzerland; yi-cheng.zhang@unifr.ch
3 Walker College of Business, Appalachian State University, Boone, NC 28608, USA; xiongjj@appstate.edu
4 School of Mathematical Sciences, University of Electronic Science and Technology of China, Chengdu 610054, China; 2020110801009@std.uestc.edu.cn
5 Department of Electrical and Computer Engineering, State University of New York at Stony Brook, Stony Brook, NY 11794, USA; kunqi.li@stonybrook.edu
6 Terry College of Business, University of Georgia, Athens, GA 30602, USA; jx32164@uga.edu
* Correspondence: tangyong@uestc.edu.cn

Abstract: This research systematically analyzes the behaviors of correlations among stock prices and the eigenvalues for correlation matrices by utilizing random matrix theory (RMT) for Chinese and US stock markets. Results suggest that most eigenvalues of both markets fall within the predicted distribution intervals by RMT, whereas some larger eigenvalues fall beyond the noises and carry market information. The largest eigenvalue represents the market and is a good indicator for averaged correlations. Further, the average largest eigenvalue shows similar movement with the index for both markets. The analysis demonstrates the fraction of eigenvalues falling beyond the predicted interval, pinpointing major market switching points. It has identified that the average of eigenvector components corresponds to the largest eigenvalue switch with the market itself. The investigation on the second largest eigenvalue and its eigenvector suggests that the Chinese market is dominated by four industries whereas the US market contains three leading industries. The study later investigates how it changes before and after a market crash, revealing that the two markets behave differently, and a major market structure change is observed in the Chinese market but not in the US market. The results shed new light on mining hidden information from stock market data.

Keywords: financial big data; stock market modeling; random matrix theory; eigenvalue analysis

Citation: Tang, Y.; Xiong, J.; Cheng, Z.; Zhuang, Y.; Li, K.; Xie, J.; Zhang, Y.-C. Looking into the Market Behaviors through the Lens of Correlations and Eigenvalues: An Investigation on the Chinese and US Markets Using RMT. *Entropy* **2023**, *25*, 1460. https://doi.org/10.3390/e25101460

Academic Editor: José Roberto Iglesias

Received: 10 July 2023
Revised: 8 October 2023
Accepted: 11 October 2023
Published: 18 October 2023

1. Introduction

Thanks to the availability of financial data in a wide range of frequencies from tick to daily, it is possible to apply data mining and knowledge discovery methods beyond traditional finance but from data science, network analysis, and even physics, etc. The asset prices in the markets result from complicated dynamics of spreading and reacting to market signals and information. The market structures are embedded in the price movements, which are normally correlated with each other. As a starting point for the underlying cornerstones of finance theories like modern portfolio theory (MPT) [1] and capital asset pricing model [2], the correlation information of assets prices is always at heart for theoretical studies and finance industrial practices in portfolio management and risk management, etc.

For a portfolio of N stocks, we need a correlation matrix with $N \times N$ elements to describe the pairwise relationships. With the increase of N, the number of possible relationships snowballs, making it difficult and challenging to calculate or analyze. To extract

the hidden structure and essential information, it is necessary to simplify the network by filtering the less important elements to make it feasible to analyze portfolios even with a very large N. In the past few years, we see some methods have been introduced to simplify the stock matrices. To study the correlation behaviors of the financial markets, a correlation matrix is constructed from the price time series before we apply methods and techniques such as principal component analysis [3–6], multidimensional scaling [7], factor analysis [4], minimum spanning tree [8,9], hierarchical clustering [8,10,11], and singular value decomposition [12].

Simplification of the correlation matrix requires validation, which statistically validates the matrix and keeps those validated elements to achieve a simple matrix with fewer noises and ease of analysis. The validations provide statistical confidence in the results or insights extracted from the validated matrices. The underlying idea of design validation is to compare the empirical matrices with random ones generated from the same distributions, random shuffles, or statistical tests with which the null hypothesis is set up to be tested with empirical data. Any deviations from these *benchmarks* are considered noises and should be filtered. Similarly, given an empirical correlations matrix (and the derived distance matrices for the networks), we can consider a random matrix with the same size. A null hypothesis can be introduced to test the statistical validation of each element of the original empirical matrix by comparing the distributions. The basic idea is that any deviations from the random distribution are believed as validated with genuine information from the system. In contrast, those falling within the random distribution are pure random noises that contain no system information.

Specifically, in this study, based on a dataset covering nine years of stock prices, we systematically investigate the stock markets of China and the US using random matrix theory (RMT) to study and compare the correlation properties and the dynamics of eigenvalues and eigenvectors. The findings revealed that the two stock markets are both similar and different in many ways. The results add new insights into market behaviors with implications for finance applications such as portfolio management and optimization, market risk monitoring, and trading strategy design. Meanwhile, this study also serves as a framework for data mining and knowledge in financial big data using RMT.

This work is organized as follows. First, we review the literature in Section 2. The methodology is introduced in Section 3. In Section 4 we describe the dataset of two markets and the properties of correlation matrices. Using RMT, in Section 5, the properties and behaviors of eigenvalues and eigenvectors are analyzed with an investigation of a market switch study. Finally, Section 6 presents conclusions, discussions, and limitations.

2. Literature Review

In this section, we introduce literature from three aspects. First, RMT and its applications are introduced in Section 2.1, representative studies of applying RMT in analyzing financial markets are described in Section 2.2, as well as recent studies focusing on comparing different stock markets, especially the US and Chinese markets are discussed in Section 2.3.

2.1. RMT and Its Applications

Originating in mathematical physics, RMT was first introduced by physicists to study nuclear activities back in the 1950s [13]. Eugene Wigner used RMT to model the excited states of nuclei in reactions which was hard to obtain by using traditional methods. Instead, he proposed to analyze the eigenvalues and their spacing of a random matrix [14]. The basic idea is to analyze the statistical properties of eigenvalues of the random counterpart whereas it is practically impossible to analyze the individual eigenvalues of the original complex system. RMT provides a powerful toolbox to reveal properties of matrices whose elements are sampled from randomness, usually based on certain probability distributions. Soon, RMT was proved an efficient tool for many challenges in physics and beyond. Before long, RMT attracted significant interest from scholars in various fields with wide-spreading

applications like physics, mathematics, biology, engineering, computer science, and social science. After decades of development, RMT has become an important research field with rich theoretical implications and real applications in a variety of disciplines, such as spectrum analysis and filter in information processing, signal detection and channel estimation in wireless communication, data analysis in high dimensional space, and optimization in machine learning. Interested readers should refer to works by Potters and Tao for details on theories and applications of RMT [15,16].

2.2. Applying RMT Approaches in Financial Markets

In finance, RMT was first introduced into the study of financial markets by [17], and more recently, there are significant advances in applying RMT in finance studies and applications [18–20]. In one study, RMT is applied to analyze stock market behaviors [21]. In another study, the world stock market is analyzed with RMT [22]. Recent works also investigated various financial markets using RMT [23–25].

2.2.1. RMT in Financial Correlation Analysis

Rooted in the correlation analysis, RMT offers a new look into the structures and behaviors of the financial markets. Applying RMT to financial markets is closely related to the analysis of correlation matrices and network structures [26–30]. The market is full of noises, and the useful information in correlation matrices built from price data might be covered by the noises and make correlation analysis less meaningful [31]. To quantify the validations of correlations, recently, there are many works applying RMT into the studies of the correlation matrices of financial markets [17,31–37]. Recently, there is an emergence of research using RMT in financial markets to filter noises and reveal embedded market properties. The cross-correlations of stock prices are studied using RMT to identify correlated relationships [38]. Furthermore, free random variables are applied in RMT analysis in financial time series [39]. RMT has also been applied to return estimation and asset allocation in Markowitz mean-variance optimization [40].

2.2.2. RMT in Eigenvalue Analysis

RMT provides a powerful tool for eigenvalue analysis in financial markets. Using time-shifted series, the lagged correlation matrices are studied from the RMT approach to compute eigenvalue density and identify deviations [41]. It has been verified that the largest eigenvalue λ_{max} is a good estimator of the average correlation of the correlation matrices constructed from a sliding window approach [42]. The same results are also reported, revealing that the average correlation co-moves with the largest eigenvalue for the component stocks of S&P500 [36]. For normalized eigenvectors, the value of S_{ij} ranges from 0 to 1. In other words, the two eigenvectors change from orthogonal to exactly the same. One study reports that the effect of noises on the risk becomes insignificant in measure of the fixed portfolio while remaining important for an optimized portfolio for small values of N/L [31]. This indicates that the correlation matrix can still be valid in traditional risk management and portfolio optimization; noises cover even most information. Using simulation methods, many correlation matrix filtering approaches are tested, and the approaches based on random matrix theory are found to perform consistently well in all cases [43]. The eigenvalue distribution of the emerging stock market is different from developed markets though correlation distributions and other properties are similar. Methods based on clustering for portfolio optimization and effective size determination are proposed. The results are found to be improved compared to RMT approaches [37], which indicates that RMT might be further combined with other methods in filtering matrix and optimizing a portfolio [27].

It was found that the average of correlations in the correlation matrix can be well estimated from the largest eigenvalue as

$$\lambda_{max}/N \sim \langle C_{ij} \rangle. \quad (1)$$

Following the RMT approach, the largest eigenvalues are found to be responsible for the market mode. By removing this, the correlation matrix is cleaned to reveal the topological structures [28]. The details of the residual noise part for a market are studied, revealing that the noise band is composed of more sub-bands [11]. Using RMT, the Chinese stock market is studied [18], a similar anti-correlation relationship between sub-sectors is studied [44], and the results show that the prominent sector structure exists. The distribution of eigenvalues also reveals that the market is likely to be influenced by the Chinese government's global financial crisis and policies. In a further study on the sub-sectors of a stock market, local interaction structures are found to change during financial crises [19]. The sign information of components in eigenvectors is again used to detect the sub-sector anti-correlations [45]. Focusing on how the credit market and stock market behave before and after a financial crisis, RMT is applied and finds that the largest eigenvalue of the credit market precedes that of the stock market [46]; this indicates that the pattern changes of eigenvalues have potential implications in the understanding of interrelationships between different markets. Market contagion is also investigated from financial network analysis and, naturally, RMT. Market contagion is an important indicator of market stability. By looking into the structural changes in networks and properties revealed by RMT, one can identify and predict the market contagion and thus major market switches [47–51].

2.2.3. RMT in Eigenvalue Distributions

Since the introduction of RMT into the study of financial markets, much literature investigated different markets. An earlier study points out that the lower bound is positive and no eigenvalues fall between 0 and λ_{min} also vanish above λ_{max} [17]. Since the empirical values of N and L are limited far from ∞, the edges are blurred with some eigenvalues falling beyond the bounds [32]. The distribution of the spacings of eigenvalues $s \equiv \lambda_{i+1} - \lambda_i$ are found to agree with a Wigner distribution of the energy spacing levels [34]. This provides evidence indicating that the empirical correlation matrix is consistent with its random matrix counterpart. Many empirical studies reveal that only a small fraction of eigenvalues and their corresponding eigenvectors contain system information while most are embedded in noises [17,52–54]. It has been reported that the portion of the largest eigenvalues deviating from the theoretical prediction of the counterpart random matrix is 6% [17], 4.7% [54], 2% [34], 11% [53], and 1% [35].

Furthermore, the study of [55] adds new evidence that not all eigenvalues that fall into the theoretical interval predicted by the random matrix are purely random noise but still carry some information. Derived from the eigenvector-eigenvalue identity, a study showed that dominant eigenvalues, super eigenvalues, and maximum eigenvalues could help to analyze the spectrum of the financial correlation matrix in depth [56]. In computational results and applications in financial markets, one study reviewed the previous works, including some real-world applications, and presented promising analytical techniques from random matrix theory [26,57]. Another study proposed general, exact formulas for the overlaps between the eigenvectors of large correlated random matrices with noises [58]. Besides the intro-relationship of stock markets, another study revealed a deep relationship between news and world financial indices using tools of random matrix theory [59]. Economic policy is another field that has a significant influence on the stock market, and [60] analyzed the correlation matrix and different stock network structures to reveal the implication of the correlation matrix components. The work of [61] fused previous models, which made predictions based on the arbitrarily long time horizon and introduced an ensemble of random rectangular matrices from the observations of independent Lévy processes over a fixed-time horizon. To summarize and compose a benchmark for the study of correlated time-series signals, ref. [62] used supersymmetric theory to generate the statistics of eigenvectors of the cross-correlations of correlated time-series. Another study investigated the correlations of Chinese stocks before and during the 2008 crisis based on the random matrix analysis [63].

2.3. Comparative Studies on Different Markets

In another thread, there are abundant studies dedicated to the comparative studies on the two major stock markets, namely the Chinese and US markets [29,64–67]. Although RMT has been applied to stock markets, there is still a lack of comprehensive studies using RMT to analyze the Chinese and US markets. How the correlations and eigenvalues behavior are related to the market switches between bull and bear markets is still not sufficiently investigated. There is a thread of literature on comparing the dynamics of markets in different countries [29,30]. Considering the signs of eigenvector components, sub-sectors of positive and negative signs can be derived from sectors in anti-correlation. The sub-sectors are detected with strong appearances in the Chinese stock market but weaker in the US stock market [44]. US and British stock exchanges are studied by using RMT on the asymmetric correlation matrix with a lag of τ [3]. One work revealed the different strengths of correlations between stocks, especially the oil sector and banking stocks in the Nigerian Stock Market (NSM) and Johannesburg Stock Exchange (JSE), for the period of 2009 to 2013, using random matrix theory [68]. Comparative analyses on two different stock markets—the S&P 500 (USA) and Nikkei 225 (JPN) via the power mapping method from the random matrix theory, and found strong consistency between the states of the two stock markets as well as the feasibility to predict critical state (market crash) [69].

Particularly, some works investigated the markets of the US and China [64,66]. According to the strong connection between financial assets and institutions and the diversity as well as the localization of the stock market, one study previously analyzed the topological structure of financial networks of two major markets of China and the US with complex network theory [29]. Several studies investigated the two markets from aspects of comovement [70], impacts of trade conflicts and pandemic [65,67,71], and conditional correlations [72]. These studies revealed the different behaviors of the two major stock markets. However, there is still a lack of comprehensive studies on the Chinese and US stock markets from the perspective of RMT. In this sense, this work aims to fill this gap by systematically investigating the two markets using correlation analysis and RMT.

3. Methodology

3.1. Construction of Correlation Matrices

For an empirical correlation matrix C of size $N \times N$ generated from N returns series of length L, we can construct the elements as

$$C = \frac{1}{L} M M^T, \tag{2}$$

where M is a $N \times L$ matrix with normalized return $y_i(t)$ for each stock at every time t, where

$$y_i(t) = \frac{Y_i(t) - \langle Y_i(t) \rangle}{\sigma_i}, \tag{3}$$

where $Y_i(t)$ stands for the return at time t.

The study of [73] provides a study of the eigenvalues spectrum for the Chinese stock market with a sliding window approach. The inverse participation ratio is defined as

$$I^k = \sum_{l=1}^{N} \left[u_l^k \right]^4, \tag{4}$$

where u_l^k is the components of eigenvector v^k, to measure the deviation degree of eigenvectors [53]. A criterion of fractional Gaussian noise (fGn) is used to evaluate the autocorrelation matrix of stocks showing agreement with fGn, though the stock returns are non-Gaussian [20].

3.2. Eigenvalue Analysis Using RMT

RMT is a powerful tool in the analysis of eigenvalues of noisy data in various fields [15,16,74,75]. According to RMT [15,16], the eigenvalue distribution of a pure random matrix C_{random} with the same size of C follows

$$p(\lambda)_{random} = \frac{Q}{2\pi}\frac{\sqrt{(\lambda_{max}-\lambda)(\lambda-\lambda_{min})}}{\lambda}, \tag{5}$$

where λ_{min} and λ_{max} are the theoretical minimum and maximum eigenvalue bounds of random matrix, the Q is the ratio of L/N satisfying the requirement that $Q > 1$, $L \to \infty$, and $N \to \infty$ [17]. Using the empirical data, we can also get the empirical distribution as

$$p(\lambda)_{random} = \frac{1}{N}\frac{dn(\lambda)}{d\lambda}. \tag{6}$$

Theoretically, with the knowledge of Q, we can determine the theoretical eigenvalue bounds as

$$\lambda_{min,max} = 1 + \frac{1}{Q} \mp 2\sqrt{\frac{1}{Q}}. \tag{7}$$

With these calculations, we can construct and determine the theoretical distribution of a null hypothesis random matrix. The empirical eigenvalues that fall within the interval of $[\lambda_{min}, \lambda_{max}]$ are pure random noises, and those that fall beyond the interval are the validated eigenvalues carrying true information of the system. In this way, we also get the validated corresponding eigenvectors for those validated eigenvalues. Also, we can go further to investigate the statistical validation of the eigenvectors. The distribution of the eigenvector components in v_i for eigenvalue λ_i follows the Porter-Thomas distribution [17] as

$$P(v_i) = \frac{1}{\sqrt{2\pi}}e^{-\frac{v_i^2}{2}}, \tag{8}$$

with which we can validate the eigenvector components by comparing the distributions. It has been reported that the distribution of eigenvector components of the largest eigenvalues shows a great difference from the theoretical predictions [17].

In short, we first construct the correlation matrix for the N stocks and calculate the corresponding theoretical bounds of eigenvalues predicted with RMT, and analyze the eigenvalues with special attention to the largest and second largest eigenvalues.

4. Data and Correlation Matrices

4.1. Data

In this paper, we study the stock markets of China and the United States. There are three considerations in choosing these two markets. First, both markets are major stock markets in the world with tremendous total market scales and a large number of stocks that are actively traded. Second, the two markets both experienced major market shifts between bull and bear markets demonstrating rich market dynamics and behaviors. Third, the US market and Chinese market are representatives of a much-matured market and still-developing market, respectively. We collected the daily price data of the components of the China Securities Index 300 (CSI300) and Standard & Poor's 500 (S&P500) between 4 January 2007 and 6 November 2015. In total, the dataset covers 2149 trading days for CSI300, and 2228 trading days for S&P500. The data of CSI300 are retrieved from the CSMAR Solution Database of Shenzhen GTA Education Tech. Ltd. The data of S&P500 are extracted from Yahoo Finance service. We further selected 163 stocks from CSI300 with at least 2000 trading dates without continuous 100 non-trading dates, whereas we selected 468 stocks with at least 2100 trading dates from S&P500. Later, we refer to the screened stocks as CSI163 and S&P468, respectively [29].

4.2. Correlation Matrices

In a stock market, the prices of stocks fluctuate constantly showing complex behaviors. It is important to investigate the performance of individual stocks as well as the interactive behaviors among stocks. To evaluate the interactive co-movement behaviors among the prices of assets, the correlation is a fundamental concept widely used in studies of price dynamics and is used in traditional theories. When the correlation is considered, in traditional theories, like in MPT where the correlation matrices are actually inputs for the portfolio optimization [1], the correlation is assumed as fixed. Still, in the real world, the correlations fluctuate and demonstrate some collective behaviors in market crashes. As a starting point for studying the structure and behavior of markets, correlation analysis is found to be useful not only in theory but also in practices of portfolio risk estimation and optimization [33,76]. Especially during periods of crisis, highly collected co-movements of the stocks are very likely to cause significant losses for a portfolio, so it is necessary to watch the portfolio's correlations. Also, to understand the market structure and the dynamics, it is interesting to investigate the correlations [8,33,35,77–79].

Following the definition and notation widely used in the literature, the Pearson correlation coefficient [8]

$$\rho_{ij} = \frac{\langle Y_i Y_j \rangle - \langle Y_i \rangle \langle Y_j \rangle}{\sqrt{\left(\langle Y_i^2 \rangle - \langle Y_i \rangle^2\right)\left(\left\langle Y_j^2 \right\rangle - \langle Y_j \rangle^2\right)}} \tag{9}$$

can be calculated for each stock pair of s_i and s_j using the logarithmic return

$$Y_i = \ln P_i(t) - \ln P_i(t-1). \tag{10}$$

The value of ρ_{ij} ranges from -1 to -1, indicating a dynamic relationship for the two stocks from a complete anti-correlation to a complete correlation. For a perfect uncorrelated pair, $\rho_{ij} = 0$ by definition. If there are N stocks in consideration, then there will be N^2 correlation coefficients fitting into a $N \times N$ correlation matrix. Correlation analysis has been applied in the study of market structures [8,28,80] and portfolio optimization [31,37,43,54].

In the RMT approach, the statistics of the eigenvalues distribution and the deviation between empirical distribution and the distribution generated from a random fashion are discussed to describe the information contribution of these deviated eigenvalues and the corresponding components of the eigenvectors. But first, the empirical results are tested against a random matrix case [31].

5. Eigenvalues and Eigenvectors for CSI163 and S&P468

5.1. Eigenvalues

Based on the correlation matrices we built in the previous section, we are ready to investigate the eigenvalues and eigenvectors of both markets. First, we use all the logged daily returns data of both two markets, CSI163 and S&P468 over the whole study period, which is 4 January 2007 and 6 November 2015 covering 2149 trading dates for the former and 2228 trading dates for the latter. We present the probability density distributions (PDF) of eigenvalues from the empirical correlation matrix and theoretically predicted by using random matrix theory for CSI163 in Figure 1 and for S&P468 in Figure 2, respectively. For both markets, we find that most empirical eigenvalues are within the RMT predicted interval with some exceptions. As shown in Figure 1, for CSI163, the theoretical predicted eigenvalues bounds are $\lambda_{min} = 0.5250$ and $\lambda_{max} = 1.6267$. We see that there are 7 eigenvalues are larger than the largest eigenvalue predicted by RMT, i.e., 4.29% of all eigenvalues fall beyond the interval. The largest eigenvalue $\lambda_1 = 60.2252$ is nearly 37 times the predicted largest eigenvalue, i.e., $\lambda_1/\lambda_{max} = 37.0238$. For S&P468, as shown in Figure 2, the largest eigenvalue $\lambda_1 = 189.5698$ which is almost 89 times the bound predicted by RMT.

There are 12 eigenvalues that are larger than the bound, i.e., 3.56% are beyond the interval and carry real market information.

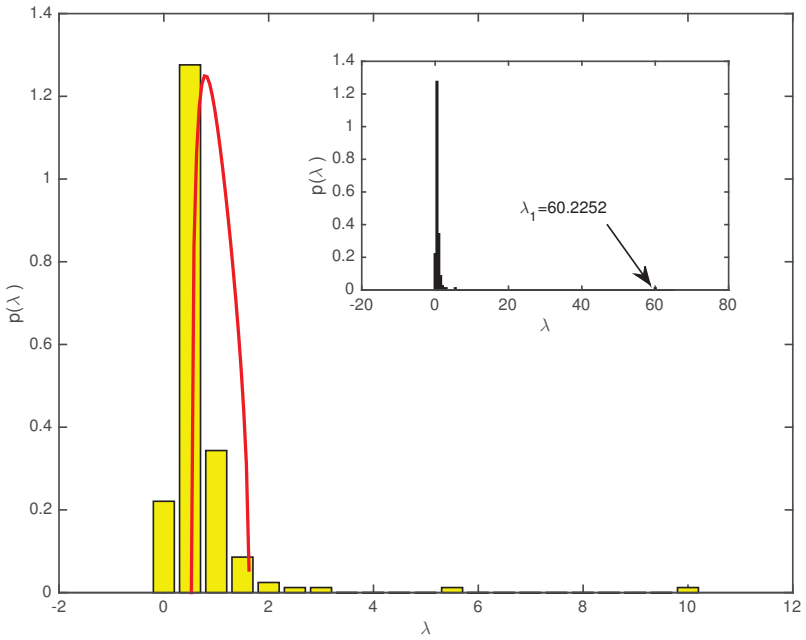

Figure 1. The eigenvalue distributions for CSI163 correlation matrix over the whole study period. The yellow bars are distributions of all eigenvalues calculated from the empirical correlation matrix of 163 daily log return time series, and the red curve is the theoretical distribution predicted from the random matrix theory by using a random matrix of the same size as the empirical correlation matrix. The upper bound is $\lambda_{max} = 1.6267$. The inset is a plot of all empirical eigenvalues including the largest eigenvalue $\lambda_1 = 60.2252$.

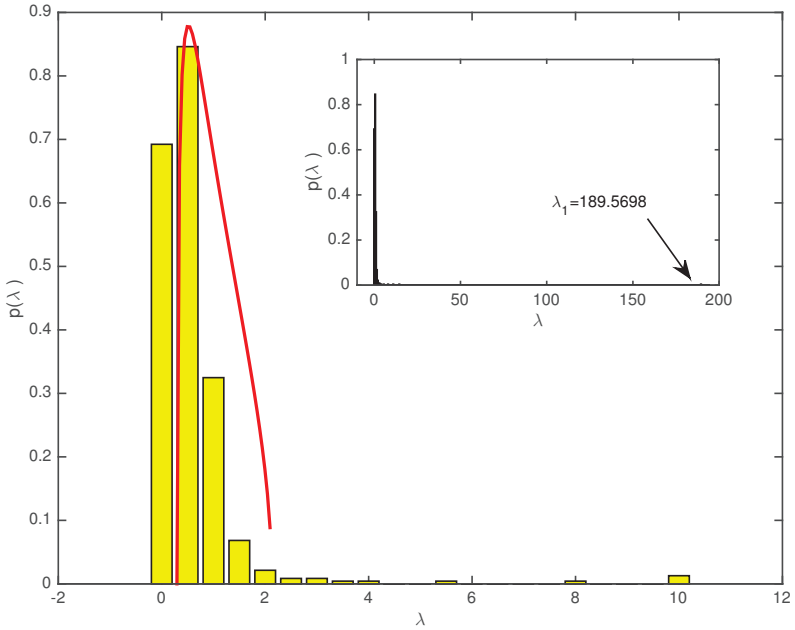

Figure 2. The eigenvalue distributions for S&P468 correlation matrix over the whole study period. The yellow bars are distributions of all eigenvalues calculated from the empirical correlation matrix of 468 daily logged return series, and the red curve is the theoretical distribution predicted from the random matrix theory by using a random matrix of the same size as the empirical correlation matrix. The upper bound is $\lambda_{max} = 2.130$. The inset is a plot of all empirical eigenvalues, including the largest eigenvalue $\lambda_1 = 189.5698$.

Using the sliding window approach, we can investigate the dynamic properties of eigenvalue distributions. For CSI163 and S&P468, we use the window size $L_{csi163} = 170$ and $L_{S\&P468} = 500$, respectively, to satisfy the requirement of $Q = L/N > 1$. In choosing the window sizes, basically, we desire a window that is large enough to cover significant market periods. A shorter window might lead to short-term noises that do not reflect the fundamental dynamics of the markets. Furthermore, the window moves at a step of one trading date; this allows our sliding windows to move smoothly with the finest possible granularity and capture detailed market behaviors. For each sliding window, we use the data of N stocks to calculate the pairwise correlation matrix C, from which we further calculate the λ_1/N and average correlation $\langle C_{ij} \rangle = \sum C_{ij}/N^2$. As shown in Figure 3a,b, we see that for both markets, the values of λ_1/N and the average correlation $\langle C_{ij} \rangle$ correlated very well over the whole study period indicating that λ_1/N is a good estimator of the average correlation $\langle C_{ij} \rangle$ as we have introduced previously.

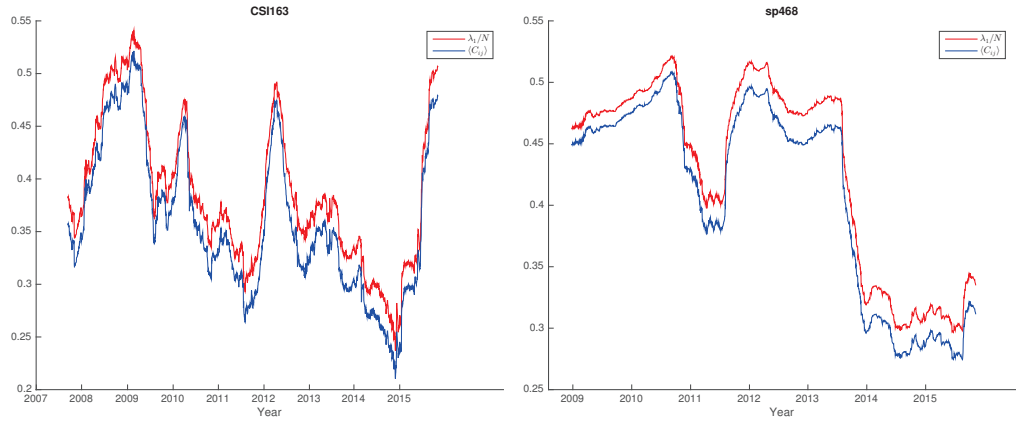

(**a**) (**b**)

Figure 3. The largest eigenvalue λ_1/N and the average correlation $\left\langle C_{ij} \right\rangle$ for all sliding windows of CSI163 (**a**) and S&P468 (**b**). We see that the two curves fit very well.

In Figure 4a,b, we plot the largest eigenvalue λ_1/N and the index close prices of CSI300 (a) and S&P500 (b). After the left shifting, we find that λ_1/N and the index itself show similar trends. This shows that λ_1/N is also an indicator of the index itself. For CSI163, the trend similarity is relatively more obvious than that of S&P468. If we do not perform left shifts, we find that λ_1/N is anti-co-move with the index showing that during market crashes, the λ_1/N (also the average correlation $\langle C_{ij} \rangle$) becomes larger, i.e., the stocks of the market are correlated, whereas during calm periods, the λ_1/N becomes small indicating fewer correlations among stocks.

To see how the eigenvalues distributed in the whole study period. In Figures 5 and 6, we plot the distributions of the eigenvalues (excluding the largest eigenvalue) of all sliding windows over the study periods CSI163 and S&P468, respectively. As the figures show, most eigenvalues are very small. Though many eigenvalues are within the bounds of prediction based on RMT, we also observe some eigenvalues are larger than the upper bound $\lambda_{max} = 3.9172$ for CSI163 and $\lambda_{max} = 3.8709$ for S&P468. We define the fraction of eigenvalues that are larger than the predicted λ_{max} using RMT as

$$p^d = \frac{|\lambda > \lambda_{max}|}{N}, \tag{11}$$

i.e., the ratio of the number of eigenvalues deviated beyond λ_{max} to the total number of eigenvalues N. Since the eigenvalues carry meaningful information about the market, this ratio can be employed as an indicator describing how much information is embedded in the distribution of the empirical eigenvalues. Using the sliding window approach, we

calculate the fraction for each window and plot with the index close price for CSI163 in Figure 7 and S&P468 in Figure 8, respectively.

For better visualizations, we shrink the index values of 200,000 times for $CSI163_{close}$ and 100,000 times for $S\&P468_{close}$, respectively. As we can see, the values of p^d stay unchanged between sudden changes, so the curves of p^d show a shape of discrete stages with ups and downs. More interestingly, we find that the changes of p^d coincide with the changes in index closing prices. As shown in Figure 7 for CSI163 and Figure 8 for S&P468, the changing points of the p^d precisely mark out the local minimums (marked with yellow dots) and local maximums (marked with red dots) of the index itself.

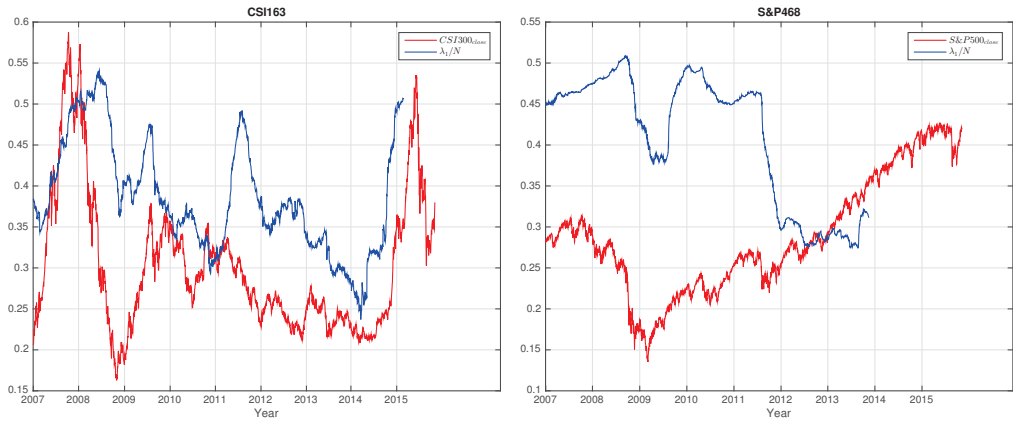

(**a**) (**b**)

Figure 4. The largest eigenvalue λ_1/N and the index close price of CSI300 (**a**) and S&P500 (**b**). The largest eigenvalue λ_1/N curves are left shifted 170 trading dates for CSI300 and 500 trading dates for S&P500, for the window size is 170 for CSI163 and 500 for S&P468. For better visualizations, we shrink the indices of CSI300 and S&P500 10,000 times and 5000 times, respectively. We see that the shifted curves of λ_1/N are similar to the indices.

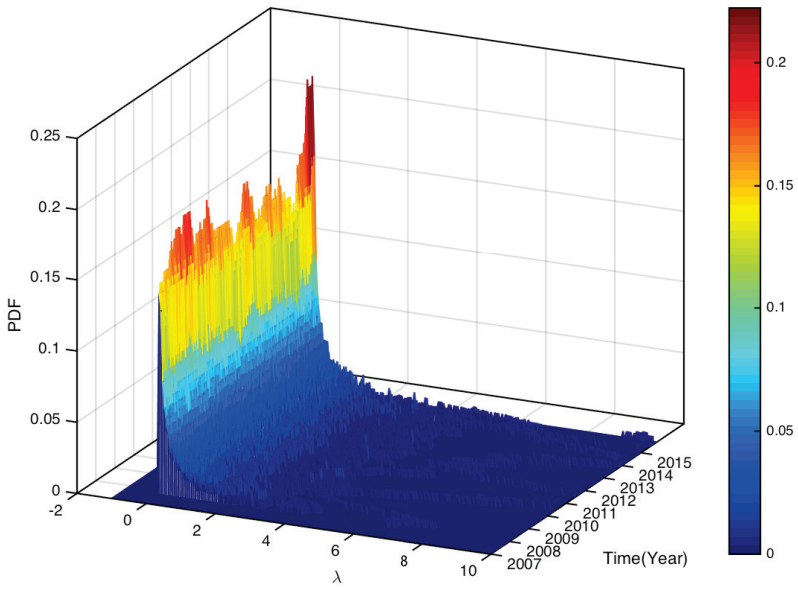

Figure 5. The PDF of all eigenvalues (excluding the largest eigenvalue λ_1) distribution for all sliding windows over the study period of CSI163.

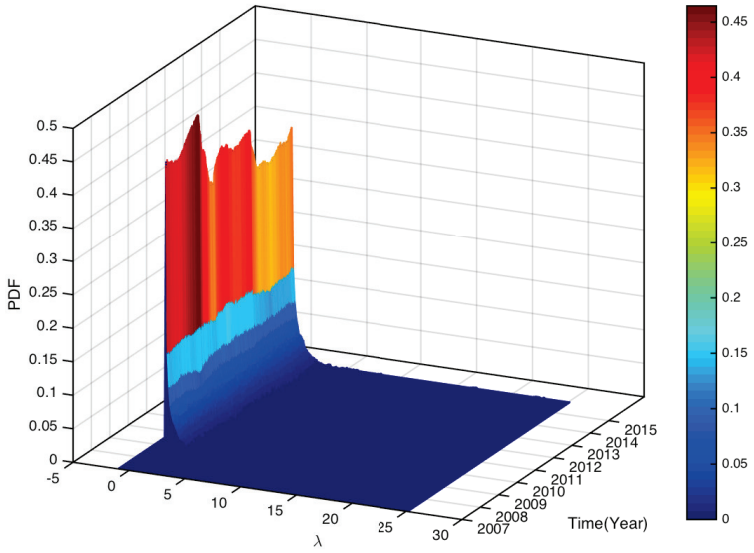

Figure 6. The PDF of all eigenvalues (excluding the largest eigenvalue λ_1) distribution for all sliding windows over the study period of S&P468.

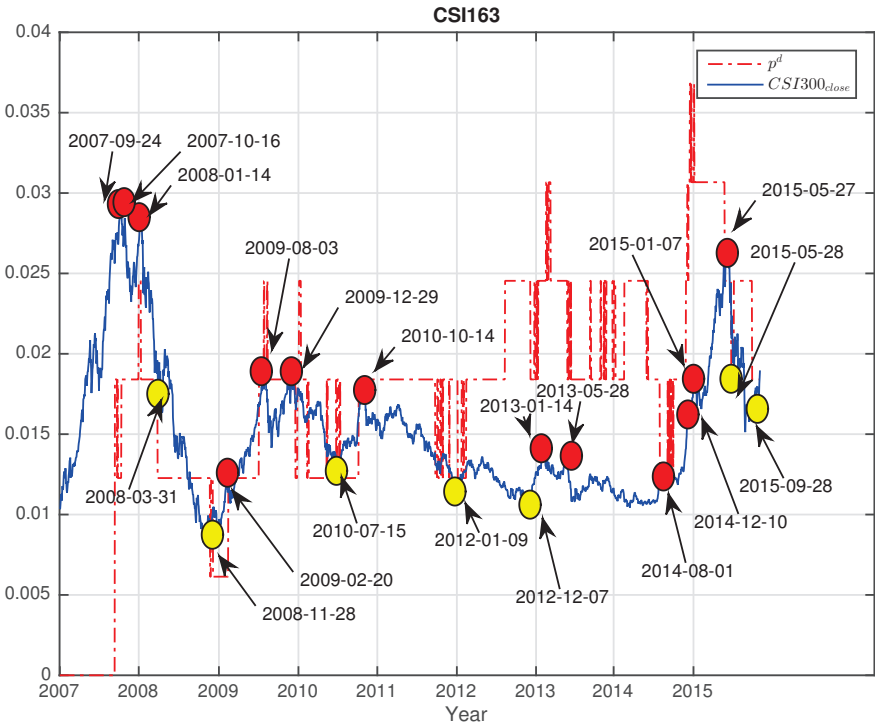

Figure 7. The fraction p^d of eigenvalues beyond the predicted largest eigenvalue versus the index close price for CSI163 over the study period. For better visualization, we rescale the index values by shrinking 200,000 times. The coincidences of changes of fraction p^d and the index closing price are marked out in red dots for local maximums and yellow dots for local minimums on the price curve with dates.

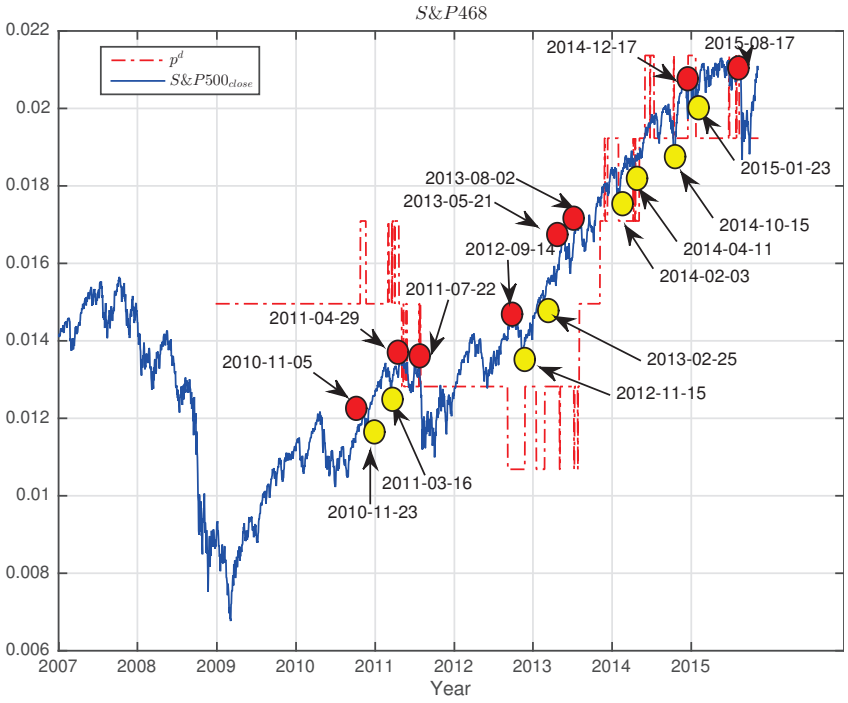

Figure 8. The fraction p^d of eigenvalues beyond the predicted largest eigenvalue versus the index close price for S&P468 over the study period. For better visualization, we rescale the index values by shrinking 100,000 times. The coincidences of changes of fraction p^d and the index closing price are marked out in red dots for local maximums and yellow dots for local minimums on the price curve with dates.

We see that p^d is relatively stable with many fixed periods, but the changes of p^d can match with the significant market changes in index closing prices. Some of them are even leading the index for several days. This observation indicates that p^d has the potential to monitor the market situation. Once the p^d changes value, investors must be cautious and pay particular attention to the market fluctuations both of surges and crashes. This information might also be useful in designing trading strategies to catch major market mode switches.

In Table 1, we summarize the properties of eigenvalues that deviate beyond the λ_{max}. We see that only a very small fraction of eigenvalues is larger than the theoretically predicted eigenvalue. On average, only 3.0268 eigenvalues for CSI163 and 7.2250 eigenvalues for S&P468 are beyond the bounds. The average fraction is $\left\langle p^d \right\rangle = 0.0186$ for CSI163 and $\left\langle p^d \right\rangle = 0.0154$ for S&P468, respectively.

Table 1. Properties of eigenvalue deviation fraction p^d for CSI163 and S&P468. The avg. number is the average number of eigenvalues deviated beyond the predicted upper bounds λ_{max}.

Market	Avg. Number	p^d_{min}	p^d_{max}	$\left\langle p^d \right\rangle$
CSI163	3.0268	0.0061	0.0368	0.0186
S&P468	7.2250	0.0107	0.0214	0.0154

5.2. Largest Eigenvalue

To study the eigenvector u^1 corresponding to the largest eigenvalue λ_1, we take an average of all eigenvector components. Since the λ_1 stands for the whole market, we expect that the average components are related to the index. We plot the $\langle u^1_i \rangle$ with the index close prices of both markets for each sliding window in Figure 9a,b. As shown in the figures, the value of $\langle u^1_i \rangle$ changes happened on the dates or periods of major market changes.

For the eigenvector u^1, we also confirm that all components have the same sign, either positive or negative [81], i.e., all stocks contribute to the movement of the market on the eigenvector u^1 in the same direction; they either climb or fall. It is worth noting that, in practice, one might choose to remove the market mode of the largest eigenvalue before analyzing the eigenvalues. Here, we directly analyze the second-largest eigenvalue and the corresponding eigenvector for simplicity.

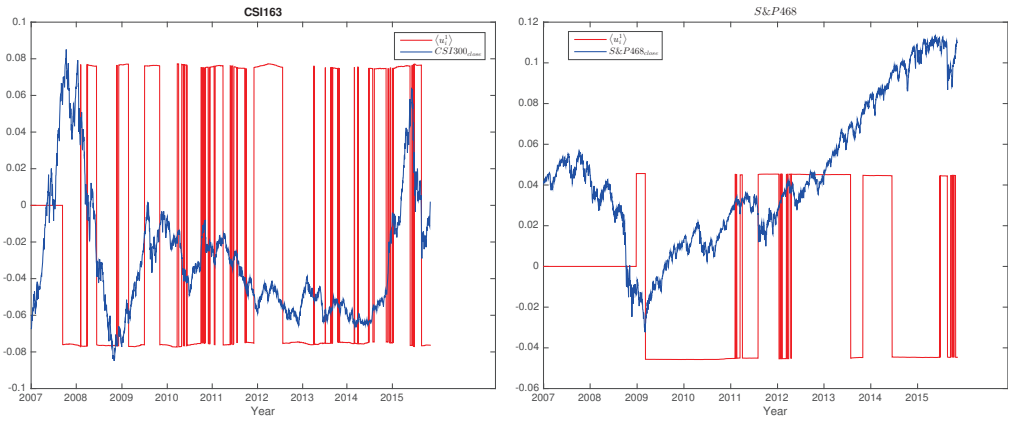

(**a**) (**b**)

Figure 9. The average of eigenvector components corresponding to the largest eigenvalue $\langle u_i^1 \rangle$ and the index close price of both CSI300 (**a**) and S&P500 (**b**). For better visualizations, we shrink the index close price by 25,000 times and 10,000 times for CSI300 and S&P500, respectively. We see that the changes of $\langle u_i^1 \rangle$ happen on the dates when the markets change.

5.3. Second Largest Eigenvalue

It is believed that the largest eigenvalue λ_1 stands for the market mode itself, whereas the second largest λ_2 eigenvalue and its corresponding eigenvector u^2 contain more information about the market. Now, we focus on the distribution of the components in u^2. As we know, the values of components in eigenvectors represent the weights for the corresponding eigenvector; the best idea to allocate investment in portfolio management is that we long the assets with positive signs and short the assets with negative signs. The eigenportfolio based on eigenvector u^j is given as:

$$P_j = \sum_{i=1}^{N} \frac{1}{\sqrt{\lambda_j}} \frac{u_i^j}{\sigma_i} Y_i, \tag{12}$$

where N is the number of assets, U_i^j is the component for asset s_i in eigenvector u_j, and Y_i is the return for asset s_i. This indicates that larger eigenvalues λ_i bring fewer weights for assets in a risky portfolio, whereas smaller eigenvalues bring smaller risks with greater weights on the assets.

For industry I_i, the contribution of I_i is defined as

$$I_i^j(t) = \sum_{k \in I_i} \left(u_k^j\right)^2, \tag{13}$$

where u_k^j is the value of the stock belonging to industry I_i. By dividing over the total values of all industries, we get the normalized contribution for industry I_i

$$\overline{I}_i^j(t) = \frac{I_i^j(t)}{\sum_i I_i^j(t)}. \tag{14}$$

Compared with another approach [73], the normalized values allow comparison between any two industries, thus making the ranking of industries possible. Of course, Equation (14) also indicates that $\sum_i \overline{I}_i^j(t) = 1$.

Using Equations (13) and (14), we calculate and rank all industries in all sliding windows for both CSI163 and S&P468. For a given date, we can get the contributions from all sectors to the eigenvector components for the second largest eigenvalue u^2. We investigate which industries appear in the components with the largest values. In Figure 10a,b, we plot the histograms for industries that appeared for CSI163 and S&P468, respectively. We find that four industries appeared for CSI163, which are finance and insurance, pharmaceuticals, machinery, and metals, whereas for S&P468, we find only three industries appeared, which are utilities, financials, and energy. This reveals the leading industrial sectors for the two markets over the whole study period.

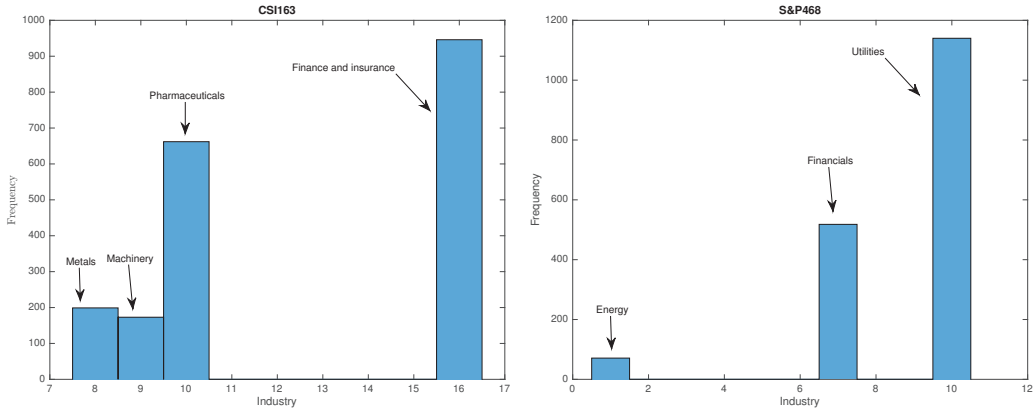

(**a**) (**b**)

Figure 10. The frequencies of industries appearing in the largest values of eigenvector components of CSI163 (**a**) and S&P468 (**b**). For CSI163, four industries appear in the largest eigenvector components, whereas there are three industries for that of S&P468.

5.4. Market Switching

Both the Chinese and US markets experienced significant fluctuations during our study period covering some major market mode changes of bull markets and bear markets. In our study period between 4 January 2007 and 6 November 2015, the Chinese stock market enjoyed a bull market period from 2007 to 2008 and surged to its historical height in 2008 but soon suffered a major crash and only partially recovered in the middle of 2008 and stepped into bear market mode before long. This bear market mode lasted for almost seven years, and only finished in 2015, being replaced by a rocket bull market mode. Unfortunately, the 2015 bull market was very short and tumbled greatly into bear market mode again with huge drops. For S&P500, the US stock markets also suffered a great market crisis in 2008, but the market changed into a very long climbing bull market in 2009.

To investigate how the u^2 changes before and after a market crash, we choose a case study period between 24 July 2008 and 16 February 2009 for CSI300 centering with a market turning point on 4 November 2008, covering 135 trading days and a period between 26 December 2008 and 2 June 2009, and for S&P500 centering with a market turning point on 9 March 2009, covering 108 trading days. We denote the ranking for stock s_i at time t as $R_i(t)$ according to the normalized values. For a period of $[t_s, t_e]$ of length $L_{s,e}$, the averaged ranking for s_i is

$$\langle R_i(t) \rangle = \frac{1}{L_{s,e}} \sum_{t=t_s}^{t_e} R_i(t), \tag{15}$$

where $L_{s,e} = t_e - t_s + 1$ is the number of trading dates in the period. By calculating all

averaged rankings for all of the stocks in both periods before and after the market crash, we can get the top and bottom 10 stocks for CSI163 and S&P468. The top and bottom 10 stocks according to the averaged ranking for CSI163 in the *Fall* stage and *Climb* stage are presented in Tables 2 and 3, respectively. The same lists are presented in Tables 4 and 5 for the Fall and Climb stages of S&P468.

Table 2. The top ten and bottom ten stocks of the second largest eigenvalue u^2 of CSI163 ranked by the average u^2 components values in the Fall stage between 24 July 2008 and 4 November 2008.

Top 10 Rank	**Tick**	**Stock Name**	**Industry**
1	2007	Hualan Biological Engineering Inc.	Pharmaceuticals
2	600,867	Star Lake Bioscience Co., Inc.	Pharmaceuticals
3	600,085	Beijing Tongrentang Co., Ltd.	Pharmaceuticals
4	963	Huadong Medicine Co., Ltd.	Wholesale
5	600,332	Sichuan Hongda Co., Ltd.	Metals
6	600,108	Gansu Yasheng Industrial (Group) Co., Ltd.	Agriculture
7	600,535	Nanjing Chixia Development Co., Ltd.	Real estate
8	600,277	Jiangsu Hengrui Medicine Co., Ltd.	Pharmaceuticals
9	600,089	TBEA Co., Ltd.	Machinery
10	999	Sanjiu Medical & Pharmaceutical Co., Ltd.	Pharmaceuticals
Bottom 10 Rank	**Tick**	**Stock Name**	**Industry**
154	46	Oceanwide Construction Group Co., Ltd.	Real estate
155	601,988	China Construction Bank	Finance
156	2	China Vanke Co., Ltd.	Real estate
157	600,048	Poly Real Estate Group Co., Ltd.	Real estate
158	601,398	Guangshen Railway	Transportation
159	600,016	China Minsheng Banking Corp. Ltd.	Finance
160	600,015	Hua Xia Bank Co., Ltd.	Finance
161	1	Shenzhen Development Bank Co., Ltd.	Finance
162	600,036	China Merchants Bank Co., Ltd.	Finance
163	600,000	Shanghai Pudong Development Bank	Finance

The tables reveal some exciting results. In Table 2, we see that stocks of finance and real estate occupy the bottom ten while stocks of pharmaceuticals dominate the top 10 in the Fall stage of CSI300, and this phenomenon remains unchanged during the Climbing stage after the market turning point. This indicates and confirms again that financials are not the only dominating players in the Chinese stock market. In the Climbing stage, as shown in Table 2, stocks of pharmaceuticals still dominate the top 10, and the stocks of finance remain at the bottom part. This shows that the internal structure of the CSI300 market remains almost unchanged before and after the market crashes.

Being opposite to CSI163, S&P468 demonstrates a different behavior before and after the crash period. As shown in Table 4, stocks of financials dominate the top positions with the smallest rankings; in other words, stocks of financials play significant roles in the Fall stage; however, stocks of energy collectively occupy the bottom 10. When the market entered the Climb stage, passing the turning point, the whole rankings reversed with stocks of energy becoming the top stocks whereas the financials stocks fell to the bottom, as shown in Table 5.

Table 3. The top ten and bottom ten stocks of the second largest eigenvalue u^2 of CSI163 ranked by the average u^2 components values in the Climb stage between 4 November 2008 and 16 February 2009.

Top 10			
Rank	**Tick**	**Stock Name**	**Industry**
1	999	Sanjiu Medical & Pharmaceutical Co., Ltd.	Pharmaceuticals
2	2007	Hualan Biological Engineering Inc.	Pharmaceuticals
3	629	Panzhihua New Steel & Vanadium Co., Ltd.	Metals
4	600,089	TBEA Co., Ltd.	Machinery
5	600,085	Beijing Tongrentang Co., Ltd.	Pharmaceuticals
6	538	Yunnan Baiyao Industry Co., Ltd.	Pharmaceuticals
7	963	Huadong Medicine Co., Ltd.	Wholesale
8	729	Beijing Yanjing Brewery Co., Ltd.	Food & Beverage
9	600,535	Nanjing Chixia Development Co., Ltd.	Real estate
10	600,332	Sichuan Hongda Co., Ltd.	Metals
Bottom 10			
Rank	**Tick**	**Stock Name**	**Industry**
459	157	Changsha Zoomlion Heavy Industry	Machinery
460	600,030	CITIC Securities Co., Ltd.	Finance
461	600,585	Jiangsu Changjiang Electronics Technology	Electronics
462	601,988	China Construction Bank	Finance
463	601,398	Guangshen Railway	Transportation
464	1	Shenzhen Development Bank Co., Ltd.	Finance
465	600,015	Hua Xia Bank Co., Ltd.	Finance
466	600,016	China Minsheng Banking Corp. Ltd.	Finance
467	600,036	China Merchants Bank Co., Ltd.	Finance
468	600,000	Shanghai Pudong Development Bank Co., Ltd.	Finance

Table 4. The top ten and bottom ten stocks of the second largest eigenvalue u^2 of S&P468 ranked by the average u^2 components values in the Fall stage between 26 December 2008 and 9 March 2009.

Top 10			
Rank	**Tick**	**Stock Name**	**Industry**
1	STI	SunTrust Banks	Financials
2	ZION	Zions Bancorp	Financials
3	MTB	M&T Bank Corp.	Financials
4	CMA	Comerica Inc.	Financials
5	WFC	Wells Fargo	Financials
6	BBT	BB&T Corporation	Financials
7	JPM	JPMorgan Chase & Co.	Financials
8	RF	Regions Financial Corp.	Financials
9	LEN	Lennar Corp.	Consumer Discretionary
10	PNC	PNC Financial Services	Financials
Bottom 10			
Rank	**Tick**	**Stock Name**	**Industry**
459	EOG	EOG Resources	Energy
460	MUR	Murphy Oil	Energy
461	OXY	Occidental Petroleum	Energy
462	HP	Helmerich & Payne	Energy
463	NBL	Noble Energy Inc.	Energy
464	XEC	Cimarex Energy	Energy
465	APC	Anadarko Petroleum Corp.	Energy
466	DO	Diamond Offshore Drilling	Energy
467	DVN	Devon Energy Corp.	Energy
468	APA	Apache Corporation	Energy

Table 5. The top ten and bottom ten stocks of the second largest eigenvalue u^2 of S&P468 ranked by the average u^2 components values in the Climb stage between 10 March 2009 and 2 June 2009.

Top 10			
Rank	**Tick**	**Stock Name**	**Industry**
1	APA	Apache Corporation	Energy
2	DVN	Devon Energy Corp.	Energy
3	ETR	Entergy Corp.	Utilities
4	DO	Diamond Offshore Drilling	Energy
5	NBL	Noble Energy Inc.	Energy
6	APC	Anadarko Petroleum Corp.	Energy
7	FE	FirstEnergy Corp.	Utilities
8	OXY	Occidental Petroleum	Energy
9	MUR	Murphy Oil	Energy
10	XOM	Exxon Mobil Corp.	Energy
Bottom 10			
Rank	**Tick**	**Stock Name**	**Industry**
459	USB	US Bancorp	Financials
460	JPM	JPMorgan Chase & Co.	Financials
461	RF	Regions Financial Corp.	Financials
462	WFC	Wells Fargo	Financials
463	BBT	BB&T Corporation	Financials
464	PNC	PNC Financial Services	Financials
465	ZION	Zions Bancorp	Financials
466	CMA	Comerica Inc.	Financials
467	MTB	M&T Bank Corp.	Financials
468	STI	SunTrust Banks	Financials

6. Conclusions and Discussion

In this study, we applied random matrix theory to study the eigenvalues and their eigenvectors of the US and Chinese stock markets. The correlation properties are studied, and some eigenvalues of the correlation matrices beyond the predicted bounds are observed in both markets. The largest eigenvalues λ_1 are dozens of times larger than the predicted λ_{max}. They are found to be potential market indicators. Eigenvalue deviation fractions beyond the predicted largest eigenvalue are observed to pinpoint market turning points. For the two markets, the most influential industry sectors are identified. They behave differently when the market crashes. These findings provide information on the dynamics of eigenvalues and eigenvectors. This is useful for investors and regulators to monitor the markets. On the other hand, the eigenvalues are related to factor models. The largest eigenvalue stands for the market itself and the corresponding eigenvector has impacts on most stocks, described as the single factor model for stock s_i: $r_i = \beta_i r_M + e_i$, where r_M is the market return, for N stocks, the correlation matrix has one dominant eigenvalue. The CAMP is a special case of a single factor model. However, other eigenvalues are beyond the predicted λ_{max}. It is natural to model the returns in multi-factors as proposed in arbitrage pricing theory (APT), $r_i = \sum \beta_{ki} f_k + e_i$, where f_k is the kth factor. Since the eigenvalues embedded in the predicted bounds represent noises, it is natural to choose the top k largest eigenvalues $\lambda_{max-k}, \ldots, \lambda_{max-1}$; thus, we get k corresponding eigenvectors $v_{max-k}, \ldots, v_{max-1}$. In other words, the k principle components in the PCA. To simplify the model, it is reasonable to consider the sector information revealed in the eigenvectors; in other words, the corresponding eigenvector components belonging the the sector are reserved.

Last but not least, the present work still has several limitations that should not be neglected and are worth further efforts in future works. First, this work only considered two major markets in an outdated time period. More global markets and updated periods can be considered in future work. Second, this work provides findings largely through empirical analysis rather than rigorous statistical approaches. In order to further validate the findings,

statistical testing should be considered. Third, this work only reports observations, and no practical applications are developed to further evaluate the values of the methodology and findings. In the future, applications like quantitative trading strategies, portfolio management, and risk management can be developed around the findings to demonstrate the values in financial practices.

Author Contributions: Conceptualization, Y.T.; methodology, Y.T. and Y.Z. (Yicheng Zhang); formal analysis, Y.T., J.X. (Jason Xiong), Z.C., Y.Z. (Yan Zhuang), K.L., J.X. (Jingcong Xie) and Y.Z. (Yicheng Zhang); data curation, Y.T., writing—original draft preparation, Y.T., writing—review and editing, Y.T., J.X. (Jason Xiong), Z.C., Y.Z. (Yan Zhuang), K.L., J.X. (Jingcong Xie) and Y.Z. (Yicheng Zhang), visualization, Y.T. All authors have read and agreed to the published version of the manuscript.

Funding: This research received no external funding.

Institutional Review Board Statement: Not applicable.

Informed Consent Statement: Not applicable.

Data Availability Statement: All data used in this study are publicly available from financial websites.

Acknowledgments: The authors would like to thank editors and anonymous reviewers for their constructive discussions, comments, and patience.

Conflicts of Interest: The authors declare no conflict of interest.

References

1. Markowitz, H. Portfolio Selection. *J. Financ.* **1952**, *7*, 77–91. [CrossRef]
2. Sharpe, W.F. Capital Asset Prices: A Theory of Market Equilibrium under Conditions of Risk. *J. Financ.* **1964**, *19*, 425–442. [CrossRef]
3. Livan, G.; Rebecchi, L. Asymmetric correlation matrices: An analysis of financial data. *Eur. Phys. J. B—Condens. Matter Complex Syst.* **2012**, *85*, 213. [CrossRef]
4. Wang, D.; Podobnik, B.; Horvatić, D.; Stanley, H.E. Quantifying and modeling long-range cross correlations in multiple time series with applications to world stock indices. *Phys. Rev. E* **2011**, *83*, 046121. [CrossRef] [PubMed]
5. Fenn, D.J.; Porter, M.A.; Williams, S.; McDonald, M.; Johnson, N.F.; Jones, N.S. Temporal evolution of financial-market correlations. *Phys. Rev. E* **2011**, *84*, 026109. [CrossRef]
6. Di Matteo, T.; Pozzi, F.; Aste, T. The use of dynamical networks to detect the hierarchical organization of financial market sectors. *Eur. Phys. J. B—Condens. Matter Complex Syst.* **2010**, *73*, 3–11. [CrossRef]
7. Tilak, G.; Széll, T.; Chicheportiche, R.; Chakraborti, A. Study of Statistical Correlations in Intraday and Daily Financial Return Time Series. In *Econophysics of Systemic Risk and Network Dynamics, New Economic Windows*; Abergel, F., Chakrabarti, B.K., Chakraborti, A., Ghosh, A., Eds.; Springer: Milan, Italy, 2013; pp. 77–104.
8. Mantegna, R.N. Hierarchical structure in financial markets. *Eur. Phys. J. B* **1999**, *11*, 193–197. [CrossRef]
9. Nobi, A.; Maeng, S.E.; Ha, G.G.; Lee, J.W. Network Topologies of Financial Market During the Global Financial Crisis. *arXiv* **2013**, arXiv:1307.6974.
10. Tumminello, M.; Lillo, F.; Mantegna, R.N. Correlation, hierarchies, and networks in financial markets. *J. Econ. Behav. Organ.* **2010**, *75*, 40–58. [CrossRef]
11. Dimov, I.I.; Kolm, P.N.; Maclin, L.; Shiber, D.Y.C. Hidden noise structure and random matrix models of stock correlations. *Quant. Financ.* **2012**, *12*, 567–572. [CrossRef]
12. Bouchaud, J.P.; Laloux, L.; Miceli, M.A.; Potters, M. Large dimension forecasting models and random singular value spectra. *Eur. Phys. J. B—Condens. Matter Complex Syst.* **2007**, *55*, 201–207. [CrossRef]
13. Dyson, F.J. Statistical Theory of the Energy Levels of Complex Systems. I. *J. Math. Phys.* **1962**, *3*, 140–156. [CrossRef]
14. Wigner, E.P. Characteristic Vectors of Bordered Matrices with Infinite Dimensions I. In *The Collected Works of Eugene Paul Wigner: Part A: The Scientific Papers*; Wightman, A.S., Ed.; Springer: Berlin/Heidelberg, Germany, 1993; pp. 524–540. ._35. [CrossRef]
15. Potters, M.; Bouchaud, J.P. *A First Course in Random Matrix Theory: For Physicists, Engineers and Data Scientists*; Cambridge University Press: New York, NY, USA, 2020.
16. Tao, T. *Topics in Random Matrix Theory*; American Mathematical Society: Providence, RI, USA, 2023; Volume 132.
17. Laloux, L.; Cizeau, P.; Bouchaud, J.P.; Potters, M. Noise Dressing of Financial Correlation Matrices. *Phys. Rev. Lett.* **1999**, *83*, 1467–1470. [CrossRef]
18. Chen, H.; Mai, Y.; Li, S.P. Analysis of network clustering behavior of the Chinese stock market. *Phys. A Stat. Mech. Appl.* **2014**, *414*, 360–367. [CrossRef]
19. Jiang, X.F.; Chen, T.T.; Zheng, B. Structure of local interactions in complex financial dynamics. *Sci. Rep.* **2014**, *4*, 5321. [CrossRef]

20. Jamali, T.; Jafari, G.R. Spectra of empirical autocorrelation matrices: A random-matrix-theory-inspired perspective. *EPL (Europhys. Lett.)* **2015**, *111*, 10001. [CrossRef]
21. Kumar, S.; Kumar, S.; Kumar, P. Diffusion entropy analysis and random matrix analysis of the Indian stock market. *Phys. A Stat. Mech. Appl.* **2020**, *560*, 125122. [CrossRef]
22. Saeedian, M.; Jamali, T.; Kamali, M.; Bayani, H.; Yasseri, T.; Jafari, G.R. Emergence of world-stock-market network. *Phys. A Stat. Mech. Appl.* **2019**, *526*, 120792. [CrossRef]
23. Raei, R.; Namaki, A.; Vahabi, H. Analysis of collective behavior of Iran banking sector by random matrix theory. *Iran. J. Financ.* **2019**, *3*, 60–75. [CrossRef]
24. Vahabi, H.; Namaki, A.; Raei, R. Comparing the collective behavior of banking industry in emerging markets versus mature ones by random matrix approach. *Front. Phys.* **2022**, *10*, 896303. [CrossRef]
25. Taştan, B.; Imamoglu, H. The analysis of cross-correlation between Istanbul Stock Exchange and major stock markets and indices: An empirical analysis using Random Matrix Theory. *Concurr. Comput. Pract. Exp.* **2022**, *34*, e7113. . [CrossRef]
26. Bun, J.; Bouchaud, J.P.; Potters, M. Cleaning large correlation matrices: Tools from random matrix theory. *Phys. Rep.* **2017**, *666*, 1–109. [CrossRef]
27. Heidari Haratemeh, M. Portfolio Optimization and Random Matrix Theory in Stock Exchange. *Innov. Manag. Oper. Strateg.* **2021**, *2*, 257–267. [CrossRef]
28. Namaki, A.; Shirazi, A.H.; Raei, R.; Jafari, G. Network analysis of a financial market based on genuine correlation and threshold method. *Phys. A Stat. Mech. Appl.* **2011**, *390*, 3835–3841. [CrossRef]
29. Tang, Y.; Xiong, J.J.; Jia, Z.Y.; Zhang, Y.C. Complexities in Financial Network Topological Dynamics: Modeling of Emerging and Developed Stock Markets. *Complexity* **2018**, *2018*, 4680140. [CrossRef]
30. Tang, Y.; Xiong, J.J.; Luo, Y.; Zhang, Y.C. How Do the Global Stock Markets Influence One Another? Evidence from Finance Big Data and Granger Causality Directed Network. *Int. J. Electron. Commer.* **2019**, *23*, 85–109. [CrossRef]
31. Pafka, S.; Kondor, I. Noisy covariance matrices and portfolio optimization II. *Phys. A Stat. Mech. Appl.* **2003**, *319*, 487–494. [CrossRef]
32. Laloux, L.; Cizeau, P.; Potters, M.; Bouchaud, J.P. Random matrix theory and financial correlations. *Int. J. Theor. Appl. Financ.* **2000**, *3*, 391–397. [CrossRef]
33. Mantegna, R.N.; Stanley, H.E. *An Introduction to Econophysics: Correlations and Complexity in Finance*; Cambridge University Press: New York, NY, USA, 2000.
34. Plerou, V.; Gopikrishnan, P.; Rosenow, B.; Amaral, L.A.N.; Stanley, H.E. A random matrix theory approach to financial cross-correlations. *Phys. A Stat. Mech. Appl.* **2000**, *287*, 374–382. [CrossRef]
35. Plerou, V.; Gopikrishnan, P.; Rosenow, B.; Amaral, L.A.N.; Stanley, H.E. Econophysics: Financial time series from a statistical physics point of view. *Phys. A Stat. Mech. Appl.* **2000**, *279*, 443–456. [CrossRef]
36. Plerou, V.; Gopikrishnan, P.; Rosenow, B.; Amaral, L.A.N.; Stanley, H.E. Collective behavior of stock price movements—A random matrix theory approach. *Phys. A Stat. Mech. Appl.* **2001**, *299*, 175–180. [CrossRef]
37. Tola, V.; Lillo, F.; Gallegati, M.; Mantegna, R.N. Cluster analysis for portfolio optimization. *J. Econ. Dyn. Control* **2008**, *32*, 235–258. [CrossRef]
38. Rosenow, B.; Plerou, V.; Gopikrishnan, P.; Amaral, L.A.N.; Stanley, H.E. Application of random matrix theory to study cross-correlations of stock prices. *Int. J. Theor. Appl. Financ.* **2000**, *03*, 399–403. [CrossRef]
39. Burda, Z.; Jarosz, A.; Nowak, M.A.; Jurkiewicz, J.; Papp, G.; Zahed, I. Applying free random variables to random matrix analysis of financial data. Part I: The Gaussian case. *Quant. Financ.* **2011**, *11*, 1103–1124. [CrossRef]
40. Bai, Z.; Liu, H.; Wong, W.K. Enhancement of the applicability of Markowitz's portfolio optimization by utilizing random matrix theory. *Math. Financ.* **2009**, *19*, 639–667. [CrossRef]
41. Biely, C.; Thurner, S. Random matrix ensembles of time-lagged correlation matrices: Derivation of eigenvalue spectra and analysis of financial time-series. *Quant. Financ.* **2008**, *8*, 705–722. [CrossRef]
42. Luo, Y.; Xiong, J.; Dong, L.G.; Tang, Y. Statistical correlation properties of the SHIBOR interbank lending market. *China Financ. Rev. Int.* **2015**, *5*, 91–102. [CrossRef]
43. Pafka, S.; Kondor, I. Estimated correlation matrices and portfolio optimization. *Phys. A Stat. Mech. Appl.* **2004**, *343*, 623–634. [CrossRef]
44. Jiang, X.F.; Zheng, B. Anti-correlation and subsector structure in financial systems. *EPL (Europhys. Lett.)* **2012**, *97*, 48006. [CrossRef]
45. Ouyang, F.; Zheng, B.; Jiang, X. Spatial and temporal structures of four financial markets in Greater China. *Phys. A Stat. Mech. Appl.* **2014**, *402*, 236–244. [CrossRef]
46. Lim, K.; Kim, M.J.; Kim, S.; Kim, S.Y. Statistical properties of the stock and credit market: RMT and network topology. *Phys. A Stat. Mech. Appl.* **2014**, *407*, 66–75. [CrossRef]
47. Namaki, A.; Raei, R.; Ardalankia, J.; Hedayatifar, L.; Hosseiny, A.; Haven, E.; Jafari, G.R. Analysis of the Global Banking Network by Random Matrix Theory. *Front. Phys.* **2021**, *8*, 586561. [CrossRef]
48. Glasserman, P.; Young, H.P. Contagion in Financial Networks. *J. Econ. Lit.* **2016**, *54*, 779–831. [CrossRef]
49. Elliott, M.; Golub, B.; Jackson, M.O. Financial Networks and Contagion. *Am. Econ. Rev.* **2014**, *104*, 3115–3153. [CrossRef]

50. Li, F.; Kang, H.; Xu, J. Financial stability and network complexity: A random matrix approach. *Int. Rev. Econ. Financ.* **2022**, *80*, 177–185. [CrossRef]
51. Amini, H.; Cont, R.; Minca, A. RESILIENCE TO CONTAGION IN FINANCIAL NETWORKS. *Math. Financ.* **2016**, *26*, 329–365. [CrossRef]
52. Plerou, V.; Gopikrishnan, P.; Rosenow, B.; Amaral, L.A.N.; Guhr, T.; Stanley, H.E. Random matrix approach to cross correlations in financial data. *Phys. Rev. E* **2002**, *65*, 066126. [CrossRef]
53. Alaoui, M.E. Random matrix theory and portfolio optimization in Moroccan stock exchange. *Phys. A Stat. Mech. Appl.* **2015**, *433*, 92–99. [CrossRef]
54. Sharifi, S.; Crane, M.; Shamaie, A.; Ruskin, H. Random matrix theory for portfolio optimization: A stability approach. *Phys. A Stat. Mech. Appl.* **2004**, *335*, 629–643. [CrossRef]
55. Kwapień, J.; Drożdż, S.; Oświe¸cimka, P. The bulk of the stock market correlation matrix is not pure noise. *Phys. A Stat. Mech. Appl.* **2006**, *359*, 589–606. [CrossRef]
56. Nie, C.X. Analyzing financial correlation matrix based on the eigenvector–eigenvalue identity. *Phys. A Stat. Mech. Appl.* **2021**, *567*, 125713. [CrossRef]
57. Pharasi, H.K.; Sharma, K.; Chakraborti, A.; Seligman, T.H., Complex Market Dynamics in the Light of Random Matrix Theory. In *New Perspectives and Challenges in Econophysics and Sociophysics*; Abergel, F., Chakrabarti, B.K., Chakraborti, A., Deo, N., Sharma, K., Eds.; Springer International Publishing: Cham, Switaerland, 2019; pp. 13–34. [CrossRef]
58. Bun, J.; Bouchaud, J.P.; Potters, M. Overlaps between eigenvectors of correlated random matrices. *Phys. Rev. E* **2018**, *98*, 052145. [CrossRef]
59. García-Medina, A.; Sandoval, L.; Bañuelos, E.U.; Martínez-Argüello, A. Correlations and flow of information between the New York Times and stock markets. *Phys. A Stat. Mech. Appl.* **2018**, *502*, 403–415. [CrossRef]
60. Ji, J.; Huang, C.; Cao, Y.; Hu, S. The network structure of Chinese finance market through the method of complex network and random matrix theory. *Concurr. Comput. Pract. Exp.* **2019**, *31*, e4877.
61. Zitelli, G.L. Random matrix models for datasets with fixed time horizons. *Quant. Financ.* **2020**, *20*, 769–781. [CrossRef]
62. Baruccaand, P.; Kieburg, M.; Ossipov, A. Eigenvalue and eigenvector statistics in time series analysis. *EPL (Europhys. Lett.)* **2020**, *129*, 60003. [CrossRef]
63. Han, R.Q.; Xie, W.J.; Xiong, X.; Zhang, W.; Zhou, W.X. Market Correlation Structure Changes Around the Great Crash: A Random Matrix Theory Analysis of the Chinese Stock Market. *Fluct. Noise Lett.* **2017**, *16*, 1750018. [CrossRef]
64. Yang, Y. Comparison and Analysis of Chinese and United States Stock Market. *J. Financ. Risk Manag.* **2020**, *9*, 44. [CrossRef]
65. Zhang, Y.; Mao, J. COVID-19's impact on the spillover effect across the Chinese and U.S. stock markets. *Financ. Res. Lett.* **2022**, *47*, 102684. [CrossRef]
66. Jin, Z.; Guo, K. The Dynamic Relationship between Stock Market and Macroeconomy at Sectoral Level: Evidence from Chinese and US Stock Market. *Complexity* **2021**, *2021*, 6645570. [CrossRef]
67. Chen, Y.; Pantelous, A.A. The U.S.-China trade conflict impacts on the Chinese and U.S. stock markets: A network-based approach. *Financ. Res. Lett.* **2022**, *46*, 102486. [CrossRef]
68. Urama, T.C.; Ezepue, P.O.; Nnanwa, C.P. Analysis of Cross-Correlations in Emerging Markets Using Random Matrix Theory. *J. Math. Financ.* **2017**, *7*, 18. [CrossRef]
69. Pharasi, H.K.; Sharma, K.; Chatterjee, R.; Chakraborti, A.; Leyvraz, F.; Seligman, T.H. Identifying long-term precursors of financial market crashes using correlation patterns. *New J. Phys.* **2018**, *20*, 103041. [CrossRef]
70. Batondo, M.; Uwilingiye, J. Comovement across BRICS and the US Stock Markets: A Multitime Scale Wavelet Analysis. *Int. J. Financ. Stud.* **2022**, *10*, 27. [CrossRef]
71. Vuong, G.T.H.; Nguyen, M.H.; Huynh, A.N.Q. Volatility spillovers from the Chinese stock market to the U.S. stock market: The role of the COVID-19 pandemic. *J. Econ. Asymmetries* **2022**, *26*, e00276. [CrossRef]
72. Pan, Q.; Mei, X.; Gao, T. Modeling dynamic conditional correlations with leverage effects and volatility spillover effects: Evidence from the Chinese and US stock markets affected by the recent trade friction. *N. Am. J. Econ. Financ.* **2022**, *59*, 101591. [CrossRef]
73. Ren, F.; Zhou, W.X. Dynamic Evolution of Cross-Correlations in the Chinese Stock Market. *PLoS ONE* **2014**, *9*, e97711. [CrossRef]
74. Said, S.; Heuveline, S.; Mostajeran, C. Riemannian statistics meets random matrix theory: Toward learning from high-dimensional covariance matrices. *IEEE Trans. Inf. Theory* **2022**, *69*, 472–481. [CrossRef]
75. Zhu, W.; Ma, X.; Zhu, X.H.; Ugurbil, K.; Chen, W.; Wu, X. Denoise Functional Magnetic Resonance Imaging With Random Matrix Theory Based Principal Component Analysis. *IEEE Trans. Biomed. Eng.* **2022**, *69*, 3377–3388. [CrossRef]
76. Bouchaud, J.P.; Potters, M. *Theory of Financial Risk and Derivative Pricing: From Statistical Physics to Risk Management*; Cambridge University Press: New York, NY, USA, 2003.
77. Rosenow, B.; Gopikrishnan, P.; Plerou, V.; Stanley, H.E. Dynamics of cross-correlations in the stock market. *Phys. A Stat. Mech. Appl.* **2003**, *324*, 241–246. [CrossRef]
78. Giardina, I.; Bouchaud, J.P.; Mézard, M. Microscopic models for long ranged volatility correlations. *Phys. A Stat. Mech. Appl.* **2001**, *299*, 28–39. [CrossRef]
79. Kenett, D.Y.; Huang, X.; Vodenska, I.; Havlin, S.; Stanley, H.E. Partial correlation analysis: Applications for financial markets. *Quant. Financ.* **2015**, *15*, 569–578. [CrossRef]

80. Iori, G.; Masi, G.D.; Precup, O.V.; Gabbi, G.; Caldarelli, G. A network analysis of the Italian overnight money market. *J. Econ. Dyn. Control* **2008**, *32*, 259–278. [CrossRef]
81. Tanaka-Yamawaki, M.; Yang, X.; Kido, T.; Yamamoto, A. Extracting Market Trends from the Cross Correlation between Stock Time Series. In *Advanced Techniques for Knowledge Engineering and Innovative Applications: Proceedings of the 16th International Conference, KES 2012, San Sebastian, Spain, 10–12 September 2012*; Revised Selected Papers; Tweedale, J.W., Jain, L.C., Eds.; Springer: Berlin/Heidelberg, Germany, 2013; pp. 25–38. [CrossRef]

entropy

MDPI

Article

A Wealth Distribution Agent Model Based on a Few Universal Assumptions

Matheus Calvelli [1] and Evaldo M. F. Curado [1,2,*]

[1] Centro Brasileiro de Pesquisas Físicas, Rio de Janeiro 22290-180, RJ, Brazil; matheus.calvelli@gmail.com
[2] National Institute of Science and Technology for Complex Systems, Rua Xavier Sigaud 150, Rio de Janeiro 22290-180, RJ, Brazil
* Correspondence: evaldo@cbpf.br

Abstract: We propose a new agent-based model for studying wealth distribution. We show that a model that links wealth to information (interaction and trade among agents) and to trade advantage is able to qualitatively reproduce real wealth distributions, as well as their evolution over time and equilibrium distributions. These distributions are shown in four scenarios, with two different taxation schemes where, in each scenario, only one of the taxation schemes is applied. In general, the evolving end state is one of extreme wealth concentration, which can be counteracted with an appropriate wealth-based tax. Taxation on annual income alone cannot prevent the evolution towards extreme wealth concentration.

Keywords: agent-based; economy; information; taxation; complex systems; income distributions

Citation: Calvelli, M.; Curado, E.M.F. A Wealth Distribution Agent Model Based on a Few Universal Assumptions. *Entropy* **2023**, *25*, 1236. https://doi.org/10.3390/e25081236

Academic Editor: José Roberto Iglesias

Received: 15 June 2023
Revised: 8 August 2023
Accepted: 10 August 2023
Published: 19 August 2023

1. Introduction

The study of wealth distributions dates back to the late 19th century, when Pareto studied the distribution of land in Italy—an equivalent proxy, at the time, to wealth—and found that, for higher incomes, it was distributed according to a power law, with an exponent α. Later, he found that this distribution was also applicable to Europe as a whole, with an average value $\alpha \simeq 3/2$, according to Pareto estimates [1]. This new discovery led many economists to believe that this was a robust and stable phenomenon and that, with sufficient data, the same behavior would be found in most other countries in the world, as indeed it was. Clearly, if this behavior is valid in general, it must be based on very general trade behaviors common to all countries in the world, regardless of geographic region, culture, religion, etc.

Trying to have insight into some of these basic behaviors in trade that are common to all countries and that are important for a better understanding of the socioeconomic origins of these distributions, such as those obtained by Pareto, is one of the contributions of this paper. We will discuss some of these common behaviors in trade and their influence on this type of distribution.

The probability density function, $P(x)$, associated with Pareto distribution can be written, in general form, as

$$P(x) = \begin{cases} F(x) & \text{for } x < x_c, \\ \frac{\lambda}{x^{\alpha+1}} & \text{for } x \geq x_c \text{ where } \lambda > 0 \text{ is a parameter} \end{cases} \tag{1}$$

where for $x < x_c$ (x can be land, money, etc., in general, any kind of wealth), we have a function $F(x)$, but for $x > x_c$, a power law appears, having a typical exponent α. The Pareto distribution, $\mathcal{P}(x)$, is usually associated with the cumulative distribution function for the higher values of x, i.e.,

$$\mathcal{P}(x) = \int_x^\infty dx' P(x') \,. \tag{2}$$

Since then, the nature of this distribution of wealth has changed drastically. In particular, the 20th century saw the creation of a strong middle class in some countries ([2,3]), as the industrial revolution, war, and hyperinflation changed the economy of many countries [4]. Interestingly, however, the Pareto distribution would still better describe the tail, while the Boltzmann–Gibbs distribution would best describe the broader part of society (poor and middle class), as can be seen in the income distributions for the US and UK in Figure 1. Therefore, it is not surprising that the ability of the Pareto distribution to describe the wealthier parts of society leads economists to further reinforce their past ideas about its robustness and stability.

Nevertheless, as time goes by and the economic turmoil of the 20th century ends, inequality began to grow at an alarming pace [5], with some economists even predicting a return to 19th-century levels of inequality [5] in some countries, something that many economists thought impossible, further putting into question the stability of the distribution. This increasingly stimulates the theoretical study of the nature of this distribution, trying to better understand its basic causes.

It is important to note that among the various attempts to quantify a little more the measure of inequality, the so-called Lorenz curve, proposed by Max O. Lorenz in 1905 [6], is one of the most important and is used to calculate the Gini index, introduced by Corrado Gini, in 1912 [7], which is currently the standard measure of inequality. Essentially, the Lorenz curve is a graphical representation of inequality, be it wealth inequality or annual income inequality. In this representation, we plot on the abscissa the fraction of the population according to the annual income or wealth and on the vertical axis the fraction of the accumulated wealth or annual income. The Gini index is defined as twice the area contained between the line corresponding to complete equality, i.e., the curve connecting the origin to the point $(1, 1)$, and the Lorenz curve.

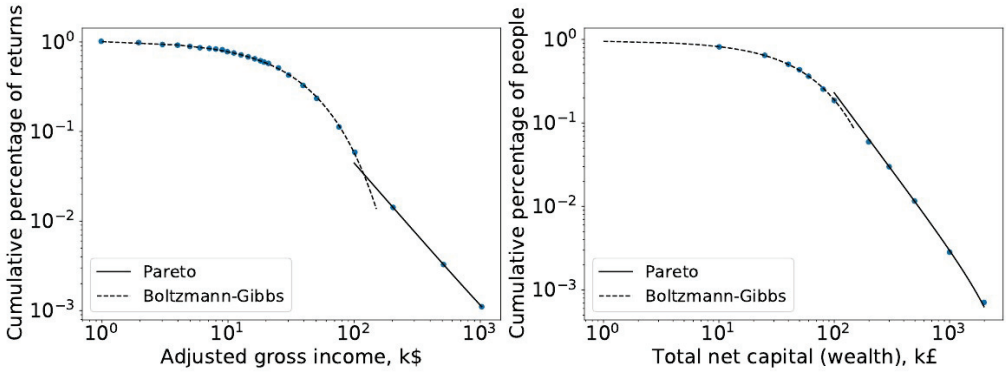

Figure 1. The cumulative probability distribution of net wealth in the US (**left**, 1997) and UK (**right**, 1996) shown in log–log scales. Points represent data from the IRS/HMRC, and solid lines are the fitted lines to the exponential (Boltzmann–Gibbs) and power-law (Pareto) [1].

Among those that studied the inequality from a theoretical point of view, however, agent-based models seem to lead to better results, closer to reality. For example, in [8,9], Chatterjee, A., and Chakrabarti, B. K., considered a simple gaslike model and developed it with increasing levels of complexity. In it, they explore how different types of exchanges can affect a system where, an important point, money is always conserved in any trade interaction ($m_i(t) + m_j(t) = m_i(t+1) + m_j(t+1)$); debt cannot occur; and transactions, where a Δm fraction of money is exchanged, happen randomly between agents. Their model leads, as expected, to a steady state, which is a Gibbs state. Sequentially, the authors added a uniform saving parameter that models the system's propensity to save, and hence, the amount exchanged has changed. This in turn leads the distribution of wealth to a gamma distribution, thus showing how an additional constraint can change the shape of the distributions. Then, the authors allowed the saving propensity to be distributed among each agent by $\rho(\lambda)$ and showed that, regardless of the shape of $\rho(\lambda)$, the asymptotic form

of the distribution was always a Pareto one. This result matches the work conducted by Chakraborti and Patriarca [10], which shows that a system composed of subsystems with different degrees of freedom (the propensity to save) leads to a Pareto power law.

Another important work was conducted by Braunstein, Macri, and Iglesias in [11], where they show how, in a complex network, there is a strong link between wealth and the connectivity of agents.

However, when we take a step back from the simulations and look at the data, we can clearly see from the works of Dragulescu in [12] and Banerjee and Yakovenko in [3] and many others ([2,13–28]) how fundamental and widespread these distributions are, and hence, we expect that this behavior must arise from very basic and common commercial features and interactions.

Therefore, in order to analyze the influence of these universal aspects on trading in distributions, we propose here an agent-based model that is able to bridge these gaps between real-world modeling and fundamental understanding. With this aim, we propose some very basic fundamental (universal) assumptions that are common to any commercial exchange, trying to understand their effects on the distribution of wealth. One of these assumptions is to consider a direct link between information (we further explain this interpretation in the next chapters), represented as the number of connections an agent makes, and wealth. Another assumption, also very general, is the slight trade advantage that a wealthier agent generally has over a poorer agent in any given trade event. Finally, we consider two different types of taxation, a taxation on wealth and a taxation on annual income. In this paper, we will only consider in each scenario (by scenario, we are considering the time evolution of wealth distribution satisfying a set of rules on the connectivity of agents and the trade advantage they have depending on the wealth of the agents, and also the application of only one of two types of taxation, on wealth or on annual income) a single taxation scheme.

We then show how each of these assumptions contributes to the distribution of wealth over time and how they help us understand how different taxation schemes can affect these distributions.

2. Outline of the Model

Our goal with this work is to construct a simple agent-based model, rooted in very basic assumptions of business relationships. To do this, we have built our model step by step, introducing complexity along the way, while always maintaining its basic features. Hence, the description of the model, as well as its results, is presented in the same manner, as a step-by-step model built from its simplest form to its most complex, in order to help us understand what the effect of each part is and why it matters. We also separate the description of each version of the model from its results in order to discuss the impact of each parameter and to understand why we have chosen some appropriate numerical values for some of these parameters.

2.1. Fundamental Characteristics

We consider a collection of N agents, each starting with a given value w_0 of a continuous variable w_i, representing the wealth of the agents. The evolution is probabilistic, where, in each Monte Carlo step, each agent is chosen once and trades with other agents, chosen randomly. As the system evolves, agents interact and trade according to four different scenarios. In these interactions, agents can either gain or lose a net amount of money based on the combined wealth of both agents i and j,

$$\Delta w_{i,j} = \mu(w_i w_j)/(w_i + w_j)\,, \tag{3}$$

where μ is a constant $\in [0, 1]$. This function is chosen because it reflects well the relationship of the difference in buying power among agents: the bigger the difference in buying power of one agent relative to another, the greater is its ability to set the amount of money exchanged. This also makes it impossible for agents to trade more wealth than they

currently have, a basic requirement. It is important to note, however, that this function is not special and that any other function with a similar qualitative behavior would also work.

At each interaction, both agents play according to a probability distribution and wealth is not conserved, as it happens in reality. Therefore, possibilities where both agents gain (wealth creation) and where both agents lose (wealth destruction) are possible. Since wealth is not conserved in each trade exchange, the total wealth of the system is normalized at the end of each Monte Carlo step.

Basic Assumptions

Here, we will introduce the three very basic assumptions that we have adopted and that we believe are generally valid anywhere in the world. Of course, each of these assumptions will be adequately mathematized.

Our first basic assumption, which we believe should be self-evident, is

Assumption 1 (First basic assumption)**.** *The number of trades an agent makes increases with his wealth.*

These agents will then randomly interact with others according to a given connection function, which we define as $f_c(w_i)$, which gives how many connections/interactions each agent can make, based on his wealth. For example, if $f_c(w_i) = 1$, each agent in turn, regardless of its wealth, will perform one interaction, and therefore one transaction, per Monte Carlo step. Notice that in one Monte Carlo step, a given agent may perform more than $f_c(w_i)$ interactions, as it may be chosen by other agents in their time.

Therefore, according to the assumption, the connection function $f_c(w)$ mentioned above must be a monotonically increasing function. We will assume here the simplest one, a linear function. Clearly, any other type of monotonically increasing function could be adopted, but the qualitative behavior of the evolution of the system will not change by reasonable choices of the connection function. Only the way the system evolves will change, but not the patterns of the distribution. This assumption will be used in the second, third, and fourth scenarios presented below.

Our second basic assumption, which is also self-evident, is

Assumption 2 (Second basic assumption)**.** *The probability of winning a trade transaction increases with the difference in wealth between the richest and poorest.*

We will introduce a probability of winning a trade exchange that depends on the difference in wealth between the two agents trading. The richer an agent is relative to each other, the higher the probability of winning (in terms of simulation, this means that two "coins" are tossed, one for each agent; hence, they both can win or lose, and situations where one wins and the other loses are also possible) a trade, as is usually the case in any trade negotiation. Hence, when $w_i > w_j \rightarrow P(w_i|w_j) > P(w_j|w_i)$. The aim is to model the fact that the richest agent in a given trade is usually the one who takes the least risk. This assumption will be used in the third and fourth scenario.

2.2. Taxation

Here, we have our third basic assumption:

Assumption 3 (Third basic assumption)**.** *The tax is a monotonic increasing function of wealth.*

We have essentially two main types of taxation: wealth taxation and income taxation (income or capital gains during 1 year, i.e., one stage).

2.2.1. Taxation on Wealth

After a certain number of Monte Carlo steps, here adopted as five, we have what we call a stage, which we can consider equivalent to 1 year. At the end of each stage, a tax

is applied on the amount of wealth the agent has at the end of the period. The standard pattern should be that the tax increases with wealth, so we have our third basic assumption.

We then define as a taxation function, to be applied to the wealth of each agent at the end of a stage, the simplest one, a linear function:

$$\text{Tax}(w_i) = \begin{cases} 0, & \text{if } w_i \leq w_o \\ \gamma(w_i - w_0) + \sigma w_0, & \text{if } 0 < w_i < w^* \text{ and} \\ \tau, & \text{if } \quad w_i > w^* \,, \end{cases} \tag{4}$$

where $\gamma, \tau, \sigma \in [0, 1]$; γ indicates the growth rate of the tax according to wealth, σ the base tax rate, τ the maximum adopted tax rate, and $w^* = [\tau + (\gamma - \sigma)\, w_0]/\gamma$. It is worth noting that taxation here means taxation to be applied on the wealth each agent has. We will consider in this paper only progressive taxation, as it should be; thus, the parameter γ is considered non-negative. Of course, scenarios with negative values of γ will contribute to concentrate more wealth in the hands of fewer agents. The parameter τ could be relevant and is an important political issue today in many countries. The parameter σ, the initial tax rate, is a parameter that is not important at all, but we keep it here for the sake of completeness.

It is also important to note that there is nothing special about the form of this function, chosen here as a linear function. It could also be another type of increasing function, such as a power law. What matters is its behavior—it grows with wealth and has an upper bound. In fact, we explored the quadratic function, and the visible difference was on how quickly the simulations reached their different patterns.

This taxation is then applied to the share of each agent's wealth w_i above a given minimum w_0 at the end of a fixed number of Monte Carlo steps (called stages), where w_0 is each agent's wealth at the beginning of the simulation.

The total tax charged to the N agents at the end of a stage is then

$$C_T = \sum_{i=1}^{N} \text{Tax}(w_i)\, w_i \ . \tag{5}$$

This total tax collected at the end of a stage is then redistributed equally among all agents (different scenarios in which, for example, the redistribution favors the poor are also possible and certainly lead to different results and conclusions). Thus, if we let $C_T =$ total tax collected, then $C_{i,T} = C_T/N$ is the amount of tax that is returned to each agent at the end of a stage.

In the fourth scenario (see Sections 2.7 and 3.4), we will consider taxation on annual income, but the same third assumption applies: taxation increases with income earned during the previous year.

2.2.2. Taxation on Income or Capital Gain

We have discussed in Section 2.2.1 how to tax the wealth of agents at the end of each year (stage) rather than taxing income or capital gains, which is the much more common form of tax. Therefore, instead of taxing all agents' wealth w_i above the minimum w_0, we now tax an agent's annual capital gain whenever it is above the minimum gain ξ. Hence, regardless of how much wealth an agent has, if he has enough capital gain over a year, i.e., a stage, above this minimum (ξ), the agent will be taxed on that amount, in a monotonically increasing way. Then, we can define

$$\text{Capital Gain} \equiv G_i = w_{i,t} - w_{i,t-1} \,, \tag{6}$$

where t indexes the t-th year, i.e., the t-th stage—as defined in (Section 2.3). Hence, taxation

to be applied to the capital gain of each agent can now be assumed as

$$\text{Tax}(G_i) = \begin{cases} 0, & \text{if } G_i \leq \xi \\ \gamma(G_i - \xi), & \text{if } \xi < G_i < G^* \text{ and} \\ \tau, & \text{if } \ G_i > G^* \,, \end{cases} \tag{7}$$

where $\xi \in [0, w_0]$ (therefore, it is never greater than the starting point of the systems) and $G^* = (\tau + \gamma\xi)/\gamma$; γ is the the growth rate of the tax according to capital gain.

Notice, however, that here, at the end of a year (a stage), we tax anyone with a capital gain above ξ, regardless of their current (wealth) condition. Therefore, a poor agent ($w_i < 1$) who has capital gains above the minimum ($G_i > \xi$) at a given time t will be taxed, even though he is poor. Note, however, that the order of magnitude of taxes in this case (earnings in a year) is very different from the case of a wealth tax. It is important to note that there are many types of taxes that can be collected during the year. There are consumption taxes, which are regressive, affecting poor agents more than rich ones, and taxes on annual income, which are progressive, hurting the rich more. All types of taxes collected during an agent's year are called here the agent's annual income tax. By annual here, we mean the earning received during a stage, of course.

Therefore, while in the wealth tax model an agent with $w_i >> w_0$ can be taxed heavily, since the tax is applied over the agent's total wealth above w_0, it also allows poorer agents to build wealth, since they are not taxed until their wealth is at least $w_i = w_0$. Here, in the case of income tax, the opposite may be true. No matter how poor an agent is, whenever he has a good year, he will be taxed, thus making it difficult for him to build wealth. Meanwhile, extremely wealthy agents could pay almost nothing—relative to their wealth—if their capital gain is not important.

As with taxation on wealth, at the end of the stage (year), the total tax collected that year, which is $\sum_i \text{Tax}(G_i)G_i$, is redistributed equally among all agents.

Note, however, that in each scenario analyzed in this paper, only one of these two types of taxation is applied, either on wealth or on annual income.

2.3. Simulation Setup

We initiate every agent with $w_i = w_0$ and define a Monte Carlo step when each agent (N) in the system finishes his turn, which means

The agent i, with income w_i and number of connections $f_c(w_i) = k$, performs all k interactions in one step. These k interactions are randomly chosen.

The system has no distance (every agent can interact with $f_c(w_i)$ other agents, chosen at random). Therefore, since the interacting agents are randomly selected, a given agent i may perform more than $f_c(w_i)$ interactions per step, since other agents may in turn randomly choose agent i.

We then define that **five Monte Carlo steps** constitute a **stage**, and every step is synchronous: the state of an agent (increase/decrease in wealth) is only updated when the Monte Carlo step is completed (all agents have been updated). Tax collection and redistribution occur only once at the end of the stage. Therefore, Monte Carlo steps can be interpreted as the passage of months, while a stage as the passage of an entire year (annual tax).

We also separate the population in two groups:

1. Agents with $w_i \geq 1$, which are shown in the distributions;
2. Agents with $w_i < 1$, which are taken as the poverty rate and only appear as a percentage.

In the following chapters, we explore different simulation settings (interaction rules, probability, and connection functions) and discuss some of the properties of the model. Note, however, that the functions we have chosen have nothing special about them—we particularly choose the simplest functions whenever possible—it is just their qualitative behaviors that matter. In fact, in the beginning, we tested alternative functions, and the

resulting patterns remained unchanged (the speed of evolution may, as mentioned earlier, change depending on the functions chosen).

2.4. First Scenario: Raw Model and Taxation on Wealth

This is the simplest, unbiased scenario. Consider a system with the trade rules defined at the beginning of Section 2, with an equal probability of winning a commercial exchange; i.e., the probability that agent i will win a commercial exchange with agent j is

$$P(w_i|w_j) = \frac{1}{2}\,. \tag{8}$$

We also consider the connection function—which, as it is defined in Section 2.1, means how many interactions/transactions an agent will choose at each step—as

$$f_c(w_i) = 1\,, \tag{9}$$

for any value of w_i, implying that at each step, each agent chooses only one other agent to trade with.

The numerical simulation results for this model can be seen in Section 3.1.

2.5. Second Scenario: The Wealth–Connection Model with Wealth Taxation

In this scenario, we go one step further. We present a simple connection function that links the wealth of an agent with his number of connections,

$$f_c(w_i) = \begin{cases} \alpha \frac{(w_i - w_0)}{w_0} + 1 & \text{if} \quad w_i \geq w_0 \\ 1 & \text{if} \quad w_i < w_0\,, \end{cases} \tag{10}$$

where $\alpha \in [0, 1]$. The probability of an agent i winning a commercial exchange with an agent j is still given by Equation (8).

According to the function (10), note that agents will always make at least one interaction and that $f_c(w_i)$ is continuous. In order to reproduce this, agents with $f_c(w_i) \in \mathbb{R}$ have an equivalent probability of having an extra interaction at each Monte Carlo step. For example, an agent i with $f_c(w_i) = 3.14$ will have three connections plus an extra connection with a probability of 14%. A random number will be drawn, and if it is below 0.14, the agent will obtain an extra connection, while if it is above, the agent will only obtain three connections in this round. The numerical simulations associated with this scenario are shown in Section 3.2.

2.6. Third Scenario: Favoring the Rich on Transactions and Wealth Taxation

Now, according to our second basic assumption, we introduce a higher probability of winning a commercial transaction for the agent with greater wealth. Until now, each agent had an equal probability of winning a commercial exchange, but now the probability of an agent i winning a transaction with an agent j will be given by the asymmetric function

$$P(w_i|w_j) = \frac{2 + \exp(\beta \delta w_{i,j})}{5 + \exp(\beta \delta w_{i,j})}\,, \tag{11}$$

where $\delta w_{i,j} = w_i - w_j$ and $\beta \in [0, 1]$. This function aims to model the economic bargaining power of an agent. The greater the difference between the wealths of agent i and agent j, the greater the chance that agent i will make a favorable transaction, modeling the fact that the richer agent takes less risk in a trade transaction. At each step, a random number is drawn, and an agent plays this probability with each of the other agents he trades with. Wealth, as always, is not necessarily conserved: if both agents win, wealth is created (both agents earn Δw, Equation (3)); if only one wins, wealth is conserved (one agent loses Δw, while the other wins); and if both lose, wealth is destroyed. In Figure 2, we can see the behavior of this probability function as a function of β. Notice how the decrease in the probability of winning for the poorer agent is small, while the increase for the rich is significant. The

function is not symmetric. This is because if the commercial negotiation is too unfavorable for an agent, he simply does not make the trade (except in very exceptional cases, which are not considered here).

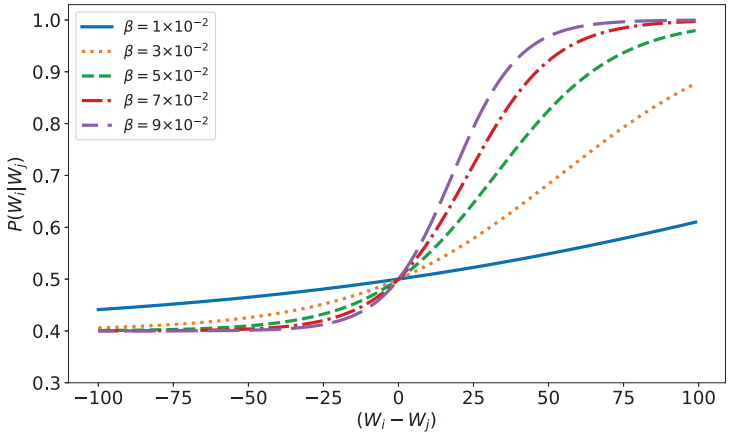

Figure 2. Probability function, Equation (11).

Here, once again, the chosen function is not special, and any other function with similar behavior would work. What matters is the advantage that the rich agent has.

2.7. Fourth Scenario: Favoring the Rich in Transactions and Taxation on Annual Income (Capital Gains)

In this scenario, we consider a connection function given by Equation (10), a probability to win a commercial exchange given by Equation (11), and a tax on income earned during a year given by Equation (7).

3. Results

Essentially, μ, β, and α only control how fast the system evolves and, therefore, how quickly it goes through the different stages. Higher rates of any of these variables will mean that some of the intermediate distributions will inevitably be skipped because the system will evolve too fast. Therefore, these parameters will be kept constant in all our simulations since we are more interested in following the different stages of evolution (after some tests we adopt from now on the values $\mu = 0.1$, $\beta = 0.01$, and $\alpha = 1$) . Similarly, σw_0, our base tax rate, will be kept at 5% of w_0 ($\sigma w_0 = 0.05$). The parameters w_0 and ξ are simply scale parameters, and therefore, their values do not affect the results. Therefore, they are also kept fixed ($w_0 = 10$ and $\xi = 0$) during all numerical simulations.

On the other hand, however, γ and τ could completely change both the evolution of the system and the possible equilibrium states. Therefore, our analysis will consist of varying essentially these two parameters, keeping all others constant.

3.1. Raw Model

As defined in Section 2.4, the raw model describes a system without any assumptions that privilege any of the agents. The richest and the poorest have equal opportunities. Therefore, its probability function (bargaining power) and connection function are given by Equations (8) and (9). All results presented in this section are for N = 100,000 (number of agents) averaged over 100 samples. Taxation is over wealth, given by Equation (4).

Statistics

In Figure 3, we can see that even in a system without any kind of privilege, where no agent has any kind of advantage over another agent, with equitable redistribution of the wealth collected with taxes among agents, there is still some inequality, with the Gini coefficient reaching 0.32. In Figure 3a, we can see that the 99 quantile (quantiles are

equivalent to percentiles, and they represent the point that separates the top x% of the population from the rest; for example, the 90 quantile (or q90) separates the top 10% of the population from the other 90%) has a value not greater than 2.5 w_0, which is not very unequal. In Figure 3b, it can be seen that the 10% richest agents own about 20% of the total wealth, which seems quite reasonable.

However, even in the context of this raw model, where a perfectly egalitarian system still creates inequality, it is easy to infer that in any normal circumstance, where agents do not have perfectly equal opportunities and taxation is not applied to an agent's total wealth, inequality will likely continue to increase.

The big problem for any society is to avoid great inequalities in order to avoid serious social problems, not necessarily to eliminate them.

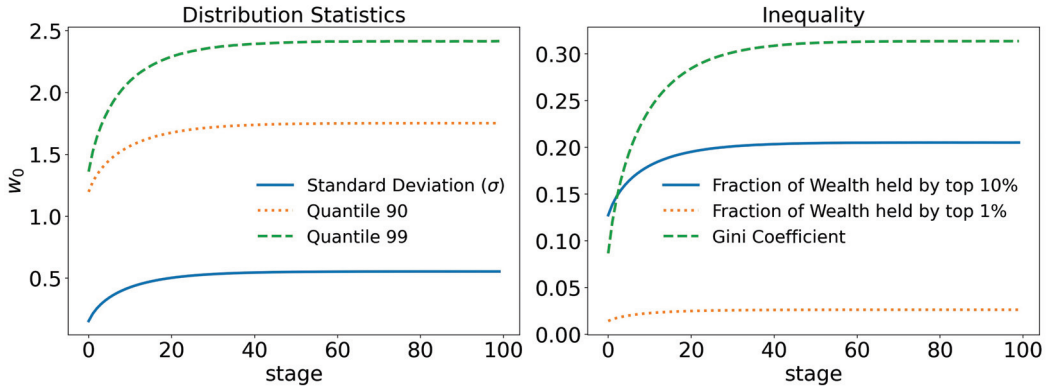

Figure 3. Raw model with taxation on wealth: $\gamma = 10^{-3}$ and $\tau = 0.4$. In the figure on the left, we can see the average wealth held by the 90 and 99 quantiles, i.e., the 10% and 1% richest agents, respectively, compared with the standard deviation. On the right, the fraction of wealth held by the 10% and 1% richest agents is shown. The time evolution of the Gini index is also shown, stabilizing slightly above 0.3.

3.2. Wealth–Trade Link

As defined in Section 2.5, the wealth–connection model describes a system in which the richer the agent, the greater his number of connections (trade exchanges). Therefore, since his bargaining power remains at 50% at all commercial exchanges, due to fluctuations, the wealthier agents end up having higher profits than the poorer agents. The functions that define this scenario are given by Equations (8) and (10). All results presented in this section are for N = 100,000 averaged over 100 samples. Taxation is on wealth, given by Equation (4).

Statistics

In Figure 4, we can see that the link between wealth and connections allows for greater inequality. Whereas, before, the 99th quantile stabilized around 2.4 w_0, it now stabilizes at 3.1 w_0, a 30% increase. Similar differences can also be seen for other statistics. The Gini index went from 0.31 to 0.37, an increase of 20%. The total wealth of the richest 10% went from 20% to 24%, an increase of 20%, and so on.

Therefore, the small advantage of allowing the agent with more wealth to have more connections at each step, which is a fact, and even if his chance of winning a trade exchange is 1/2; i.e., without any advantage, the chances of the agent increasing his wealth increase, leading to a growth of inequality in the population.

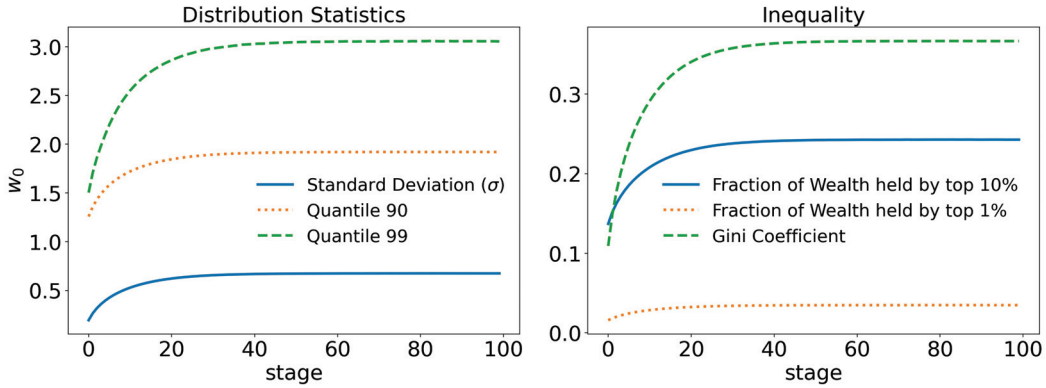

Figure 4. Statistics for the wealth–connection linked model and taxation on wealth: $\gamma = 10^{-3}$ and $\tau = 0.4$. In the figure on the left, we can see the average wealth held by the 90 and 99 quantiles, i.e., the 10% and 1% richest agents, respectively, compared with the standard deviation. Note that these values are larger than in the raw case, Figure 5. On the right, the fraction of wealth held by the 10% and 1% richest agents is shown. The increase in wealth concentration is evident. Consequently, the Gini index also increases. The time evolution of the Gini index is also shown, stabilizing just below 0.4.

3.3. Favoring the Rich on Transactions

As defined in Section 2.6, this model describes a system where an agent's bargaining power, $P(w_i|w_j)$, given by Equation (11), and his number of connections, $f_c(w_i)$, given by Equation (10), are linked to his wealth. The taxation here is on wealth, given by Equation (4). Therefore, as an agent becomes richer, his risk decreases both by his increasing bargaining power and by the number of transactions he makes. All results presented in this section are for N = 100,000 averaged over 500 simulations.

3.3.1. Distributions

First, we start by exploring the evolution of the wealth distribution in this scenario, which is the main focus of this research: can the model reproduce real-world wealth distribution scenarios with these simple assumptions? The parameter values adopted are $\tau = 0.4$ and $\gamma = 1/10{,}000$ (Figures 5 and 6), and $\gamma = 1/100$ (Figure 7).

On the left-hand side of Figure 5, we can see that at the beginning of the simulation, the system quickly evolves into a Gibbs-type form. However, at stage 5, as the poverty rate (orange line) begins to increase, what resembles a Pareto tail begins to appear. At stage 10, when the poverty rate has passed 0.5% and continues to increase, the Pareto-shaped tail starts to become clearer. At stage 23, its shape reaches exactly the expected behavior, as can be seen in the fitted curve in Figure 6: Gibbs-like middle and poor classes, with a Pareto-shaped tail for the upper 10% of the population and a poverty rate just above 1%. Interestingly, however, as the system reaches that point, the poverty rate begins to decrease due to the wealth tax, as inequality increases. At stage 38, we see that a "secondary" Pareto tail appears with a higher coefficient, much like the distribution for Japanese firms shown by Aoyama et al in [14], showing that, in practice, if given enough time, even the rich begin to differentiate themselves, some much richer than others. Then, at stage 45, poverty continues to decrease, around 0.1% (remember that taxation is levied on wealth), even though inequality is still present and evolving. The much richer, due to the taxation on wealth, rather than annual income, help reduce poverty. The rounded part of the curve for higher values of wealth is due to finite size effects. By increasing the number of agents, this rounded part of the curve shifts to the right. To the right of the distributions, we have a graph of the number of interactions at each stage. We would like to note that, due to the not-so-large number of agents, we cannot claim that these behaviors are true power laws. For this, we would have to run simulations for at least 100 times larger number of agents, which is beyond our scope at the moment. Until the last stage presented in the

image (stage 45), the system does not seem to have reached an equilibrium state yet. The tendency towards a condensate state is clear.

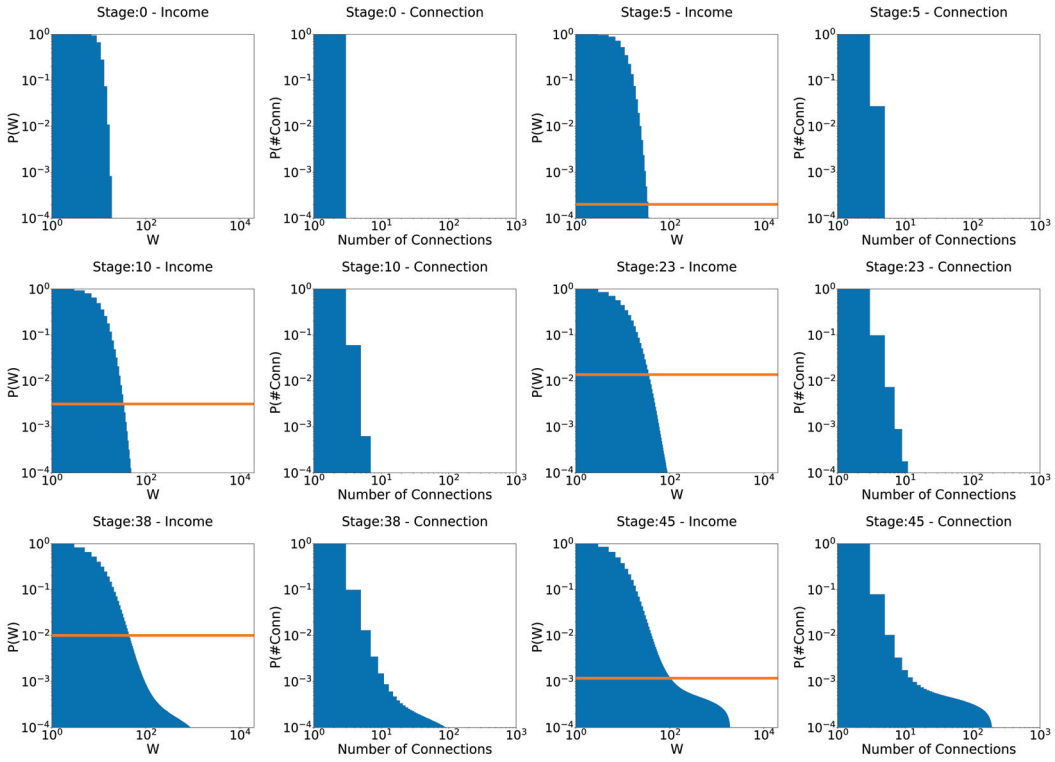

Figure 5. Evolution of the distributions for the model that favors the rich: $\gamma = 10^{-4}$ and $\tau = 0.4$. At each stage, the figure on the left is the distribution of income, and the figure on the right is the distribution of the number of connections. The orange line is the poverty rate.

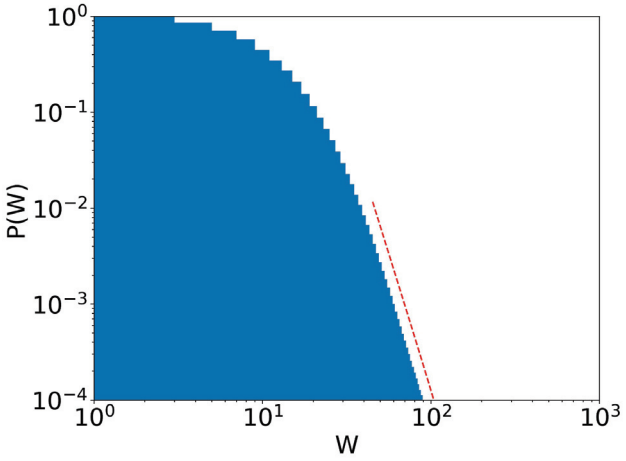

Figure 6. Stage 23 of Figure 5. Pareto tail (dotted red line) is clear, with Pareto exponent $\alpha = 5.63$. $\gamma = 10^{-4}$ and $\tau = 0.4$.

Now, when we increase taxation 10 times (γ = 1/10,000 $\rightarrow$ γ = 1/1000), as can be seen in Figure 7, the system still evolves to the expected behavior. However, by reducing inequality, tax revenue is also reduced, and, therefore, the redistribution of wealth. This makes the system apparently reach an equilibrium state (from stage 42 to stage 99) faster and much more egalitarian, but with a much higher poverty rate. This is an important point. It shows that there is a level of taxation above which the system apparently stabilizes, at least for a long time. Now, just as in the previous chapters—where the rules of the system were more egalitarian—inequality still exists. This shows us three things about

a system that favors the wealthy (note that, again, this is in the context of a model with perfectly equal tax redistribution; unequal redistribution—those that favor the poor, for example—could lead to different results):

1. The problem of poverty is not simply solved with higher tax rates. How to redistribute the tax collected is also an essential point. Here, the tax has been redistributed equally among agents. A redistribution of tax that favors the poor is likely to decrease the level of poverty. However, this has not been considered in this work, and it would be interesting to analyze this issue in a future work.
2. A strong tax system does not necessarily mean lower poverty rates. As said before, how to redistribute taxes is also a key point.
3. It is not necessary to eliminate inequality in order to end poverty. If the rich are taxed properly—on wealth—and redistribution favors the poor, poverty can be virtually eliminated.

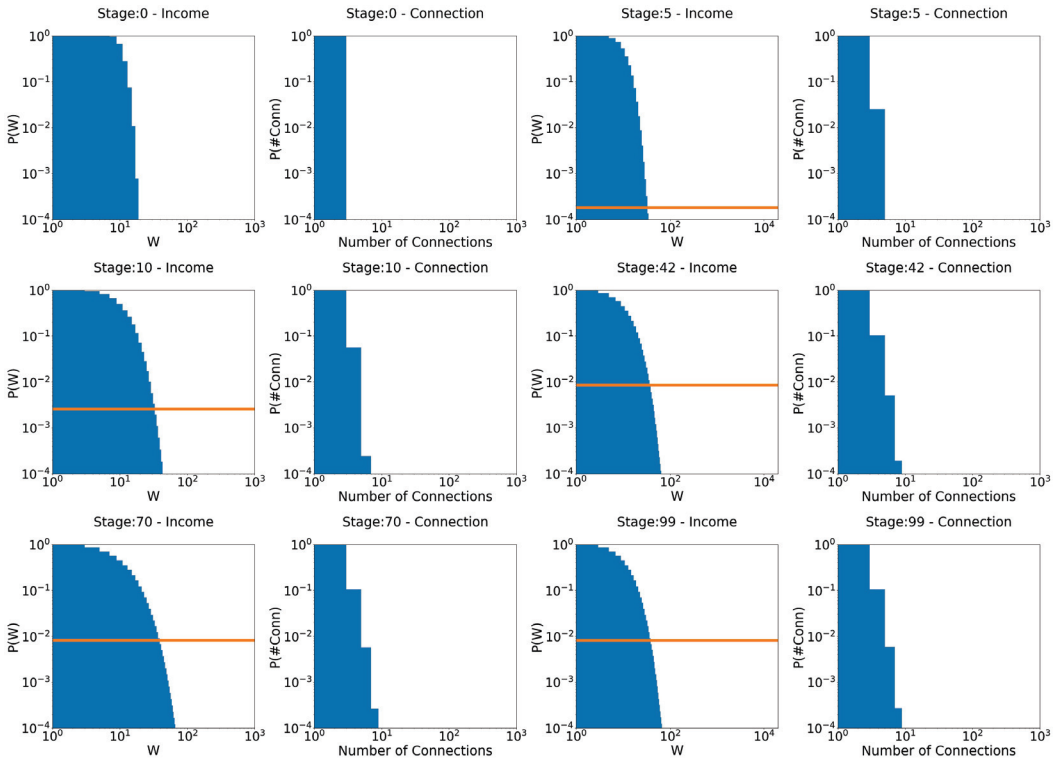

Figure 7. Evolution of distributions for the model that favors the rich: $\gamma = 10^{-3}$ and $\tau = 0.4$. The orange line is the poverty rate.

Therefore, these simulations show us a lot about the model. First, it shows that the model is perfectly capable of reproducing, qualitatively, the behavior of wealth distributions in the real world, from more egalitarian societies to strongly unequal societies, where even the richest end up separated into different classes. Second, it shows us that a certain level of inequality generally always exists, but this poverty can be combated with effective taxation on wealth and effective redistribution of these taxes.

3.3.2. Statistics

In order to better analyze the effects of the parameters of the model over its time evolution of the distributions, let us examine some of its statistics. The total tax revenue can be seen in Figure 8 for several values of γ. As the system evolves, lower tax rates lead to higher tax revenues that are applied to fewer and fewer agents. This is because lower tax rates allow a greater concentration of wealth, so fewer and fewer people can reach the minimum wealth required to pay taxes ($w_0 = 10$). This becomes clearer when we look at

Figures 9 and 10, which show the evolution of the top 10% and top 1% of the population, respectively. We can see that the 90 quantile initially grows to 2 times w_0 and then suddenly falls around stage 40 for lower tax rates, although the percentage of wealth held by the top 10% continues to increase. This means that wealth is concentrated in a group of agents (much) smaller than the 10%. This quantifies the effects we saw in the last section: even among the richest agents, a differentiation starts, with some much richer than others (the second Pareto tail we saw). Meanwhile, the simulation with the highest tax rate ($\gamma = 0.001$) quickly reaches equilibrium (which can be better visualized in Figure 11) and inequality is greatly reduced, although, as we saw in the distributions, poverty is more prevalent. This can be further understood by looking at the Gini coefficient in Figure 11; see how $\gamma = 0.0001$ (tax rate) leads to lower inequality than a value 10 times higher ($\gamma = 0.001$). Moreover, notice that in Figure 11, all simulations eventually reach equilibrium, with a stable standard deviation.

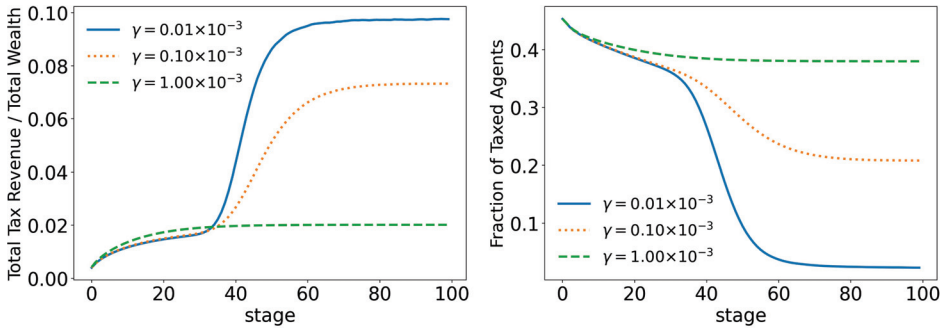

Figure 8. Evolution of total tax revenue and total taxed agents for different values of γ (tax growth rate according to wealth).

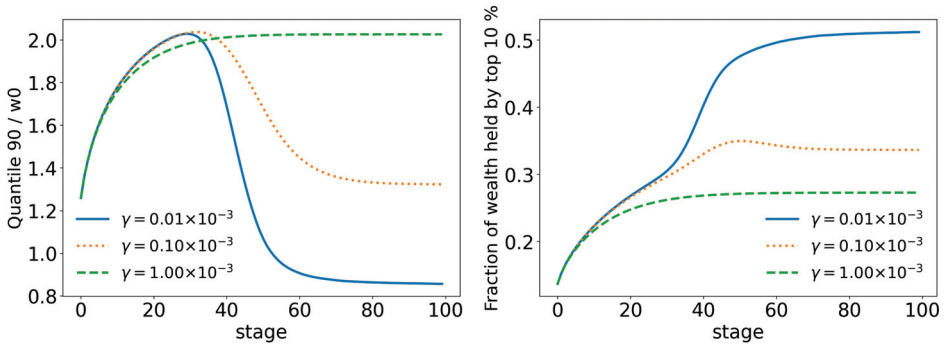

Figure 9. Evolution of the top 10% of agents for different values of γ (tax growth rate according to wealth).

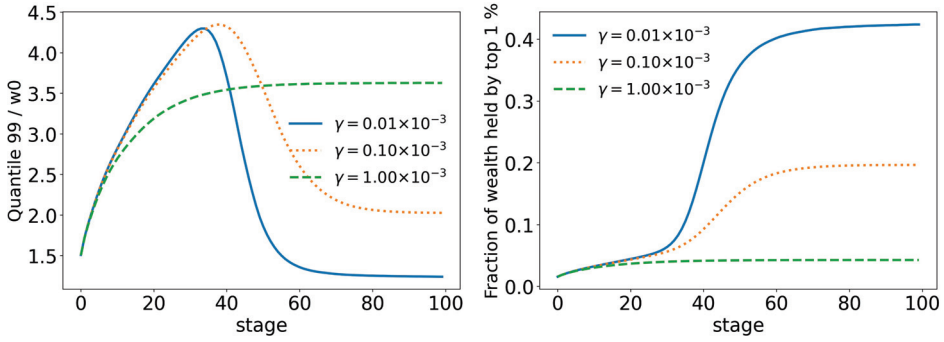

Figure 10. Evolution of the top 1% of agents for different values of γ (tax growth rate according to wealth).

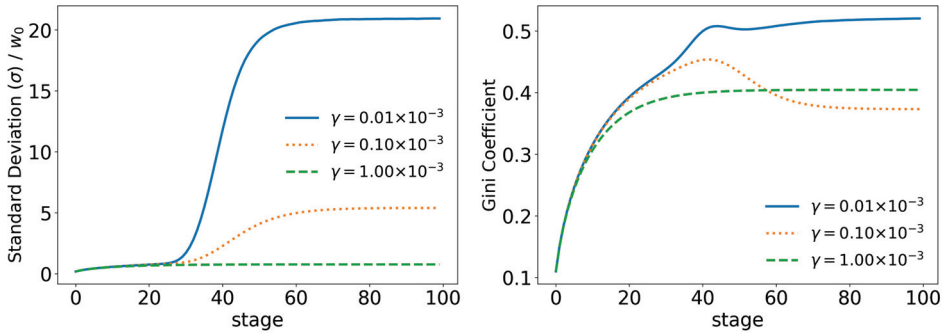

Figure 11. Evolution of the standard deviation (σ) and the Gini coefficient for different values of γ (tax growth rate according to wealth).

3.4. Annual Income Tax Model

This scenario is similar to the model described in Section 3.3, where an agent's bargaining power ($P(w_i|w_j)$) and number of connections are linked ($f_c(w_i)$) to his wealth. The difference in this section is how taxation works. Here, instead of taxing the total wealth of an agent at the end of a stage, we tax the amount the agent earned at the last stage, which we call capital gain or annual income. This is the last scenario we are considering, as it is the closest representation to the taxation most commonly used around the world. Therefore, as a connection function, we use Equation (10); as bargaining power, we use Equation (11); and as taxation, Equation (7) is used. All results presented in this section are for $N = 100{,}000$ averaged over 500 simulations.

3.4.1. Distributions

The evolution of wealth distributions for the scenario with annual income taxation can be seen in Figure 12. In accordance with what we saw in the previous section, the Gibbs and Pareto tail appears again; see Figure 12, stage 30 (for a proper fit, refer to Figure 13). This time, however, we can see an even steeper second Pareto tail at stage 41 (see Figure 14), showing that inequality among the rich (top 0.1%) has increased even more. In addition, we see a reduction in poverty rate between stages 41 and 51, although we have the highest concentration rate so far. However, as the system continues to evolve, not only does inequality seem to keep growing, but so does poverty, with no signs of reaching equilibrium. This is because, since we are taxing only annual earnings, as the ultrarich possess more and more wealth, there is less and less capital gain to be had in interaction with other agents (since the very rich are few), so tax revenues decrease and the welfare state collapses. These numerical results confirm the widespread intuition among many economists that taxation of annual income fails to balance the concentration of income in a country that, with this type of taxation, always tends towards an ever more extreme concentration. Consequently, according to the model, taxation of wealth and not only of annual incomes seems to be an inevitable policy to avoid a growing concentration of income.

Now, analyzing the results of the shift from wealth taxation to taxation on annual earnings, which is the most widely used type of taxation today in most countries, only confirms the most important part of the model—its ability to represent qualitatively real world wealth distributions based on a few very simple assumptions widely spread around the world. Just these few basic assumptions are already sufficient to represent qualitatively the actual wealth distributions. Of course, we can greatly increase the complexity of the model by adding new economic variables, which also increases the number of parameters, all of which have been incorporated in one way or another in the few parameters used in this model, a kind of coarse-grained one. However, we believe that to understand the basic facts behind the unequal distribution of wealth around the world, the advantages that the rich have in trading more and being more likely to win a deal are among the most important and, as we have seem, are already sufficient to reproduce the qualitative

(Pareto) aspects of countries' wealth distributions in general. Wealth concentration, as these scenarios suggest, is an inevitable fact if there are no effective fiscal policies and a redistribution of wealth with priority to low-income agents. This work suggests that the market alone is incapable of properly handling the problem of wealth concentration, which seems to be circumvented only through effective taxation on wealth, at least in the case of equal redistribution of revenues. This is the scenario that the model clearly shows.

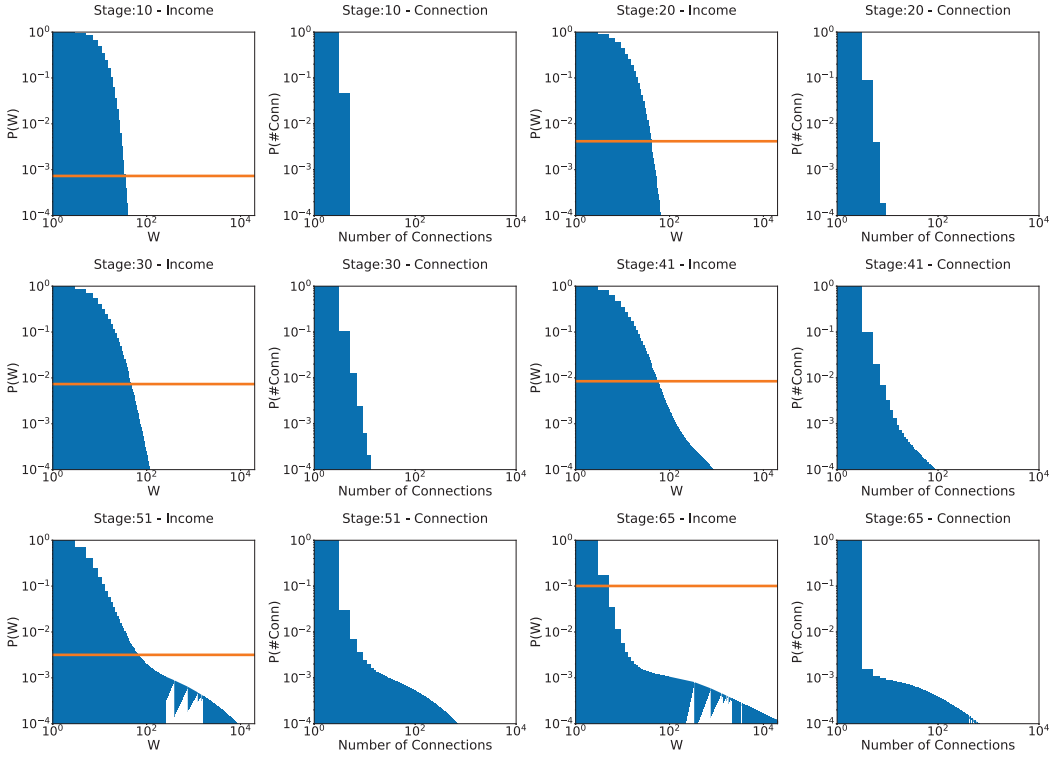

Figure 12. Evolution of probability distributions for the model with capital gain taxation: $\gamma = 0.1$ and $\tau = 0.4$. The orange line is the poverty rate.

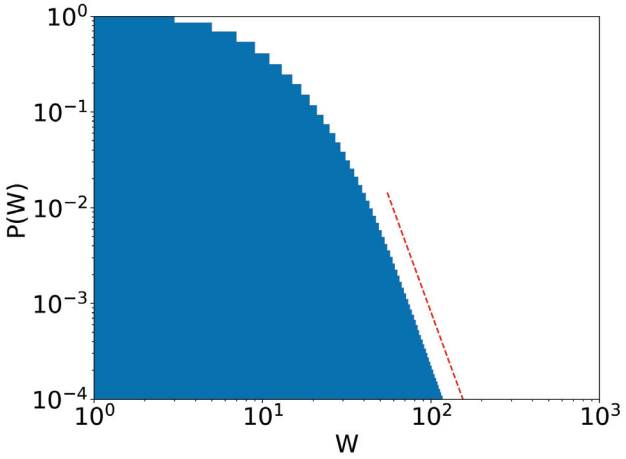

Figure 13. Stage 30 of Figure 12. There is a Pareto tail (dotted red line) with $\alpha = 4.82$.

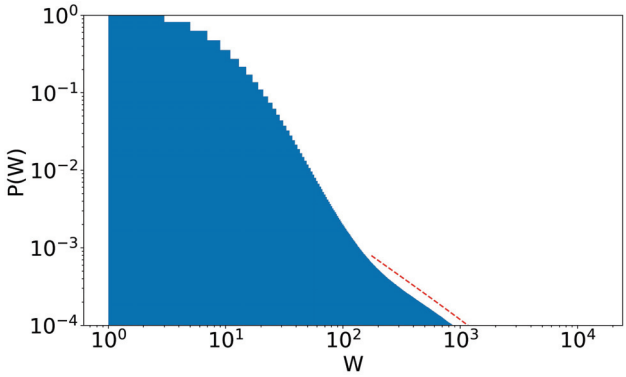

Figure 14. Stage 41 of Figure 12, scenario of annual income taxation. A second Pareto tail appears, with $\alpha = 1.06$ (dotted red line). $\gamma = 1/10$ and $\tau = 0.4$.

3.4.2. Statistics

If we start by looking at the taxes in Figure 15, we already have a good idea of the impact that the upper tax limit (τ) has on the model. We can see that higher tax limits slow down the time evolution of the model at some stages, but that inevitably they all follow the same path. We can also see that due to the new form of taxation, tax revenues are much lower in all stages. The same behavior can be seen in all other statistics: top 10%, Figure 16; top 1%, Figure 17; standard deviation and Gini coefficient, Figure 18. Here, however, the concentration reaches much higher levels, with the richest 1% holding more than 80% of the total wealth of the population in some cases, while Gini coefficients reach more than 0.8.

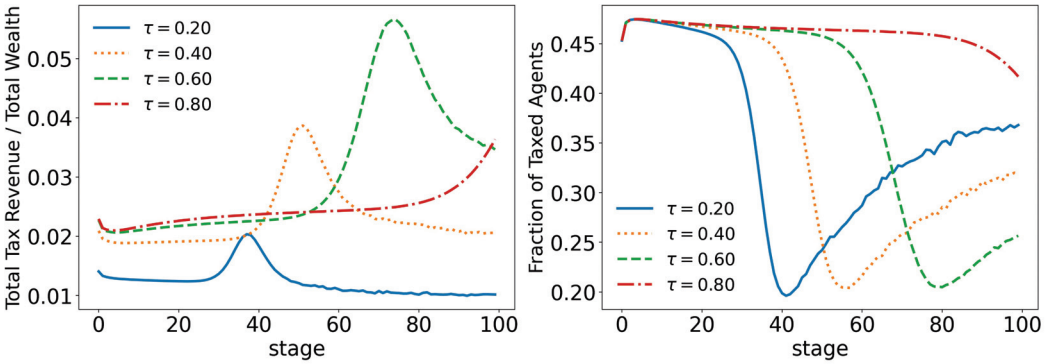

Figure 15. Evolution of total tax revenue and total taxed agents for different values of τ (tax limit). $\gamma = 0.1$.

Moreover, as we saw in the last section, the change among the rich happens in a faster and stronger way. This time, the 90 quantile reaches two times w_0 much earlier (stage 20 vs. stage 40 in the wealth tax model) than before and drops to much lower values: in scenario 3, the lowest value of the 90 quantile is just above $0.8w_0$ (Figure 9), whereas now it is only $0.25w_0$ (Figure 16). A similar trend can also be seen at the 99 quantile (Figure 17). This shows us that the wealth of the population is not, in fact, in the hands of the richest 10% or even the richest 1%, but, actually, in the hands of the 0.0% group (top 0.001%, 0.0001%, 0.00001%, etc.).

Therefore, the impact of the highest level of taxation, τ, does not seem to change the qualitative behavior of the time evolution of the stages; it just delays the same pattern, and it is not a pattern-changing parameter. Then, the important aspects seem to be (i) the value of the parameter γ, (ii) the type of taxation (on wealth or on annual income), and (iii) how the total tax revenue is redistributed (to be analyzed in a future work). All other parameters do not change the tendency of wealth concentration, according to our simulations.

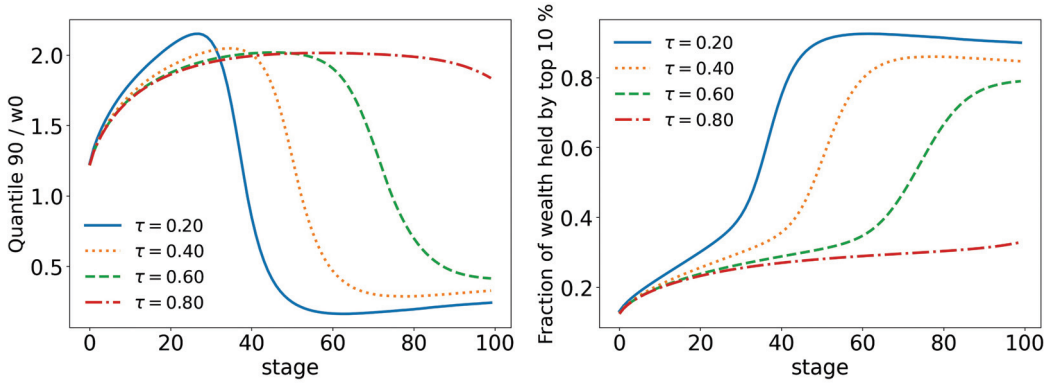

Figure 16. Evolution of the top 10% of agents for different values of τ (tax limit) and $\gamma = 0.1$.

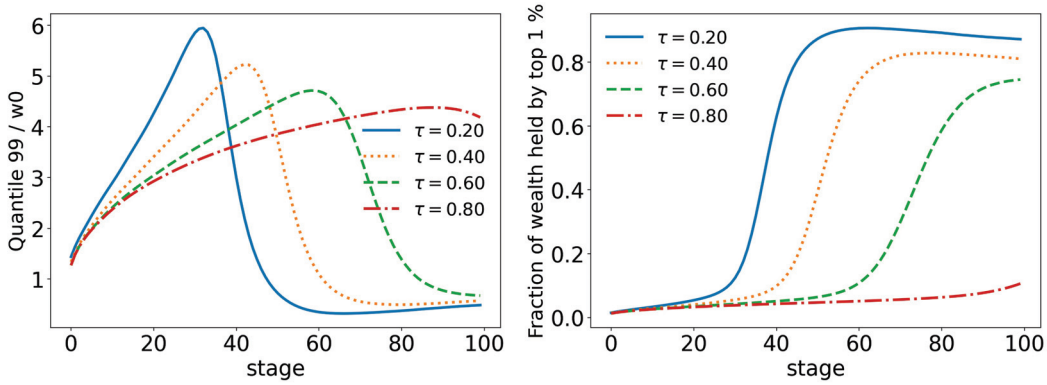

Figure 17. Evolution of the top 1% of agents for different values of τ (tax limit) and $\gamma = 0.1$.

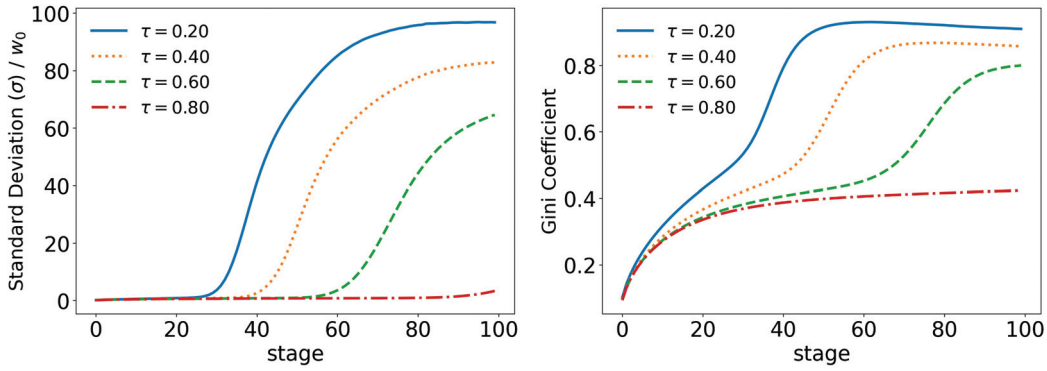

Figure 18. Evolution of the standard deviation (σ) and the Gini coefficient for different values of τ (tax limit) and for $\gamma = 0.1$.

4. Conclusions

We show that a simple model that links wealth with trade and favors the rich in commercial transactions can qualitatively reproduce the current wealth/income distributions, with their middle and poor classes having a Gibbs-type distribution and a Pareto tail for the richest parts of the population. Moreover, we show that for capital gain/annual income taxation, the equilibrium state provided by this model is of extreme concentration, while for a wealth tax, it is possible, depending on the parameter values, to reach an equilibrium state that is not the one of extreme concentration of wealth.

The model also shows us that, first, simply increasing taxes does not necessarily lead to lower rates of inequality, because high tax rates lead to a much smaller number of tax-paying agents, thus decreasing the tax revenue to be redistributed, as in standard economic theory. Therefore, in general, higher taxes lead to lower rates of inequality, but there is a special combination of the parameters where this may not be the case; see Figure 11.

However, while it is important to note that this conclusion about the relationship between higher taxes and inequality would likely change if redistribution favored the poor, its fundamental features are still highly likely to be correct. Second, it also shows us that the lower risks (greater bargaining power) and greater number of opportunities (connections) associated with wealthy agents are a central part of the inequality equation, so it is not simply a matter of taxing these agents more, but reducing these differences as well. A high concentration scenario does not exist when opportunities are equal and/or markets are regulated.

Furthermore, the model also shows us that this extreme concentration/inequality can be avoided by taxing wealth, even at low rates, allowing an effective welfare state to functionally eradicate poverty while allowing a healthy economic elite to exist.

Additionally, we can also state with a certain level of confidence that, given the model's ability to qualitatively reproduce current global trends in economic inequality, as well as its ability to provide results consistent with economic theory, we can understand the current situation based on a few basic assumptions. This means that among the main drivers of inequality, we should consider the problem of unequal opportunities and the difference in risks associated with doing business. Richer agents have much more access to business and a much lower risk rate than the rest of society and, therefore, a much higher probability of winning in any scenario analyzed. The temporal evolution of this scenario leads to growing inequality, inevitably. In addition, the model also makes it very clear that inequality appears naturally and must be actively combated; otherwise, the tendency towards extreme concentration is unstoppable. Therefore, given current global trends, with low taxation, no matter how egalitarian a society may be at the beginning, the system will tend to evolve towards an ever greater concentration.

Moving a little further away from the realm of the model, but based on its findings, we could say that inequality is a problem with multiple origins, but which, at its core, is driven by privileged access to trade and therefore lower risk. However, it is only when this privilege is boundlessly associated with commercial transactions, allowing large corporations to buy and sell as they please, that inequality truly spirals out of control. The market, as we have seen, inevitably creates some level of inequality, which in itself is not a problem if that inequality is not so high. However, when we allow agents with great bargaining power unregulated access to the market, the system truly falls apart.

Looking back while building this model, we also considered much more complex situations, such as distance-based trading advantages between agents, which is also a realistic factor, among others. However, all these more complex alternatives, with many more parameters, exhibited similar behaviors and patterns, making it increasingly clear that the fundamental and simpler characteristics chosen for this model were the driving factors in its behavior.

Finally, the analysis of the effects of unequal redistribution, favoring the poorest, is very important, as it will certainly offer new reasonable scenarios, avoiding the extreme concentration of income we currently see. The study of a hybrid taxation system, in which both taxation on wealth and taxation on annual income coexist, is also an aspect to be considered in future studies.

Author Contributions: Conceptualization, E.M.F.C.; Methodology, E.M.F.C.; Software, M.C.; Investigation, E.M.F.C. and M.C.; Data curation, M.C.; Writing–original draft, M.C.; Writing–review & editing, E.M.F.C.; Project administration, E.M.F.C. All authors have read and agreed to the published version of the manuscript.

Funding: We thank the financial support from the Brazilian scientific agencies Conselho Nacional de Desenvolvimento Científico e Tecnológico (CNPq) and Fundação de Amparo à Pesquisa do Estado do Rio de Janeiro (FAPERJ).

Institutional Review Board Statement: Not applicable.

Data Availability Statement: Not applicable.

Conflicts of Interest: The authors declare no conflict of interest.

References

1. Chakrabarti, B.; Chakraborti, A.; Chakravarty, S.; Chatterjee, A. *Econophysics of Income and Wealth Distributions*, 1st ed.; Cambridge University Press: Cambridge, UK, 2013.
2. Drăgulescu, A.; Yakovenko, V.M. Exponential and power-law probability distributions of wealth and income in the united kingdom and the united states. *Physica A* **2001**, *299*, 213. [CrossRef]
3. Banerjee, A.; Yakovenko, V.M. Universal patterns of inequality. *New J. Phys.* **2010**, *12*, 075032. [CrossRef]
4. Parsson, J.O. *Dying of Money: Lessons of the Great German and American Inflations*, 1st ed.; Dog Ear Publishing: Indianapolis, IN, USA, 2011.
5. Piketty, T. *Capital in the Twenty-First Century*, 1st ed.; The Belknap Press of Harvard University Press: Cambridge, MA, USA, 2014.
6. Lorenz, M.O. *Methods of Measuring the Concentration of Wealth*; American Statistical Association: Alexandria, VA, USA, 1905; Volume 9, pp. 209–219. [CrossRef]
7. Ceriani, L.; Verme, P. The Origins of the Gini Index: Extracts from Variabilità e Mutabilità (1912) by Corrado Gini. *J. Econ. Inequal.* **2012**, *10*, 421. [CrossRef]
8. Chatterjee, A.; Chakrabarti, B.K. Kinetic exchange models for income and wealth distributions. *Eur. Phys. J. B* **2007**, *60*, 135. [CrossRef]
9. Chatterjee, A.; Chakrabarti, B.K. Kinetic market models with single commodity having price fluctuations. *Eur. Phys. J. B* **2006**, *54*, 399. [CrossRef]
10. Chakraborti, A.; Patriarca, M. Variational principle for the pareto power law. *Phys. Rev. Lett.* **2009**, *103*, 228701. [CrossRef] [PubMed]
11. Braunstein, L.A.; Macri, P.A.; Iglesias, J.R. Study of a market model with conservative exchanges on complex networks. *Physica A* **2013**, *392*, 1788. [CrossRef]
12. Drăgulescu, A. Applications of physics to economics and finance: Money, income, wealth, and the stock market. *arXiv* **2003**, arXiv:0307341v2.
13. Queiros, S.M.D.; Anteneodo, C.; Tsallis, C. Power-law distributions in economics: A nonextensive statistical approach. In *Noise and Fluctuations in Econophysics and Finance*; SPIE: Bellingham, WA, USA, 2005; Volume 5848.
14. Aoyama, H.; Nagahara, Y.; Okazaki, M.; Souma, W.; Takayasu, H.; Takayasu, M. Pareto's law for income of individuals and debt of bankrupt companies. *Fractals* **2000**, *8*, 293. [CrossRef]
15. Clementi, F.; Gallegati, M. Pareto's Law of Income Distribution: Evidence for Germany, the United Kingdom, and the United States. In *Econophysics of Wealth Distributions*, 1st ed.; Springer: Milan, Italy, 2005.
16. Siciliani, I.D.; Tragtenberg, M. Kinetic theory and brazilian income distribution. *Physica A* **2019**, *513*, 166. [CrossRef]
17. Saez, E.; Zucman, G. *The Triumph of Injustice: How the Rich Dodge Taxes and How to Make Them Pay*, 1st ed.; W. W. Norton: New York, NY, USA, 2019.
18. Steinbaum, M. *Effective Progressive Tax Rates in the 1950s*; Roosevelt Institute: New York, NY, USA, 2017. Available online: https://rooseveltinstitute.org/2017/08/08/effective-progressive-tax-rates-in-the-1950s/ (accessed on 12 February 2021).
19. Iglesias, J.R.; de Almeida, R.M.C. Entropy and equilibrium state of free market models. *Eur. Phys. J. B* **2012**, *85*, 85. [CrossRef]
20. Tesfatsion, L.; Judd, K. *Handbook of Computational Economics, Vol. 2: Agent-Based Computational Economics*, 1st ed.; Staff General Research Papers; Iowa State University, Department of Economics: Ames, IA, USA, 2006.
21. Moran, J.; Bouchaud, J.-P. May's instability in large economies. *Phys. Rev. E* **2019**, *100*, 032307. [CrossRef] [PubMed]
22. de Oliveira, P. Investment/taxation model: Investors in groups. *Physica A* **2020**, *537*, 122588. [CrossRef]
23. de Oliveira, P. Investment/taxation/redistribution model criticality. *Eur. Phys. J. B* **2020**, *93*, 196. [CrossRef]
24. Iglesias, J.R.; Cardoso, B.-H.F.; Gonçalves, S. Inequality, a scourge of the XXI century. *Commun. Nonlinear Sci. Numer. Simul.* **2021**, *95*, 105646. [CrossRef]
25. Cardoso, B.-H.F.; Iglesias, J.R.; Gonçalves, S. Wealth concentration in systems with unbiased binary exchanges. *Physica A* **2021**, *579*, 126123. [CrossRef]
26. Cardoso, B.-H.F.; Gonçalves, S.; Iglesias, J.R. Wealth distribution models with regulations: Dynamics and equilibria. *Physica A* **2020**, *551*, 124201. [CrossRef]
27. de Oliveira, P.M.C. Rich or poor: Who should pay higher tax rates? *Eur. Phys. Lett.* **2017**, *119*, 40007. [CrossRef]
28. Fujiwara, Y.; Souma, W.; Aoyama, H.; Kaizoji, T.; Aoki, M. Growth and fluctuations of personal income. *Physica A* **2003**, *321*, 598. [CrossRef]

entropy

MDPI

Article

Taxes, Inequality, and Equal Opportunities

José Roberto Iglesias [1,2,3,*,†], Ben-Hur Francisco Cardoso [4,†] and Sebastián Gonçalves [1,†]

[1] Instituto de Física, Universidade Federal do Rio Grande do Sul, Porto Alegre 91501-970, RS, Brazil; sgonc@if.ufrgs.br
[2] Instituto Nacional de Ciência e Tecnologia de Sistemas Complexos, CBPF, Rio de Janeiro 22290-180, RJ, Brazil
[3] Escola de Gestão e Negócios, Programa de Pós-Graduação em Economia, UNISINOS, Porto Alegre 91330-002, RS, Brazil
[4] Departamento de Economia e Relações Internacionais, Universidade Federal de Santa Catarina, Florianópolis 88015-400, SC, Brazil; benhur.phys@gmail.com
* Correspondence: joseroberto.iglesias@gmail.com
† These authors contributed equally to this work.

Abstract: Extreme inequality represents a grave challenge for impoverished individuals and poses a threat to economic growth and stability. Despite the fulfillment of affirmative action measures aimed at promoting equal opportunities, they often prove inadequate in effectively reducing inequality. Mathematical models and simulations have demonstrated that even when equal opportunities are present, wealth tends to concentrate in the hands of a privileged few, leaving the majority of the population in dire poverty. This phenomenon, known as condensation, has been shown to be an inevitable outcome in economic models that rely on fair exchange. In light of the escalating levels of inequality in the 21st century and the significant state intervention necessitated by the recent COVID-19 pandemic, an increasing number of scholars are abandoning neo-liberal ideologies. Instead, they propose a more robust role for the state in the economy, utilizing mechanisms such as taxation, regulation, and universal allocations. This paper begins with the assumption that state intervention is essential to effectively reduce inequality and to revitalize the economy. Subsequently, it conducts a comparative analysis of various taxation and redistribution mechanisms, with a particular emphasis on their impact on inequality indices, including the Gini coefficient. Specifically, it compares the effects of fortune and consumption-based taxation, as well as universal redistribution mechanisms or targeted redistribution mechanisms aimed at assisting the most economically disadvantaged individuals. The results suggest that fortune taxation are more effective than consumption-based taxation to reduce inequality.

Keywords: econophysics; exchange models; inequality

Citation: Iglesias, J.R.; Cardoso, B.-H.F.; Gonçalves, S. Taxes, Inequality, and Equal Opportunities. *Entropy* **2023**, *25*, 1346. https://doi.org/10.3390/e25091346

Academic Editor: Damián H. Zanette

Received: 3 July 2023
Revised: 4 September 2023
Accepted: 14 September 2023
Published: 16 September 2023

1. Introduction

In capitalist economies, social and economic inequality has become an ingrained characteristic. While a certain degree of inequality can serve as a motivator for individuals to strive for progress, excessive inequality poses a significant barrier to the fundamental driver of the economy: trade. Consequently, individuals in dire poverty are marginalized from participating in economic transactions, resulting in reduced circulation of money and diminished consumption of goods. From the insights of Adam Smith [1] to the perspectives of contemporary neo-liberals [2], including proponents of the Austrian School and minimal state intervention [3], orthodox economic theory has long posited that the inherent mechanisms of the market will naturally alleviate disparities in wealth. This theory argues that by providing individuals with opportunities for advancement, everyone will have a chance to improve their circumstances, thereby reducing inequality [4]. One of the early studies in income distribution was developed by Italian economist Vilfredo Pareto [5].

Pareto's analysis of income data from the 19th century revealed a striking phenomenon: income distribution follows a power law, with the exponent now known as the Pareto exponent. He went beyond this observation, asserting that the non-Gaussian nature of income distribution suggested that individuals or enterprises took deliberate actions leading to higher income. This notion still finds support today, despite the fact that there are more critics of meritocracy [6,7] than proponents. In any case, a persistent hypothesis prevails in capitalist societies: that with "equal opportunities", individuals of sufficient intelligence and effort can ascend the social pyramid.

Nevertheless, the current state of affairs deviates markedly from this idyllic conception. Recent data from the USA paint a highly contrasting picture: a mere 1% of the economic elite possesses almost half (50%) of the total wealth, with the top quantile (20%) of the population owns a overwhelming 88% of available resources, as indicated by Wolff's research in 2017 [8]. As highlighted by Piketty [7], the chronological progression of the wealthiest segment of society's assets expands at a swifter pace than the overall economy. Adding to this stark reality, the once-promising notion of social mobility stands exposed as a mere illusion, as considerable fortunes persist through the channels of inheritance, as highlighted in Fernholz's work in 2023 [9].

Even simple exchange models used in econophysics to simulate trade and economic exchanges demonstrate this phenomenon. In two recent papers [10,11], we have demonstrated that exchange models considered *fair*, where agents participating in trade have equal chances of earning money, inevitably lead to the total concentration of wealth in the hands of a single individual or a select few. Moreover, most microscopic models of exchange among economic agents exhibit this behavior (see ref. [12]).

These models consider an ensemble of interacting agents that exchange a fixed or random amount of their total wealth. The exchanged wealth is susceptible to several interpretations. It could be the money given for some service or commodity or an *error* during the exchange [13], and it may be attributed to a profit or *plus valia*. Analogous to physical systems where particles exchange energy through binary conservative collisions, these models [14–17] consider a set of interacting agents that exchange wealth. If the exchanged amount of wealth is a random fraction of the wealth of each agent, the resulting wealth distribution follows a Gibbs exponential distribution [17]. However, such models lack fairness, as the values each agent puts at stake may differ significantly.

One of the most used models of wealth exchange among economic agents is the so-called Yard-Sale model. This model, in its original version, is a fair model because each agent has the same possibility of winning the same amount of money. The basic idea is that no one can receive, in any trade, more than he/she is putting at stake during the exchange.

Numerical [12] and analytical [18] results with the Yard-Sale model, or some variations of it, point to *condensation*, i.e., a continuous concentration of all available wealth in just one or a few agents, leading to an absorbing state where no more wealth is exchanged [10]. The phenomenon of *condensation*, while well-known to experts in the field, might appear to challenge a fundamental principle of thermodynamics because it leads to a situation seemingly at odds with the second law of thermodynamics. In the conventional Kinetic Theory of Gases, as formulated by Boltzmann, random energy exchanges propel the system towards the equal distribution of energy, culminating in a state of maximum entropy. However, when energy (or wealth) exchanges are restricted from exceeding the inherent energy, a distinct scenario unfolds. This outcome corresponds to a state of minimum entropy or, conversely, maximum information. While the second law predicts a *thermal death of the universe*, characterized by the uniform distribution of energy and a uniform temperature, alternative models of equitable exchange envision a *thermal death of trade*, marked by large disparities in wealth (comparable to temperature differences), ultimately leading to a cessation of trade. Nevertheless, the current path of the global economy, characterized by the persistent growth of inequality [7], seems to bring us uncomfortably close to this ominous scenario.

Different modifications have been introduced in the Yard-Sale model to overcome condensation. For example, increasing the probability of favoring the poorest agent in a transaction [19,20] or introducing a taxation mechanism [13,21,22], wherein all agents periodically contribute taxes, and the collected amount is subsequently distributed among them. This approach closely resembles real-world political systems adopted by various countries. Therefore, our focus will be on examining the impact of taxes on wealth redistribution and inequality reduction.

In the following section, we will describe the exchange model we are going to use, i.e., the Yard-Sale model. In Section 3, we review previous findings with taxation on wealth; in Section 4, we present the novel results with taxation on exchanges and redistribution, and the impact in reducing inequality.

2. The Model

We consider an ensemble of interacting economic agents, where two of them are selected sequentially and at random to exchange a predetermined fraction of their wealth. Agents do not risk all of their capital in each exchange, but they save a fraction, which depends on their risk aversion [19,20,23–26]. Therefore, the attributes of each agent i are the risk-aversion factor β_i and its wealth w_i. Both are initially drawn from random uniform distributions in the $[0, 1)$ interval (for the exchange-tax system, we use another distribution for β, that is the same value for all agents, therefore becoming a parameter of the model, which is varied to check on its effect), but while β_i stays constant for each agent, w_i (simulations are insensitive to the initial distribution of w_i) changes because of exchanges involving that agent.

It is worth noting that certain models introduce the possibility of wealth creation or destruction during these exchanges [27]. However, for the purposes of our discussion, we will limit ourselves to conservative models, where the total wealth remains constant.

Let us assume an exchange of wealth between agents i and j. Supposing that i wins an amount of wealth from j; we have that

$$w_i^* = w_i + dw \;\text{ and }\; w_j^* = w_j - dw,$$

where $w^*_{i(j)}$ is the wealth of the agent $i(j)$ after the exchange.

The most widely used rule to determine the quantity dw transferred from the loser to the winner is the *fair* one, which states that $dw = \min[(1-\beta_i)w_i(t); (1-\beta_j)w_j(t)]$. It is considered *fair* because the amount of wealth exchanged is the minimum of the quantities risked by the two agents and the same regardless of who wins, and it is the basis of the Yard-Sale model [28].

As we stressed before, numerical and analytical studies with the Yard-Sale model, as well as its variations, consistently lead to condensation. Recently, we have given a general proof that all models following a *fair* principle, including the Yard-Sale, inevitably lead to condensation [10,11]. To overcome this fate, different rules of interaction have been applied, for example increasing the probability of favoring the poorer agent in a transaction [19,20] or introducing a cut-off that avoids interactions between agents below and above this cut-off [29]. One particular choice is to use a rule suggested by Scafetta [12,19], where, in the exchange between the agents i and j, the probability of favoring the poorer partner is given by the following:

$$p = \frac{1}{2} + f \times \frac{|w_i(t) - w_j(t)|}{w_i(t) + w_j(t)}, \tag{1}$$

and f is a factor that we call the *social protection* factor, which goes from 0 (equal probability for both agents) to $1/2$ (highest probability of favoring the poorer agent). In each interaction, the poorer agent has a probability p of earning a quantity dw, whereas the richer one has a probability of $1 - p$. It is evident that the higher the difference in wealth in a given pair of agents, the higher the influence of f in the probability; thus, f is a good indicator of the

degree of application of social policies of wealth distribution. This rule have been studied in full generality in some previous articles [12,30].

We have provided a concise overview of the impacts of the social protection factor. For a more in-depth examination of this approach to diminishing inequality, we direct interested readers to the comprehensive review by Chakraborti et al. [31,32].

While this simple mechanism helps to reduce inequality, some critics argue that real-world exchanges tend to favor wealthier agents. In addition, a consensus has not yet been reached on how to accurately correlate the protection factor with tangible economic measures. Consequently, it seems that a more logical way to reduce inequality is through the redistribution of the taxes collected. Therefore, we will focus on the effects of taxes. In the next section, we will delve into the simplest tax system: tax on wealth.

3. Taxes on Fortune

In this section, we present previously published results [33] concerning the implementation of a simple flat tax on wealth. Our simulation revolves around a society consisting of N agents who engage in wealth exchanges based on the Yard-Sale model. At each time-step, two agents are randomly selected, facilitating a monetary exchange where one participant emerges as the winner while the other becomes the loser. Regarding the tax collection mechanism in our simulation, it operates as follows: after every Monte Carlo Step (MCS), i.e., following $N/2$ exchanges, all agents contribute the same fraction λ of their wealth as taxes. (It is worth noting that the wealth tax shares similarities with property or fortune taxes, albeit being less prevalent than income taxes.) Consequently, the redistribution of money can manifest in two distinct ways: a universal allocation, wherein funds are distributed evenly among the entire population, or a focused approach, wherein the funds are specifically directed towards individuals with lower wealth.

All results presented here are averages over 10^3 samples for three system sizes N: $10^3, 10^4$, and 10^5. As the obtained results are almost independent of the size, we have plotted just the outcome for $N = 10^5$ and $N = 10^4$ agents. The saving propensity factor β, as well as the initial wealth of each agent, are chosen at random from a uniform probability distribution in the interval $(0, 1)$. While the individual wealth changes along the simulation because on the exchange interactions, the saving factor of each agents is fixed.

3.1. Universal Redistribution

The most straightforward type of redistribution is universal, wherein the entire tax revenue collected is distributed equally among all individuals, irrespective of their wealth. Similar taxation mechanisms have been proposed in prior studies [13,21], albeit with the assumption of β values close to 1 and in the context of the small transaction limit approximation. Notwithstanding these differences, our findings, which have been published elsewhere [33], qualitatively correspond with prior research; they show that the Gini index decreases as the tax percentage increases, as expected; so, the taxation mechanism can effectively mitigate inequality. However, the effect of the tax percentage is non monotonic; indeed, it is more effective at small values. Effectively, 10% of taxes makes a huge change in the Gini index, lowering it from 1 (no taxes) to 0.5, while increasing taxes up to 25% lowers the Gini index to 0.3. More details on the quantitative effect of the universal taxes on the Gini index can be seen in Figure 1-right, (blue curve). We cannot expect, in real societies, a tax percentage above 25%. Recent contributions [22,34] have explored related systems of universal redistribution, where the tax percentage depends on wealth.

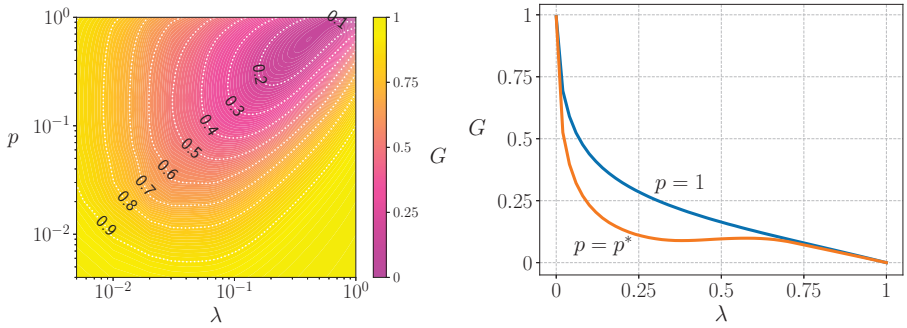

Figure 1. (**Left**): Gini index represented as a heat map plus iso-Gini curves, as a function of the tax fraction (λ) and the bottom fraction of agents that receive the collected taxes (p). (**Right**): Gini index as a function of λ for $p = 1$ (universal case) and $p = p^*$ (optimal targeted case). Both figures were obtained for a system of $N = 10^4$ agents (from ref. [33]).

3.2. Focused Redistribution

In the targeted scenario, the total tax collection is distributed among the p poorest fraction of the population, referred to as the targeted population. The universal case corresponds to $p = 1$. Figure 1-left illustrates the relationship between the Gini index and both λ and p. Notably, when the allocation is limited to less than 1% of the population ($p \leq 10^{-2}$), which aligns with many governmental initiatives aimed at assisting the unemployed and extremely impoverished individuals, the impact on the Gini coefficient is almost negligible. To achieve a noticeable effect in reducing inequality, it becomes necessary to extend assistance to at least the poorest 3–4% of the population. Additionally, Figure 1 reveals an optimal value of $p = p^*$ that minimizes inequality for each tax rate λ, indicating an intriguing non-trivial relationship between λ and p in this context.

Finally, in Figure 1-right, we compare the Gini index as a function of λ for two cases: $p = 1$ (universal case) and $p = p^*$ (optimal targeted case). Notably, for intermediate values of λ, particularly around $\lambda \approx 0.3$, the regulatory mechanism of assisting only a fraction of the population proves to be more effective in significantly reducing inequality.

4. Taxes on Exchanges

One common taxation in many countries is the VAT (value-added tax), or IVA in Spanish-speaking countries. A slightly different tax, called ICMS (tax on the circulation of goods and services) is applied in Brazil. This is a tax that everybody pays when buying goods or paying for services.

We simulate the VAT system by taxing each exchange with a fixed percentage on the exchanged quantity dw. In practice, the tax collection works as follows: two agents, i and j, are randomly selected to exchange wealth in such a way that agent j will lose an amount of wealth $(1-\beta)\min(w_i, w_j)$ while agent i will receive this value reduced by a factor $(1-\lambda)$. Thus,

$$w_i^* = w_i + (1-\lambda)(1-\beta)\min(w_i, w_j) \quad \text{and} \quad w_j^* = w_j - (1-\beta)\min(w_i, w_j), \tag{2}$$

where λ is the tax rate. The collected taxes $\lambda(1-\beta)\min(w_i, w_j)$ of each exchange are accumulated during one MCS, that is, along $N/2$ exchanges. After this period, the collected taxes are equally distributed among all agents. We denote the liquidity of the system L as the total value received by the agents in exchanges along one MCS. The reader may have already noticed that here, we make use of a constant and universal saving factor β, in order to simplify the calculations. But, there are no obstacles to using an individual β_i for each agent.

As before, we again use the Gini index to measure inequality. We show in Figure 2 the Gini index as a function of the tax fraction λ for different values of β. We observe that the higher the tax rate, the lower the inequality, as expected, and inequality also decreases if

the risk aversion increases, similarly to what was obtained in the models without taxes. In the trivial case ($\lambda = 0$), we recover the $G = 1$ result (condensation).

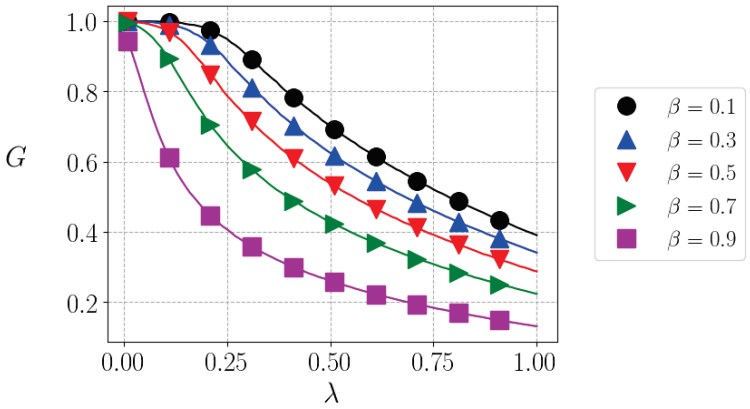

Figure 2. Equilibrium Gini index as a function of λ, the tax index, for different values of β. Lines correspond to simulations with $N = 10^4$ agents and symbols, with $N = 10^5$.

In Figure 3, we depict the liquidity as a function of λ, for different values fo β. Here, an interesting feature is observed. While the behavior of liquidity with β is not simple, it generally decreases as the risk aversion increases, which is expected. However, for each value of β, there is an optimum value of $\lambda = \lambda^*$, such that the liquidity $L = L^*$ is maximum—and inequality is minimum. It is clear that very low or very high taxes are a burden to trade; therefore, an intermediary, not trivial value appears as a function of β to maximize liquidity. Nevertheless, such maximization has to be counterbalanced with the minimization of the Gini index. In the next figure, Figure 4, we show that the optimum tax rate (λ^*) decreases as a function of β.

Finally, in Figure 5, we show how the Gini index and liquidity behave as a function of β, when the optimum tax rate is applied. We can observe a a trade-off between equality and liquidity for different values of β.

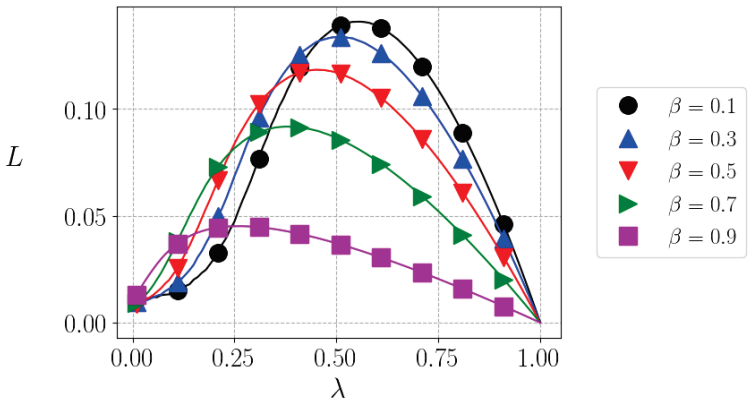

Figure 3. Equilibrium liquidity as a function of λ, the tax index, for different values of β. Lines correspond to simulations with $N = 10^4$ agents and symbols, with $N = 10^5$.

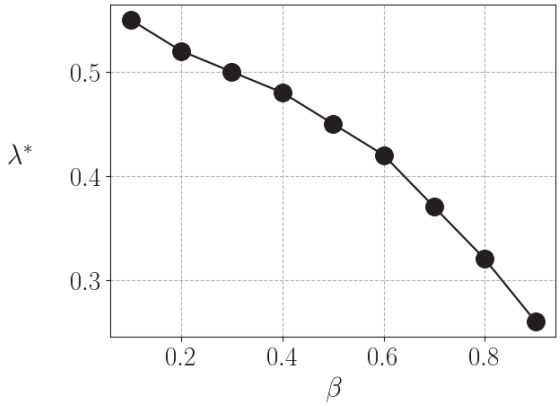

Figure 4. Optimum value of λ as a function of d β. The line is just a guide for the eyes, points are the results of the simulations for different values of β.

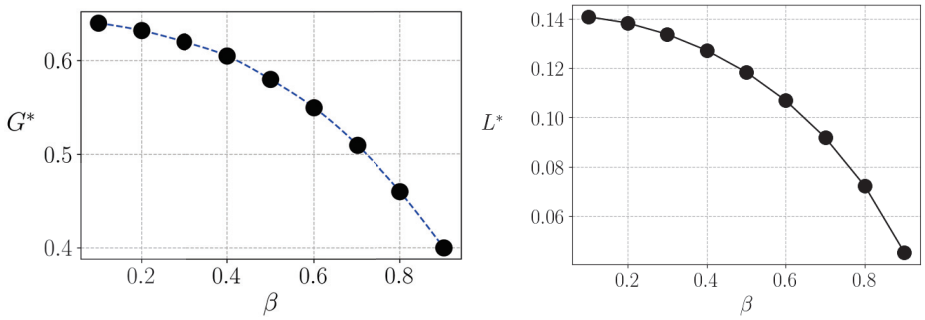

Figure 5. Equilibrium Gini index (**left**) and liquidity (**right**) at $\lambda = \lambda^*$ as a function of β. Lines are just guides for the eyes, points are the results of the simulations for different values of β.

5. Discussion and Conclusions

Recent studies in the field of econophysics have unveiled an intriguing phenomenon: fair models that allocate equal chances of winning to individuals may, in fact, result in maximum inequality. This implies that despite initially equal opportunities, there is a need for redistribution mechanisms to ensure greater equality in outcomes.

In this article, we delve into the topic of taxation and explore how different taxation mechanisms can contribute to reducing inequality. Specifically, we juxtapose the findings of earlier research [10]—which delved into wealth taxes—with the concept of transaction taxes—akin to a value-added tax (VAT) on consumption. Taxation can be a potent tool for redistributing wealth and resources from the affluent to the less privileged. However, the type of taxation system implemented can have vastly different impacts on the level of inequality in society.

Through our research, we analyze various types of taxation models, including a flat wealth tax with universal and directed redistribution, as well as a wealth-transaction tax with universal redistribution.

Our research has identified that a small fraction of wealth tax can significantly contribute to reducing inequality. Our analysis reveals that by implementing targeted redistribution mechanisms that specifically cater to the poorest individuals in society, the impact of wealth tax can be even stronger. By providing resources and support to those who are most in need, we can foster greater social and economic equality.

However, while a higher tax rate consistently leads to a decrease in inequality, the volume of economic activity follows an inverted U-shaped curve in response to changes in the tax rate. In other words, we can identify an optimal tax rate that maximizes economic activity. Nevertheless, the specific optimal tax rate varies depending on the average saving rate of individuals in a society. We have obtained an optimal tax rate that can range from 0.25 to 0.55, depending on the average saving rate.

When analyzing the outcomes, it is crucial to acknowledge that we are working within a basic fair exchange model. Despite retaining the fundamental aspects of trade, this model does not encompass goods production or economic expansion. These constraints mean that while the impact of taxes and redistribution evidently diminishes inequality, as seen in the practices of certain nations through social allocations, the numerical outcomes should be considered as instructive rather than definitive predictions.

To sum up, even though equitable models that distribute equal opportunities might seem just, they can paradoxically lead to heightened disparities in actual outcomes. This research underscores the importance of adopting efficient redistribution mechanisms, such as levying wealth taxes on both wealth and transactions—where the former proves more effective than the latter—in order to foster heightened levels of societal and economic parity.

Author Contributions: Conceptualization, J.R.I.; Methodology, J.R.I., B.-H.F.C. and S.G.; Software, B.-H.F.C.; Validation, B.-H.F.C. and S.G.; Formal analysis, J.R.I., B.-H.F.C. and S.G.; Investigation, J.R.I., B.-H.F.C. and S.G.; Data curation, B.-H.F.C.; Writing—original draft, J.R.I. and S.G.; Writing—review & editing, J.R.I., B.-H.F.C. and S.G.; Visualization, B.-H.F.C.; Supervision, J.R.I.; Project administration, S.G. All authors have read and agreed to the published version of the manuscript.

Funding: B.-H.F.C. acknowledges the Brazilian agency Conselho Nacional de Desenvolvimento Científico e Tecnológico (CNPq) for the scholarship. J.R.I. and S.G. acknowledge Brazilian agency Conselho Nacional de Desenvolvimento Científico e Tecnológico (CNPq) for support. S.G. acknowledges FAPERGS-Brazil for PqG-19/2551-0001973-4.

Institutional Review Board Statement: Not applicable.

Data Availability Statement: On request to benhur.phys@gmail.com.

Conflicts of Interest: The authors declare no conflict of interest.

References

1. Smith, A. *The Wealth of Nations: An Inquiry into the Nature and Causes of the Wealth of Nations*; Harriman House Limited: Petersfield, UK, 2010.
2. Hoover, K. *The New Classical Macroeconomics*; Edward Elgar Publishing: Cheltenham, UK, 1992.
3. Hayek, F.A. *The Road to Serfdom: Text and Documents—The Definitive Edition*; University of Chicago Press: Chicago, IL, USA, 2009; Volume 2.
4. Rassekh, F. The convergence hypothesis: History, theory, and evidence. *Open Econ. Rev.* **1998**, *9*, 85–105. [CrossRef]
5. Pareto, V. *Cours d'Économie Politique*; Rouge: Lausanne, Switzerland, 1897.
6. Sandel, M.J. *The Tyranny of Merit: What's Become of the Common Good?* Picador Paper: New York, NY, USA, 2021.
7. Piketty, T. *Capital in the 21st Century*; Harvard University Press: Cambridge, MA, USA, 2014.
8. Wolff, E.N. *Household Wealth Trends in the United States, 1962 to 2016: Has Middle Class Wealth Recovered?* Technical report; National Bureau of Economic Research: Cambridge, MA, USA, 2017.
9. Fernholz, R.T.; Hagler, K. Rising Inequality and Declining Mobility in the Forbes 400. *Econ. Lett.* **2023**, *230*, 111235. [CrossRef]
10. Cardoso, B.H.F.; Iglesias, J.R.; Gonçalves, S. Wealth concentration in systems with unbiased binary exchanges. *Phys. A Stat. Mech. Its Appl.* **2021**, *579*, 126123. [CrossRef]
11. Cardoso, B.H.F.; Gonçalves, S.; Iglesias, J.R. Why equal opportunities lead to maximum inequality? The wealth condensation paradox generally solved. *Chaos Solitons Fractals* **2023**, *168*, 113181. [CrossRef]
12. Caon, G.; Gonçalves, S.; Iglesias, J. The unfair consequences of equal opportunities: Comparing exchange models of wealth distribution. *Eur. Phys. J. Spec. Top.* **2007**, *143*, 69–74. [CrossRef]
13. Li, J.; Boghosian, B.M.; Li, C. The Affine Wealth Model: An agent-based model of asset exchange that allows for negative-wealth agents and its empirical validation. *Phys. A Stat. Mech. Its Appl.* **2019**, *516*, 423–442. [CrossRef]
14. Ispolatov, S.; Krapivsky, P.L.; Redner, S. Wealth distributions in asset exchange models. *Eur. Phys. J. B Condens. Matter Complex Syst.* **1998**, *2*, 267–276. [CrossRef]
15. Boghosian, B.M.; Devitt-Lee, A.; Johnson, M.; Li, J.; Marcq, J.A.; Wang, H. Oligarchy as a phase transition: The effect of wealth-attained advantage in a Fokker–Planck description of asset exchange. *Phys. A Stat. Mech. Its Appl.* **2017**, *476*, 15–37. [CrossRef]
16. Patriarca, M.; Heinsalu, E.; Chakraborti, A. Basic kinetic wealth-exchange models: Common features and open problems. *Eur. Phys. J. B* **2020**, *10*, 186. [CrossRef]
17. Yakovenko, V.M.; Rosser, J.B. Colloquium: Statistical mechanics of money, wealth, and income. *Rev. Mod. Phys.* **2009**, *81*, 1703. [CrossRef]

18. Moukarzel, C.F.; Gonçalves, S.; Iglesias, J.R.; Rodríguez-Achach, M.; Huerta-Quintanilla, R. Wealth condensation in a multiplicative random asset exchange model. *Eur. Phys. J. Spec. Top.* **2007**, *143*, 75–79. [CrossRef]
19. Scafetta, N.; Picozzi, S.; West, B.J. Pareto's law: A model of human sharing and creativity. *arXiv* **2002**, arXiv:cond-mat/0209373.
20. Iglesias, J.R.; Gonçalves, S.; Pianegonda, S.; Vega, J.L.; Abramson, G. Wealth redistribution in our small world. *Phys. A Stat. Mech. Its Appl.* **2003**, *327*, 12–17. [CrossRef]
21. Bustos-Guajardo, R.; Moukarzel, C.F. Wealth distribution under Yard-Sale exchange with proportional taxes. *Int. J. Mod. Phys. C* **2016**, *27*, 1650094. [CrossRef]
22. Lima, H.; Vieira, A.R.; Anteneodo, C. Nonlinear redistribution of wealth from a Fokker-Planck description. *arXiv* **2020**, arXiv:2007.11680.
23. Sinha, S. Stochastic maps, wealth distribution in random asset exchange models and the marginal utility of relative wealth. *Phys. Scr.* **2003**, *2003*, 59. [CrossRef]
24. Chatterjee, A.; Chakrabarti, B.K.; Manna, S. Pareto law in a kinetic model of market with random saving propensity. *Phys. A Stat. Mech. Its Appl.* **2004**, *335*, 155–163. [CrossRef]
25. Chakraborti, A.; Chakrabarti, B.K. Statistical mechanics of money: How saving propensity affects its distribution. *Eur. Phys. J. B Condens. Matter Complex Syst.* **2000**, *17*, 167–170. [CrossRef]
26. Patriarca, M.; Chakraborti, A.; Kaski, K. Statistical model with a standard Γ distribution. *Phys. Rev. E* **2004**, *70*, 016104. [CrossRef]
27. Quevedo, D.S.; Quimbay, C.J. Non-conservative kinetic model of wealth exchange with saving of production. *Eur. Phys. J. B* **2010**, *73*, 145–153. [CrossRef]
28. Hayes, B. Computing science: Follow the money. *Am. Sci.* **2002**, *90*, 400–405. [CrossRef]
29. Das, A.; Yarlagadda, S. An analytic treatment of the Gibbs–Pareto behavior in wealth distribution. *Phys. A Stat. Mech. Its Appl.* **2005**, *353*, 529–538. [CrossRef]
30. Cardoso, B.H.F.; Gonçalves, S.; Iglesias, J.R. Wealth distribution models with regulations: Dynamics and equilibria. *Phys. A Stat. Mech. Its Appl.* **2020**, *551*, 124201. [CrossRef]
31. Chakraborti, A.; Muni Toke, I.; Patriarca, M.; Abergel, F. Econophysics review: I. Empirical facts. *Quant. Fin.* **2011**, *11*, 991–1012. [CrossRef]
32. Chakraborti, A.; Muni Toke, I.; Patriarca, M.; Abergel, F. Econophysics review: II. Agent-based models. *Quant. Fin.* **2011**, *11*, 1013–1041. [CrossRef]
33. Iglesias, J.R.; Cardoso, B.H.F.; Gonçalves, S. Inequality, a scourge of the XXI century. *Commun. Nonlinear Sci. Numer. Simul.* **2021**, *95*, 105646. [CrossRef]
34. De Oliveira, P.M.C. Rich or poor: Who should pay higher tax rates? *EPL (Europhys. Lett.)* **2017**, *119*, 40007. [CrossRef]

entropy

MDPI

Article

A Hybrid Opinion Formation and Polarization Model

Baizhong Yang [1], Quan Yu [2,3,*] and Yi Fan [2,3]

[1] School of Mathematics and Statistic, Guizhou University, Guiyang 550025, China
[2] School of Mathematics and Statistic, Qiannan Normal University for Nationalities, Duyun 558000, China
[3] Key Laboratory of Complex Systems and Intelligent Optimization of Guizhou Province, Duyun 558000, China
* Correspondence: quanyu@sgmtu.edu.cn

Abstract: The last decade has witnessed a great number of opinion formation models that depict the evolution of opinions within a social group and make predictions about the evolution process. In the traditional formulation of opinion evolution such as the DeGroot model, an agent's opinion is represented as a real number and updated by taking a weighted average of its neighbour's opinions. In this paper, we adopt a hybrid representation of opinions that integrate both the discrete and continuous nature of an opinion. Basically, an agent has a 'Yes', 'Neutral' or 'No' opinion on some issues of interest and associates with its Yes opinion a support degree which captures how strongly it supports the opinion. With such a rich representation, not only can we study the evolution of opinion but also that of support degree. After all, an agent's opinion can stay the same but become more or less supportive of it. Changes in the support degree are progressive in nature and only a sufficient accumulation of such a progressive change will result in a change of opinion say from Yes to No. Hence, in our formulation, after an agent interacts with another, its support degree is either strengthened or weakened by a predefined amount and a change of opinion may occur as a consequence of such progressive changes. We carry out simulations to evaluate the impacts of key model parameters including (1) the number of agents, (2) the distribution of initial support degrees and (3) the amount of change of support degree changes in a single interaction. Last but not least, we present several extensions to the hybrid and progressive model which lead to opinion polarization.

Keywords: opinion dynamics; opinion formation; opinion polarization

Citation: Yang, B.; Yu, Q.; Fan, Y. A Hybrid Opinion Formation and Polarization Model. *Entropy* **2022**, *24*, 1692. https://doi.org/10.3390/e24111692

Academic Editor: José Roberto Iglesias

Received: 23 October 2022
Accepted: 14 November 2022
Published: 19 November 2022

1. Introduction

In social life, opinions and beliefs significantly affect human choices and also drive their actions [1]. Therefore, it is important to understand opinion dynamics, i.e., the evolution process of opinion spreading and forming in social networks. Opinion dynamics can be applied in various aspects [2–8]. For example, in political elections, Bravomarquez et al. [9] conducted an empirical study on the opinion time series in the 2008 American election by using Twitter data. In market research, Castro et al. [10] proposed a recommendation system based on opinion dynamics to help users choose the right product or service in a scenario of excessive information. In research on transportation, Hashemi et al. [11] proposed an opinion dynamics method to improve the reliability of the speed estimator. In other fields, Noah et al. [12] studied the evolution of the American people's opinions on a series of issues related to the Iraq war. Carmela et al. [13] explained the mechanism of consensus reached by 178 countries in the 2015 Paris Climate Change Agreement, etc. In this way, researchers have deepened their understanding of the formation and evolution of opinions and aroused interest from other fields.

Models in opinion dynamics usually include three elements: expression formats of opinions, fusion rules and dynamic environments of opinions. In particular, the agents in the group express initial opinions through a special expression format. According to fusion rules, the opinions of the agents are updated repeatedly. Finally, the opinions of all agents form a stable state: consensus, polarization or fragmentation. According to whether the

opinion values are discrete or not, the opinion dynamics can be divided into two categories: (1) discrete opinion models, e.g., the Ising model [14–19], the Sznajd model [20–22], the Voter model [23–28], the majority-vote model [29–33], and (2) continuous opinion models, e.g., the Deffuant–Weisbuch (DW) model [34–37] and the Hegselmann–Krause (HK) model [38–42]. The former type usually describes situations in which agents have a finite number of opinions. As for the latter type, the DW model updates asynchronously and allows two agents to interact with each other if their opinions are close to some extent, while the HK model updates synchronously and allows a crowd of agents to do so simultaneously if their opinions are somewhat similar. In addition, both the DW and the HK models rely on the idea of repeated averaging under a confidence threshold. Considering these works, we believed that both discrete and continuous models have disadvantages and thus we will propose a hybrid model where opinions are discrete (support, oppose, feel neutral) while support degrees are continuous (lying in the range of $[0, 1]$ with 0 meaning absolutely oppose and 1 meaning absolutely support). First discrete opinions are tailored for some situations, one of which may be voting for some representatives in congress or parliament. Second continuous support degrees reflect delicate feelings and emotions, which are natural in real life.

Most studies on continuous opinion dynamics take a weighted average of agent opinions in any single interaction [43–45]. However, in reality, when an agent is exposed to its same opinion, its confidence in this opinion will be strengthened. Moreover, when two agents meet with different opinions, they may not be able to make their opinions the same immediately. In fact, there are many versions of opinion dynamics models that take into account the "support" or "conviction" of an agent. For example, Roy et al. [46] studied this public and private opinion dynamics and the critical behaviour of the consensus-forming transitions using a kinetic exchange model; Szurlej et al. [47] studied the binary q-voter model with generalized anticonformity on random Erdős–Rényi graphs; Lallouache et al. [48] proposed a minimal multiagent model for the collective dynamics of opinion formation in society by modifying kinetic exchange dynamics studied in the context of income, money or wealth distributions in a society; Scheufele et al. [49] studied how the opinion climate affects participatory behaviour with or without public expression of opinion. Yet none of these studies allows opinions to be strengthened when like-minded agents meet. Therefore, in this paper, we will propose a novel model called progressive opinion evolution (POE) which exploits a slow and continuous accumulation updating strategy to deal with the drawbacks above. Based on this model, we will mainly discuss how agents interact and update their opinions.

To be specific, we proposed an updating rule for agents' support degrees, i.e., how strongly they support an opinion, and thus constructed a mathematical model accordingly. Moreover, we conducted simulations to test parameter sensitivity on evolution processes. Our main contributions are summarized as follows: (1) a framework for opinion formation through progressive opinion change; (2) three mechanisms for opinion polarization.

The remainder of this paper is organized as follows. Section 2 presents some necessary preliminaries. Section 3 describes our progressive evolution model. Section 4 presents empirical evaluations of the effects of different parameters on opinion evolution. Section 5 discusses polarization mechanisms as well as related simulations. Finally, Section 6 concludes this paper and discusses future works.

2. Preliminaries

In the simulations part, we discuss groups of agents whose support degrees about an opinion follow certain distributions, so we introduce notations concerning some probability distributions here. We use $X \sim \mathsf{U}[a, b]$ to denote that X follows a uniform distribution over $[a, b]$. Moreover, we use $X \sim \mathcal{N}(\mu, \sigma^2)$ to denote that X follows a normal distribution with μ and σ^2 as its mean and variance, respectively. On the other hand, we use $X \sim beta(\alpha, \beta)$ to denote that X follows a beta distribution, where $\alpha > 0$ and $\beta > 0$, respectively. Moreover, we sometimes talk about a range of values, so for simplicity, we use $\mathcal{E}(a, t, b)$ to denote a

set of numbers that begin with a and do not exceed b with t as a single step, i.e., $\mathcal{E}(a,t,b) = \{a + k \cdot t | a + k \cdot t \leq b, k \in \mathbb{Z}, k \geq 0\}$.

3. The Proposed Model

Consider a set of agents, $A = \{a_1, \cdots, a_N\}$, and a discrete-time stamp $t \in \{0, \cdots, \infty\}$ at which opinions update. To demonstrate how strongly an agent supports an opinion, we first introduce the definitions of *support degree* and *opinion* as below.

Definition 1. *Given an agent a_i and a time stamp t, we define its support degree $s_i(t)$ as a function with a range $[0,1]$. Moreover, we define opinions as*

$$x_i(t) = \begin{cases} 1, & \text{if } s_i(t) > 0.5; \\ 0, & \text{if } s_i(t) = 0.5; \\ -1, & \text{if } s_i(t) < 0.5. \end{cases} \tag{1}$$

In our setting, if an agent's support degree is greater than (resp. smaller than) 0.5, we say that it supports (opposes) an issue. Otherwise, we say that he remains neutral about an issue. In what follows, we use $0 \leq \delta \leq 1$ to denote support degree change (SDC), the increase or decrease of an agent's support degree. The larger δ is, the more significant an agent's support degree update.

Below, we present the definition of *support degree profile* which describes the support degree of all agents.

Definition 2. *Given a time stamp t, the support degree profile (SDP) at time t, denoted by $S(t)$, is defined as $\langle s_1(t), \cdots, s_N(t) \rangle$, which is a vector of support degrees of all agents.*

Below, we define special cases which will be useful for introducing what we mean by consensus.

Definition 3. *If $s_i(t) > 0.5$ (resp. $s_i(t) < 0.5$, $s_i(t) = 0.5$) for all $1 \leq i \leq N$, we say that $S(t)$ is a positive (resp. negative, neutral) SDP.*

In this paper, we will only be interested in cases where the initial SDP is neither positive nor negative nor neutral. Next, we define a special case that will be useful in discussing polarization.

Definition 4. *If $\exists 1 \leq h \neq l \leq N$ s.t.*

1. $s_h(t) < s_l(t)$;
2. $\forall 1 \leq i \leq N, s_i(t) \notin (s_h(t), s_l(t))$;
3. $\exists j, k$ *s.t.* $s_j(t) \leq s_h(t)$ *and* $s_k(t) \geq s_l(t)$,
4. *and* $s_l(t) - s_h(t) > 0.5$;

*then we say that $S(t)$ is a τ-*gap *SDP, where $\tau = s_l(t) - s_h(t)$.*

Now, we show the intuition of the notion of a τ-gap SDP. (1) Item 2 implies that no agents have support degree between that of $s_h(t)$ and $s_l(t)$; i.e., the support degrees of a_h and a_l must be adjacent to each other in the sorted form of $S(t)$. (2) Item 3 indicates that there must exist agents whose support degrees lie at both sides of that of a_h and a_l in the sorted form of $S(t)$. (3) Item 4 ensures that our definition is well-defined as is stated in Proposition 1.

Proposition 1. *At some certain time stamp, if an SDP is τ-gap, then it cannot be τ'-gap where $\tau' \neq \tau$.*

Proof. (by contradiction) Assume that there exists a profile $S(t)$ that is both τ-gap and τ'-gap where $\tau \neq \tau'$. According to Definition 4, $\tau > 0.5$ and $\tau' > 0.5$. Since $S(t)$ is τ-gap, there must exist an interval of length τ where no agents have support degrees. Similarly, there must exist another interval of length τ' where no agents have support degrees. In this sense, the intervals above are disjoint. Therefore, the length of their union is $\tau + \tau' > 1$ that exceeds the length of the interval $(0, 1)$ which is 1.The contradiction falsifies our assumption and thus confirms the validity of our proposition. □

Notice that given an SDP $S(t)$, if $s_i(t) \in \{0, 1\}$ for $1 \leq i \leq N$, then it is a one-gap profile. Below, we have a proposition that asserts that in a τ-gap SDP there cannot be any neutral agents and there must exist agents with opposite opinions.

Proposition 2. *If $S(t)$ is a τ-gap SDP for some τ, then*

1. $\nexists\, 1 \leq i \leq N$ *s.t.* $s_i(t) = 0.5$;
2. $\exists 1 \leq j \neq k \leq N$ *s.t.* $s_i(t) > 0.5$ *and* $s_j(t) < 0.5$.

Based on the proposition above, we are ready to understand the notion of most swinging agents as well as their implications.

Definition 5. *If $S(t)$ is a τ-gap SDP, $s_h(t) = \max\limits_{s_i(t)<0.5} s_i(t)$ and $s_l(t) = \min\limits_{s_j(t)>0.5} s_j(t)$, then we say that a_h (resp. a_l) is a/the most swinging agent involved in $S(t)$ that opposes (resp. supports) an issue.*

In this sense, considering all agents, the opinions of a_h and a_l are the closest to neutral. To some extent, they are the most able to be persuaded and then converted. Hence, it is reasonable to adopt their support degrees to measure the difference between the supporting sub-group and the opposing sub-group. The larger the support degree difference between a_h and a_l, the more polarized the two sub-groups. This leads to the proposition below, in which the rationality of Definition 4 is shown.

Proposition 3. *Suppose $S(t)$ is a τ-gap SDP, a_h and a_l are a/the most swinging agent involved in $S(t)$ that opposes and supports an issue, respectively, then $s_l(t) - s_h(t) = \tau$.*

Since we studied opinion dynamics empirically, we introduce definitions below which give exact meanings of observations. Below, we present what we mean by observing a process of opinion evolution that follows a certain model.

Definition 6. *If $\mathcal{R} = \langle S(0), \cdots, S(T)\rangle_{\mathcal{M}}$ is a sequence of observed profiles that follows $\mathcal{M}$, where T is a specified time stamp, then we say that $\mathcal{R}$ is an observed process of opinion evolution that follows $\mathcal{M}$ and T is the cutoff. Or we say that $\mathcal{R}$ is an observed evolution process for short if understood from the context.*

Below, we show the meaning of observing consensus or polarization of length $(T - t^*)$.

Definition 7. *Suppose that $\mathcal{R} = \langle S(0), S(1), \cdots, S(T)\rangle_{\mathcal{M}}$ is an observed evolution process.*

1. *if there exists $1 \leq t^* \leq T$, s.t. $S(t)$ is a positive (resp. negative, neutral) SDP for $t^* \leq t \leq T$, but $S(t^* - 1)$ is not, then we say that $\mathcal{R}$ is observed to form a consensus of length $(T - t^*)$.*
2. *if there exists $1 \leq t^* \leq T$, and τ_0, s.t. $S(t)$ is a τ-gap SDP for $t^* \leq t \leq T$ with $\tau \geq \tau_0$ but $S(t^* - 1)$ is not, then we say that $\mathcal{R}$ is observed to form a τ_0-polarization of length $(T - t^*)$.*

In our setting, at each time stamp, exactly two agents meet each other, which is similar to the DW model [34]. According to their support degrees before the meeting, there are six combinations of support degrees that need to be considered (as is shown by ①∼⑥ in Table 1 (Since this table is symmetric, the below left part is ignored)):

1. Both are greater than 0.5;
2. One is greater than 0.5 while the other is less than 0.5;
3. One is greater than 0.5 while the other is equal;
4. Both are less than 0.5;
5. One is less than 0.5 while the other is equal;
6. Both equal 0.5.

Then our update rules will be defined based on the cases above. For example, when two agents with the same opinion meet each other, both their support degrees will be increased or decreased, depending on whether they support or oppose an issue.

Example 1. *Suppose that two agents both have the same support degree change δ,*

1. *(both positive) if their previous support degrees are* 0.6 *and* 0.7*, then their degrees will increase to* $0.6 + \delta$ *and* $0.7 + \delta$*, respectively;*
2. *(both negative) if their previous support degrees are* 0.2 *and* 0.3*, then their degrees will decrease to* $0.2 - \delta$*, and* $0.3 - \delta$*, respectively.*

When two agents with opposite opinions meet each other, their support degrees will be increased or decreased and get close to each other.

Example 2. *Suppose that two agents both have the same support degree change δ, if their previous support degrees are* 0.4 *and* 0.5*, then their support degrees will come close to being* $0.4 + \delta$ *and* $0.5 - \delta$*, respectively.*

Table 1. Cases that are considered.

a_i \ a_j	> 0.5	< 0.5	$= 0.5$
> 0.5	①	②	③
< 0.5	-	④	⑤
$= 0.5$	-	-	⑥

Both are greater than 0.5 (See ①). One is greater than 0.5 while the other is less than 0.5 (See ②). One is greater than 0.5 while the other is equal(See ③). Both are less than 0.5 (See ④). One is less than 0.5 while the other is equal (See ⑤). Both equal 0.5 (See ⑥).

In addition, if an agent feels neutral about an issue, its opinion will be dragged and thus changed by any other one that supports or opposes this issue.

Our progressive opinion evolution (POE) model adopts asynchronous update rules, i.e., at every time stamp, two or more agents are randomly selected to communicate with each other and then update their support degrees. Yet in our models, we only allow interactions between exactly two agents. When two agents, namely a_i and a_j, meet each other at time t, their support degree updates can be described as follows, and are divided into several cases depending mainly on whether they have the same or different opinions.

1. The most trivial case is that both agents are neutral; then no updates are needed, so the rule, in this case, is as below.

$$\begin{cases} s_i(t+1) = s_i(t), \\ s_j(t+1) = s_j(t) \end{cases} \tag{2}$$

2. If both agents are positive (resp. negative) at time t, their confidence will be strengthened and thus their support degrees will be increased (resp. decreased) by δ, as shown in Equations (3) and (4).

$$\begin{cases} s_i(t+1) = s_i(t) + \delta, \\ s_j(t+1) = s_j(t) + \delta \end{cases} \tag{3}$$

$$\begin{cases} s_i(t+1) = s_i(t) - \delta, \\ s_j(t+1) = s_j(t) - \delta \end{cases} \tag{4}$$

3. If two agents with opposite opinions meet each other, their confidence in previous opinions will be weakened, i.e., one support degree will be increased while the other will be decreased. Without loss of generality, we assume that $s_i(t) < s_j(t)$ and the respective updates are described below.

$$\begin{cases} s_i(t+1) = s_i(t) + \delta, \\ s_j(t+1) = s_j(t) - \delta \end{cases} \tag{5}$$

In addition, since support degrees cannot lie outside the interval $[0, 1]$, we apply the function $\prod_{[0,1]}$ below to limit the results obtained from Equations (2)–(5).

$$\prod_{[0,1]}(x) = \begin{cases} 1, & \text{if } x > 1 \\ x, & \text{if } 0 \leq x \leq 1 \\ 0, & \text{if } x < 0 \end{cases} \tag{6}$$

For example, Equation (5) will turn into the following in our implementation.

$$\begin{cases} s_i(t+1) = \prod_{[0,1]}(s_i(t) + \delta), \\ s_j(t+1) = \prod_{[0,1]}(s_j(t) - \delta) \end{cases} \tag{7}$$

Proposition 4. *Suppose $\mathcal{R} = \langle S(0), S(1), \cdots, S(T) \rangle_{\mathcal{M}}$ is an observed evolution process that follows our POE model. If there exist $1 \leq t^* \leq T$, s.t. $S(t^*)$ is a positive (resp. negative, neutral) profile, then $S(t)$ is also a positive (resp. negative, neutral) profile for $t^* < t \leq T$.*

Proof. We simply prove the case for positive profiles and the other two are similar. In order to prove that $S(t)$ is positive for $t^* < t \leq T$, we simply need to prove that $S(t^* + 1)$ is also positive.

Without loss of generality, we assume that two agents, namely a_j and a_k, are picked for interactions upon $S(t^*)$. According to Definition 3, $s_i(t^*) > 0.5$ for $1 \leq i \leq N$; thus $s_j(t^*) > 0.5$ and $s_k(t^*) > 0.5$. According to Equation (3), $s_j(t^* + 1) = s_j(t^*) + \delta > 0.5$ since $\delta > 0$. Similarly, $s_k(t^* + 1) > 0.5$. On the other hand, for any $1 \leq l \leq N$, s.t. $l \neq j$ and $l \neq k$, $s_l(t^* + 1) = s_l(t^*) > 0.5$, so $s_i(t^* + 1) > 0.5$ for $1 \leq i \leq N$, which in turn confirms that $S(t^* + 1)$ is a positive profile. □

4. Simulations with POE Model

We visualized the properties of our model through Matlab simulations. To be specific, we demonstrated the effects of three parameters including (1) the *support degree change* δ, (2) the distribution of their initial *SDP* $\langle s_1(0), \cdots, s_N(0) \rangle$ as well as (3) the group size N.

For each of the three parameters above, we evaluated how they influence the speed of convergence. So given a model with all parameters specified, we use t^* to represent the average number of iterations needed to achieve convergence (see [50] for more details). Moreover, in order to observe convergence in a convenient way, we used an additional parameter $t_{\max}$ which means the number of iterations we perform in a particular run.

4.1. Comparing Different Values of Support Degree Change δ

For the simulations in this subsection, N and $t_{\max}$ were set to 200 and 10,000, respectively. To evaluate the impacts of δ, we tested each value in $\mathcal{E}(0.05, 0.02, 0.49)$ for this parameter. For each such value, we conducted simulations 500 times and obtained the t^* value over these runs.

Since simulations showed that different δ values present similar trends concerning convergence, we took two runs as examples in which δ was set to 0.2 and 0.6, respectively,

and we present them in Figure 1 here. Among all simulations, we found that those models with $\delta < 0.5$ quickly converge (form a consensus) while those with $\delta > 0.5$ failed to do so within $t_{\max}$ iterations, as is vividly shown in the two sub-figures of Figure 1.

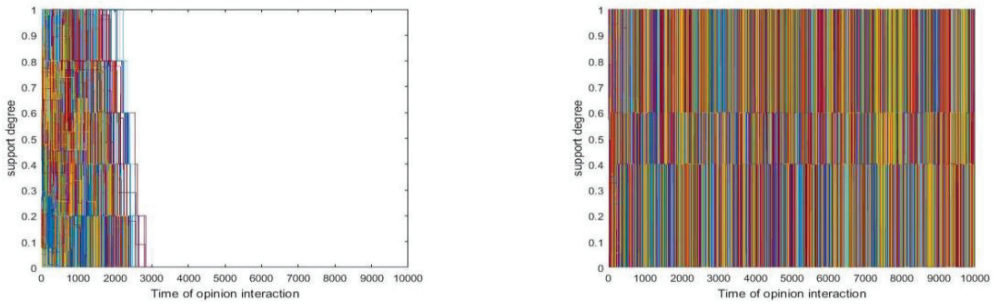

(**a**) $\delta = 0.2$ (**b**) $\delta = 0.6$

Figure 1. The average t^* values for different δ values. (**a**) $\delta = 0.2$. (**b**) $\delta = 0.6$. Other parameters: $N = 200$, $t_{\max} = 10,000$, $s_i(0) \sim \mathrm{U}[0,1]$ where $1 \leq i \leq 200$.

Furthermore, we present t^* values with respect to different δ values in Figure 2.

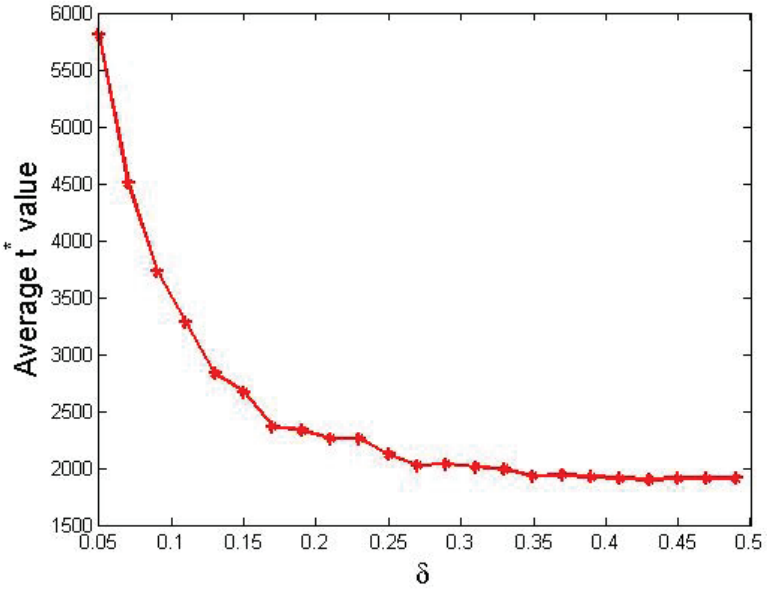

Figure 2. The average t^* values for different δ values. Other parameters: $N = 200$, $t_{\max} = 10,000$, $s_i(0) \sim \mathrm{U}[0,1]$ where $1 \leq i \leq 200$.

From Figure 2, we obtained the following observations.

1. In general, the value of t^* clearly decreased as δ increased from 0.05 to 0.49.
2. The decreasing trend of t^* wrt. δ was sharp in the first half where δ ranged from 0.05 to 0.25 but became smooth in the second half, where δ is greater than 0.25.

Now, we analyze the performances visualized in Figure 2. When δ is small, agents can only update their support degree in small steps, so a great number of steps are needed to achieve consensus. In contrast, when δ is relatively big, a small amount steps are in need. On the other hand, when $\delta > 0.5$, agents' support degrees update too fiercely so that no consensus was observed within $t_{\max}$ iterations.

Remark 1. *In practice, given a society, when an average agent is reluctant to change its idea, it will take longer for the society to form a consensus. On the other hand, if an average agent is too open-minded, its opinion may keep changing and thus a consensus is difficult to achieve.*

4.2. Comparing Different Distributions of Initial SDP

We considered different distributions of agents' initial *SDP* $\langle s_1(0), \cdots, s_N(0) \rangle$, and evaluated their impacts on the result and speed of convergence. To be specific, we conducted two lists of simulations.

1. The former list evaluated the influences of different proportions of opinions, where the support degree distribution is uniform in both the positive and the negative groups.
2. The latter list simulated those initial *SDP*s that follow the beta and normal distribution, compared to those that follow the uniform distribution.

4.2.1. The Effects of Different Proportions of Opinions

Given a fixed number of N agents, we partitioned them into two groups, those who support or oppose an issue. In this sense, we use N_p and N_n to denote the number of agents in these groups, respectively, and obviously, $N = N_p + N_n$.

Since simulations showed that different (N_p, N_n) values present similar results about convergence, we took two runs as examples in which (N_p, N_n) were set to $(150, 50)$ and $(50, 150)$, respectively, and we presented them in Figure 3 here.

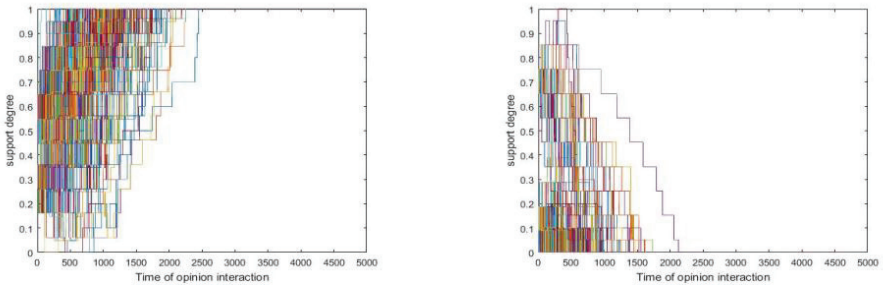

(**a**) $(150, 50)$ (**b**) $(50, 150)$

Figure 3. The effects for different (N_p, N_n) values. $\delta = 0.1$, $N = 200$, $t_{\max} = 10{,}000$. (**a**) $(150, 50)$. $s_i(0) \sim \mathsf{U}[0.5, 1]$ where $1 \leq i \leq 150$. $s_{151}(0), \cdots, s_{200}(0) \sim \mathsf{U}[0, 0.5]$. (**b**) Parameter settings are analogous.

From Figure 3, we obtained the following.

1. Figure 3a showed simulations where N_p and N_n were 150 and 50, respectively, and this simulation formed a consensus where all agents were positive.
2. Figure 3b showed similar situations where N_p and N_n were 50 and 150 and finally, all agents became negative.

From Figure 3, we conjectured that $N_p > N_n$ leads to a consensus where all agents are positive, while $N_p < N_n$ causes the opposite. To verify this claim, we conducted four groups of simulations where (N_p, N_n) were set to $(180, 20)$, $(120, 80)$, $(90, 110)$ and $(30, 170)$, respectively. In each group, we conducted 500 simulations and in the end, we made observations that fitted this conjecture.

Remark 2. *In practice, if everyone is open-minded to some extent, then their meeting is likely to form a consensus that is consistent with majority votes, provided a sufficient number of interactions.*

4.2.2. Evaluating Beta and Normal Distributions of Initial SDP

In reality, agents' support degrees can be concentrated to some extent. To be specific, there are two types of interesting distributions: (1) distributions where the majority are quite indifferent between supporting or opposing an issue, and (2) those where the majority have polarized support degrees. Rigorously, we think that the beta and the normal distributions are interesting because they reflect the two situations above. Hence, we redid the simulations in Section 4.1, but replaced the uniform distribution there with *beta*$(0.1, 0.1)$ and $\mathcal{N}(0.5, 0.1)$, respectively. Then we visualized the results of these 3 distributions and placed their curves together in Figure 4.

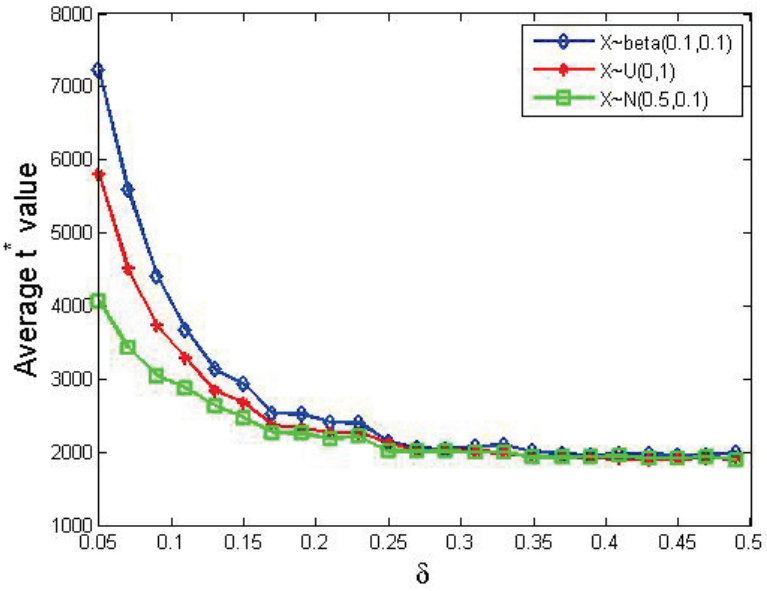

Figure 4. The influence of distributions of initial SDPs. Other parameters: $N = 200$, $t_{max} = 10,000$; the blue, red and green curves correspond to the beta, uniform and normal distribution, respectively.

From Figure 4, we obtained the following.

1. Obviously, the three curves shared similar trends with the one in Figure 2.
2. The beta distribution took the longest to form a consensus, while the normal distribution took the shortest time when δ is relatively small.

Further simulations showed that no consensus would be reached when $\delta > 0.5$. All in all, this figure illustrated that more concentrated distributions lead to sooner consensus among agents.

Remark 3. *In reality, when most agents have initial support degrees that are similar, such agents can easily persuade others to accept their ideas. In contrast, if there exists a considerable amount of agents with polarized support degrees, it will take longer to persuade them to accept intermediate ideas.*

4.3. The Effects of Group Size

We redid the simulations in Section 4.1, but replaced the value of N with 100, 200, 500 and 1000, respectively. Since simulations showed that different N values present similar trends concerning convergence, we took two runs as examples in which N was set to 100 and 500, respectively, and we presented them in Figure 5 here. Furthermore, we visualized the results of 200, 500 and 1000 agents and placed their curves together in Figure 6.

In Figure 5, we found the following.

1. Both runs formed a consensus.
2. Larger groups of agents led to later consensus.

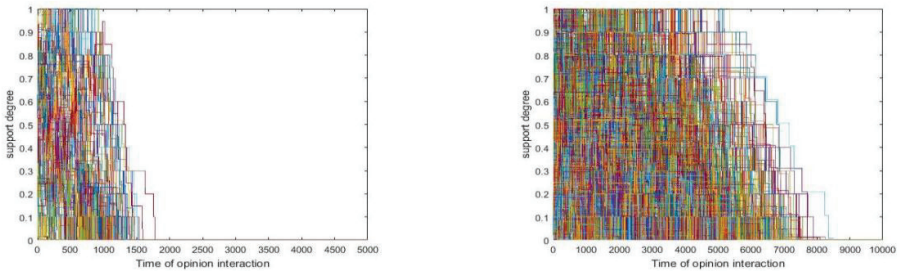

(**a**) $N = 100$ (**b**) $N = 500$

Figure 5. Influence of N. (**a**) $N = 100$. (**b**) $N = 500$. Other parameters: $\delta = 0.1$, $t_{\max}^{(a)} = 5,000$, $t_{\max}^{(b)} = 10,000$, the initial support degrees are uniformly and randomly selected from $[0, 1]$.

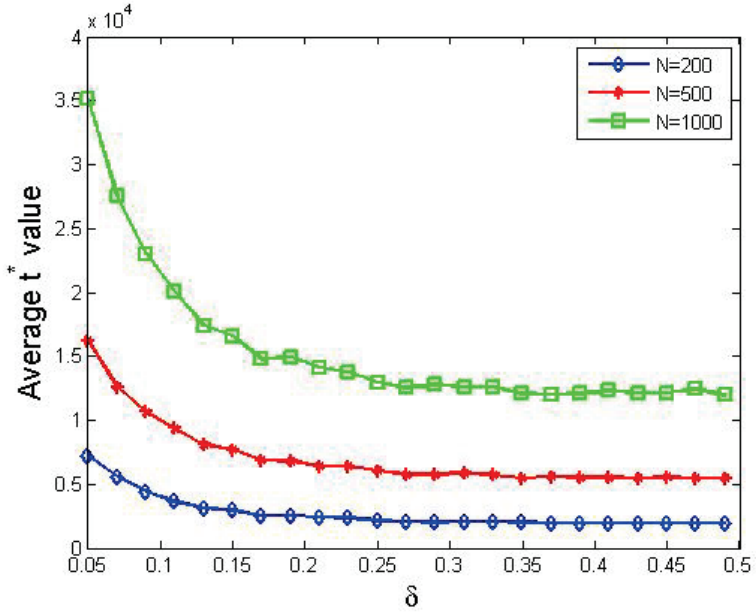

Figure 6. The average t^* values for different δ values. Other parameters: the initial support degree is uniformly and randomly selected from $[0, 1]$. The blue, red and green curves correspond to parameter combinations, namely (1) $N = 200$, $t_{max} = 10,000$; (2) $N = 500$, $t_{max} = 50,000$; and (3) $N = 1,000$, $t_{max} = 50,000$, respectively.

From Figure 6, we obtained the following.

1. Obviously, the three curves shared similar trends with the one in Figure 2, which indicated that whether their support degrees converge does not depend on the number of agents involved.
2. The situation in Figure 5 also occurred in the three cases here.

Remark 4. *In a society where communications are primitive, to be specific, in each time stamp, only two agents are allowed to interact with each other, the time needed to form a consensus is proportional to the number of agents.*

4.4. Non-Uniform SDCs in A Group

In previous simulations, all agents have the same SDC. Alternatively, any two agents update their support degree with the same increase or decrease. In this subsection, we considered agents that could have individual SDCs, so we redid the simulation in Section 4.1, but replaced the uniform SDC among agents with individual ones.

We conducted two simulations in which individual SDCs follow uniform distributions over $[0.1, 0.4]$ and $[0.1, 0.8]$, respectively. In what follows, we use δ_i to denote the a_i's SDC. Since simulations showed that different runs present similar trends concerning convergence,

we took two of them as examples in which $\delta_i \sim \mathrm{U}[0.1, 0.4]$ and $\delta_i \sim \mathrm{U}[0.1, 0.8]$, respectively, where $1 \leq i \leq 200$, and we presented them in Figure 7 here.

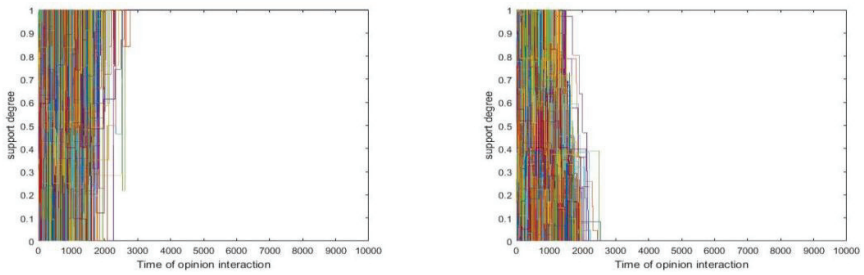

(**a**) $\delta_i \in [0.1, 0.4]$ (**b**) $\delta_i \in [0.1, 0.8]$

Figure 7. Non-uniform SDCs in a group. (**a**) $\delta_i \in [0.1, 0.4]$. (**b**) $\delta_i \in [0.1, 0.8]$. Other parameters: $N = 200$, $t_{max} = 10,000$, $s_i(0) \sim \mathrm{U}[0, 1]$ where $1 \leq i \leq 200$.

In Figure 7, we found the following.

1. Both initial distributions formed a consensus in the end.
2. In Figure 7b, even though there were a significant proportion of agents whose SDCs were greater than 0.5, a consensus was formed eventually.

Furthermore, we considered other intervals namely $[0.1, b]$ where $b \in \{0.2, 0.3, \cdots, 1\}$. and each of them was tested 500 times. Then, we visualized the relation between b and t^* in Figure 8 below.

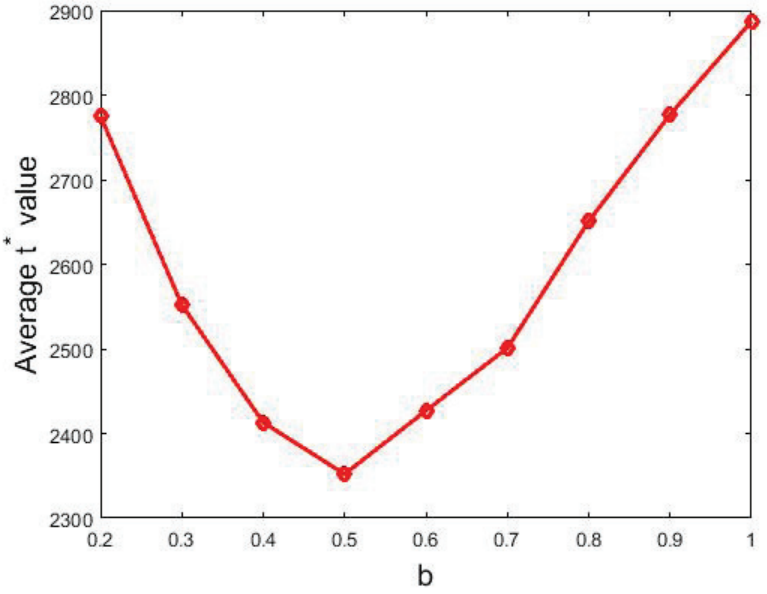

Figure 8. The relation between the average t^* value and the right endpoint b. Other parameters: $N = 200$, $t_{max} = 10,000$, $s_i(0) \sim \mathrm{U}[0, 1]$ where $1 \leq i \leq 200$.

From Figure 8, we obtained the following.

1. Even though there could be a significant proportion of agents who were more open-minded, i.e., they updated their support degrees considerably, a consensus was still reached.
2. The $b - t^*$ curve presented a decrease when $b < 0.5$ but then showed an increase until b reached 1. This indicated that larger SDC values generated an earlier consensus when they were smaller than 0.5. Moreover, it revealed that more open-minded agents with SDC value greater than 0.5 produced a later consensus.

Now, we analyze this phenomenon.

1. Since there was a fair proportion of agents with SDC values less than 0.5, they constituted a core that served as a foundation for opinion evolution. Such a core persuaded those open-minded agents with SDC values greater than 0.5 to eventually agree with the opinions of the core.
2. As to the speed of convergence, when δ was small, it took longer to form a consensus which coincided with the mechanism beneath Figure 2. However, when $b \geq 0.5$, agents' support degrees update quite fiercely, so it is not easy to reach a consensus, which was why more time was needed to reach a consensus.

Remark 5. *As mentioned above, if agents in a society are too open-minded, they will hardly form a consensus. However, if there exist plenty of agents who are willing to update their support degrees in small steps, they will constitute a core and this core will gradually persuade those open-minded ones and finally turn them into their like-minded companions.*

5. Three Mechanisms for Polarization

Group polarization is a hot topec in recent research of opinion dynamics [50–57]. In this section, we propose three extensions of our POE model which served for polarization.

5.1. Communications Limited by Support Degree Differences

In reality, there can be communication barriers between agents whose support degrees differ too much. More concretely, if two agents have different opinions, their communication cannot occur unless their support degrees are close to some extent, i.e., the difference between their support degrees is smaller than a certain specified confidence threshold.

Based on our POE model above, we introduce a bounded confidence threshold ϵ, where $0 \leq \epsilon \leq 1$, which permits or prohibits communications between agents with different opinions. Actually, our intuition for this is as follows.

1. Agents with the same opinion communicate with each other effectively.
2. Only when two agents meet with different opinions, do we exert a threshold.

Formally, in Cases ②, ③ and ⑤ in Table 1, agents' support degrees update only when $|s_i(t) - s_j(t)| \leq \epsilon$ for some confident specified threshold ϵ. Combining these rules and the ones in Equations (2)–(4) in Section 3, we have a novel model, named ϵ-POE model, for communications that are limited by support degree differences. Notice that such a model will degenerate to the POE model when $\epsilon = 1$. In addition, since support degrees cannot lie outside the interval $[0, 1]$, we implement this model in the same way as Equation (7).

Since simulations showed that different ϵ values present similar trends in polarization, we took two particular runs as examples in which ϵ were set to 0.1 and 0.6, respectively, and we presented them in Figure 9 here.

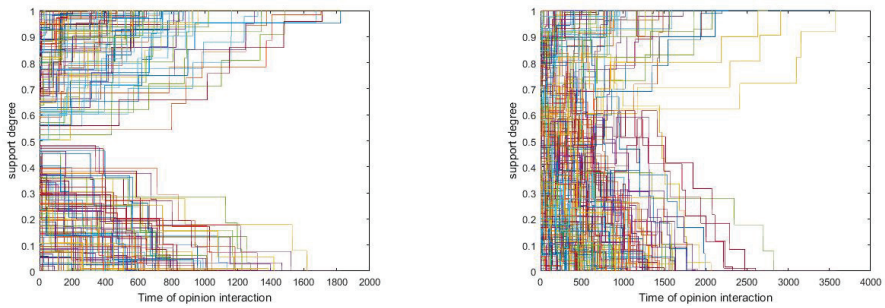

(**a**) $\epsilon = 0.1$ (**b**) $\epsilon = 0.6$

Figure 9. The influence of ϵ. (**a**) $\epsilon = 0.1$. (**b**) $\epsilon = 0.6$. Other parameters: $\delta = 0.1$, $N = 200$, $t_{max} = 10,000$, $s_i(0) \sim \mathrm{U}[0, 1]$ where $1 \leq i \leq 200$.

Figure 9 shows that both the ϵ-POE modes (with $\epsilon = 0.1$ and $\epsilon = 0.6$, respectively) polarized.

Next, we tested all combinations of $\langle \delta, \epsilon \rangle \in \mathcal{E}(0.1, 0.05, 0.4) \times \mathcal{E}(0, 0.1, 1)$ and ran simulations 500 times with each of them. In this sense, we defined *polar ratio* as the proportion of runs that achieved polarization. The relation between polar ratios and bounded confidence is presented in Figure 10, in which each curve corresponds to a specific δ value.

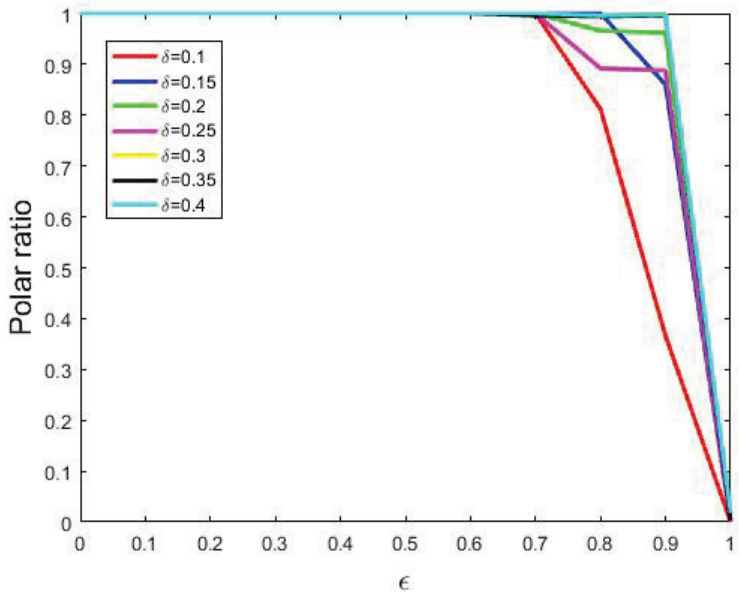

Figure 10. The effects of bounded confidence. Other parameters: $N = 200$, $t_{max} = 10{,}000$, $s_i(0) \sim \mathsf{U}[0,1]$ where $1 \leq i \leq 200$.

From Figure 10, we found that larger bounded confidence led to smaller polar ratios, i.e., small bounded confidence tended to polarize. The reason may be that smaller bounded confidence results in less willingness to update one's opinions.

Remark 6. *More trust between agents with different opinions leads to less polarization.*

Actually, we have a proposition below which shows that in our ϵ-POE mode, once an SDP becomes 1-gap, it will preserve this property till the end of our observation.

Proposition 5. *Suppose that $\mathcal{M}$ is an ϵ-POE model, and $\mathcal{R} = \langle S(0), S(1), \cdots, S(T) \rangle_{\mathcal{M}}$ is an observed evolution process. If there exists $1 \leq t^* \leq T$, s.t. $s_i(t^*) \in \{0, 1\}$ for all $1 \leq i \leq N$, then $S(t^*) = S(t^* + 1) = \cdots = S(T)$.*

5.2. Polarization through More Effective Interaction with Like-Minded Agents

In reality, like-minded agents tend to communicate somewhat effectively. In this sense, like-minded agents cause more updates compared to those with different opinions. To distinguish between the effects resulting from like-minded agents and that from opposite-minded ones, we introduce an extra parameter $0 \leq c \leq 1$ for perturbation which helps depict such prejudice. More specifically, we believe that support degree changes between like-minded agents should be enlarged by a factor of $1 + c$, while those between different-minded agents should be shrunk by a factor of $1 - c$. Hence, when like-minded agents meet, the update should be $\delta(1 + c)$, which is greater than that in previous sections. Analogously, when opposite-minded agents meet, the update should be $\delta(1 - c)$. If $c = 0$, this model degenerates to the POE model above. By considering these issues, we have a model below which depicts such a situation.

1. The most trivial case is that both agents are neutral and the update rules are just the same as before, i.e., no updates are needed.

2. If both agents are positive (resp. negative) at time t, their confidence will be strengthened and thus their support degrees will be increased (resp. decreased) by $\delta(1+c)$, as is shown in Equations (8) and (9).

$$\begin{cases} s_i(t+1) = s_i(t) + \delta(1+c), \\ s_j(t+1) = s_j(t) + \delta(1+c) \end{cases} \tag{8}$$

$$\begin{cases} s_i(t+1) = s_i(t) - \delta(1+c), \\ s_j(t+1) = s_j(t) - \delta(1+c) \end{cases} \tag{9}$$

3. If two agents with different opinions meet each other, one support degree will be increased while the other will be decreased. So their support degrees will still get close, even though by a smaller step in this case. Without loss of generality, we assume that $s_i(t) < s_j(t)$ and the respective updates are described below.

$$\begin{cases} s_i(t+1) = s_i(t) + \delta(1-c), \\ s_j(t+1) = s_j(t) - \delta(1-c) \end{cases} \tag{10}$$

In addition, since support degrees cannot lie outside the interval $[0,1]$, like in previous situations, we implement this model in the same way as Equation (7).

Since simulations showed that different c values present similar trends, we took two specific runs as examples in which c were set to 0.5 and 0.7, respectively, and we presented them in Figure 11 here.

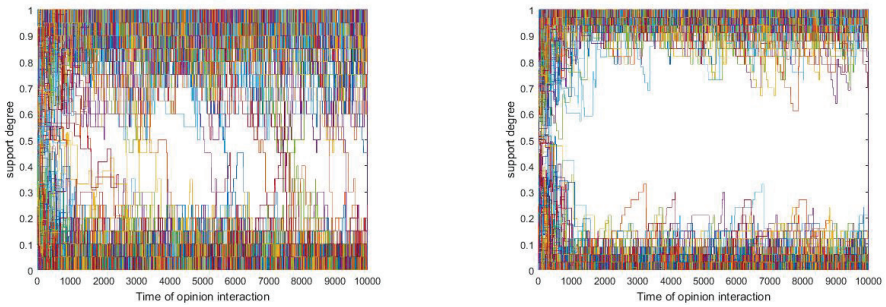

(**a**) $c = 0.5$ (**b**) $c = 0.7$

Figure 11. The influence of c. (**a**) $c = 0.5$. (**b**) $c = 0.7$. Other parameters: $\delta = 0.1$, $N = 200$, $t_{max} = 10,000$, $s_i(0) \sim \mathsf{U}[0,1]$ where $1 \leq i \leq 200$.

In Figure 11, neither consensus nor τ_0-polarization was observed with $\tau_0 \geq 0.8$. Yet detailed observations showed that τ_0-polarization was observed with $\tau_0 > 0.6$. To better depict this phenomenon, we propose Definition 8 below.

Definition 8. *(dynamic polar) We counted the number of people in the interval* $[0,r]$, *and* $[1-r,1]$, *which are separately denoted by* η, *and* μ, *if* $|\frac{\eta}{N} - \frac{\mu}{N}| \leq p$, *and* $\frac{\eta}{N} + \frac{\mu}{N} > q$, *where* $0 < r \leq 1$, $0 \leq p \leq 1$, *and* $0 \leq q \leq 1$, *then we say that a dynamic polar among the agents is reached at time* t, *which concerns* r, p *and* q.

Below, in each simulation, we set $r = 0.4$, $p = 0.2$ and $q = 0.95$. Then, we considered all combinations of $\delta \in \mathcal{E}(0.1, 0.05, 0.4)$ and $c \in \mathcal{E}(0.1, 0.1, 0.9)$, and we ran simulations 500 times with each combination. Finally, we reported dynamic polarization ratios in Figure 12, in which each curve corresponded to a δ value.

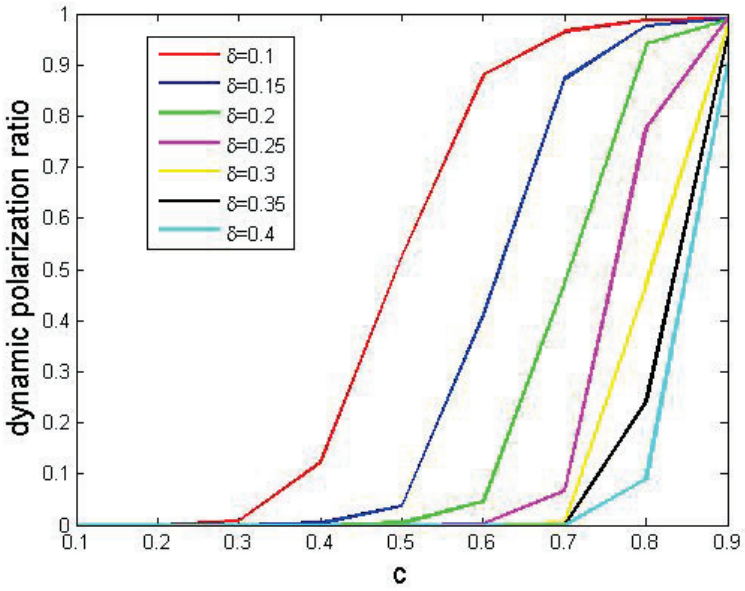

Figure 12. The effects of the perturbation parameter c. Other parameters: $N = 200$, $t_{max} = 10,000$, $s_i(0) \sim \mathsf{U}[0,1]$ where $1 \leq i \leq 200$.

In Figure 12, we found that bigger δ values produced smaller dynamic polarization ratios, which indicated that small δ values tend to cause polarization. Moreover, we noticed that larger perturbation values led to greater dynamic polarization ratios.

Now, we analyze the performances. With bigger δ, agents' support degrees fluctuate sharply so that it is difficult to realize dynamic polarization. On the other hand, if agents communicate much more effectively with like-minded ones compared to opposite-minded ones, their support degrees rarely come close to the average level among them.

Remark 7. *First, we considered a conservative society in which the majority are stubborn, i.e., they are little willing to change their support degrees. The less their willingness is, the more likely they are to form a dynamic polar.*

Second, we considered a society where individual agents have obvious prejudice, i.e., they update their support degrees more strongly with like-minded companions. The greater their prejudice is, the more probable it is that they will reach a dynamic polar.

5.3. Polarization through the Higher Chance of Interaction with Like-Minded Agents

Inspired by the Barnum Effect [58], we considered a case where agents desire to interact with like-minded companions. Such interactions can positively reinforce one's own beliefs. However, in the POE model, we assume that any two agents have equal opportunities for interactions. To be specific, each agent is chosen for communications with a probability about $\frac{1}{N}$, where N is the number of agents. In this sense, they have a $50/50$ chance of being like-minded.

Given a particular agent a_i, we use $\rho(a_i)$ to denote the proportion of agents that share the same opinion with agent a_i, so the proportion of agents that have different opinions is $1 - \rho(a_i)$. Then we introduce a bias parameter $0 \leq b \leq 1$, which helps increase the probability that an agent meets like-minded companions. More specifically in our setting, if an agent a_i supports or opposes an issue, it will meet like-minded companions at a probability of $\min\{\rho(a_i) + b, 1\}$ while it meets other agents at a probability of $1 - \min\{\rho(a_i) + b, 1\}$. However, if agent a_i feels neutral about that issue, it will meet any other agent with equal probability. Notice that such a model will degenerate to the POE model above when $b = 0$.

Our model here is the same as the POE model before with a single exception that we pick agents for communications by Algorithm 1.

Algorithm 1: PickAgentPair.

input: An agent set A, a time stamp t, SDP at time t, i.e., $\langle s_1(t), \cdots, s_{|A|}(t) \rangle$, a bias parameter b

output: Two agents for communications

```
a_i ← a random agent in A;
if a_i feels neutral then
    a_j ← a random agent other than a_i;
else
    p ← min{ρ(a_i) + b, 1}; // prob of meeting a like-minded one
    x ← a random number that follows U[0, 1]; // for prob determination
    if x < p then
        // with probability p
        a_j ← a random agent that shares opinions;
    else
        // with probability 1-p
        a_j ← a random agent that has different opinions;
return a_i and a_j for communications;
```

In addition, since support degrees cannot lie outside the interval $[0, 1]$, like in previous situations, we excluded unreasonable values in the same way as Equation (7).

Below, in each simulation, we set $r = 0.4$, $p = 0.2$ and $q = 0.95$. Then, we considered all combinations of $\delta \in \mathcal{E}(0.1, 0.05, 0.4)$ and $b \in \mathcal{E}(0.1, 0.05, 0.5)$ and then tested their effects. We found that the results were similar to those presented in Figure 11; therefore, we also used Definition 8 to depict such phenomena. We ran simulations with all combinations of parameters, 500 times for each. Finally, we reported dynamic polarization ratios in Figure 13, in which each curve corresponded to a δ value.

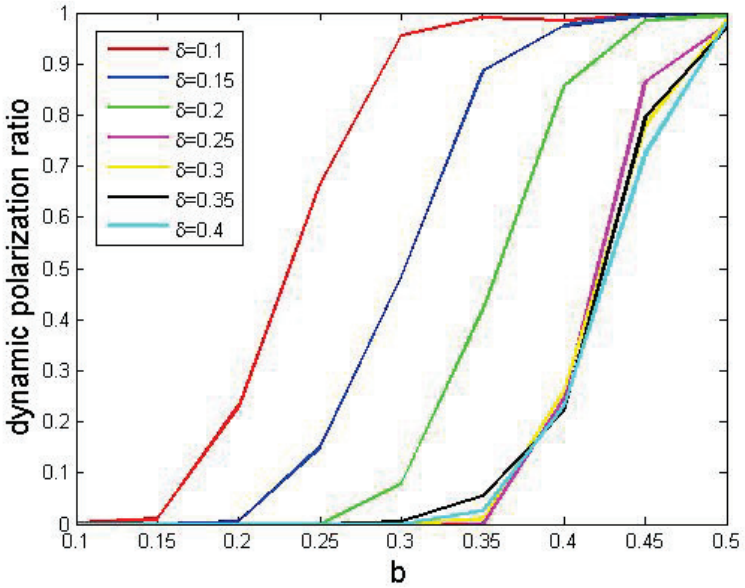

Figure 13. The effects of perturbation parameters. Other parameters: $N = 200$, $t_{max} = 10,000$, $s_i(0) \sim \mathsf{U}[0, 1]$ where $1 \leq i \leq 200$

In Figure 13, we found the following.

1. Obviously, those curves shared similar trends with the one in Figure 12.
2. More perturbation resulted in higher dynamic polarization ratios.

Based on such observations, we conjectured that more concentration on like-minded companions could cause more dynamic polarization.

Remark 8. *In a society where agents tend to communicate with like-minded companions, their support degrees will probably be increased by each other. Hence, the society may be divided into several subgroups each of which shares close support degrees. In other words, these agents will likely form a dynamic polar.*

6. Conclusions

In this paper, we proposed a hybrid opinion dynamic model based on progressive opinion evolution with a discrete component, namely agents' opinions, as well as a continuous one, namely support degrees. It has two distinguishing features as follows. (1) When agents meet with someone with the same opinions, their opinions will be strengthened; to be specific, their support degrees could increase or decrease simultaneously. (2) Agents may not be able to achieve an agreement (to have the same support degree) in a single interaction. Moreover, we proposed several extensions to this POE model which serve as mechanisms of opinion polarization. To be specific, the first extension introduced a further component, namely confident threshold, that limited communications between different-minded agents. The second extension considered prejudice on different-minded agents, more specifically, like-minded agents produced greater updates while different-minded agents generated smaller ones. The third brought about more opportunities for communication between like-minded agents.

We conducted a series of simulations to explore the behaviour of our models. In particular, we evaluated the impacts of several components and model parameters on the results and speeds of convergence. The results of these simulations show that our models reflected some aspects of social reality and thus simulated some social phenomena.

For future works, we will explore models with dictatorships. Moreover, it will be interesting to investigate an agent society with interactions that involve more than two agents.

Author Contributions: Conceptualization, B.Y., Y.F. and Q.Y.; methodology, Q.Y. and B.Y.; software, B.Y., Y.F. and Q.Y.; validation, Q.Y.; formal analysis, B.Y. and Q.Y.; investigation, B.Y., Q.Y. and Y.F.; resources, Q.Y.; writing—original draft preparation, B.Y.; writing—review and editing, B.Y., Q.Y. and Y.F.; supervision, Q.Y.; project administration, Q.Y.; funding acquisition, Q.Y. All authors have read and agreed to the published version of the manuscript.

Funding: Quan Yu (the corresponding author) was funded in part by the Foundation Project for Talents of Qiannan Science and Technology Cooperation Platform Supported by the Department of Science and Technology, Guizhou ([2019]QNSYXM-05), in part by the Educational Department of Guizhou under Grant (KY[2019]067), in part by the Foundation Project for Professors of Qiannan Normal University for Nationalities (QNSY2018JS010). Yi Fan was funded in part by the Special Foundation for Talents in Qiannan Normal University for Nationalities in 2019 (02-721901029), in part by the Project for Growing Youth Talents of the Educational Department of Guizhou (No.KY[2019]201), and in part by the Foundation Project of Science and Technology Plans of Qiannan under Grant 2020XK05ST.

Institutional Review Board Statement: Not applicable.

Data Availability Statement: Not applicable.

Conflicts of Interest: The authors declare no conflict of interest.

References

1. Srbu, A.; Loreto, V.; Servedio, V.; Tria, F. *Opinion Dynamics: Models, Extensions and External Effects*; Springer International Publishing: Berlin/Heidelberg, Germany, 2017. [CrossRef]
2. Le Pira, M.; Inturri, G.; Ignaccolo, M.; Pluchino, A.; Rapisarda, A. Simulating Opinion Dynamics on Stakeholders' Networks through Agent-based Modeling for Collective Transport Decisions. *Procedia Comput. Sci.* **2015**, *52*, 884–889. [CrossRef]
3. Li, Q.; Braunstein, L.; Havlin, S.; Stanley, G. Strategy of Competition between Two Groups based on an Inflexible Contrarian Opinion Model. *Am. Phys. Soc.* **2012**, *86*, 066101. [CrossRef] [PubMed]

4. Varma, V.S.; Morarescu, I.C.; Lasaulce, S.; Martin, S. Opinion dynamics aware marketing strategies in duopolies. In Proceedings of the 2017 IEEE 56th Annual Conference on Decision and Control (CDC), Melbourne, VIC, Australia, 12–15 December 2017. [CrossRef]
5. Kozuki, A.; Mahmassani, H.S. Information Acquisition and Social Interaction Mechanisms in Opinion Formation and Market Adoption of Transportation Services. In Proceedings of the 88th Annual Meeting of the Transportation Research Board, Washington, DC, USA, 11–15 January 2009.
6. Crokidakis, N. Effects of mass media on opinion spreading in the Sznajd sociophysics model. *Phys. Stat. Mech. Its Appl.* **2011**, 391, 1729–1734. [CrossRef]
7. Wu, Y.; Liu, S.; Yan, K.; Liu, M.; Wu, F. Opinion Flow: Visual Analysis of Opinion Diffusion on Social Media. *Vis. Comput. Graph. IEEE Trans.* **2014**, *20*, 1763–1772. [CrossRef] [PubMed]
8. Ding, Z.; Liang, H.; Dong, Y.; Chiclana, F.; Herrera-Viedma, E.; Cabrerizo, F.J. An opinion control rule with minimum adjustments to support the consensus reaching in bounded confidence model. *Procedia Comput. Sci.* **2016**, *91*, 617–624. [CrossRef]
9. Bravo-Marquez, F.; Gayo-Avello, D.; Mendoza, M.; Poblete, B. Opinion Dynamics of Elections in Twitter. In Proceedings of the 2012 Eighth Latin American Web Congress, Cartagena, Colombia, 25–27 October 2012; pp. 32–39. [CrossRef]
10. Castro, J.; Lu, J.; Zhang, G.; Dong, Y. Opinion Dynamics-Based Group Recommender Systems. *IEEE Trans. Syst. Man Cybern. Syst.* **2018**, *48*, 2394–2406. [CrossRef]
11. Hashemi, E.; Pirani, M.; Khajepour, A.; Fidan, B. Opinion Dynamics-Based Vehicle Velocity Estimation and Diagnosis. *IEEE Trans. Intell. Transp. Syst.* **2018**, *19*, 2142–2148. [CrossRef]
12. Friedkin, N.E.; Proskurnikov, A.V.; Tempo, R.; Parsegov, S.E. Network science on belief system dynamics under logic constraints. *Science* **2016**, *354*, 321–326. [CrossRef]
13. Bernardo, C.; Wang, L.; Vasca, F.; Hong, Y.; Shi, G.; Altafini, C. Achieving consensus in multilateral international negotiations: The case study of the 2015 Paris Agreement on climate change. *Sci. Adv.* **2021**, *7*, eabg8068. [CrossRef]
14. Montroll, E.W.; Badger, W.W. *Introduction to Quantitative Aspects of Social Phenomena*; Gordon & Breach: London, UK, 1974. [CrossRef]
15. Shukla, P. Hysteresis in the zero-temperature random-field Ising model on directed random graphs. *Phys. Rev. E* **2018**, *98*, 032144. [CrossRef]
16. Li, L.; Fan, Y.; Zeng, A.; Di, Z. Binary opinion dynamics on signed networks based on Ising model. *Phys. Stat. Mech. Appl.* **2019**, *525*, 433–442. [CrossRef]
17. Domínguez, A.R.; Arroyo-Duarte, R.; Rincón-Vieyra, F.; Alvarado-Mentado, M. Modeling cancer immunoediting in tumor microenvironment with system characterization through the ising-model Hamiltonian. *BMC Bioinform.* **2022**, *23*, 200. [CrossRef]
18. Takabatake, K.; Yanagisawa, K.; Akiyama, Y. Solving Generalized Polyomino Puzzles Using the Ising Model. *Entropy* **2022**, *24*, 354. [CrossRef]
19. Zukovic, M. Massive Degeneracy And Anomalous Thermodynamics in a Highly Frustrated Ising Model On Honeycomb Lattice; In Proceedings of the International ECMS Conference on Modelling and Simulation, Alesund, Norway, 30 May–3 June 2022; pp. 336–341. [CrossRef]
20. Sznajd-Weron, K.; Sznajd, J. Opinion evolution in closed community. *Int. J. Mod. Phys.* **2000,** *11*, 1157–1165. [CrossRef]
21. Giménez, M.C.; Revelli, J.A.; Wio, H.S. Non Local Effects in the Sznajd Model: Stochastic resonance aspects. *EAI Endorsed Trans. Complex Syst.* **2012**, *1*, e3. [CrossRef]
22. Chen, H.; Shu, J. *Sznajd2: A Community-Aware Opinion Dynamics Model*; IEEE: Piscataway, NJ, USA, 2016; pp. 1477–1484. [CrossRef]
23. Liggett, H. Ergodic Theorems for Weakly Interacting Infinite Systems and the Voter Model. *Ann. Probab.* **1975**, *3*, 643–663. [CrossRef]
24. Chiyomaru, K.; Takemoto, K. Adversarial attacks on voter model dynamics in complex networks. *Phys. Rev. E* **2021**, *106*, 014301. [CrossRef]
25. Majmudar, J.R.; Krone, S.M.; Baumgaertner, B.O.; Tyson, R.C. Voter models and external influence. *J. Math. Sociol.* **2020**, *44*, 1–11. [CrossRef]
26. Latoski, L.C.F.; Dantas, W.G.; Arenzon, J.J. Curvature-driven growth and interfacial noise in the voter model with self-induced zealots. *Phys. Rev. E* **2022**, *106*, 014121. [CrossRef]
27. Doniec, M.; Lipiecki, A.; Sznajd-Weron, K. Consensus, Polarization and Hysteresis in the Three-State Noisy q-Voter Model with Bounded Confidence. *Entropy* **2022**, *24*, 983. [CrossRef]
28. Golebiowska, M.; Sznajd-Weron, K. The Evolution of Political Views Within the Model with Two Binary Opinions. In *Lecture Notes in Computer Science;* Springer: Berlin/Heidelberg, Germany, 2021; Volume 12744, pp. 302–308. [CrossRef]
29. Galam, S. Application of statistical physics to politics. *Phys. Stat. Mech. Appl.* **1999**, *274*, 132–139. [CrossRef]
30. Balankin, A.S.; Martínez-Cruz, M.; Gayosso Martínez, F.; Mena, B.; Tobon, A.; Patiño-Ortiz, J.; Patiño-Ortiz, M.; Samayoa, D. Ising percolation in a three-state majority vote model. *Phys. Lett. A* **2017**, *381*, 440–445. [CrossRef]
31. Vilela, A.L.; Pereira, L.F.C.; Dias, L.; Stanley, H.E.; da Silva, L.R. Majority-vote model with limited visibility: An investigation into filter bubbles. *Phys. Stat. Mech. Appl.* **2021**, *563*, 125450. [CrossRef]
32. Chen, H.; Wang, S.; Shen, C.; Zhang, H.; Bianconi, G. Non-Markovian majority-vote model. *Phys. Rev. E* **2020**, *102*, 062311. [CrossRef] [PubMed]

33. Neshov, N.N.; Tonchev, K.; Velchev, Y.; Manolova, A.; Poulkov, V. *SoftVotingSleepNet: Majority Vote of Deep Learning Models for Sleep Stage Classification from Raw Single EEG Channel*; IEEE: Piscataway, NJ, USA, 2022; pp. 298–302. [CrossRef]
34. Guillaume.; Deffuant.; Gérard.; Weisbuch.; Frederic.; Amblard.; David.; Neau. Mixing beliefs among interacting agents. *Adv. Complex Syst.* **2000**, *3*, 11. [CrossRef]
35. Zhang, J.; Hong, Y. Opinion evolution analysis for short-range and long-range Deffuant–Weisbuch models. *Phys. Stat. Mech. Appl.* **2013**, *392*, 5289–5297. [CrossRef]
36. Luo, Y.; Li, Y.; Sun, C.; Cheng, C. Adapted Deffuant–Weisbuch model with implicit and explicit opinions. *Phys. Stat. Mech. Appl.* **2022**, *596*, 127095. [CrossRef]
37. Chen, G.; Su, W.; Mei, W.; Bullo, F. Convergence properties of the heterogeneous Deffuant-Weisbuch model. *Automatica* **2020**, *114*, 108825. [CrossRef]
38. Hegselmann, R.; Krause, U. Opinion dynamics and bounded confidence: models, analysis and simulation. *J. Artif. Soc. Soc. Simul.* **2002**, *5*, 1–33.
39. Xu, H.; Cai, H.; Wu, S.; Ai, K.; Xu, M. HKML: A Novel Opinion Dynamics Hegselmann-Krause Model with Media Literacy. In Proceedings of the 2020 IEEE International Conference on Systems, Man, and Cybernetics, SMC 2020, Toronto, ON, Canada, 11–14 October 2020; IEEE: Piscataway, NJ, USA, 2020; pp. 52–57. [CrossRef]
40. Cheng, C.; Yu, C. Social conformity creates consensus and strong diversity of Hegselmann-Krause opinion dynamics. *Sci. China Inf. Sci.* **2022**, *65*, 129202:1–129202:3. [CrossRef]
41. Zhao, Y.; Xu, M.; Dong, Y.; Peng, Y. Fuzzy inference based Hegselmann-Krause opinion dynamics for group decision-making under ambiguity. *Inf. Process. Manag.* **2021**, *58*, 102671. [CrossRef]
42. Atas, F.; Demirci, A.; Özemir, C. Bifurcation analysis of Friedkin-Johnsen and Hegselmann-Krause models with a nonlinear interaction potential. *Math. Comput. Simul.* **2021**, *185*, 676–686. [CrossRef]
43. Li, K.A.; Liang, H.A.; Kou, G.B.; Dong, Y.A. Opinion dynamics model based on the cognitive dissonance: An agent-based simulation. *Inf. Fusion* **2020**, *56*, 1–14. [CrossRef]
44. Baccelli, F.; Chatterjee, A.; Vishwanath, S. Pairwise stochastic bounded confidence opinion dynamics: Heavy tails and stability. In Proceedings of the IEEE INFOCOM 2015—IEEE Conference on Computer Communications, Hong Kong, China, 26 April–1 May 2015. [CrossRef]
45. Dong, Q.; Zhou, X.; Martínez-López, L. A hybrid group decision making framework for achieving agreed solutions based on stable opinions. *Inf. Sci.* **2019**, *490*, 227–243. [CrossRef]
46. Roy, S.; Biswas, S. Opinion dynamics: public and private. *Philos. Trans. R. Soc. Math. Phys. Eng. Sci.* **2022**, *380*, 20210169. [CrossRef]
47. Abramiuk-Szurlej, A.; Lipiecki, A.; Pawłowski, J.; Sznajd-Weron, K. Discontinuous phase transitions in the q-voter model with generalized anticonformity on random graphs. *Sci. Rep.* **2021**, *11*, 17719. [CrossRef]
48. Lallouache, M.; Chakrabarti, A.S.; Chakraborti, A.; Chakrabarti, B.K. Opinion formation in kinetic exchange models: Spontaneous symmetry-breaking transition. *Phys. Rev. E* **2010**, *82*, 056112. [CrossRef]
49. Scheufele, D.A.; Eveland, W.P., Jr. Perceptions of 'Public Opinion' and 'Public' Opinion Expression. *Int. J. Public Opin. Res.* **2001**, *13*, 25–44. [CrossRef]
50. Liang, H.; Li, C.; Dong, Y.; Jiang, Y. The fusion process of interval opinions based on the dynamic bounded confidence. *Inf. Fusion* **2016**, *29*, 112–119. [CrossRef]
51. Dinkelberg, A.; O'Sullivan, D.J.P.; Quayle, M.; MacCarron, P. Detecting Opinion-based Groups and polarization in Survey-based attitude Networks and estimating Question Relevance. *Adv. Complex Syst.* **2021**, *24*, 2150006:1–2150006:37. [CrossRef]
52. Gaitonde, J.; Kleinberg, J.M.; Tardos, É. Polarization in Geometric Opinion Dynamics. In Proceedings of the EC '21: 22nd ACM Conference on Economics and Computation, Budapest, Hungary, 18–23 July 2021; ACM: New York, NY, USA, 2021; pp. 499–519. [CrossRef]
53. Biondi, E.; Boldrini, C.; Passarella, A.; Conti, M. Dynamics of opinion polarization. *arXiv* **2022**, arXiv:2206.06134.
54. Wu, T.; Zuheros, C.; Liu, X.; Herrera, F. Managing minority opinions in large-scale group decision making based on community detection and group polarization. *Comput. Ind. Eng.* **2022**, *170*, 108337. [CrossRef]
55. Zafeiris, A. Opinion Polarization in Human Communities Can Emerge as a Natural Consequence of Beliefs Being Interrelated. *Entropy* **2022**, *24*, 1320. [CrossRef] [PubMed]
56. Dai, J.; Zhu, J.; Wang, G. Opinion influence maximization problem in online social networks based on group polarization effect. *Inf. Sci.* **2022**, *609*, 195–214. doi: 10.1016/j.ins.2022.07.086. [CrossRef]
57. Ye, Y.; Zhang, R.; Zhao, Y.; Yu, Y.; Du, W.; Chen, T. A Novel Public Opinion Polarization Model Based on BA Network. *Systems* **2022**, *10*, 46. [CrossRef]
58. Ernst, E.; Resch, K. The Barnum effect in complementary medicine. *Complement. Ther. Med.* **1995**, *3*, 134–137. [CrossRef]

entropy

MDPI

Article

A Social Recommendation Model Based on Basic Spatial Mapping and Bilateral Generative Adversarial Networks

Suqi Zhang [1,*], Ningjing Zhang [2], Wenfeng Wang [2], Qiqi Liu [3] and Jianxin Li [4]

[1] School of Information Engineering, Tianjin University of Commerce, Tianjin 300134, China
[2] School of Science, Tianjin University of Commerce, Tianjin 300134, China; zhangningjing@stu.tjcu.edu.cn (N.Z.); wangwenfeng@stu.tjcu.edu.cn (W.W.)
[3] School of Artificial Intelligence and Data Science, Hebei University of Technology, Tianjin 300401, China; qiqi.liu@hebut.edu.cn
[4] School of IT, Deakin University, Burwood, VIC 3125, Australia; jianxin.li@deakin.edu.au
* Correspondence: suqizhang@tjcu.edu.cn

Abstract: Social recommender systems are expected to improve recommendation quality by incorporating social information when there is little user–item interaction data. Therefore, how to effectively fuse interaction information and social information becomes a hot research topic in social recommendation, and how to mine and exploit the heterogeneous information in the interaction and social space becomes the key to improving recommendation performance. In this paper, we propose a social recommendation model based on basic spatial mapping and bilateral generative adversarial networks (MBSGAN). First, we propose to map the base space to the interaction and social space, respectively, in order to overcome the issue of heterogeneous information fusion in two spaces. Then, we construct bilateral generative adversarial networks in both interaction space and social space. Specifically, two generators are used to select candidate samples that are most similar to user feature vectors, and two discriminators are adopted to distinguish candidate samples from high-quality positive and negative examples obtained from popularity sampling, so as to learn complex information in the two spaces. Finally, the effectiveness of the proposed MBSGAN model is verified by comparing it with both eight social recommendation models and six models based on generative adversarial networks on four public datasets, Douban, FilmTrust, Ciao, and Epinions.

Keywords: recommendation algorithm; social recommendation; generative adversarial network; nonlinear mapping

Citation: Zhang, S.; Zhang, N.; Wang, W.; Liu, Q.; Li, J. A Social Recommendation Model Based on Basic Spatial Mapping and Bilateral Generative Adversarial Networks. *Entropy* **2023**, *25*, 1388. https://doi.org/10.3390/e25101388

Academic Editors: Éloi Bossé and José Roberto Iglesias

Received: 14 June 2023
Revised: 15 September 2023
Accepted: 25 September 2023
Published: 28 September 2023

1. Introduction

With the development and popularity of the internet, people are facing an increasingly serious problem of information overload [1]. As an important information filtering technology, recommendation algorithms can provide users with personalized information that meets their interests and needs, saving their time and improving the efficiency of information utilization. Recommendation algorithms have been used widely in many fields [2,3], for example, e-commerce platforms and music and video streaming services. The emergence of social platforms has sparked some analysis regarding social networks [4]. At the same time, the rise of social networking platforms provides a large amount of user-related data for social recommendation, which can effectively improve recommendation quality and user satisfaction by using social relationships and extracting potential user interest features from them. Therefore, social recommendation technology has become an important research direction and research hotspot in the field of recommendation systems [5,6].

Currently, social recommendation models are mainly based on the assumption of homogeneity, users with social relationships have similar interests [7]. However, this assumption is not realistic. In reality, the social behavior of users in the social space and the interaction behavior of users in the interaction space are both diverse and contingent.

Therefore, it is believed that the heterogeneous information in the two spaces: the social space and the interaction space, shall not be directly fused [8].

Among them, the fusion of heterogeneous information refers to the process of combining and harmonizing data from different sources or formats, such as text, images, videos, and user profiles. For example, in a recommender system, integrating information from various sources like product descriptions, user reviews, and social media data to provide personalized recommendations. For example, a user follows and comments on content related to high-calorie food in the social space, while he or she often searches for and buys sports-related goods in the interaction space. Although these two behaviors may not seem to be directly related, the common feature behind them is the user's pursuit of healthy living. If the information in the interaction space and social space is directly fused, it may recommend high-calorie food to users and ignore their pursuit of healthy life; thus affecting their user experience. Therefore, directly utilizing users' social behavior to recommend products can introduce a lot of noise, and how to effectively fuse heterogeneous information has become a fundamental problem in the field of social recommendation. At the same time, how to further capture the common features hidden behind heterogeneous information on the basis of effective fusion of heterogeneous information is a problem that needs to be solved.

Apart from the fusion of heterogeneous information, social recommendation models also focus on how to better mine the data information in the social and interaction spaces to improve recommendation quality. There are a lot of traditional data information mining strategies such as classification, clustering, generative adversarial network (GAN), and regression. Among these, generative adversarial networks [9] are a powerful deep learning model that can generate data with high similarity and have been used widely in areas such as deep learning [10–12]. Among them, the mining of data information involves extracting valuable insights and patterns from a large volume of data. It includes techniques such as data preprocessing, feature extraction, and data analysis. For instance, in the field of customer relationship management, mining customer data to identify patterns of customer behavior and preferences for targeted marketing campaigns. In recent years, more and more researchers have started to explore how GAN can be applied to social recommendation to improve recommendation accuracy. The challenge of generative adversarial networks is the design of adversarial ideas, constructing more effective generators and discriminators, so as to use the generative power of generative adversarial networks. In the scope of social recommendations, GAN can be used to generate candidate items [13] or candidate friends [14], in order to facilitate more accurate recommendations. However, most GAN-based approaches only consider either the social space or the interaction space, failing to capture the bilateral information at the same time.

The organizational structure is as follows: Section 2 introduces the relevant work; Section 3 introduces the specific implementation process and details of the MBSGAN model; in Section 4, the effectiveness of the model was verified through two sets of comparative experiments; finally, the conclusions, limitations, and potential research directions of this study were summarized.

2. Related Work

In this section, two lines of related work are presented, namely, the social relationship-based recommendation model and the generative adversarial network-based recommendation model.

The user's social relationship information, as an important factor influencing the user's decision making, has been widely incorporated into social relationship-based recommendation models to improve the accuracy and performance of recommendation models. SBPR [15] transforms social relations into a kind of weight, which is used to strengthen interaction between users, so as to combine social information and interactive information. Sorec [16] is based on probabilistic matrix decomposition, which decomposes the user–item interaction matrix into two low-dimensional matrices and the authors improved the accu-

racy and performance of the recommendation model by introducing a social network factor matrix between these two matrices to effectively fuse the social and interaction information. DSCF [17] is based on collaborative filtering, in which an attention layer is adopted to fuse interaction and social information. DiffNet++ [18], as a neural network based approach, aggregates higher-order neighbors in the social network and interaction network to obtain user expressions separately and uses a graph attention mechanism to fuse the two user expressions. All of the social recommendation models mentioned above make recommendations by sharing a unified user expression, which achieves the fusion of the two types of information. The advantage of these models is that sharing user expressions can fill in missing data and improve recommendation effectiveness by integrating information from multiple spaces, especially in situations with sparse data. However, these studies overlook the fact that users typically interact with different goals in the interaction space and social space, and the underlying motivations and influencing factors are different, leading to heterogeneity in interaction and social behavior [19]. To solve the above heterogeneity problem, in some social recommendation models, researchers attempt to learn user feature vectors in the interaction space and social space separately, and use these learned user feature vectors to make recommendations. DASO [20] is based on generative adversarial networks, which fuse interaction information and social information by mapping them to each other's space. DcRec [21] is a graph neural network-based social recommendation model that separates user information in the social space and item space by contrast learning, and then the user feature vectors in the two spaces are fused for recommendation tasks using an attention-based fusion mechanism. Although the above methods solve the problem of heterogeneity by learning users separately, these two models do not take into account that the interaction and social behavior of users are influenced by their own values and personality characteristics, and the two behaviors also share common characteristics, which cannot completely erase the similarity between them [22]. Continuing with the example in the introduction, considering only the user's interest in high-calorie food content and their social relationship with fitness influencers separately, without considering the underlying features that connect them, can still lead to incorrect judgments, assuming that users both enjoy eating high-calorie food and following fitness influencers. Therefore, they did not fully utilize the common features behind user interaction and social behavior [23].

Generative adversarial networks have been widely used to learn the distribution of user–item interaction data. Liu et al. [24] proposed solution generates reasonable user–item pairs by the relevance score function and the discriminator discriminates between real user–item pairs and the generator-generated user–item pairs. In CFGAN [25], the generator generates reasonable user purchase vectors, and the discriminator discriminates between the real user purchase vectors and the generator-generated user purchase vectors. GCGAN [26] uses convolutional neural networks to generate user purchase vectors based on CFGAN. RSGAN [13] is a social recommendation model based on generative adversarial networks, in which the generator samples the items that friends of the user frequently interact with, the user's preferred items, and the discriminator is responsible for distinguishing the items sampled by the generator from the real interaction items, so that the items generated by the generator become closer to the user's preferences through adversarial training. ESRF [14] is also a social recommendation model based on GAN, in which the generator samples a fixed number of friends, and the discriminator is responsible for distinguishing between the ratings of the items sampled by the generator and the user's own preferences, and the ratings of the items by the average opinions of the sampled friends. By doing this, the friends generated by the generator become more and more reliable through adversarial training, and the recommendations are assisted by the opinions of the friends. GANRec [27] proposes a negative sampling model based on the generative adversarial network, which improves the accuracy of the recommendation system by using GAN to generate negative samples. However, the above recommendation model only considers the use of the bilateral generative adversarial networks in the interaction space. Therefore, in this paper, we build a bilateral generative adversarial network, and use the

generative adversarial network in each space to learn user feature vectors in the social space and interaction space at the same time, so as to improve the accuracy of recommendation algorithms.

3. MBSGAN Model

Users' values and personality traits developed over time directly influence their interaction and social behavior. The way of fully extracting common features between these two spaces will have a great influence on the social recommendation. Therefore, this paper introduces a base feature space to fuse interaction and social information, which contains common user characteristics behind user interaction and social behavior, such as user values, personality, family background, and education. In addition, we constructed a bilateral generative adversarial network in both spaces in order to deeply explore and learn the complex data information in both spaces. While solving the problem of heterogeneity effectively, this better captures the common features behind the two spaces and utilizes bilateral generative adversarial networks to learn information from both spaces simultaneously.

3.1. Overview of the Model Framework

In this paper, we propose a social recommendation model based on basic spatial mapping and bilateral generative adversarial networks (MBSGAN), called MBSGAN, based on spatial mapping and bilateral generative adversarial networks to utilize the underlying feature space to capture the common features behind user interaction and social behavior. Among them, adversarial learning in the interaction space obtains candidate recommended items by learning the interaction information between users and items, while in the social space, candidate friends are obtained by learning the social information between users and their friends. Both modules are adversarial models, but they are based in different data spaces and have different goals. These two adversarial networks are the core content of bilateral adversarial training in this paper. In MBSGAN, the fusion of interaction and social information through spatial mapping and bilateral generative adversarial networks can help deeply explore the interaction information in their respective spaces, so as to improve the accuracy of recommendations.

The model framework is shown in Figure 1, and the model consists of three modules: a "User Vector Mapping" module, an "Interaction Space Adversarial Learning" module and a "Social Space Adversarial Learning" module.

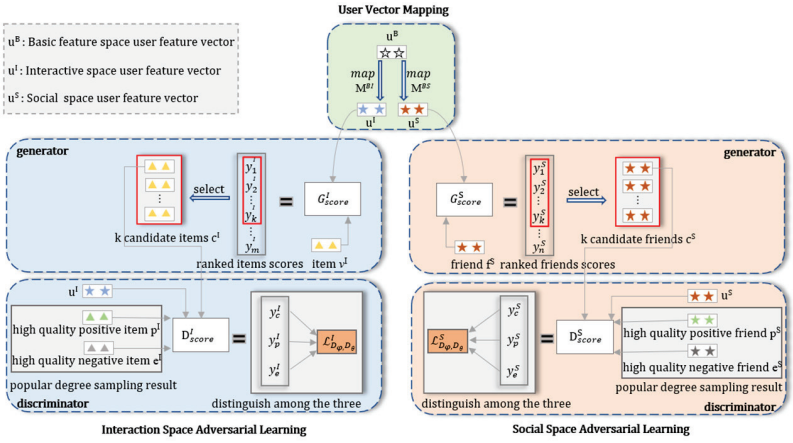

Figure 1. An overview of the proposed MBSGAN framework. u^{B}, u^{I}, u^{S} represent vector representations of users in the basic feature space, interaction space, and social space, respectively. v^I, f^S, respectively, represent the item expression and user friend expression. c^I, c^S represent the candidate items and friends selected by the generator; p^I, e^I, p^S, e^S represent high-quality positive and negative examples selected from interactive and social data (please refer to Sections 3.3.2 and 3.4.2 for detailed interpretation).

The "User Vector Mapping" module contains the user's basic feature vector u^B and two mapping functions M_{B-I} and M_{B-S}. First, the user's base feature vector u^B is mapped through the mapping function M_{B-I} to the interaction space, to obtain the user vector in the interaction space u^I. At the same time, the user base feature vector u^B is mapped to the social space by the mapping function M_{B-S} to the social space, to obtain the user expression in the social space u^S. Finally, the u^I and u^S are input to the "Interaction Space Adversarial Learning" module and the "Social Space Adversarial Learning" module, respectively, for adversarial training.

The "Interaction Space Adversarial Learning" module consists of a generator and a discriminator. First, the user feature vector of the interaction space u^I and item vectors v^I are both input into the score function $G^I{}_{score}$ (the definition of $G^I{}_{score}$ will be given in Equation (4) of Section 3.3). The top k items with the highest scores are selected as candidate items. Then, the user feature vector u^I and the high quality positive items p^I, high quality negative items e^I sampled by popularity and the candidate items c^I generated by the generator are input together into the score function D^I_{score} (the definition of D^I_{score} will be given in Equation (6) of Section 3.3), and then we obtain the correlation scores of users with high-quality positive and negative items ${y_p}^I$, ${y_e}^I$ and the correlation scores between the user and the candidate items ${y_c}^I$. Finally, the loss function $\mathcal{L}^I_{D_\varphi}$ (the definition of $\mathcal{L}^I_{D_\varphi}$ will be given in Equation (8) of Section 3.3) is used to make ${y_c}^I$ both away from ${y_p}^I$ and away from ${y_e}^I$ as far as possible, thus distinguishing the candidate items.

The "Social Space Adversarial Learning" module also includes a generator and a discriminator. First, the user feature vector of the social space u^S and the friend vector f^S are both input into the score function G^S_{score} (the definition of G^S_{score} will be given in Equation (11) of Section 3.4), the relevance scores of the user and all friends are obtained, and the top k friends with the highest scores are selected as candidate friends. Then, the user feature vector u^S and the high-quality positive friends p^S, high-quality negative friends e^S are sampled by popularity and the candidate friends c^S generated by the generator are input together into the score function G^S_{score} to obtain the correlation score between the user and the high-quality positive and negative friends ${y_p}^S$, ${y_e}^S$, and the correlation score between the user and the candidate friends ${y_c}^S$. Finally, the loss function $\mathcal{L}^S_{D_\varphi}$ (the definition of $\mathcal{L}^S_{D_\varphi}$ will be given in Equation (14) of Section 3.4) is used as far as possible to make ${y_c}^S$ both away from ${y_p}^S$ and away from ${y_e}^S$, thus distinguishing the candidate friends.

After the above bilateral adversarial training process, the candidate items obtained from the interaction space generator are recommended to the user as the items to be recommended. In the following, we will introduce the "User Vector Mapping" module in Section 3.2, the "Interaction Space Adversarial Learning" module and the "Social Space Adversarial Learning" module in Sections 3.3 and 3.4. Finally, in Section 3.5, we describe the entire adversarial training process of the model.

3.2. "User Vector Mapping" Module

The base feature space is a space that is deeper and more in line with the essence of things than the interaction space and social space. The decisions made by users in any scenario are influenced by their own values, which reflect a user's orientation and thinking or viewing anything and distinguishing right from wrong, and these values have a certain degree of stability and persistence. Unlike the characteristic factors in social and shopping scenarios, values will not undergo significant changes in a short period of time. Using the base feature space to reflect users' basic values, and the feature factors of the base feature space can include users' pursuit of a better life, freedom, and equality, etc. The social and interactive behaviors of users in both social and shopping scenarios are influenced by their own values. Therefore, we believe that the base feature space can be transformed into the interaction space and social space through mapping functions.

We transfer user information from the base feature space (*B*: the basic space) to the interaction space (*I*: the interaction space) and the social space (*S*: the social space) by a nonlinear mapping operation. Specifically, the user's representation in the base feature

space ${u_i}^B$ is mapped to the interaction space and the social space by a mapping function, and the user's expression in the interaction space ${u_i}^I$ and the user's expression in the social space ${u_i}^S$ are obtained. As shown in Equation (1), the nonlinear mapping function from the base feature space to the interaction space is defined as follows:

$$u_i^I = M_{p-I}\left(u_i^B\right) = W_L^I \cdot \left(\cdots \alpha\left(W_2^I \cdot \alpha\left(W_1^I \cdot u_i^B + b_1^I\right) + b_2^I\right)\cdots\right) + b_L^I \tag{1}$$

In the above equation, the ${W_S}^I$ and ${b_S}^I$ are the weights and biases of the L layer neural network (the number of layers in this article is set to 2), respectively, and α is the nonlinear activation function. Similarly, the nonlinear function from the underlying feature space to the social space is shown in Equation (2):

$$u_i^S = M_{p-S}\left(u_i^B\right) = W_L^S \cdot \left(\cdots \beta\left(W_2^S \cdot \beta\left(W_1^S \cdot u_i^B + b_1^S\right) + b_2^S\right)\cdots\right) + b_L^S \tag{2}$$

where the ${W_S}^S$ and ${b_S}^S$ are the weights and biases of the L layer neural network, respectively, and β is the nonlinear activation function. Equations (1) and (2) represent two multilayer perceptrons with L layers, respectively.

The user expression mapped through the base feature space will be used for adversarial learning in the interaction space and adversarial learning in the social space, respectively, which will be introduced below. Therefore, the base feature space and bilateral generative adversarial networks are combined to jointly mine information and improve recommendation performance.

3.3. "Interaction Space Adversarial Learning" Module

To better learn user and item representations, we use the generative adversarial network in the interaction space because of its powerful ability to learn complex data distributions to capture users' preferences in selecting items. As shown in the lower left part of Figure 1, the interaction space adversarial training module consists of two parts: the generator attempts to select as many items that can best match the user's interests as candidates as possible; the discriminator's goal is to try to override the candidates generated by the generator.

3.3.1. The Generator in the Interaction Space

The goal of the generator is to approximate the potential true conditional distribution ${P_{real}}^I\left(v^I \mid {u_i}^I\right)$ and generate the most relevant candidate samples. First, we use ${g_{score}}^I\left({u_i}^I, {v_j}^I\right)$ to denote the item's ${v_j}^I$ click or purchase likelihood by the user ${u_i}^I$, as shown in Equation (3):

$$g_{score}^I\left(u_i^I,\ v_j^I\right) = \left(u_i^I \cdot v_j^I\right) + \varphi_g^I \tag{3}$$

where φ_g^I is the bias. After normalizing the probabilities by using the softmax function, we obtain the generator score function in the interaction space G_{score}^I as shown in Equation (4):

$$G_{score}^I = \frac{exp\left(g_{score}^I\left(u_i^I,\ v_j^I\right)\right)}{\sum_{v_j \in V} exp\left(g_{score}^I\left(u_i^I,\ v_j^I\right)\right)} \tag{4}$$

Second, we use this score function to obtain the user ${u_i}^I$ prediction scores for all items ${y_1}^I, {y_2}^I \cdots {y_m}^I$ and after sorting these items, we select the items with the top k items as candidate items.

3.3.2. The Discriminator in the Interaction Space

After the generator generates the candidate items, the discriminator is responsible for overriding the candidate items generated by the generator. The advantage of the popularity sampling method over other common sampling methods lies in its simplicity

and ability to handle cold-start problems. So the discriminator improves its discriminative power by utilizing a two-part prevalence-based sampling strategy [28]. The prevalence-based sampling strategy is used to accurately obtain positive and negative example items for adversarial training. The discrimination between positive items, negative items and candidate items is designed for the continuous game between generator G and discriminator D to better learn the true data distribution in the training data.

The main process of the popularity-based sampling strategy is as follows. First, the popularity of an item is expressed in terms of the number of users who have interacted with n_j. Second, a popularity mean (Mean) is calculated to reflect the average popularity of all items. Items above the mean popularity value are defined as high-popularity items and those below the mean popularity value are defined as low-popularity items. The mean popularity value is calculated in Equation (5).

$$Mean = \frac{1}{J}\sum_{j=1}^{J} n_j \tag{5}$$

where the n_j is the first j the prevalence of the first item, and J is the total number of items.

According to the definition of popularity, we believe that among the positive examples of items that users have interacted with, the low-popularity items represent the users' true interest preferences. Similarly, among the negative example items that the user has interacted with, the high popularity items reflect the user's true aversion tendency. Therefore, the high-quality positive items, p^I, will be obtained by intersecting the user's positive items with the low-popularity items, and similarly, the high-quality negative items, e^I, will be obtained by intersecting the user's negative example items with the high popularity items, as shown in Figure 2.

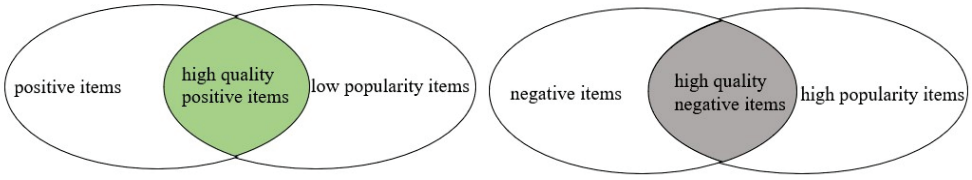

Figure 2. Schematic diagram of prevalence sampling.

The main idea of discriminating between positive and negative items and candidate items is that users' preferences for predicted candidate items shall not be higher than the users' preference for high-quality positive items; the users' preference for predicted candidate items shall not be lower than the users' preference for high-quality negative items.

The score function of the discriminator in the interaction space ${D_{score}}^I$ is shown in Equation (6):

$$D^I_{score} = \frac{exp\left(f^I_{score}(u_i,\ v_j)\right)}{\sum_{v_j \in V} exp\left(f^I_{score}(u_i,\ v_j)\right)} \tag{6}$$

$$f^I_{score}(u_i, v_j) = (u_i \cdot v_j) + \varphi^I_f \tag{7}$$

where ${\varphi_f}^I$ is the bias. As in Equation (7), we can obtain the prediction score of each item in the discriminator.

In the stage of training discriminator D, the user ratings of high-quality positive and negative example items, as well as candidate items, are fed into the discriminator D with the aim of overriding the candidate items generated by the generator. The discriminator loss function $\mathcal{L}^I_{D_\varphi}$ is trained to maximize the difference between users' ratings of candidate items and users' ratings of high-quality positive examples and maximize the difference between

users' ratings of candidate items and users' ratings of high-quality negative examples. The objective function of discriminator D is shown in Equation (8):

$$\min_{D_\varphi} \mathcal{L}^I_{D_\varphi} = -E\left[\left(log\sigma\left(y_p^I - y_c^I\right) + log\sigma\left(y_c^I - y_e^I\right)\right)\right] \tag{8}$$

where the ${y_p}^I$, ${y_e}^I$ denote the user's prediction scores for high-quality positive items and high-quality negative items obtained by using the prevalence-based sampling strategy, and ${y_c}^I$ denotes the user's prediction scores for the candidate items generated by the generator.

In the stage of training the generator G, the user's ratings of high-quality positive example items and candidate items are fed into the generator G, with the aim of generating candidate items that better match the user's true preferences. The difference between the user's rating of candidate items and the user's rating of high-quality positive examples is minimized by training, i.e., maximizing the generator loss function $\mathcal{L}^I_{G_\theta}$. The objective function of the generator G is shown in Equation (9):

$$\max_{G_\theta} \mathcal{L}^I_{G_\theta} = -E\left[log\sigma\left(y_p^I - y_c^I\right)\right] \tag{9}$$

where ${y_c}^I$ denotes the user's the predicted rating of the candidate item, the ${y_p}^I$ denotes the user's prediction scores for the positive example items. The generator G is trained to fight against the discriminator D, until the discriminator D cannot distinguish the candidate items from the real data.

3.4. "Social Space Adversarial Learning" Module

In order to better learn user expressions from a social perspective, we utilize another generative adversarial network in social space for social information learning. Again, adversarial learning in the social space contains two parts, a generator and a discriminator, as shown in the lower right part of Figure 1. The generator tries to use the generator score function to select friends that are as similar as possible to the mapped user expressions as candidate friends; the discriminator aims to distinguish candidate friends from real friends by the discriminator score function.

3.4.1. The Generator in the Social Space

The goal of the generator is to approach the underlying true conditional distribution through adversarial training ${P_{real}}^S\left(f^S \mid {u_i}^S\right)$ and let the user ${u_i}^S$ generate the most relevant candidate friends. Similarly, we use ${g_{score}}^S\left({u_i}^S, {f_j}^S\right)$ to denote ${f_j}^S$ is the friend of the user ${u_i}^S$, as shown in Equation (10):

$$g^S_{score}\left(u_i,\ k_j\right) = \left(u_i^S \cdot f_j^S\right) + \varphi_g^S \tag{10}$$

where ${\varphi_g}^S$ is the bias. After normalizing the probabilities by using the softmax function, we obtain the score function of the generator in the social space ${G_{score}}^S$ as shown in Equation (11):

$$G^S_{score} = \frac{exp\left(g^S_{score}\left(u_i^S,\ f_j^S\right)\right)}{\sum_{k_j \in K} exp\left(g^S_{score}\left(u_i^S, f_j^S\right)\right)} \tag{11}$$

In the following, we use this score function to arrive at the user u_i^S prediction scores for all friends ${y_1}^S$, ${y_2}^S \cdots {y_n}^S$ and after sorting, we select the top k friends as candidate friends.

3.4.2. The Discriminator in the Social Space

The goal of the discriminator is to override the candidate friends generated by the generator. The discriminator also consists of two parts: a sampling strategy based on

popularity and a method for discriminating between positive and negative examples and candidate friends.

Similarly, we use a popularity-based sampling strategy to select high-quality positive friends and high-quality negative friends. The high-quality positive friends, p^S, were obtained by intersecting the user's friends with the low-popularity friends, and similarly, the high-quality negative friends, e^S, will be obtained by intersecting the user's negative friends (friends who have no social relationship with the user) with the high popularity friends.

The main idea of discriminating between high-quality positive and negative example friends, and candidate friends is that the similarity between the user and the predicted candidate friend shall not be higher than the similarity between the user and the high-quality positive example friend, and the similarity between the user and the predicted candidate friend shall not be lower than the similarity between the user and the high quality negative example friend.

The score function of the discriminator in social space ${D_{score}}^S$ is shown in Equation (12):

$$D^S_{score} = \frac{exp\left(f^S_{score}(u_i,\ k_j)\right)}{\sum_{k_j \in K} exp\left(f^S_{score}(u_i,\ k_j)\right)} \tag{12}$$

$$f^S_{score}(u_i,\ k_j) = (u_i \cdot k_j) + \varphi^S_f \tag{13}$$

where ${\varphi_f}^S$ is the bias. With Equation (13), we can obtain the predicted scores of the user and each friend in the discriminator. Similarly, the objective function for the social space discriminator D adversarial training is shown in Equation (14):

$$\min_{D_\varphi} \mathcal{L}^S_{D_\varphi} = -E\left[\left(log\sigma\left(y^S_p - y^S_c\right) + log\sigma\left(y^S_c - y^S_e\right)\right)\right] \tag{14}$$

where ${y_p}^S$, ${y_e}^S$ denotes the user's prediction scores for the high-quality positive and high-quality negative friends obtained by using the popularity-based sampling strategy, and ${y_c}^S$ denotes the user's prediction scores for the candidate friends generated by the generator.

In the stage of training the optimized social space generator G, the users' ratings of positive examples and high-quality candidate friends are fed into the objective function of the generator G, with the aim of generating candidate friends that better match the users' true preferences. The objective function for generator G is shown in Equation (15):

$$\max_{G_\theta} \mathcal{L}^S_{G_\theta} = -E\left[log\sigma\left(y^S_p - y^S_c\right)\right] \tag{15}$$

where ${y_c}^S$ denotes the user's predicted score of the candidate friend, the ${y_p}^S$ denotes the user's prediction scores for the positive friend. The generator G is trained to fight against the discriminator D so that the discriminator D cannot distinguish the candidate friends from the real data, and in order to make the candidate friends generated by the generator closer to the real data, then the goal is to make the difference between ${y_p}^S$ and ${y_c}^S$ becomes smaller and smaller. Thus, let ${\mathcal{L}_G}^S{}_\theta$ be maximized.

3.5. Adversarial Training Process of the Model

In order to show the training process of the MBSGAN model more clearly, we present the adversarial training algorithm of the MBSGAN model in Algorithm 1. The training of each cycle is mainly divided into three parts: base feature space mapping, adversarial training in the social space and adversarial training in the interaction space, as shown below.

Algorithm 1: MBSGAN adversarial training algorithm.

Input: datasets
Output: recommendation list
Randomly split the dataset (item, social) into training set (80%) and testing set (20%)
for each epoch **do**
  obtain the mapped user vector u^I, u^S from the primary feature space
  pretrain the generator and the discriminator of social space
  get high-quality positive friends p^S and negative friends e^S by popularity sampling
  for each batch of adversarial training **do** (social space)
    use current G^S_{score} to obtain all friends' prediction scores
    select the **top k** friends as candidate friends c^S
    update generator based on Equation (15)
    use D^S_{score} to obtain user's prediction scores for p^S, e^S and c^S
    update discriminator based on Equation (14)
  end
  pretrain the generator and the discriminator of interaction space
  get high-quality positive items p^I and negative items e^I by popularity sampling
  for each batch of adversarial training **do** (interaction space)
    use current G^I_{score} to obtain all items' prediction scores
    select the **top k** items as candidate items c^I
    update generator based on Equation (9)
    use D^I_{score} to obtain user's prediction scores for p^I, e^I and c^I
    update discriminator based on Equation (8)
  end
  recommend the **top k** items with the highest scores (interaction space)
  calculate precision, recall, NDCG and RMSE, MAE (testing set)
end

4. Experimental Study

To validate the effectiveness of the MBSGAN model's performance, the effects of spatial mapping and bilateral adversarial training on model performance are explored, as well as the effects of parameter variations in the model on the results. In this section, two sets of experiments are analyzed in Sections 4.2 and 4.3 to verify the effectiveness of MBSGAN model performance by analyzing the social recommendation model and the adversarial training recommendation model; model ablation experiments are compared in Section 4.4 to verify the effects of vector mapping and bilateral adversarial training on the model; finally, the selection of the number of candidate samples k values is analyzed in Section 4.5 to verify the effects of model parameter variations on MBSGAN model performance.

4.1. Dataset and Evaluation Metrics

In this work, four benchmark datasets, Douban, FilmTrust, Ciao, and Epinions, are used to study the performance of the proposed MBSGAN. The Douban data comes from Douban, which contains users' ratings of movies and social information among users; FilmTrust is a movie dataset from the FilmTrust website, which also contains users' ratings of movies and social information among users; Ciao comes from an online social platform, which includes users' ratings of purchased products and social information among users; the Epinions dataset comes from an online social platform where people can review products, which includes users' ratings of products and social information among users; The specific statistics of the four public datasets are shown in Table 1.

Table 1. Dataset statistics.

Data Items	User Volume	Item Volume	Rating Amount	Social Relationships
Douban	2848	39,586	894,887	35,770
FilmTrust	1508	2071	35,497	1853
Ciao	7375	105,114	284,086	111,781
Epinions	40,163	139,738	664,824	442,980

To evaluate the performance of the model, the evaluation metrics are Precision@ k, Recall@ k, Normalized Cumulative Discount Gain@ k, Mean Absolute Error MAE (Mean Absolute Error), and Root Mean Squared Error RMSE (Root Mean Squared Error). In the top k recommendation task, k is taken as 10 to calculate the first three metrics, and the evaluation metrics are shown below.

Precision: the proportion of all predicted positive samples that contain true positive samples. The definition is as follows:

$$precision = \frac{TP}{TP + TN} \tag{16}$$

where TP (True Positive) represents the number of positive samples predicted as positive and FP (False Positive) represents the number of negative samples predicted as positive.

Recall (recall): the proportion of true positive samples that are predicted to be positive, which is defined as follows.

$$Recall = \frac{TP}{TP + FN} \tag{17}$$

where FN (False Negative) represents the number of negative samples predicted as negative. Recall@ k represents the proportion of true positive samples that are predicted as positive in the first k samples.

Normalized discounted cumulative gain (*NDCG*) is a composite assessment score that evaluates the combined quality of relevance and ranking of items in the test set in the top k recommendation list. Higher NDCG values indicate better ranking results.

$$NDCG = \frac{DGG}{IDGG} \tag{18}$$

$$DCG = \sum_{i=1}^{|REL|} \frac{2^{rel_i} - 1}{log_2(i+1)} \tag{19}$$

where $|REL|$ denotes the results are sorted in the order of relevance from largest to smallest in the best way. rel_i denotes the relevance score of item i. *DCG* (discounted cumulative gain) calculates the score of items in user u's recommendation list by considering both relevance and order factors, and *IDCG* (ideal discounted cumulative gain) is the result of *DCG* normalization.

Mean absolute error (*MAE*): the mean value of the error between the model predicted scores and the true scores, reflecting the degree of similarity between the predicted scores and the true scores. The definition is as follows:

$$MAE = \frac{\sum_{(u,i) \in R_{test}} |r_{ui} - r'_{ui}|}{|R_{test}|} \tag{20}$$

where $|R_{test}|$ denotes the number of user ratings of items in the test set, the r_{ui} and r'_{ui} are the real ratings and the ratings predicted by the algorithm, respectively.

Root mean squared error (*RMSE*) is the square root of the ratio of the square of the predicted score to the true score error to the number of observations n, as defined below:

$$RMSE = \sqrt{\frac{\sum_{(u,i)\in R_{test}} \left(r_{ui} - r'_{ui}\right)^2}{|R_{test}|}} \tag{21}$$

When *precision*, *recall*, and *NDCG* values are larger, it indicates better recommendation performance. *MAE* and *RMSE* reflect the difference between predicted and true scores, and smaller values indicate higher accuracy of recommendations.

4.2. Parameter Settings

The parameter settings in the experiment are shown in Table 2. $\boldsymbol{k}$ is the number of candidate samples, $\boldsymbol{d}$ denotes the vector dimension, $\boldsymbol{\lambda}$ is the regularization coefficient, ***batch*** is the batch size, and ***lr*** is the learning rate. In the experiment, the number of epochs for Douban and FilmTrust was set to 30, and ciao was set to 40.

Table 2. Parameter Settings.

Dataset	k	D	λ	*batch*	*Lr*
Douban	15	32	1×10^{-7}	512	5×10^{-5}
FilmTrust	15	32	1×10^{-6}	512	5×10^{-5}
Ciao	20	32	2×10^{-5}	1024	5×10^{-4}
Epinions	20	32	2×10^{-5}	1024	5×10^{-4}

4.3. Experimental Comparison of Social Recommendation Models

To demonstrate the advantages of the MBSGAN model proposed in this paper over other social recommendation models, the experimental results of the MBSGAN model are compared with eight baseline social recommendation models on four publicly available datasets. Among them, SBPR and SoMA are Bayesian-based social recommendation models; Diffnet++, Light_NGSR, and GNN-DSR are graph convolutional neural network-based social recommendation models; RSGAN, DASO, and ESRF are social recommendation models incorporating generative adversarial networks. Each of the eight baseline social recommendation models is described as follows:

(1) SBPR [15] (2014): for the first time, social relationships were added to the Bayesian personalized ranking algorithm (BPR), arguing that users are more biased towards items preferred by their friends than items with negative feedback or no feedback.
(2) SoMA [29] (2022): a social recommendation model based on the Bayesian generative model that exploits the displayed social relationships and implicit social structures among users to mine their interests.
(3) DiffNet++ (2020): a social recommendation model using graph convolutional networks, by aggregating higher-order neighbors in the social relationship graph and item interaction graph, respectively, and by distinguishing the influence of neighbors on users with an attention mechanism.
(4) Light_NGSR [30] (2022): a social recommendation model based on the GNN framework, which retains only the neighborhood aggregation component and drops the feature transformation and nonlinear activation components. It aggregates higher-order neighborhood information from user–item interaction graphs and social network graphs.
(5) GNN-DSR [31] (2022): a social recommendation model using graph convolutional networks, which considers dynamic and static representations of users and items and combines their relational influences. It models the short-term dynamic and long-term static interaction representations of user interest and item attractiveness, respectively.
(6) RSGAN (2019): a social recommendation model that uses GAN and social reconstruction, where generators generate items that friends interact with as items that users

like, and discriminators are used to distinguish items that friends interact with from items that users really like themselves.

(7) DASO (2019): a social recommendation model based on GAN that fuses heterogeneous information by mapping each other in interaction space and social space. The generator picks samples that are likely to be of interest to users, and the discriminator distinguishes between real samples and generated samples.

(8) ESRF (2020): a social recommendation model using generative adversarial networks and social reconstruction, where the generator generates friends with similar preferences to the user and the discriminator distinguishes between the user's personal preferences and the average preferences of friends.

To verify the effectiveness of MBSGAN combined with vector mapping and bilateral generative adversarial networks, we separate the experimental results into two different types according to the two main tasks of the recommender system: "Top-N recommendation" and "rating prediction". Meanwhile, since the SoMA, Light_NGSR, and GNN-DSR codes are not available, we only compare the MAE and RMSE metrics on the Ciao and Epinions datasets, as shown in Table 3.

Table 3. Experimental results of social recommendation model (Top-N recommendation).

Model	Douban			FilmTrust			Ciao		
	Precision@3	Recall@3	NDCG@3	Precision@3	Recall@3	NDCG@3	Precision@3	Recall@3	NDCG@3
SBPR	0.182	0.013	0.208	0.221	0.094	0.267	0.022	0.008	0.024
DiffNet++	0.204	0.016	0.220	0.375	0.201	0.416	0.025	0.012	0.028
RSGAN	0.211	0.015	0.217	0.347	0.203	0.385	0.029	0.014	0.033
DASO	0.224	0.017	0.239	0.400	0.234	0.445	0.033	0.023	0.038
ESRF	0.223	0.017	0.238	0.380	0.232	0.392	0.032	0.016	0.037
MBSGAN	0.237	0.018	0.248	0.430	0.236	0.459	0.034	0.029	0.039

The MBSGAN model was compared with five social information-based recommendation models with the following results:

By observing the experimental results in Table 3, it can be seen that the MBSGAN proposed in this paper obtains optimal values in terms of each metric in the Douban, FilmTrust, and Ciao datasets compared to the baseline model. Further analysis of the experimental results leads to the following conclusions: Diffnet++, RSGAN, DASO, ESRF, and MBSGAN perform better compared to the traditional social recommendation method SBPR because the four baseline models of the latter incorporate the network model in deep learning, because deep learning models have multiple layers and nonlinear activation functions that can capture complex nonlinear relationships between users and projects. Traditional recommendation models often rely on linear or shallow models, which cannot effectively capture the complex and nonlinear nature of user–item interactions. And compared with SBPR, which only considers the first-order neighbors of users, the use of network models can tap more information about user–item interactions and the association information in social relationships to obtain a richer user representation. Compared with RSGAN and ESRF using GAN, DASO and MBSGAN outperform these two models in all metrics, indicating that RSGAN and ESRF share the same user representation in both interaction and social spaces, which limits the learning of user representation, while DASO and MBSGAN learn user representation in the social space and interaction space separately to learn more fully the information in each space. This is because learning user expressions separately can reduce irrelevant interference. Separating user representations in social spaces and interaction spaces can avoid interference between spaces and improve the independence and accuracy of the model for information in each space. The MBSGAN model performs better than DASO, demonstrating the effectiveness of basic feature space mapping.

By observing the experimental results in Table 4, we can see that, compared with the baseline model, the MBSGAN proposed in this paper obtains the better result in terms of

MAE metrics of the Ciao dataset and on the MAE and RMSE metrics of Epinions. Further analysis of the experimental results leads to the following conclusions: compared with SoMA, Light_NGSR, and GNN-DSR, which use only social relationships, the experimental results of MBSGAN on two real datasets almost outperform these baseline models, indicating that the application of generative adversarial networks in social recommendation is beneficial to improving the accuracy of the models and reducing scoring errors.

Table 4. Experimental results of social recommendation model (rating prediction).

Model	Ciao		Epinions	
	MAE	RMSE	MAE	RMSE
SoMA	0.785	0.998	1.050	1.189
Light_NGSR	0.736	0.973	0.835	1.084
GNN-DSR	0.697	0.944	0.801	1.057
MBSGAN	0.704	0.807	0.765	0.931

4.4. Experimental Comparison of Pairwise Training Recommendation Models

To demonstrate the advantages of the MBSGAN model proposed in this paper over other generative adversarial network-based recommendation models, the experimental results of the MBSGAN model are compared with six baseline adversarial training recommendation models on three publicly available datasets. Among them, CFGAN, GCGAN, and GANRec [27] are collaborative filtering recommendation models based on generative adversarial networks, and RSGAN, DASO, and ESRF are social recommendation models based on generative adversarial networks. The other three baseline adversarial training recommendation models that are different from the social recommendation model experiments are described as follows:

(1) CFGAN (2018): a collaborative filtering recommendation model based on generative adversarial networks, where the generator generates the user's purchase vector, and the discriminator is responsible for distinguishing between the generator's "fake" purchase vector and the real user's purchase vector.
(2) GCGAN (2021): Based on CFGAN, the discriminator captures the latent features of users and items through a graph convolutional network to distinguish whether the input is a "fake" purchase vector by the generator or a real user purchase vector.
(3) GANRec (2023): a collaborative filtering model based on generative adversarial networks, where the generator picks out items that the user may like as negative samples and the discriminator distinguishes between real positive samples and generator-generated negative samples.

In order to verify the effectiveness of MBSGAN combined with vector mapping and bilateral generative adversarial networks, we divided the experimental results into two different types according to the two major tasks of the recommendation systems: "Top-N recommendation" and "rating prediction", respectively. The results of comparing the MBSGAN model with several generative adversarial network-based recommendation models on the Top-N recommendation task were as follows.

By observing the experimental results in Tables 5 and 6, it is evident that the proposed MBSGAN obtains optimal values for each metric in the Douban, FilmTrust, and Ciao datasets compared to the six baseline models. Further analysis of the experimental results leads to the following conclusions: compared with the three collaborative filtering recommendation models CFGAN, GCGAN, and GANRec, RSGAN, DASO, and ESRF perform better because the latter three models incorporate social information, indicating that the proper use of social relationships can help alleviate the sparsity problem and lead to more accurate recommendation results. A social relationship is a direct relationship between people. The addition of social relationships provides more information and basis for recommendation algorithms, making the recommendation results more accurate. Compared with RSGAN and ESRF, DASO and MBSGAN outperformed them on almost

all three datasets, indicating that constructing bilateral generative adversarial networks in both spaces can more fully exploit the information in the interaction and social spaces than unilateral adversaries, thus improving the accuracy of the models and reducing scoring errors. This is because the bilateral adversarial network not only mines the interaction information in the interaction space, but also uses it to learn information in the social space, alleviating the noise problem in both spaces and improving recommendation accuracy.

Table 5. Experimental results of the recommendation model based on adversarial training (Top-N recommendation).

Model	Douban			FilmTrust			Ciao		
	Precision@3	Recall@3	NDCG@3	Precision@3	Recall@3	NDCG@3	Precision@3	Recall@3	NDCG@3
CFGAN	0.203	0.011	0.204	0.239	0.073	0.252	0.023	0.011	0.025
RSGAN	0.211	0.015	0.217	0.347	0.203	0.385	0.029	0.014	0.033
DASO	0.224	0.017	0.239	0.380	0.234	0.392	0.033	0.023	0.037
ESRF	0.223	0.017	0.238	0.400	0.232	0.445	0.032	0.016	0.038
GCGAN	0.190	0.014	0.218	0.212	0.229	0.229	0.021	0.010	0.022
GANRec	0.204	0.015	0.217	0.249	0.231	0.230	0.022	0.011	0.026
MBSGAN	0.237	0.018	0.248	0.436	0.268	0.473	0.034	0.029	0.039

Table 6. Experimental results of the recommendation model based on adversarial training (score prediction).

Model	Douban		FilmTrust		Ciao	
	MAE	RMSE	MAE	RMSE	MAE	RMSE
CFGAN	1.233	1.529	0.981	1.151	1.199	1.423
RSGAN	1.255	1.561	1.022	1.370	1.245	1.560
DASO	0.883	1.224	0.994	1.101	0.859	1.228
ESRF	0.900	1.256	1.683	1.849	1.701	1.869
GCGAN	0.898	1.253	0.956	1.005	0.889	1.255
GANRec	0.922	1.215	1.001	1.059	0.998	1.253
MBSGAN	0.820	1.187	0.895	0.946	0.704	0.807

4.5. Comparison of Ablation Experiments of Models

In order to verify the effectiveness of introducing spatial mapping and bilateral generative adversarial networks in the model, this paper compares the MBSGAN model with the MBSGAN-P model with the vector mapping being removed, and with the MBSGAN-SocGAN model with the social spatial adversarial learning being removed, through ablation experiments. The comparison results are shown in Figures 3 and 4, respectively.

By analyzing the experimental results presented in Figure 3 as well as Figure 4, it can be observed that, after removing the spatial vector mapping part of the base features or bilateral generative adversarial networks, the experimental results of each metric become worse on all three datasets, indicating that both of the above modules have a positive impact on the model performance. The introduction of the spatial mapping part better explores the common features behind different user interactions, which leads to more accurate user expressions. The basic feature space mapping can help the model better discover and extract the common features of users in different spaces. By integrating and mapping user characteristics across different spaces, it is possible to model the similarities and correlations between users in different spaces, thereby more accurately capturing user interests and preferences. In addition, it can be seen that the model performance decreases if the bilateral generative adversarial networks are not used, indicating that using generative adversarial networks to learn users' social information is helpful to obtaining more accurate user expressions. The discriminator network in GAN can evaluate the difference between the generated social information and the real social information. By continuously optimizing the adversarial process between the generator and the discriminator, the generated social

information can be made closer to the real social information, thereby improving the accuracy and credibility of user expression.

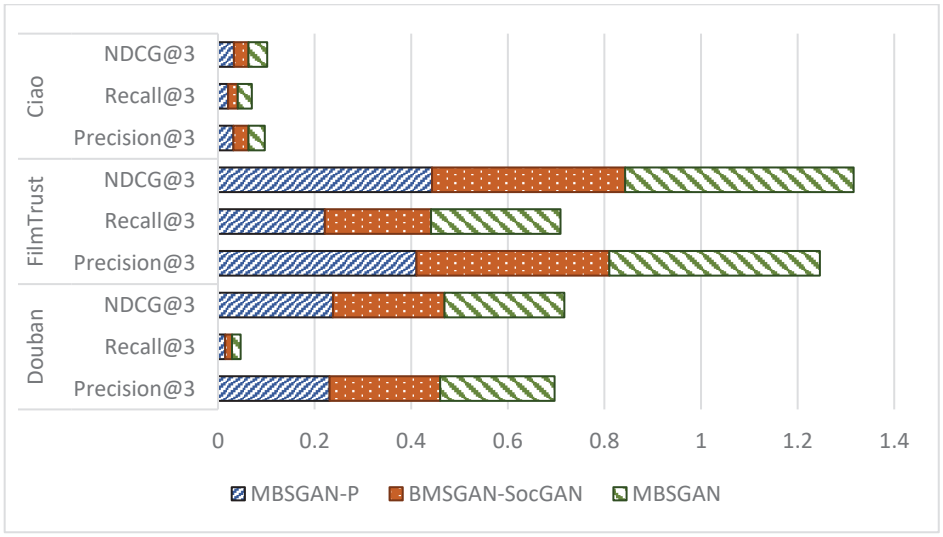

Figure 3. Comparison of ablation experimental results of MBSGAN model (Top-N recommendation).

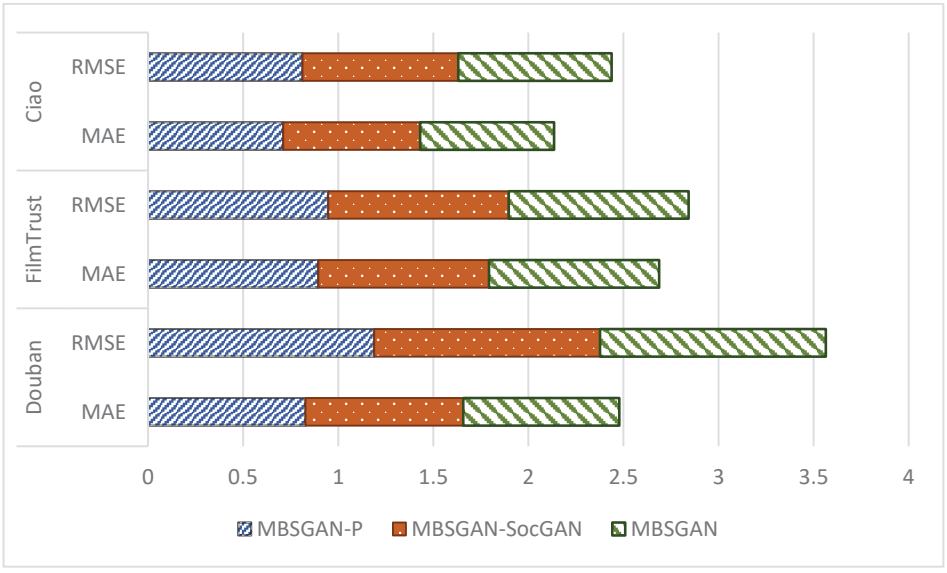

Figure 4. Comparison of ablation experimental results of MBSGAN model (score prediction).

4.6. Effect of the Number of Candidate Samples k Values

The k value is the number of candidate samples in interaction-space adversarial learning as well as social-space adversarial learning, and is used to discriminate among the three in the discriminator of the two spaces together with the high-quality positive and negative examples obtained from sampling, thus enabling the generator to more accurately select candidate samples for recommendation. In order to investigate the effect of the number of candidate samples k value on the model performance, different k values are selected to examine the performance of the proposed MBSGAN model in this paper on three publicly available datasets, and then a reasonable k value is selected as the number of candidate samples to be selected. The experimental results of the MBSGAN model corresponding to different k values are shown in Figures 5–7.

In order to present the results of Precision@3, Recall@3, and NDCG@3 with the number of candidate samples clearly in the same plot, the horizontal coordinates are set as k values and the vertical coordinates are the evaluation values, here the vertical coordinates are used

as the primary and secondary axes. The blue line represents Precision@3, the green line represents NDCG@3, and the orange line represents Recall@3. In Figures 5–7, the values of Precision@3 and NDCG @3 are based on the main axis on the left, and the Recall@3 values are based on the secondary axis on the right.

Analyzing Figures 5–7, it can be observed that the experimental results of the MBSGAN model are affected by the number of candidates k, which shows different trends on the three datasets. The model works best when k = 15 on the Douban dataset, when k = 15 on the FilmTrust dataset, and when k = 20 on the Ciao dataset. When the value of k chosen is too small, fewer candidate samples, positive and negative examples are utilized and the interaction information cannot be more fully utilized. And when the k value chosen is too large, it leads to overfitting and makes the recommendation results inaccurate.

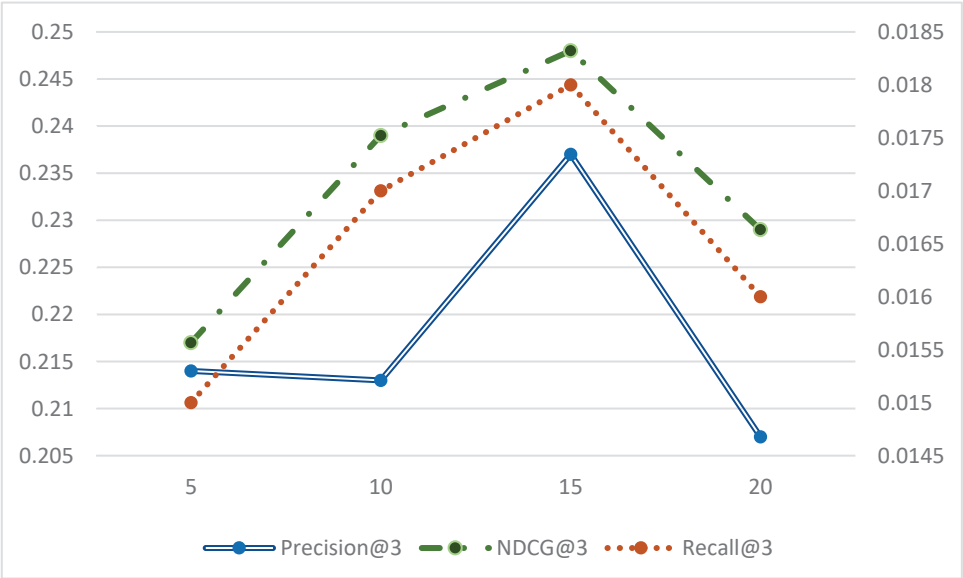

Figure 5. Experimental performance of MBSGAN models with different k values (Douban).

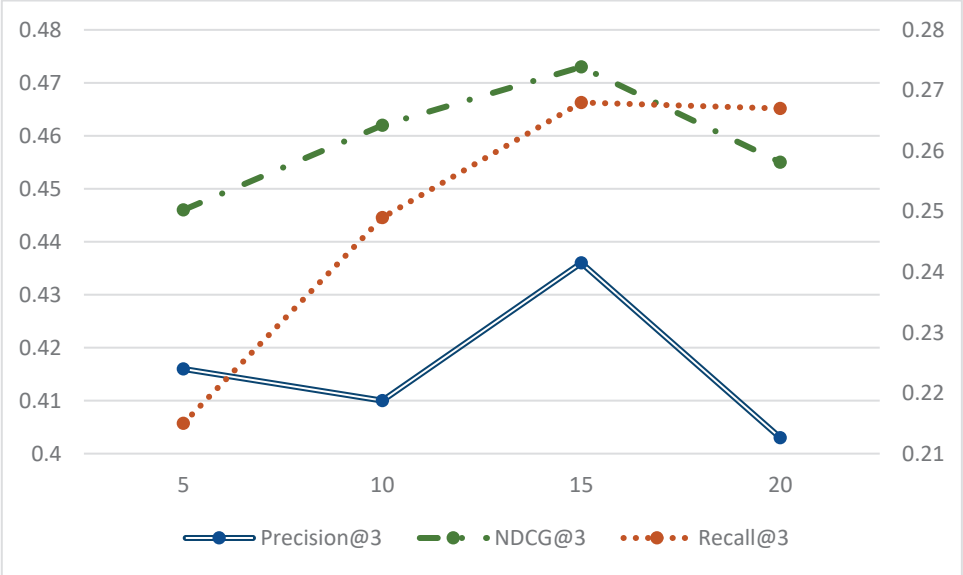

Figure 6. Experimental performance of MBSGAN model with different k values (FilmTrust).

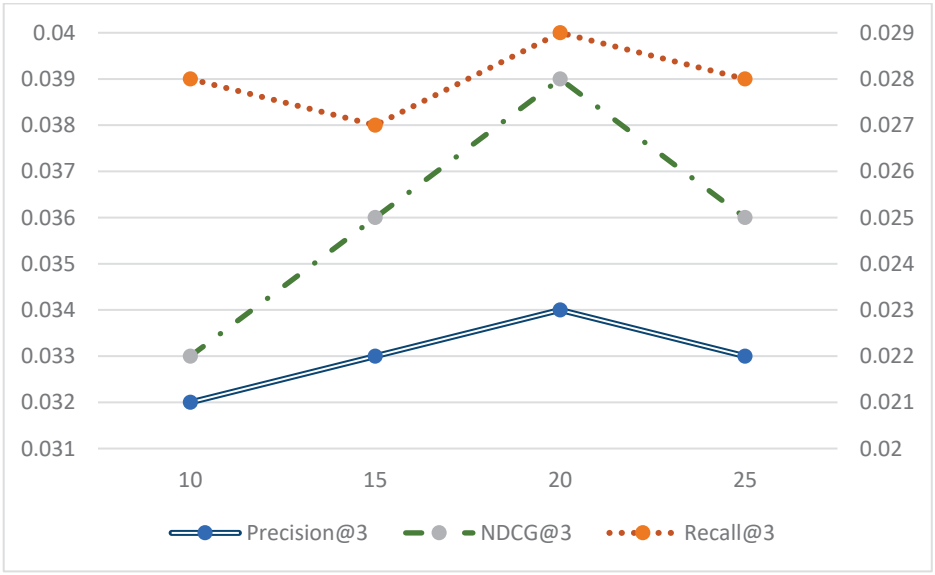

Figure 7. Experimental performance of MBSGAN model with different k values (Ciao).

4.7. Convergence of the Model

To verify the convergence of the model, we conducted experiments on three datasets: Douban, Ciao, and FilmTrust to obtain the learning curve of the MBSGAN model. Among them, the principal axis represents precision@3 and NDCG@3. The secondary coordinate axis represents recall@3 and the horizontal axis represents the number of epochs.

From Figure 8, it can be seen that the MBSGAN model has achieved convergence on all three datasets. Among them, on the Douban and FilmTrust datasets, the model converges when the number of epochs reaches 30, and on the Ciao dataset, the model converges when the number of epochs reaches around 40.

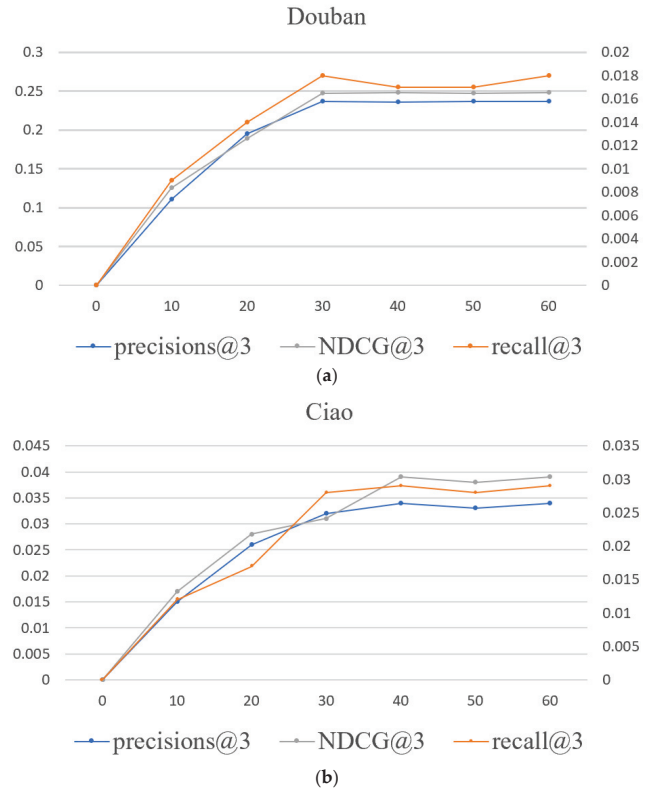

Figure 8. *Cont.*

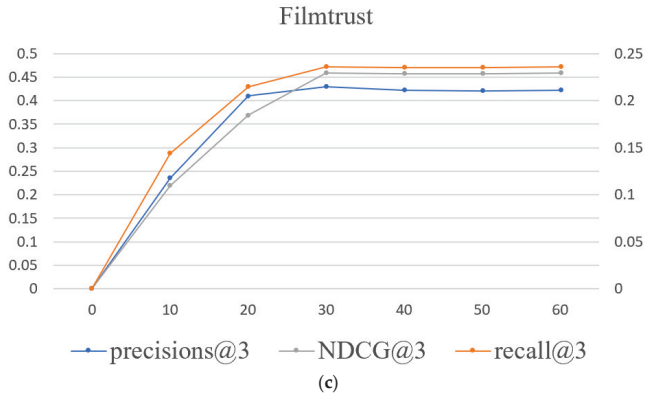

Figure 8. The learning curve of MBSGAN on three datasets. (**a**) convergence of the model on the Douban dataset. (**b**) convergence of the model on the Ciao dataset. (**c**) convergence of the model on FilmTrust dataset.

5. Conclusions

In this paper, we propose a recommendation model based on spatial mapping and bilateral generative adversarial networks (MBSGAN). We first map the base feature space to the interaction space and social space, respectively, to achieve the fusion of heterogeneous spaces and obtain more accurate user representations in both spaces. Then, bilateral generative adversarial networks are constructed in the interaction space and social space to learn the complex information in the respective spaces. Through two sets of comparative experiments, the effectiveness of using the base feature space to fuse heterogeneous information was demonstrated, and the advantages of our constructed bilateral generative adversarial networks in mining information were also verified. However, the factors that affect user interaction behavior are diverse and complex. We only consider the impact of user social information on recommendations, which is not comprehensive enough to learn the potential interaction characteristics of users. We should also consider more diverse information, such as item attribute information and user's own attribute information. Therefore, in the next work, we should consider fusing more auxiliary information for user expression and item expression in bilateral generative adversarial networks, such as knowledge graph information or user attribute information. At the same time, it is necessary to find appropriate fusion methods for this information to further enrich the feature representation of users and items, thereby improving the accuracy of recommendations.

Author Contributions: Methodology, S.Z. and N.Z.; writing—original draft, N.Z.; writing—review and editing, W.W., Q.L. and J.L. All authors have read and agreed to the published version of the manuscript.

Funding: This research was funded by Tianjin Scientific Research Innovation Project [2022SKYZ315].

Conflicts of Interest: The authors declare no conflict of interest.

References

1. Batmaz, Z.; Yurekli, A.; Bilge, A.; Kaleli, C. A review on deep learning for recommender systems: Challenges and remedies. *Artif. Intell. Rev.* **2019**, *52*, 1–37. [CrossRef]
2. Ju, C.H.; Wang, J.; Zhou, G.L. The commodity recommendation method for online shopping based on data mining. *Multimed. Tools Appl.* **2019**, *78*, 30097–30110. [CrossRef]
3. Sheu, H.S.; Chu, Z.X.; Qi, D.Q.; Li, S. Knowledge-guided article embedding refinement for session-based news recommendation. *IEEE Trans. Neural Netw. Learn. Syst.* **2022**, *33*, 7921–7927. [CrossRef] [PubMed]
4. Bonifazi, G.; Cauteruccio, F.; Corradini, E.; Marchetti, M.; Sciarretta, L.; Ursino, D.; Virgili, L. A Space-Time Framework for Sentiment Scope Analysis in Social Media. *Big Data Cognit. Comput.* **2022**, *6*, 130. [CrossRef]
5. Xu, B.; Lin, H.F.; Yang, L.; Xu, K. Cognitive knowledge-aware social recommendation via group-enhanced ranking model. *Cognit. Comput.* **2022**, *14*, 1055–1067. [CrossRef]

6. Liao, J.; Zhou, W.; Luo, F.J.; Wen, J.; Gao, M.; Li, X.; Zeng, J. SocialLGN: Light graph convolution network for social recommendation. *Inf. Sci.* **2022**, *589*, 595–607. [CrossRef]
7. Mcpherson, M.; Smith-Lovin, L.; Cook, J.M. Birds of a Feather: Homophily in social networks. *Annu. Rev. Sociol.* **2001**, *27*, 415–444. [CrossRef]
8. Shi, C.; Hu, B.B.; Zhao, W.X.; Yu, P.S. Heterogeneous information network embedding for recommendation. *IEEE Trans. Knowl. Data Eng.* **2019**, *31*, 357–370. [CrossRef]
9. Goodfellow, I.J.; Pouget-Abadie, J.; Mirza, M.; Xu, B.; Warde-Farley, D.; Ozair, S.; Courville, A.; Bengio, Y. *Generative Adversarial Networks*; NIPS: Northern Ireland, UK, 2014; pp. 2672–2680.
10. Nie, W.Z.; Wang, W.J.; Liu, A.A.; Nie, J.; Su, Y. HGAN: Holistic generative adversarial networks for two-dimensional Image-based three-dimensional object retrieval. *ACM Trans. Multimed. Comput. Commun. Appl.* **2019**, *15*, 1–24. [CrossRef]
11. Liu, D.Y.H.; Fu, J.; Qu, Q.; Nie, J.; Su, Y. BFGAN: Backward and forward generative adversarial networks for lexically constrained sentence generation. *IEEE Acm Trans. Audio Speech Lang. Process.* **2019**, *27*, 2350–2361. [CrossRef]
12. Corradini, E.; Porcino, G.; Scopelliti, A.; Ursino, D.; Virgili, L. Fine-tuning SalGAN and PathGAN for extending saliency map and gaze path prediction from natural images to websites. *Expert Syst. Appl.* **2022**, *191*, 116282. [CrossRef]
13. Yu, J.; Gao, M.; Yin, H.; Li, J.; Gao, C.; Wang, Q. Generating reliable friends via adversarial training to improve social recommendation. In Proceedings of the 2019 IEEE International Conference on Data Mining (ICDM), Beijing, China, 8–11 November 2019; IEEE: Manhattan, NY, USA, 2019; pp. 768–777.
14. Yu, J.; Yin, H.; Li, J.; Gao, M.; Huang, Z.; Cui, L. Enhancing social recommendation with adversarial graph convolutional networks. *IEEE Trans. Knowl. Data Eng.* **2020**, *34*, 3727–3739. [CrossRef]
15. Tong, Z.; Mcauley, J.; King, I. Leveraging social connections to improve personalized ranking for collaborative filtering. In Proceedings of the Proceedings of the 23rd ACM International Conference on Conference on Information and Knowledge Management, Shanghai, China, 3–7 November 2014; CIKM: Shanghai China, 2014; pp. 261–270.
16. Hao, M.; Yang, H.; Lyu, M.R.; King, I. Sorec: Social recommendation using probabilistic matrix factorization. In Proceedings of the 17th ACM Conference on Information and Knowledge Management, Napa Valley, CA, USA, 26–30 October 2008; ACM: Manhattan, NY, USA, 2008; pp. 931–940.
17. Fan, W.; Ma, Y.; Yin, D.; Wang, J.; Tang, J.; Li, Q. Deep social collaborative filtering. In Proceedings of the 13th ACM Conference on Recommender Systems, Copenhagen, Denmark, 16–20 September 2019; ACM: Manhattan, NY, USA, 2019; pp. 305–313.
18. Wu, L.; Li, J.W.; Sun, P.J.; Hong, R.; Ge, Y.; Wang, M. DiffNet++: A neural Influence and Interest diffusion network for social recommendation. *IEEE Trans. Knowl. Data Eng.* **2020**, *34*, 4753–4766. [CrossRef]
19. Jin, L.; Chen, Y.; Wang, T.; Hui, P.; Vasilakos, A.V. Understanding user behavior in online social networks: A survey. *IEEE Commun. Mag.* **2013**, *51*, 144–150.
20. Fan, W.; Derr, T.; Ma, Y.; Wang, J.; Tang, J.; Li, Q. Deep adversarial social recommendation. *arXiv* **2019**, arXiv:1905.13160.
21. Wu, J.; Fan, W.; Chen, J.; Liu, S.; Li, Q.; Tang, K. Disentangled contrastive learning for social recommendation. In Proceedings of the 31st ACM International Conference on Information & Knowledge Management, Atlanta, GA, USA, 17–21 October 2022; pp. 4570–4574.
22. Liu, C.Y.; Zhou, C.; Wu, J.; Hu, Y.; Guo, L. Social Recommendation with an Essential Preference Space. In Proceedings of the Thirty-Second AAAI Conference on Artificial Intelligence (AAAI-18), New Orleans, LA, USA, 2–7 February 2018.
23. Zhang, S.Q.; Zhang, N.J.; Li, N.N.; Xie, Z.; Gu, J.; Li, J. Social recommendation based on quantified trust and user's primary preference space. *Appl. Sci.* **2022**, *12*, 12141. [CrossRef]
24. Wang, J.; Yu, L.; Zhang, W.; Gong, Y.; Xu, Y.; Wang, B.; Zhang, P.; Zhang, D. IRGAN: A minimax game for unifying generative and discriminative information retrieval models. In Proceedings of the 40th International ACM SIGIR Conference on Research and Development in Information Retrieval, Tokyo, Japan, 7–11 August 2017; ACM: Manhattan, NY, USA, 2017; pp. 515–524.
25. Chae, D.K.; Kang, J.S.; Kim, S.W.; Lee, J.-T. CFGAN: A generic collaborative filtering framework based on generative adversarial networks. In Proceedings of the 27th ACM International Conference on Information and Knowledge Management, Torino, Italy, 22–26 October 2018; ACM: Manhattan, NY, USA, 2018; pp. 137–146.
26. Sasagawa, T.; Kawai, S.; Nobuhara, H. Recommendation system based on generative adversarial network with graph convolutional layers. *J. Adv. Comput. Intell. Intell. Inform.* **2021**, *25*, 389–396. [CrossRef]
27. Yang, Z.; Qin, J.W.; Lin, C.; Chen, Y.; Huang, R.; Qin, Y. GANRec: A negative sampling model with generative adversarial network for recommendation. *Expert Syst. Appl.* **2023**, *214*, 119155. [CrossRef]
28. Caamares, R.; Castells, P. Should i follow the crowd? a prob-abilistic analysis of the effectiveness of popularity in recommender systems. In Proceedings of the SIGIR'18: The 41st International ACM SIGIR Conference on Research & Development in Information Retrieval, Ann Arbor, MI, USA, 8–12 July 2018; pp. 415–424.
29. Liu, H.; Wen, J.; Jing, L.; Yu, J. Leveraging implicit social structures for recommendation via a Bayesian generative model. *Sci. China Inf. Sci.* **2022**, *65*, 149104. [CrossRef]

30. Yu, Y.H.; Qian, W.W.; Zhang, L.; Gao, R. A Graph-Neural-Network-Based social network recommendation algorithm using high-order neighbor information. *Sensors* **2022**, *22*, 7122. [CrossRef] [PubMed]
31. Lin, J.; Chen, S.; Wang, J. Graph neural networks with dynamic and static representations for social recommendation. In Proceedings of the World Wide Web Conference, San Francisco, CA, USA, 13–17 May 2022; DASFAA: San Francisco, CA, USA, 2022; pp. 264–271.

entropy

MDPI

Article

Resource Concentration and Clustering in Replicator Dynamics with Stochastic Reset Events

Ignacio T. Gómez Garay [1,†] and Damián H. Zanette [1,2,*,†]

[1] Centro Atómico Bariloche and Instituto Balseiro, Comisión Nacional de Energía Atómica, Universidad Nacional de Cuyo, Av. E. Bustillo 9500, San Carlos de Bariloche 8400, Argentina
[2] Consejo Nacional de Investigaciones Científicas y Técnicas, Bariloche 8400, Argentina
* Correspondence: damian.zanette@ib.edu.ar
† These authors contributed equally to this work.

Abstract: As a model for economic and ecological systems, replicator dynamics represent a basic form of agent competition for finite resources. Here, we investigate the effects of stochastic resetting in this kind of processes. Random reset events abruptly lead individual resources to a small value from which dynamics must start anew. Numerical results show that resource distribution over the population of competing agents develops highly nonuniform profiles, exhibiting clustering and fluctuations with anomalous dependence on the population size. This non-standard statistical behavior jeopardizes an analytical treatment based on mean-field assumptions. We propose alternative simplified analytical approaches which provide a stylized description of entropy evolution for the clustered distribution of resources and explain the unusually slow decrease of fluctuations.

Keywords: replicator population; stochastic resetting; resource distribution; anomalous fluctuations; clustering

Citation: Gómez Garay, I.T.; Zanette, D.H. Resource Concentration and Clustering in Replicator Dynamics with Stochastic Reset Events. *Entropy* **2023**, *25*, 99. https://doi.org/10.3390/e25010099

Academic Editor: José Roberto Iglesias

Received: 10 November 2022
Revised: 7 December 2022
Accepted: 11 December 2022
Published: 3 January 2023

1. Introduction

In theoretical biology, a *replicator* is an abstract unit capable of creating copies of itself through interaction with the environment [1,2]. This very generic concept—which provides a unified tool for studying evolutionary dynamics at several levels—encompasses such entities as nucleic-acid molecules (RNA and DNA), genes, cells, and, of course, living organisms. In the theory of cultural evolution, an analogous notion applies to memes, the units of cultural information, thus extending the same theoretical framework to social and economic phenomena [3]. The concept of replicator turned out to be especially fruitful within evolutionary game theory, as a model for biological evolution under natural selection. In this context, replicators represent strategies whose individual profit, measured by their relative reproduction success, depends on both their intrinsic fitness and their mutual interaction [4].

Replicator dynamics is a mathematical model, used in evolutionary game theory, that describes how the relative prevalence of different strategies changes in time [5,6]. If, in a large population, $x_i(t)$ is the fraction of players adopting strategy i at time t, replicator dynamics prescribe that

$$\dot{x}_i = x_i \left[f_i(\mathbf{x}) - \sum_{j=1}^{N} f_j(\mathbf{x}) x_j \right], \tag{1}$$

($i = 1, 2, \ldots, N$), where $f_i(\mathbf{x})$ denotes the fitness of strategy i, and generally depends on all the components of $\mathbf{x} = (x_1, x_2, \ldots, x_N)$. It can be seen that the N-dimensional simplex, given by $\sum_i x_i = 1$ with $x_i \geq 0$ for all i, is invariant under Equation (1), and also acts as a global attractor for all non-negative initial conditions. From the perspective of population dynamics, Equation (1) can be interpreted as the time evolution of N interacting species with fitnesses $f_i(\mathbf{x})$, additionally subjected to a global mechanism of growth

limitation, given by the second term in the brackets, which asymptotically constrains populations to the subspace where $\sum_i x_i = 1$. In this work, we adopt a similar interpretation, where x_i represents the resources (richness) of an economic agent i in a population of N interacting agents.

In the simplest version of replicator dynamics, all fitnesses are constant: $f_i(\mathbf{x}) = \lambda_i$ for all i [7]. In this situation, the first term in the right-hand side of Equation (1) induces an exponential growth of the resources x_i, at rate λ_i. The opposing effect of the second term, however, limits this growth. For sufficiently long times, in fact, the system approaches the N-dimensional simplex. The outcome of these contrary trends is that, asymptotically, the replicator with maximal fitness accumulates all the resources. Namely, for $t \to \infty$,

$$x_i = \begin{cases} 1 & \text{if } \lambda_i = \max\{\lambda_1, \lambda_2, \cdots, \lambda_N\}, \\ 0 & \text{otherwise.} \end{cases} \tag{2}$$

Thus, with constant fitnesses, the population always ends in a state where resources are trivially concentrated in just one agent. If two or more agents have identical maximal fitnesses, all the resources become shared between them in proportions depending on the initial values $x_i(0)$.

Our aim in this paper is to study the effect of reset events on the replicator dynamics with constant fitnesses. Resetting is a stochastic mechanism by which a dynamical variable—in the present case, $x_i(t)$—is occasionally brought to a prefixed value, from which its dynamics start anew. This mechanism is able to severely modify the statistical behavior of a dynamical system [8]. In the present case, we expect it to inhibit the accumulation of resources by a single agent or a small group of agents, bringing about a nontrivial resource distribution over the replicator population. To gain insight into the overall behavior of our model, which we present in Section 2, Section 3 is devoted to the numerical and analytical study of the case of a single replicator. In Section 4, we show that the combined effect of replicator dynamics and resetting in a large population with identical fitnesses results in anomalous statistical properties, with an extremely slow decrease of fluctuations as the population size grows. This unusual feature is accompanied by clustering in the amount of individual resources, which, over time, sustains a highly heterogeneous resource distribution over the population. Analytical arguments based on a toy two-cluster model are proposed to explain these numerical observations. Finally, Section 5 is devoted to discussing our main results.

2. Replicators with Resetting

Stochastic resetting was initially introduced as a mechanism of unbounded growth limitation in the context of demographic dynamics [9,10]. Remarkably, when combined with multiplicative (exponential) growth, it gives rise to long-time power-law distributions for the relevant variables [10,11]. It can therefore be used as a model for the emergence of such distributions in the broad class of phenomena where they are observed [12], ranging from biological taxon abundances [13] to economic resource sharing [14]. Since its introduction more than two decades ago, the statistical effects of stochastic resetting have been studied in a wide variety of dynamical processes, such as transport on networks [15], hydrologic phenomena [16], RNA kinetics [17], and active-particle motion [18], among many others [8].

As described in the Introduction, stochastic resetting acts on a variable $x(t)$, whose evolution is otherwise governed by certain dynamical rules, instantaneously bringing its value to a prefixed level u. Reset events are distributed at random along time, and the evolution of $x(t)$ begins de novo after each resetting. Such events emulate the effect of sudden crises or catastrophic occurrences, where the state of the system under study suffers an abrupt change in a short time [19]. This kind of phenomenon is not uncommon in social and economic contexts [11,20,21].

In replicator dynamics with constant fitnesses λ_i, we introduce reset events by proposing

$$\dot{x}_i = x_i\left(\lambda_i - \sum_{j=1}^{N}\lambda_j x_j\right) + (u_i - x_i)P_i(t), \tag{3}$$

($i = 1, 2, \ldots, N$; cf. Equation (1)). Here,

$$P_i(t) = \sum_k \delta(t - t_{i,k}) \tag{4}$$

represents a Poisson (or shot [22]) noise signal, $\delta(t)$ being the Dirac delta function. For each i, the reset times $t_{i,k}$ ($k = 1, 2, \ldots$) are randomly distributed with uniform frequency q_i, so that the average lapse between $t_{i,k}$ and $t_{i,k+1}$ is q_i^{-1} for all k. The prefactor $u_i - x_i$ in the last term of Equation (3) insures that each reset event brings $x_i(t)$ to the reset value u_i. The Markovian stochastic Equation (3) can be dealt with by means of a series of standard methods, notably, the Chapman-Kolmogorov equation, which governs the joint probability distribution of the resources $x_i(t)$ [22]. It can also be treated numerically, by a rather intuitive implementation of the Poisson process along discretized time [23]. In the following sections, we use these techniques to study the collective dynamics of the replicator population with resetting.

3. Dynamics of a Single Replicator with Resetting

As a first step in the analysis of our model, it is instructive to study the case of a single replicator, $N = 1$. Equation (3) becomes

$$\dot{x} = \lambda x(1 - x) + (u - x)P(t), \tag{5}$$

with $P(t) = \sum_k \delta(t - t_k)$. The random reset times t_k have frequency q. The first term in the right-hand side of Equation (5) makes it clear that, for a single replicator, the deterministic contribution to the dynamics is equivalent to logistic growth [24]. Due to arbitrariness in the choice of time units, the system has two independent parameters only: the ratio q/λ, and the reset value u.

Figure 1 shows a pair of realizations of $x(t)$, for $u = 0.01$ and two values of q/λ, exhibiting qualitatively different behavior. For a relatively small resetting frequency, $q/\lambda = 0.1$ (upper panel), $x(t)$ usually has enough time to reach the zone of logistic saturation, just below the level of maximal resources ($x = 1$). The evolution is only occasionally punctuated by reset events to $x = u$. On the other hand, when the resetting frequency is larger ($q/\lambda = 2.5$, lower panel), $x(t)$ barely transits the zone of exponential growth before it is interrupted by a reset event. In this latter situation, the evolution is very similar to the case where the deterministic part of the dynamics is purely multiplicative, which we have analyzed in detail in a recent contribution [19].

Assuming that the stochastic process represented by Equation (5) reaches a stationary regime for long times, the stationary distribution for x, $f^{\mathrm{st}}(x)$, can be obtained from the Chapman-Kolmogorov equation

$$\frac{\partial}{\partial t}f(x,t) + \frac{\partial}{\partial x}[v(x)f(x,t)] = q\delta(u - x) - qf(x,t) \tag{6}$$

by fixing $\partial_t f \equiv 0$. In the left-hand side of this equation, the second term represents the probability drift induced by the deterministic logistic dynamics, with $v(x) = \lambda x(1 - x)$. The two terms in the right-hand side are gain and loss contributions originating in reset events. The positive gain term is different from zero only at the reset value $x = u$, while the negative term represents uniform probability loss at frequency q for all x. On the whole, of course, the two terms compensate each other. For $x \neq u$, the effect of the delta-like gain term can interpreted as a boundary condition which connects the solution in the intervals $x < u$ and $x > u$ through the relation $v(u^+)f(u^+,t) - v(u^-)f(u^-,t) = q$ for $t > 0$, as

obtained from integration of Equation (6) around $x = u$. Using this boundary condition, the stationary solution reads

$$f^{\mathrm{st}}(x) = \frac{q}{\lambda}\left(\frac{1-u}{u}\right)^{-q/\lambda} x^{-1-q/\lambda}(1-x)^{-1+q/\lambda} \tag{7}$$

for $u \leq x < 1$, and $f^{\mathrm{st}}(x) = 0$ otherwise. This time-independent distribution behaves as a power law both for small and large values of x. For $q/\lambda > 1$, the exponent of $1 - x$ is positive, and the distribution has a maximum at $x = u$ while it decays to zero as $x \to 1$.

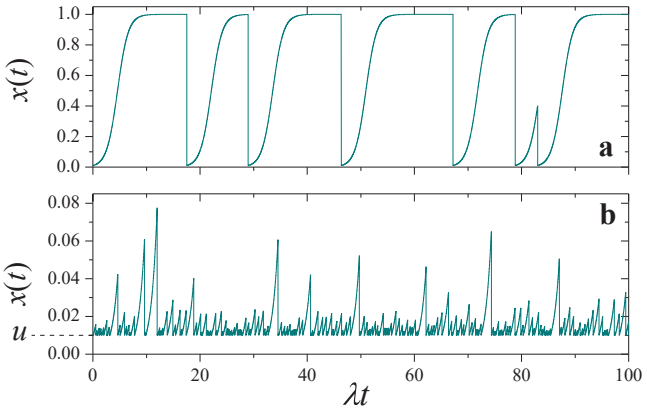

Figure 1. Two realizations of the solution to the stochastic Equation (5), for $u = 0.01$ and different values of the ratio q/λ. (**a**) $q/\lambda = 0.1$. (**b**) $q/\lambda = 2.5$. Note different scales in the vertical axes.

For $q/\lambda < 1$, on the other hand, $f^{\mathrm{st}}(x)$ exhibits a bimodal profile, with a local maximum at $x = u$ and a divergence at $x = 1$. This case is illustrated in Figure 2, where we plot the distribution as a function of both x (left panel) and $1 - x$ (right panel) for $u = 0.01$ and $q/\lambda = 0.1$. The log-log axes emphasize the power-law dependence toward the two ends. Excellent agreement between analytical and numerical results supports the assumption of a well-defined long-time stationary regime for the stochastic process. The bimodal concentration of resources at the extreme values, with the ensuing depletion in the intermediate zone, is a direct consequence of the competing effect of logistic growth, which favors accumulation near the maximum, and of reset events, which populate the zone of lower resources.

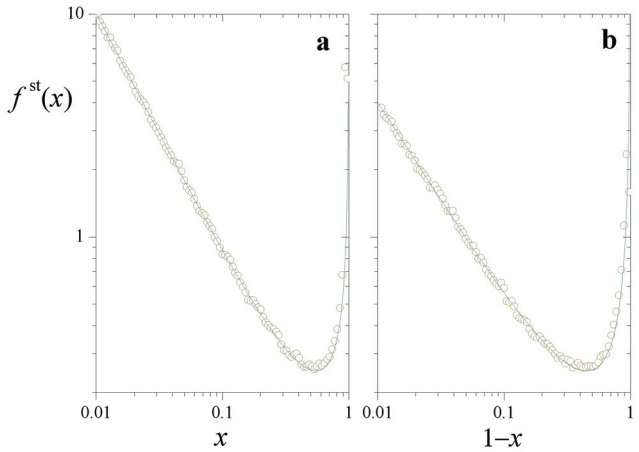

Figure 2. Stationary probability distribution for the solution to the stochastic Equation (5), $f^{\mathrm{st}}(x)$, (**a**) as a function of x and (**b**) as a function of $1 - x$, for $u = 0.01$ and $q/\lambda = 0.1$. The line stands for the analytical expression (7). Symbols correspond to a 100-column histogram, built from 4×10^5 samples of $x(t)$ taken from a numerical realization of Equation (5) every 10 time units. The numerical solution was realized by means of a standard finite-difference algorithm with a time step of 10^{-3} time units.

4. Fluctuations and Clustering in Large Homogeneous Populations

Turning now the attention to the case with $N > 1$, we consider homogeneous replicator populations, in which the parameters u_i, λ_i, and q_i in Equation (3) are the same for all agents. In this situation, agents differ from each other in the individual realizations of the sequence of stochastic reset events only. This homogeneity implies that none of them has an *a priori* advantage based on fitness, or on the frequency and strength of resetting. Thus, any nontrivial emergent collective behavior should be ascribed to the randomness in the time distribution of reset events.

For a homogeneous population, Equation (3) reads

$$\dot{x}_i = \lambda x_i(1 - x_T) + (u - x_i)P_i(t), \tag{8}$$

with $P_i(t)$ given as in Equation (4) with the same resetting frequency q for all i. In turn,

$$x_T = \sum_{j=1}^{N} x_j \tag{9}$$

stands for the total resources over the population. Assuming that, as in the case of $N = 1$, the system attains a well-defined stationary state for long times, we expect that x_T reaches a constant value if N is large enough. Of course, this requires that resource fluctuations are self-averaging over time and over the ensemble. If these conditions are fulfilled, the stationary distribution for individual resources satisfies Equation (6) with, now, $v(x) = \lambda x(1 - x_T)$. The solution is

$$f^{\mathrm{st}}(x) = \frac{q u^{q/\lambda(1-x_T)}}{\lambda(1 - x_T)} x^{-1-q/\lambda(1-x_T)}, \tag{10}$$

for $u \leq x < 1$ and 0 otherwise. The absence of a logistic nonlinearity in Equation (8) determines that $f^{\mathrm{st}}(x)$ is now a pure power law; cf. (7).

The value of x_T in Equation (10) must be obtained self-consistently, requiring that it coincides with the total resources calculated from the distribution $f^{\mathrm{st}}(x)$, namely

$$x_T = N \int_u^1 x f^{\mathrm{st}}(x) dx = \frac{Nqu}{q - \lambda(1 - x_T)}. \tag{11}$$

The only positive solution to this self-consistency equation is

$$x_T = \frac{\lambda/q - 1 + \sqrt{(\lambda/q - 1)^2 + 4Nu\lambda/q}}{2\lambda/q}. \tag{12}$$

For a given value of Nu, the total resources vary monotonically from $x_T \approx 1 - q/\lambda \approx 1$ for $q \ll \lambda$ to $x_T \approx Nu$ for $q \gg \lambda$. In the first limit, when the resetting frequency is negligible, the population is driven by almost purely replicator dynamics, and one single agent typically concentrates all the resources. When, on the other hand, reset events are dominant, the N agents always have resources close to the minimal value u. The corresponding distributions are

$$f^{\mathrm{st}}(x) \approx \begin{cases} (u^{-1} - 1)^{-1} x^{-2} & \text{for } q \ll \lambda, \\ (u^{-q/\lambda} - 1)^{-1} x^{-1-q/\lambda} & \text{for } q \gg \lambda. \end{cases} \tag{13}$$

In the remaining of this paper, we fix the attention on the case $q < \lambda$. Indeed, much as in the case of $N = 1$ analyzed in Section 3, for $q > \lambda$—when reset events dominate over resource growth—the replicator dynamics hardly manifests itself, and evolution does not essentially differ from that of a system of non-interacting multiplicative elements with resetting ([19], cf. Figure 1b). For brevity, numerical results are presented for just a few parameter sets, which we have found to be representative of more general situations.

Following the same numerical techniques used in the case of a single replicator, we have computed the stationary distribution of individual resources for populations of different sizes, with $Nu = 0.01$ and $q/\lambda = 0.1$. According to the analytical result of Equation (12), all these systems have the same total resources, $x_T \approx 0.901$. Symbols in Figure 3 show histograms of $f^{\mathrm{st}}(x)$ for three values of N, analogous to those presented in Figure 2 for $N = 1$. Lines stand for the corresponding analytical prediction (10).

It is apparent that, although numerical and analytical results follow the same general trend in the distribution of resources, there are important systematic deviations along the whole interval of the variable x. The deviations decrease in magnitude as the population grows, but are still non-negligible for a large system of 10^5 replicators. For this size and large x, the slopes of the power-law tails in the numerical estimation and the analytical prediction are very similar but, as for the values of the distributions, the former are about one order of magnitude above the latter. The difference has the opposite sign at small x, as shown in the inset. We show in the following paragraphs that these discrepancies originate in the anomalous statistical behavior of the total resources $x_T(t)$. Its fluctuations along time, in fact, decay very slowly with the system size N. This indicates that our assumption that x_T is constant, used to solve the stationary Chapman-Kolmogorov equation, may only hold for extremely large populations, drastically limiting the usefulness of the analytical approach in this kind of systems.

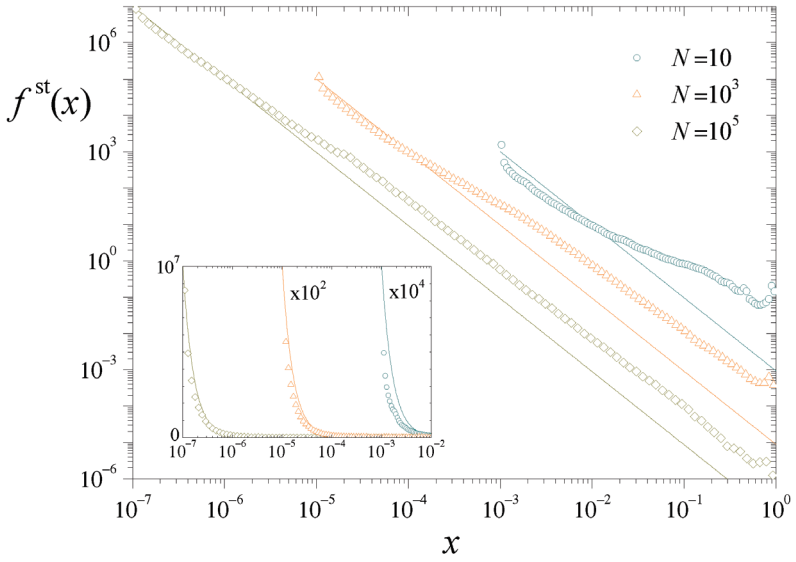

Figure 3. Symbols: Numerical estimation of the stationary distribution $f^{\mathrm{st}}(x)$ for three values of N, with $Nu = 0.01$ and $q/\lambda = 0.1$. Lines: Analytical solution (10) to the stationary Chapman-Kolmogorov equation, for the same parameters. Inset: The same data in log-linear scales, for a better appraisal in the upper part of the vertical axis. The data for $N = 10$ and 10^3 have been scaled by the factors indicated in the plot.

4.1. Anomalous Fluctuations of Total Resources

Figure 4a presents numerical estimations of the stationary distribution of x_T along time, in realizations of Equation (8) for different system sizes N. In all cases, $f^{\mathrm{st}}(x_T)$ is sharply peaked around a large value $x_T \approx 0.93$, and exhibits a broad shoulder for smaller x_T. Overall, this behavior is compatible with the analytically predicted value, $x_T \approx 0.901$, obtained from Equation (12). Note however the rather slow change of the shoulder at small x_T as N grows: a variation by a factor of 10^3 in the size of the population leads to a decrease of just above one order of magnitude in the height of the distribution in that zone.

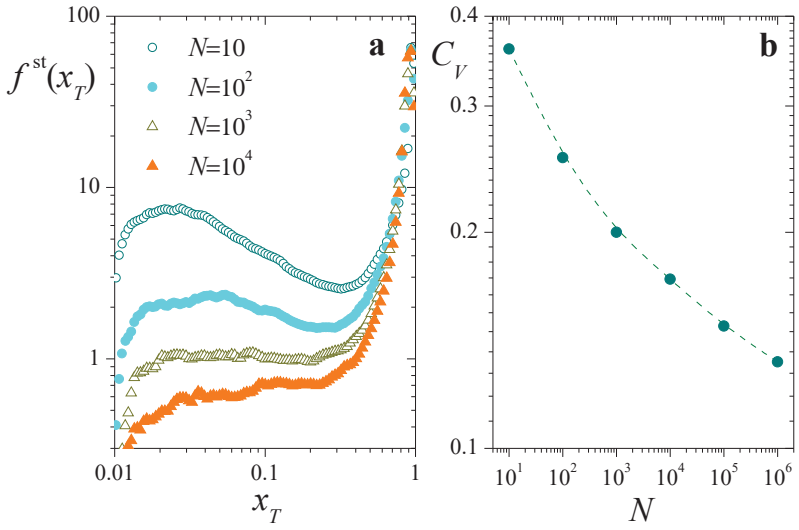

Figure 4. (**a**): Stationary distribution $f^{\mathrm{st}}(x_T)$ of total resources x_T, for four values of N, $Nu = 0.01$, and $q/\lambda = 0.1$. (**b**): Coefficient of variation C_V as a function of N. The dashed curve is a B-spline approximation included as a guide to the eye. All results are estimations obtained from numerical solutions of Equation (8) along 2×10^8 time steps.

This weak dependence on N is remarkably apparent in the coefficient of variation of x_T, defined as

$$C_V = \frac{1}{\langle x_T \rangle} \sqrt{\frac{1}{T} \int_0^T [x_T(t) - \langle x_T \rangle]^2 dt}, \tag{14}$$

where

$$\langle x_T \rangle = \frac{1}{T} \int_0^T x_T(t) dt \tag{15}$$

is the time average of $x_T(t)$, and T is a sufficiently long averaging interval. The coefficient C_V encompasses overall statistical properties of $f^{\mathrm{st}}(x_T)$ in a single quantity, as a measure of the fluctuations of $x_T(t)$ relative to its average. Figure 4b is a log-log plot of C_V as a function of N. Across the five orders of magnitude covered by the system sizes, the coefficient of variation only decreases by a factor of 3, and there is no clear indication that it might approach zero as $N \to \infty$. In fact, within this rather wide interval of N, it lacks the typical power-law trend that characterizes the system-size dependence of fluctuations in self-averaging statistical systems (usually, N^{-z} with $0 < z < 1$) [25]. This hints at a strongly heterogeneous behavior within the population, and calls for a closer look at the time evolution of individual replicators.

4.2. Heterogeneity and Clustering in the Evolution of Resources

The darkest curve in Figure 5a shows the evolution of total resources $x_T(t)$ in a population of $N = 10^4$ replicators, with $Nu = 0.01$ and $q/\lambda = 0.1$. At the initial time, all the replicators have identical resources, $x(0) = u$. We see that, most of the time, $x_T(t)$ fluctuates close to its maximum value. Intermittently, however, total resources exhibit sharp collapses where $x_T(t)$ suddenly drops to a small value, followed by a rapid recovery.

Other curves in Figure 5a show $x_i(t)$ for the three agents with highest resources at each time. These curves demonstrate the typically heterogeneous resource distribution over the population: most of the time, these three replicators accumulate a large fraction of the total resources. Comparison with $x_T(t)$, moreover, illustrates how collapses in total resources usually coincide with a reset event of the richest replicator.

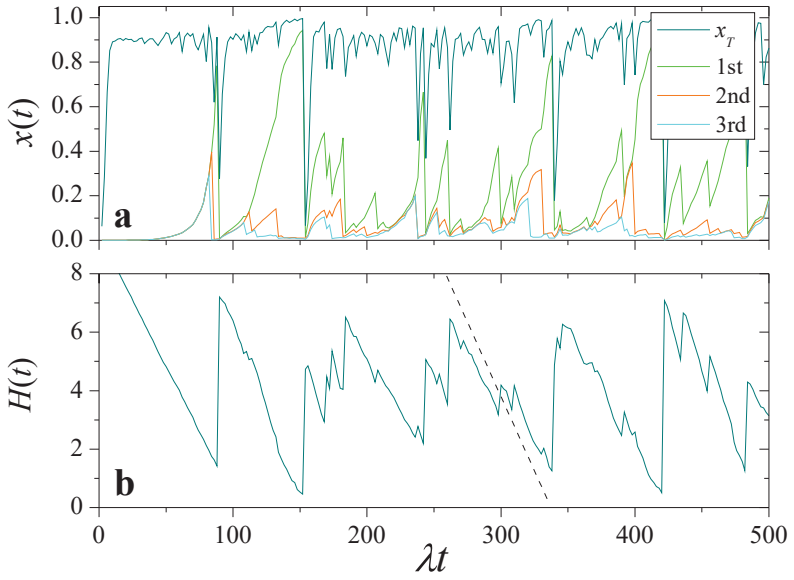

Figure 5. (**a**): Evolution of total resources, $x_T(t)$, and of individual resources for the three replicators with largest $x_i(t)$ at each time, in a realization with $N = 10^4$, $Nu = 0.01$, and $q/\lambda = 0.1$. (**b**): Entropy of individual shares, Equation (16), for the same realization. The dashed segment has the slope analytically predicted for the decrease of $H(t)$ with the two-cluster model of Section 4.3.

As a more compact characterization of heterogeneity in the distribution of resources over the population, we have computed the entropy of the individual shares x_i/x_T as a function of time:

$$H(t) = -\sum_{i=1}^{N} \frac{x_i(t)}{x_T(t)} \ln \frac{x_i(t)}{x_T(t)}. \tag{16}$$

This quantity is depicted in Figure 5b for the same realization as in the upper panel. It shows that, in the intervals between collapses of $x_T(t)$, resources progressively accumulate in less and less replicators. Resetting of one of the replicators with high resources, in turn, entails a sudden growth of $H(t)$, with an ensuing decrease as resources become increasingly concentrated.

During the intervals between collapses, we expect the population to be divided into at least two groups with different resource distributions inside each group. Those replicators that have undergone a reset event since the latest collapse should have low resources, close to the resetting level u. On the other hand, replicators that have evolved without resource resetting in the same period should possess, on the average, relatively higher resources, with a distribution closer to the equilibrium profile of Equation (10). In a succession of several consecutive collapses, the same mechanism may generate more than two groups, leading to a clustered, markedly heterogeneous resource distribution.

Clustering in the resource distribution is well illustrated by a Zipf plot, in which individual resources are represented against the rank of each replicator in a list sorted by decreasing values of x_i. Figure 6 shows snapshots of this kind of plot at four times, in a system of $N = 5000$ replicators. Other parameters are as in Figure 5. For $\lambda t = 89$, the first collapse has not taken place yet. In this situation, except for the first-rank replicator which already monopolizes practically all resources, the distribution over the population closely follows the equilibrium profile, whose slope is shown by the dashed line. As time elapses, the occurrence of collapses creates clusters, which in the Zipf plots appear as more or less flat plateaus separated by much sharper steps. In the Supplementary Video S1, which shows an animation of the Zipf plots for the same realization along time, the appearance, evolution, and fading of these plateaus is apparent.

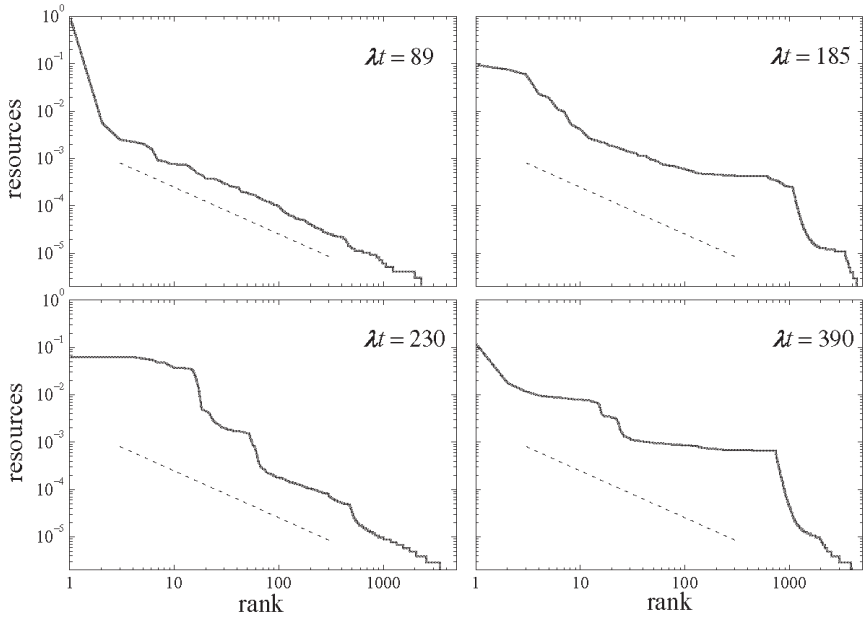

Figure 6. Four snapshots of a Zipf plot of individual resources versus rank in a decreasing list of resources, in a population of $N = 5000$ replicators with $Nu = 0.01$ and $q/\lambda = 0.1$. The dashed segments show the slope that the plot should exhibit if the population had reached the equilibrium distribution of Equation (10). Plateaus of different sizes at different times reveal the formation of groups and, thus, clustering in the resource distribution.

Intermittent collapses of total resources and the consequent clustering of resource distribution, leading to an overall highly non-uniform behavior inside the population, are likely determinants of the differences observed between analytical and numerical results, as illustrated by Figure 3, and the slow decay of fluctuations of Figure 4b. In the following, under a few simplifying assumptions, we provide a stylized description for the behavior of the entropy $H(t)$ and a prediction for the typical time between collapses, as well as an argument which explains the extremely slow decay of fluctuations in total resources as the system size grows.

4.3. Two-Cluster Model and the Decay of Fluctuations

As a simplified analytical approach to heterogeneity in the replicator population, we propose a toy model in which, at all times between collapses, total resources have the value x_T given by Equation (12), and the ensemble is divided into just two clusters. The first cluster contains the $N_r(t)$ replicators whose resources have been reset after the latest collapse, occurred at time t_c. The second cluster comprises the $N - N_r(t)$ remaining replicators. Moreover, we assume that the individual resources in the first cluster are all equal to the reset level u, while the remaining resources are homogeneously distributed over the second cluster. This implies that the total resources in each cluster are $N_r(t)u$ and $x_T - N_r(t)u$, respectively. With these assumptions, Equation (16) yields

$$H(t) = -\left[1 - \frac{N_r(t)u}{x_T}\right] \ln \frac{1 - \frac{N_r(t)u}{x_T}}{N - N_r(t)} - \frac{N_r(t)u}{x_T} \ln \frac{u}{x_T} \approx \ln[N - N_r(t)], \tag{17}$$

where the approximation of the rightmost side holds for $u \ll x_T$.

As successive reset events occur, replicators from the cluster of high resources are transferred to the other cluster at rate q so that, on the average, the number of replicators in the former satisfies the equation

$$\frac{d}{dt}[N - N_r(t)] = -q[N - N_r(t)], \tag{18}$$

with $N - N_r(t_c) = N$ at the time of the latest collapse. Namely,

$$N - N_r(t) = N\mathrm{e}^{-q(t-t_c)}. \tag{19}$$

Replacing into the approximation for the entropy in Equation (17), we find

$$H(t) \approx \ln N - q(t - t_c), \tag{20}$$

which predicts an approximate linear decay between collapses. The slanted dashed segment in Figure 5b has the slope predicted by this result, displaying very good agreement with the behavior of the numerically obtained signal for $H(t)$.

Our approximation for the entropy $H(t)$ makes it also possible to estimate the typical time between collapses, τ. In fact, in the two-cluster model a collapse will occur when just a single replicator remains in the high-resource cluster, $N - N_r(t) = 1$, accumulating essentially all the resources. In this case, $H = 0$ which, according to Equation (17), is the entropy attained at time $t = t_c + q^{-1} \ln N$. On the average, the last replicator will be reset after an additional time q^{-1}. Thus, we have

$$\tau = \frac{1 + \ln N}{q}. \tag{21}$$

In our simplified picture, τ is nothing but the period of the successive decays of $H(t)$ between its maximum and its minimum. Figure 7a shows the power spectrum $P(\nu)$ of an actual numerical calculation of $H(t)$ in a system with $N = 1000$, $Nu = 0.01$, and $q/\lambda = 0.1$. Its broad profile exposes the stochastic nature of the mechanisms at play in the variation of the entropy, but shows a clear peak at a well-defined frequency, which reveals an underlying time-periodic pattern. The vertical dashed line demonstrates that this frequency coincides quite sharply with the prediction of Equation (21), $\nu = \tau^{-1} = q/(1 + \ln N)$. We have performed this same comparison for different values of N, evaluating the main period of of numerical signals for the entropy from the position of the highest peak in their power spectra. In Figure 7b, results are compared with Equation (21), represented by the dotted line, with very good agreement.

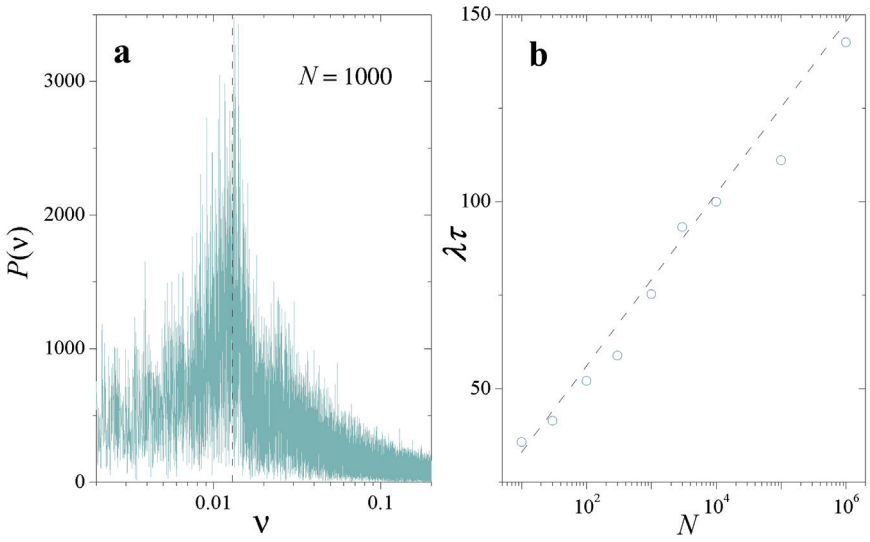

Figure 7. (**a**): Power spectrum of a time signal for the entropy $H(t)$, numerically obtained in a replicator population with $N = 1000$, $Nu = 0.01$, and $q/\lambda = 0.1$. The vertical dashed line is the frequency predicted for $H(t)$ by the two-cluster model, in the approximation $Nu \ll 1$. (**b**): Average time between collapses estimated from the power spectrum of the entropy (symbols) and from the analytical prediction ((21), dashed line), as a function of N, with the same parameters as in panel (**a**).

Finally, along the same lines of approximation, we are able to give an explanation for the extremely slow decay of fluctuations in the total resources x_T as the system size N grows, revealed by the weak dependence on N of the stationary resource distributions $f^{\mathrm{st}}(x)$ and $f^{\mathrm{st}}(x_T)$ (Figures 3 and 4a) and explicitly illustrated in Figure 4b. The time signal of $x_T(t)$ shown in Figure 5a suggests that fluctuations in total resources are mainly dominated by the collapses associated with resetting of the replicators that accumulate most of the resources. In a highly stylized model for the signal $x_T(t)$, we can assume that the statistical distribution of total resources is given by a dichotomic process, where—in the interval between collapses—x_T stays at its minimum value Nu during a "recovery time" t_R, and at its (approximate) equilibrium value $1 - q/\lambda$ during the (average) remaining time $\tau - t_R$. Namely,

$$f^{\mathrm{st}}(x_T) = \frac{t_R}{\tau}\delta(x_T - Nu) + \left(1 - \frac{t_R}{\tau}\right)\delta\Big(x_T - 1 + \frac{q}{\lambda}\Big). \tag{22}$$

From this Ansatz, the calculation of the mean value and the standard deviation of x_T is straightforward. In the limit $Nu \ll 1$, we find

$$\langle x_T \rangle = \left(1 - \frac{t_R}{\tau}\right)\Big(1 - \frac{q}{\lambda}\Big), \quad \sigma_{x_T} = \sqrt{\frac{t_R}{\tau}\left(1 - \frac{t_R}{\tau}\right)}\Big(1 - \frac{q}{\lambda}\Big), \tag{23}$$

which yields a coefficient of variation

$$C_V = \sqrt{\frac{t_R/\tau}{1 - t_R/\tau}}. \tag{24}$$

If t_R is interpreted as the time needed by $x_T(t)$ to recover from its small value just after a collapse up to its equilibrium value, we do not expect t_R to depend on N, at least for sufficiently large systems. Indeed, according to Equation (8), total resources should approximately obey $\dot{x}_T = \lambda x_T(1 - x_T) - q x_T$, which is independent of N. If this is the case, Equations (21) and (24) imply that the coefficient of variation of x_T decays as

$$C_V \sim \frac{1}{\sqrt{\ln N}} \tag{25}$$

for $N \to \infty$.

Symbols in Figure 8 correspond to results for C_V as a function of $\ln N$ for three different values of q/λ, obtained from numerical solutions of Equation (8) analogous to those of Figure 4b. Dashed lines stand for the asymptotic behavior predicted by Equation (25). Numerical results closely follow the prediction, even for relatively small values of N. On the one hand, Equation (25) shows that C_V converges to zero as N grows, which validates the Chapman-Kolmogorov formulation for sufficiently large systems. On the other, the same result proves the extremely slow decay of fluctuations with the population size. Just as an illustration, suppose that one wants to diminish fluctuations in x_T by a factor of 10, starting from results for a system of 10^4 replicators. The new system should have nothing less than 10^{400} replicators (!), a size clearly beyond the reach of any presently available computational means.

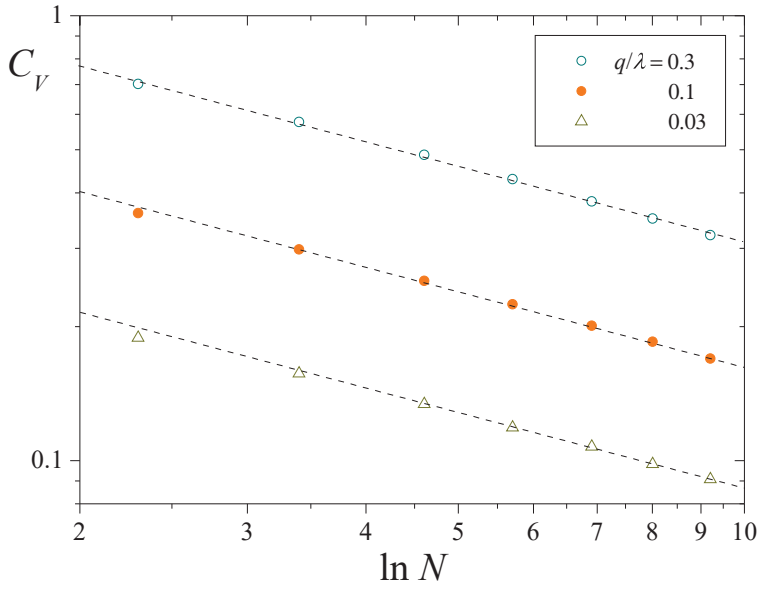

Figure 8. Coefficient of variation of total resources C_V as a function of $\ln N$, for $Nu = 0.01$ and three values of q/λ (note log-log scales). Symbols correspond to numerical results, and dashed lines stand for the asymptotic behavior predicted in Equation (25).

5. Conclusions

Replicator dynamics with constant fitnesses is a basic model of agent competition, where one or a few agents eventually accumulate all the available resources. In this paper, we have investigated whether this concentration can be mitigated by stochastic resetting in the case of a homogeneous population. Reset events are randomly distributed in time, and force the dynamics of randomly drawn agents to start anew from a small value. Analytical results based on the Chapman-Kolmogorov equation show that, in fact, the long-time distribution of individual resources approaches a smooth profile, with a power-law decay of probability as the amount of resources grows.

However, numerical evidence reveals that—even for long times and large populations—the analytical prediction is, at most, an approximation to the actually observed resource distributions. A closer inspection of the dynamics of individual agents shows that the overall behavior is still governed by a few agents, which occasionally accumulate most of the total resources. When the resources of one of these wealthier agents are reset, total resources "collapse", and the resource distribution suddenly becomes much more even. Subsequent collapses of this kind lead the distribution to develop clustering, separating the population into groups of agents with similar individual resources. This heterogeneity is responsible for the sustained differences between numerical and analytical results. These collapse-driven dynamics are also responsible for the extremely slow decay of fluctuations with the system size, which jeopardizes the use of the mean-field approach implicit in the Chapman-Kolmogorov Equation (6) for any practically attainable number of agents. Such anomalous statistical behavior is reminiscent of extreme-value statistics, whose relevance to economic processes has been emphasized in various contexts [20,26,27].

The present study complements recent work on cooperative agents subject to stochastic resetting [19], where we have shown that cooperation leads to resource redistribution, distorting the power-law distributions derived from the sole effect of reset events. These contributions represent a first attempt to characterize the collective behavior of interacting agents under the action of resetting, thus combining deterministic dynamics with stochastic ingredients. Other interactions of economic and ecological interest (e.g., parasitism, predator-prey, etc.) are worth considering in future work on the subject.

Supplementary Materials: The following supporting information can be downloaded at: https://www.mdpi.com/article/10.3390/e25010099/s1, Video S1: Animation of Zipf plots for resource distribution over the replicator population (cf. Figure 6).

Author Contributions: Both authors have equally contributed to conceptualization, methodology, software, validation, formal analysis, investigation, resources, data curation, writing, editing, visualization, and supervision. All authors have read and agreed to the published version of the manuscript.

Funding: This research received no external funding.

Institutional Review Board Statement: Not applicable.

Informed Consent Statement: Not applicable.

Data Availability Statement: Not applicable.

Conflicts of Interest: The authors declare no conflict of interest.

References

1. Dawkins, R. Replicator selection and the extended phenotype 3. *Z. Tierpsychol* **1978**, *47*, 61. [CrossRef] [PubMed]
2. Dawkins, R. *The Extended Phenotype*; Freeman: San Francisco, CA, USA, 1982.
3. Ball, J.A. Memes as replicators. *Ethol. Sociobiol.* **1984**, *5*, 145. [CrossRef]
4. Maynard Smith, J. *Evolution and the Theory of Games*; Cambridge University Press: Cambridge, UK, 1982.
5. Schuster, P.; Sigmund, K. Replicator dynamics. *J. Theor. Biol.* **1983**, *100*, 533. [CrossRef]
6. Hofbauer, J.; Sigmund, K. *Evolutionary Games and Population Dynamics*; Cambridge University Press: Cambridge, UK, 1998.
7. Eigen, M. Selforganization of matter and the evolution of biological macromolecules. *Naturwissenschaften* **1971**, *58*, 465. [CrossRef] [PubMed]
8. Evans, M.R.; Majumdar, S.N.; Schehr, G. Stochastic resetting and applications. *J. Phys. A Math. Theor.* **2020**, *53*, 193001. [CrossRef]
9. Zanette, D.H.; Manrubia, S.C. Role of intermittency in urban development: A model of large-scale city formation. *Phys. Rev. Lett.* **1997**, *79*, 523. [CrossRef]
10. Manrubia, S.C.; Zanette, D.H. Stochastic multiplicative processes with reset events. *Phys. Rev. E* **1999**, *59*, 4945. [CrossRef] [PubMed]
11. Zanette, D.H.; Manrubia, S.C. Fat tails and black swans: Exact results for multiplicative processes with resets. *Chaos* **2020**, *30*, 033104. [CrossRef] [PubMed]
12. Newman, M.E.J. Power laws, Pareto distributions and Zipf's law. *Contemp. Phys.* **2004**, *46*, 323. [CrossRef]
13. Burlando, B. The fractal dimension of taxonomic systems. *J. Theor. Biol.* **1990**, *146*, 99. [CrossRef]
14. Gabaix, X. Power laws in economics and finance. *Ann. Rev. Econ.* **2009**, *1*, 255. [CrossRef]
15. Riascos, A.P.; Boyer, D.; Herringer, P.; Mateos, J.L. Random walks on networks with stochastic resetting. *Phys. Rev. E* **2020**, *101*, 062147. [CrossRef] [PubMed]
16. Daly, E.; Porporato, A. Effect of different jump distributions on the dynamics of jump processes. *Phys. Rev. E* **2010**, *81*, 061133. [CrossRef] [PubMed]
17. Roldán, E.; Lisica, A.; Sánchez-Taltavull, D.; Grill, S.W. Stochastic resetting in backtrack recovery by RNA polymerases. *Phys. Rev. E* **2016**, *93*, 062411. [CrossRef] [PubMed]
18. Abdoli, I.; Sharma, A. Stochastic resetting of active Brownian particles with Lorentz force. *Soft Matter* **2021**, *17*, 1307. [CrossRef] [PubMed]
19. Gómez Garay, I.T.; Zanette, D.H. Collective behavior of coupled multiplicative processes with stochastic resetting. *J. Phys. Complex.* **2021**, *2*, 035020. [CrossRef]
20. Taleb, N.N. *Fooled by Randomness. The Hidden Role of Chance in Life and in the Markets*; Random House: New York, NY, USA, 2005.
21. Taleb, N.N. *The Black Swan: The Impact of the Highly Improbable*; Random House: New York, NY, USA, 2007.
22. Gardiner, C.W. *Handbook of Stochastic Methods*; Springer: Berlin, Germany, 1997.
23. Kloeden, P.E.; Platen, E. *Numerical Solution of Stochastic Differential Equations*; Springer: Berlin, Germany, 1999.
24. Drazin, P.G. *Nonlinear Systems*; Cambridge University Press: Cambridge, UK, 1992.
25. Lifshitz, I. *Self-Averaging*; Betascript: Beau Bassin, Mauritius, 2011.
26. Embrechts, P.; Klüppelberg, C.; Mikosch, T. *Modelling Extremal Events: For Insurance and Finance*; Springer: Berlin, Germany, 1997.
27. Novak, S.Y. *Extreme Value Methods with Applications to Finance*; Chapman & Hall/CRC Press: London, UK, 2011.

entropy

MDPI

Article

Can the Sci-Tech Innovation Increase the China's Green Brands Value?—Evidence from Threshold Effect and Spatial Dubin Model

Xiaofei Zhang [1], Yang Xiao [1] and Linyu Wang [2,*]

[1] School of Economics and Management, Fuzhou University, Fuzhou 350108, China
[2] School of Economics, Zhejiang University of Finance and Economics, Hangzhou 310018, China
* Correspondence: wanglinyu@zufe.edu.cn

Abstract: Based on the perspective of the innovation value chain, sci-tech innovation is divided into two stages: R&D and achievement transformation. This paper uses panel data from 25 provinces in China as the sample. We utilize a two-way fixed effect model, spatial Dubin model, and panel threshold model to discuss the impact of two-stage innovation efficiency on the value of the green brand, the spatial effect of this impact, and the threshold role of intellectual property protection in the process. The results indicate that: (1) the two stages of innovation efficiency have a positive impact on the value of green brands, and the effect of the eastern region is significantly better than that of the central and western regions. (2) The spatial spillover effect of the two stages of regional innovation efficiency on the value of green brands is evident, especially in the eastern region. (3) The innovation value chain has a pronounced spillover effect. (4) The single threshold effect of intellectual property protection is significant. When the threshold is crossed, the positive impact of the two stages of innovation efficiency on the value of green brands is significantly enhanced. (5) The influence of economic development level, openness, market size, and marketization degree on the value of green brands shows remarkable regional differences. In conclusion, this study contributes to understanding green brands' growth and provides important implications for developing independent brands in various regions of China.

Keywords: green brand value; innovation efficiency; innovation value chain; intellectual property protection; negative entropy flow; spatial Dubin model; panel threshold model

Citation: Zhang, X.; Xiao, Y.; Wang, L. Can the Sci-Tech Innovation Increase the China's Green Brands Value?—Evidence from Threshold Effect and Spatial Dubin Model. *Entropy* **2023**, *25*, 290. https://doi.org/10.3390/e25020290

Academic Editor: José Roberto Iglesias

Received: 15 November 2022
Revised: 29 January 2023
Accepted: 31 January 2023
Published: 3 February 2023

1. Introduction

Reviewing the development process of global modernization, the rapid growth of the global economy has also created many ecological and environmental problems, such as climate change/global warming, increased pollution, and resource shortages. Since the 1990s, countries worldwide have paid more attention to green coordination and sustainable development of the economy and ecological environment. Nowadays, green development, a form of economic growth and social development aimed at efficiency, harmony, and sustainability, has become a significant trend globally. Many countries worldwide consider the development of green industries essential to promoting economic restructuring.

China has entered a new stage of high-quality economic development. Developing a green economy that can reduce damage to the ecological environment and achieve sustainable development is a critical aspect of high-quality economic development. With the overall green transformation of China's economic and social development, people's consumption concepts and structure have also begun to change. More and more attention has been paid to product safety, food health, quality of the living environment, and other issues. Green consumption, a collective term for various consumption behaviors and patterns that meet human health and environmental protection standards, has gradually become popular. The popularity of green consumption has promoted the rapid development of

green markets that specialize in selling products that produce little environmental pollution during production and consumption. In order to expand the green market share, obtain differentiated competitive advantages, and establish good customer relations, the green brand strategy has become an inevitable choice for enterprises to adapt to the green consumption wave. More and more enterprises in China are seeking a green development path. Huawei released the Green Development 2030 report, pointing out that green development is the key to breaking the future of enterprises. BYD announced a "fuel cut-off", becoming the first auto company in the world to officially stop production of fuel vehicles. HSBC actively promotes "paperless bank" and "green credit". It can be seen that establishing the green brand image of enterprises, creating green brand innovation, and promoting green innovation are the mainstream trends of the future development of all kinds of enterprises. Building a green brand is an inevitable requirement in order for enterprises to enhance their competitiveness and ensure sustainable development. According to the Green Ranking released by Newsweek in 2017, 52 enterprises in China have entered the global top 500, 148 in the United States, 60 in Japan, and 32 in France. No Chinese enterprise has joined the international top 50, but there are 15 in the United States, 6 in France, and 3 in Japan. As the second-largest economy in the world, China has made some achievements in developing green brands. However, there still needs to be a gap in the quality and efficiency of green brand growth compared with the United States, Britain, Japan, and other countries. The green brand is not limited to the category of ecological and environmental protection. However, it is closely related to the sustainable development of enterprises. Developing green brands not only conforms to the development trend of the social environment, but also conforms to the wave of green consumption in the market. At the same time, it is also conducive to improving enterprises' international competitiveness and sustainable development ability. As China's green market is not mature enough, problems such as poor authenticity of green brands, "hollowing out" of green brands, and "green floating" of brands have begun to emerge, which have seriously affected consumers' enthusiasm for green brand consumption and green brand trust [1]. How to create a green brand with consumer trust and value has become a hot issue in business and academic circles.

The current research on green brands is conducted chiefly from the perspective of consumers and enterprises [2–5], and research on green brand value based on a regional perspective is rare. Previous studies have shown that innovation capability can help enterprises gain competitiveness and sustainability and thus help enterprises improve their market position, establish a brand reputation, bypass competition, make breakthroughs, and attract customers [6–9]. However, previous studies only discussed whether innovation could improve brand value and generally regarded the innovation process as a "black box", requiring more analysis of the innovation process. Only a few studies conducted independent research on green brands. In addition, the development of brands and the process of sci-tech innovation both need the protection of intellectual property rights as part of their premise. Legal and institutional means are required to protect enterprises' innovation achievements and encourage enterprises to continue to innovate to inject fresh blood into the development of enterprise brands constantly.

Given the above background and existing research, this paper, from the perspective of the innovation value chain, divides the innovation process into two stages: R&D and achievement transformation, to more clearly reveal the impact of the two stages of innovation on green brand value. As the degree of intellectual property protection varies significantly in different regions of China, taking intellectual property protection as a threshold variable, we can explore the impact of two-stage innovation on green brand value under different levels of intellectual property protection. On the one hand, we can further reveal the differences in the impact of innovation at different stages on green brand value; on the other hand, we can provide targeted policy recommendations for developing green brands in different regions. As for the impact of regional innovation on brands, existing studies usually regard the research region as a whole, which ignores the spatial relevance of innovation activities and other economic activities among regions. The establishment of

a spatial Dubin model can further discuss the impact of this spatial effect on green brand value. To provide a theoretical and practical basis for sci-tech innovation to promote the green brand value and provide targeted policy suggestions for constructing green brands in different regions of China.

2. Literature Review

2.1. Green Brand and Influencing Factors of Brand Value

Green brand refers to specific brand characteristics and attributes related to reducing environmental impact and consumers' different environmental demands [2]. Compared with nongreen brands, green brands have three characteristics: greenness, sustainability, and externality. Greenness refers to green brands' function of improving the ecological environment and social environment, which allows them to achieve a "win-win" in population, economy, environment, and other aspects. Sustainability refers to the efficient and reasonable allocation of enterprise resources due to the green nature of green brands. Externality refers to the positive impact of enterprises' development of green brands on other economic entities, such as improving the ecological environment, guiding other enterprises towards green practices, leading consumers to green consumption, etc. Scholars have carried out a series of studies in green brand-related fields, mainly from the perspective of consumer behavior. Royne et al. (2011), Hartmann & Apaolaza-Ibáez (2012), Suki (2016), and other researchers found that the main factors that affect consumers' green brand choice and purchase behavior are the deterioration of the external ecological environment and the enhancement of their health and environmental awareness [10–12]. Consumers have the motivation to choose green brands, but the actual efficiency of green brand selection is not high. From the consumers' perspective, the brand–consumer distance is too large, which is why consumers reject green brands. Enterprises can encourage consumers to establish green brand memory through green marketing, shorten the brand–consumer distance, and thus promote green brand consumption [13,14]. From the perspective of enterprises, green brand innovation is not vital, and uneven product quality is also an essential factor that restricts consumers' green consumption [15]. Therefore, enterprises should pay attention to the role of green marketing in adjusting brand environmental relevance and consumers' green brand attitude and the driving role of sci-tech innovation on the brand to enhance the value of green brands through innovation [9].

Brand value is the amount obtained by calculating all brand assets with a method similar to tangible assets evaluation [16]. Such brand assets include the value added by the brand to product sales in the market, as well as the cognition, attitude, and behavior of consumers and other stakeholders towards the brand. In short, brand value is the total value of all brand assets, expressed in monetary terms. Brand value is the most intuitive embodiment of brand competitiveness and the most direct reflection of a brand's position in the market, as well as its development and change. The mainstream evaluation methods for brand value include Interbrand, Financial World, World Brand Lab, etc. With the expansion of the influence of the World Brand Lab in China, Chinese scholars usually use the brand value data released by the World Brand Lab to conduct relevant empirical research [17–19].

Currently, the research on green brand value continues the research method of brand value and is mainly based on two perspectives of corporate finance and consumers. Chen (2010) believed that green brand value is a series of brand assets and liabilities related to enterprises' green commitments and environmental concerns [20]. Ng et al. (2014) pointed out from the consumers' perspective that green brand value is the overall evaluation of consumers' perception of green products or services and their environmental desire, sustainable expectation, and green demand [21]. With the development of society, the evaluation of corporate brands, especially green brands, should not be limited to traditional financial indicators such as market value, operating income, profitability, or the green value perceived by consumers. Whether there are positive environmental and social externalities is also an important consideration. ESG index is an evaluation standard system for enterprise, which mainly encompasses three aspects: the impact of enterprise

on the environment (E), responsibility to society (S), and internal governance (G). The three aspects are closely related to the three characteristics of the green brand (green, sustainability, and externality). The ESG index can reflect the development of green brands of enterprises to a certain extent. Therefore, this paper will measure the regional green brand value based on the brand value data released by the world brand experiment and the ESG index released by Shanghai Huazheng Index Information Service Co., Ltd.

2.2. Sci-Tech Innovation and Brand Value

The idea of sci-tech innovation as an essential source of brand value is relatively new, and issues of brand and sci-tech innovation penetration are gradually emerging in academia [22]. Aaker (1996) and Zhang et al. (2013) believe that sci-tech innovations, such as the inclusion of significant new technology attributes, may cause consumers to recognize convenience and comfort from the new technology attributes and appreciate innovation efforts and capabilities, thus creating a better image for the brand [23,24]. Kliestikova & Kovacova (2017) believe that innovation is being integrated into the construction and management of brands and use questionnaire surveys, choice analysis, and cluster analysis to empirically verify that innovation is an essential source of brand value perceived by consumers [25]. Kurt (2019) emphasized that companies focusing on R&D strategies to provide products based on technological innovation will contribute to brand value and corporate revenue in the global environment of immediate consumption, and empirical studies have shown a positive relationship between R&D expenditures, revenue, and brand value [26]. Yao et al. (2019) believe that sci-tech innovation mainly helps to improve production efficiency and product quality, thereby gaining long-term competitive advantages, which will be reflected in brand value. They also found that technical innovation has a stronger impact on improving brand value compared with nontechnical innovation [27]. Apparently, sci-tech innovation has an essential impact on brand value.

As for the relationship between sci-tech innovation and brand value, the existing research mainly carries out relevant research on two levels: firstly, at the enterprise level, based on the theory of enterprise resource base and the theory of core competitiveness; second, at the regional level, based on the theory of brand growth environment. Scholars generally argue that innovation can promote brand value by developing new products and services, improving the quality of existing products and services, increasing the added value of products and services, and other ways [28–30].

2.2.1. The Perspective of Enterprise Resource Base and Core Competence

According to the theory of enterprise resource base, the resources owned by enterprises are the material basis for the construction and development of enterprise brands. High-quality enterprise resources can promote new brands' success and help existing brands grow [28]. M'Zungu et al. (2010) pointed out that sufficient resources can guarantee enterprise' R&D and production activities, which is conducive to the development and growth of enterprise brands [31]. Han & Zhao (2008) considered that for the development of China's brands, improving product quality is the primary condition, and the quality of products depends not only on good product design but also on the skilled workers and high-quality knowledge of workers involved in enterprises [32]. Zhu & Wang (2018), based on the perspective of intellectual property rights, analyzed that enterprises' intellectual assets, such as talents, patents, and trademarks, play an essential role in promoting brand competitiveness [33]. It can be seen that the innovation resources of enterprises will have a positive effect on brand competitiveness and brand value.

An enterprise's core competence is a comprehensive system composed of the accumulation of knowledge, special skills, and related resources in the production and operation process of the enterprise. It is the power source of the sustainable competitiveness of the enterprise. Huang & He (2015) believed that brand competitiveness came from the core competence of enterprises, especially the ability to innovate independently [34]. The core competitiveness of an enterprise originates from its resources, but unique and difficult-to-

imitate essential resources can bring long-term competitive advantages to the enterprise. The innovation resources of an enterprise are usually unique to that enterprise and are scarce, nonimitative, and irreplaceable [35]. Li & Liu (2017) believe that knowledge resources dominated by core technologies are the most important manifestation of enterprise innovation resources, which are the essential resources needed to cultivate the core competence of enterprises [30]. Through the Internet industry, Helm (2007) found that for the high-tech industry, product innovation and technology development make the brand different and promote the development of the industry [36]. Wang & Wang (2020) argued that the value of China's time-honored brands comes from the accumulation of historical culture and the inheritance of core technologies, cultural endowment determines the direction of brand development, and the improvement and innovation of core technologies is the source of brand growth [37]. Based on enterprise resource theory and enterprise core competence theory, Wang et al. (2013), explored the influencing factors of independent brand creation and proposed that independent innovation is the fundamental means for Chinese enterprises to create high-quality brands while providing human capital quality is the key to enhance enterprise innovation ability [38].

To sum up, from the perspective of enterprise resources or core competence, improving enterprise innovation capability is essential to increase brand equity, improve brand competitiveness, achieve brand differentiation, and promote brand value.

2.2.2. The Perspective of Brand Growth Environment

Brand building is affected not only by internal factors of the enterprise but also by external environmental factors of the enterprise; that is, the environmental factors of the region where the brand is located. Wang & Cheng (2012) built a unitary linear regression model and found that regional technological innovation has a significant positive impact on brand value without interfering with other influencing factors [39]. Wang et al. (2019) found that regional R&D capabilities and technological environment support significantly impact brand value by building a multiple regression model [40]. Zhou et al. (2014) calculated the regional technological innovation scores of 31 provinces by factor analysis and certified that the stronger the regional technological innovation ability, the higher the brand value [41]. Qi & Liu (2015) analyzed the impact of collaborative innovation and performance on the competitiveness of brands from the regional level and found that the higher the degree of collaboration between innovation subjects, the more vital the innovation efficiency, and thus the more significant the role of improving the competitiveness of brands [42]. In addition to the innovation environment, the regional market environment, legal system environment, social environment, political environment, and natural environment in which the brand is located will have a specific impact on the construction and growth of the brand [43,44].

Intellectual property protection is crucial in technological innovation and brand building. The more perfect the legal environment is, the higher the return rate of R&D investment and brand investment is, and the stronger the motivation of enterprises to innovate. Sukarmijan & Sapong (2014) believed that based on the background of the intellectual economy, intellectual property protection plays a vital role in promoting technological progress and brand promotion [45]. Wang et al. (2015) used panel data from 25 provinces in China to demonstrate that intellectual property protection can indirectly affect brand growth by influencing regional technological innovation capability [46]. Yan (2018) stressed that the government should strengthen the protection of agricultural products' knowledge innovation, and create a good knowledge protection environment, to improve agricultural products' brand value [47].

2.3. Innovation Value Chain Theory

Previous studies usually regarded the innovation process as a "black box", which would ignore the internal structure and internal operating mechanism of innovation. From the perspective of the innovation value chain, we can explore the internal mechanism

of the innovation process and match the research on the path of innovation efficiency improvement. The innovation value chain was first proposed by Hansen & Birkinshaw (2007). They argued that the innovation value chain could be divided into three stages: the generation, transformation, and dissemination of creativity, and there is a progressive internal correlation in the three stages [48]. Chinese scholars usually regard the innovation value chain as the decomposition of sci-tech innovation links based on the perspective of production. Sci-tech innovation is a multi-stage, multi-factor value chain transmission process from the input of innovative resources to the output of innovative products, which mainly includes the following three stages: the input of innovation, the condensation of innovative knowledge, and the realization of innovative achievements [49–51]. Yu and Liu (2014) divided the sci-tech innovation process into knowledge innovation, R&D innovation, and product innovation. They investigated the innovation efficiency of different provinces at different stages using the three-stage DEA model [49]. Considering that this paper focuses on analyzing the impact of technological innovation capability and value transformation capability on the development of green brands, the innovation process is simplified into two stages: R&D and achievement transformation. R&D is the basis of innovation, focusing on knowledge creation and technological research and development. Achievement transformation is the application of innovation to realize the economic value of innovation. Both stages of innovation have input–output functions and are interrelated processes. That is, the output in the R&D stage is usually the input in the achievement transformation stage. See Figure 1 for the two-stage innovation value chain model.

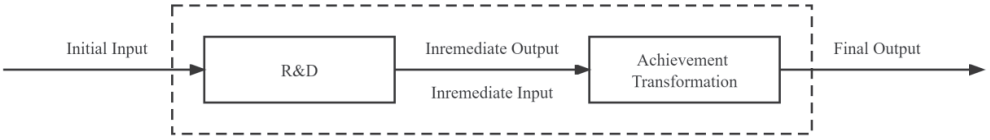

Figure 1. Two-stage innovation value chain.

2.4. Dissipative Structure Theory

In addition to being widely used in physics, chemistry, and mathematics, dissipative structure theory has gradually become a new research paradigm in economics. Its solid economic explanatory power has laid a foundation for its extensive economic application. Perrings (1986) applied the theory of dissipative structure to the analysis of economic environment systems and pointed out that economic environment systems are complex systems with dissipative structure properties [52]. The dissipative structure has four characteristics: openness, nonequilibrium, internal nonlinearity of the system, and an internal driving effect of "fluctuation" [53,54]. The brand ecosystem has four main dissipative structure characteristics as a complex economic system. As a component of the economic system, the brand ecosystem has a close exchange of capital, technology, information, and other elements with other systems in the economic system (openness). The brand ecosystem is not static, but a nonequilibrium evolution system. Technological progress or changes in market demand bring about brand changes, with which the brand ecosystem is gradually adjusted away from the original equilibrium. With the maturity of new technologies or the stability of market demand, the brand ecosystem enters a new equilibrium (nonequilibrium). The development of any brand will be affected by other brands and stakeholders. There is a complex network of associations between brands and between brands and stakeholders that compete with and promote each other [55]. It is not a simple linear relationship that can be described and depicted (in other words, it is nonlinear). "Fluctuation" originates from the change in policy, capital, technology, market, stakeholders, and other influencing factors. Any small influencing factor deviating from the original equilibrium state will be further amplified into a "huge fluctuation" that controls the evolution of the whole system through the nonlinear interaction relationship (the internal driving role of "fluctuation"). Therefore, the brand ecosystem is a system with the characteristics of a dissipative structure.

2.5. Summary of This Chapter

Scholars have conducted extensive research on the relationship between innovation and brand and have gathered rich research results. Mainly based on the theory of brand equity and brand competitiveness, they believe that innovation can increase brand equity and improve brand competitiveness, thereby improving brand value and brand influence. Brand equity theory and brand competitiveness theory are the extension and expansion of resource-based theory and core competence theory in marketing. Essentially, they both emphasize that only continuous innovation can provide inexhaustible power for the development and growth of brands.

Nevertheless, scholars seldom explore the impact of innovation on green brand value from the regional level and usually regard the research region as an independent whole, which will ignore the differences between regional development and the spatial interaction of regional economic activities. Secondly, innovation is a multi-stage and multi-output process, and the impact of innovation output at different stages on brand value may differ. Thirdly, in addition to the innovation environment in which the brand is located, the market environment, legal environment, social environment, etc., will have a particular impact on the creation and growth of the brand; in particular, the legal environment of intellectual property. On the one hand, intellectual property protection can provide a legal basis and protection for enterprises to safeguard brand rights and create a good external environment and institutional guarantee for enterprises to promote brand growth. On the other hand, it can effectively weaken the externality of innovation and avoid the phenomenon of "free riding", to protect the innovation achievements of enterprises, ensure the innovation benefits of enterprises, and improve the enthusiasm of enterprises for continuous innovation. Finally, according to the four characteristics of the dissipative structure, this paper discusses that the brand ecosystem is a system with the characteristics of the dissipative structure.

3. Study Design

3.1. Model Construction

According to the brand ecosystem theory, the brand ecosystem is a business ecosystem composed of brands and their related environments for survival and development, including government, market, sci-tech innovation, legal system, culture, and other ecological environment elements, investors, suppliers, industry associations, customers, and other relevant stakeholder elements [56]. The construction of a green brand is carried out under specific environments and conditions. It is closely related to sound economic development, a high level of opening to the outside world, a perfect market, a large market scale, and other factors. It is encouraged and constrained by various factors and relationships between all parties. Any change in these factors will affect the realization of green brand value. According to the dissipative structure theory of Prigogine (1994) [57], we can infer that if the brand ecosystem is an isolated system, then according to the principle of entropy increase, the entropy of the system will continue to increase, and the perfection of the system will certainly weaken. Suppose the brand ecosystem is an open system. In that case, the introduction of negative entropy from the surrounding environment will offset the increase in system entropy by constantly exchanging material, energy, and information with the outside world, giving the brand ecosystem the characteristics of a dissipative structure. This dissipative structure feature will make the brand ecosystem more orderly and promote green brand value in the system. Regional sci-tech innovation is an important way for the system to obtain the negative entropy flow, while protecting intellectual property rights will enhance the negative entropy flow.

For an open system with dissipative structure characteristics, its development state can be measured by calculating the total entropy change of the system [53]. The total entropy change (dS) of the system comes from the positive entropy flow (dSi, $dSi > 0$) generated by the system itself and the negative entropy flow (dSe, $dSe < 0$) formed by the system's exchange with the outside world. The formula is $dS = dSi + dSe$. When $dS < 0$,

the system will have a self-organization phenomenon and gradually evolve from the low stage to the high stage. When $dS > 0$, the system will be in a disordered state of change and degenerate from the advanced stage to the low-level stage. When $dS = 0$, it means that the system has not changed. Based on the theory of dissipative structure and the principle of entropy increase, this paper builds a relationship model between sci-tech innovation and the promotion of green brand value, as shown in Figure 2.

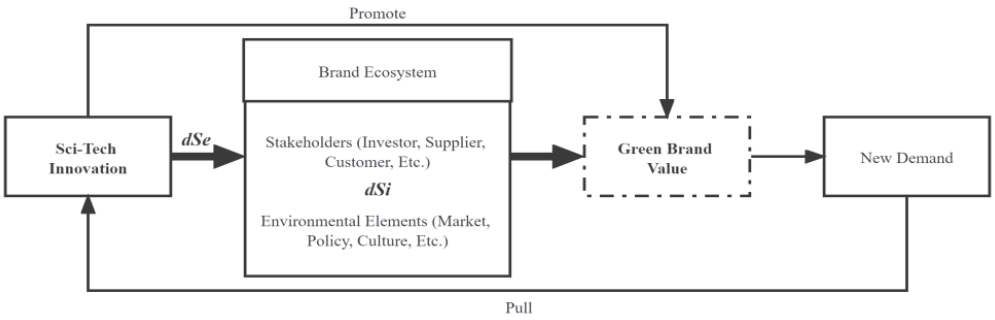

Figure 2. The relationship between sci-tech innovation and the promotion of green brand value.

Sci-tech innovation ability is the source of power to promote the development of green brands. From the regional perspective, the value of a green brand in a region is not only affected by the local brand's ecological and environmental factors, but also neighboring regions' environmental factors. In addition, the strength of intellectual property protection will affect the role of technological innovation in promoting the value of green brands. According to the above analysis, the empirical test model constructed in this paper is shown in Figure 3.

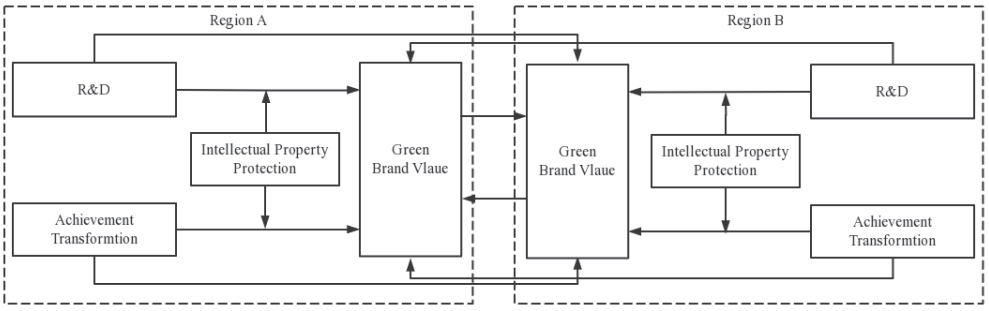

Figure 3. Influence mechanism of sci-tech innovation on green brand value.

3.1.1. Two-Way Fixed Effects Model

In order to study the impact of two-stage innovation efficiency on the value of the green brand, this paper uses the stepwise regression method to build Models (1)–(3). The specific model forms are as follows:

$$BV_{it} = \alpha_0 + \alpha_1 TRD_{it} + \alpha_2 EDL_{it} + \alpha_3 OUL_{it} + \alpha_4 MS_{it} + \alpha_5 MD_{it} + \mu_{it} \quad (1)$$

$$BV_{it} = \alpha_0 + \alpha_1 TAT_{it} + \alpha_2 EDL_{it} + \alpha_3 OUL_{it} + \alpha_4 MS_{it} + \alpha_5 MD_{it} + \mu_{it} \quad (2)$$

$$BV_{it} = \alpha_0 + \alpha_1 TRD_{it} + \alpha_2 TAT_{it} + \alpha_3 EDL_{it} + \alpha_4 OUL_{it} + \alpha_5 MS_{it} + \alpha_6 MD_{it} + \mu_{it} \quad (3)$$

The explained variable BV_{it} is the green brand value of region i in year t. The explanatory variables TRD_{it} and TAT_{it} are the R&D efficiency and achievement transformation efficiency of region i in year t; EDL_{it}, OUL_{it}, MS_{it}, and MD_{it}, respectively represent the regional economic development level, the degree of opening to the outside world, the market size and the degree of marketization. α is the regression coefficient; μ is a random error term.

3.1.2. Two-Way Fixed Effects Model

According to the application of "the first law of geography" in economics, there is a specific interaction between regional economic activities in space [58]. Commonly used spatial econometric models include the spatial Doberman model (SDM), spatial lag model (SLM), and spatial error model (SEM). SDM has more real explanatory power than the other two models because it can examine the influence of explanatory variables in adjacent areas on the explained variables [59]. Therefore, to avoid ignoring the possible model estimation bias caused by spatial effects of regional economic behavior and to make the research results more realistic, this paper explores the spatial effects of regional innovation efficiency on the value of green brands by building a SDM. The specific manifestations of the SDM are as follows:

$$\begin{aligned} BV_{it} = {} & \rho WBV_{it} + \beta_0 TRD_{it} + \beta_1 EDL_{it} + \beta_2 OUL_{it} + \beta_3 MS_{it} + \beta_4 MD_{it} \\ & + \theta_0 TRD_{it} + \theta_1 EDL_{it} + \theta_2 OUL_{it} + \theta_3 MS_{it} + \theta_4 MD_{it} + \varepsilon_{it} \end{aligned} \tag{4}$$

$$\begin{aligned} BV_{it} = {} & \rho WBV_{it} + \beta_0 TAT_{it} + \beta_1 EDL_{it} + \beta_2 OUL_{it} + \beta_3 MS_{it} + \beta_4 MD_{it} \\ & + \theta_0 TAT_{it} + \theta_1 EDL_{it} + \theta_2 OUL_{it} + \theta_3 MS_{it} + \theta_4 MD_{it} + \varepsilon_{it} \end{aligned} \tag{5}$$

$$\begin{aligned} BV_{it} = {} & \rho WBV_{it} + \beta_0 TRD_{it} + \beta_1 TAT_{it} + \beta_2 EDL_{it} + \beta_3 OUL_{it} + \beta_4 MS_{it} + \beta_5 MD_{it} \\ & + \theta_0 TRD_{it} + \theta_1 TAT_{it} + \theta_2 EDL_{it} + \theta_3 OUL_{it} + \theta_4 MS_{it} + \theta_5 MD_{it} + \varepsilon_{it} \end{aligned} \tag{6}$$

W is the spatial weight matrix; WBV_{it} is the spatial lag item of the explained variable's green brand value; $WTRD_{it}$, $WTAT_{it}$, $WEDL_{it}$, $WOUL_{it}$, WMS_{it}, and WMD_{it} are the spatial lag items of R&D efficiency, achievement transformation efficiency, and other control variables, respectively. ρ represents the spatial autocorrelation coefficient, β and θ represent the regression coefficient, and ε represents the error term.

The spatial adjacency weight matrix (W) is set according to whether provinces are adjacent geographically. If two regions are adjacent, the matrix element is set to 1. If two regions are not adjacent, the matrix element is set to 0. The spatial inverse distance matrix (W*) is set according to the Euclidean distance (d_{ij}) between the provincial capitals of each province and city and is used for the subsequent robustness test. The weight matrix elements of the spatial adjacency weight matrix (W) and spatial inverse distance matrix (W^*) are defined as follows:

$$W_{ij} = \begin{cases} 1, \text{region } i \text{ is adjacent to region } j \\ 0, \text{region } i \text{ isn't adjacent to region } j \end{cases}, i \neq j \quad W_{ij}^* = \begin{cases} \frac{1}{d_{ij}}, i \neq j \\ 0, i = j \end{cases} \tag{7}$$

3.1.3. Panel Threshold Model

This paper refers to Hansen (1999)'s panel data threshold model [60], selects intellectual property protection as the threshold variable of R&D efficiency and achievement transformation efficiency, and constructs the threshold regression model as follows:

$$\begin{aligned} BV_{it} = {} & \alpha_0 + \alpha_1 TRD_{it} I(IPR_{it} \leq \gamma) + \alpha_2 TRD_{it} I(IPR_{it} \geq \gamma) + \alpha_3 EDL_{it} \\ & + \alpha_4 OUL_{it} + \alpha_5 MS_{it} + \alpha_6 MD_{it} + \mu_{it} \end{aligned} \tag{8}$$

$$\begin{aligned} BV_{it} = {} & \alpha_0 + \alpha_1 TAT_{it} I(IPR_{it} \leq \gamma) + \alpha_2 TAT_{it} I(IPR_{it} \geq \gamma) + \alpha_3 EDL_{it} \\ & + \alpha_4 OUL_{it} + \alpha_5 MS_{it} + \alpha_6 MD_{it} + \mu_{it} \end{aligned} \tag{9}$$

IPR_{it} is the level of intellectual property protection in year t of region i, γ is the threshold value, ε is a random disturbance term, and $I(\cdot)$ is a threshold index function.

3.2. Variable Design

3.2.1. Explained Variables

Previous studies mostly explored the impact of sci-tech innovation on enterprise brand value from the enterprise level. This paper focuses on the impact of technological

innovation on the overall level of green brand value in the region from the regional level. It considers the poor availability of regional green brand value data. Therefore, this paper's regional green brand value is the sum of the regional green brand value. The measurement method is as follows: first, we count the brands that are shortlisted in China's 500 Most Valuable Brands. Secondly, according to the ESG index, we remove the enterprise brands rated below B. Finally, according to the brand value data released by the World Brand Lab, the total brand value of enterprises in a particular region with an ESG rating of B or above is estimated.

3.2.2. Explanatory Variables

This paper refers to the super-efficient SBM proposed by Tone (2002) [61] and uses the efficiency value to measure the two-stage innovation level: R&D efficiency (*TRD*) and achievement transformation efficiency (*TAT*). In the stage of R&D, R&D personnel and R&D funds are usually used as input in the initial stage of innovation. Innovation output is generally about knowledge and technology, and its manifestations are patents, inventions, monographs, and scientific papers. In the R&D stage, R&D personnel and R&D expenditure are selected as the innovation input indicators in this stage. The number of patent applications and Chinese scientific and technological papers included in three major foreign retrieval tools (SCI, EI, CPI-S) are selected as the innovation output indicators to measure technology and knowledge. Of these, the total R&D expenditure of each region is calculated as R&D capital stock (based on 2009) concerning the perpetual inventory method proposed by Pittman (1983) [62], $K_t = (1 - \delta) K_{t-1} + I_t$, where K_t is the R&D capital stock in t period. It is the R&D expenditure in period t; K_{t-1} is the R&D capital stock of period $t-1$; δ is the capital depreciation rate. The calculation of initial R&D capital stock and depreciation rate refers to the practice of Shan (2008); with the capital depreciation rate δ set as 15%, and initial R&D capital stock $K_0 = I_0/(\delta + e)$, e is the average growth rate of R&D expenditure [63]. The number of patent applications and scientific and technological papers published, as the intermediate variables of the innovation value chain, are not only the innovation output indicators in the R&D stage, but also the input indicators in the achievement transformation stage. Enterprises also need to provide corresponding financial support when developing and utilizing innovative achievements. Therefore, new product development expenditure is selected to reflect the investment of innovation funds in the achievement transformation stage. The innovation achievements will eventually provide economic benefits to the enterprise, so the sales revenue of new products and the export revenue of new products are selected as the innovation output in the achievement transformation stage. See Table 1 for the two-stage evaluation indicators of regional innovation efficiency.

Table 1. Two-stage regional innovation efficiency evaluation index system.

Stage	Indicator Type	Indicator Name
R&D	Input	R&D expenditure
		Full time equivalent of R&D personnel
	Output	Number of patent applications
		Number of scientific papers published
Achievements transformation	Input	Number of patent applications
		Number of scientific papers published
		New product development expenditure
	Output	Sales revenue of new products
		Export income of new products

3.2.3. Threshold Variables

In order to measure the level of intellectual property protection (*IPR*), the GP index method proposed by Ginarte & Park (1997) is a quantitative measurement method commonly used abroad to measure the level of intellectual property protection [64]. The GP index measures the level of protection from the legislative level of intellectual property pro-

tection. Due to the relatively imperfect legal systems of developing countries, the level of intellectual property protection measured by the GP index will be on the high side. Thence, Chinese scholars usually measure the actual level of intellectual property protection in China based on the research ideas of Han & Li (2005), taking into account the law legislation and enforcement level of intellectual property protection [65]. Hu et al. (2012) proposed a new method to objectively and comprehensively measure the level of intellectual property protection by the proportion of technology market transactions in local GDP [66]. This method does not need to trace the factors that affect intellectual property protection, which are difficult to measure. Given the measurability and objectivity of this method, this paper uses the proportion of technology market transactions in local GDP to measure the level of regional intellectual property protection.

3.2.4. Control Variables

According to the theory of brand growth environment, brand development is affected not only by the enterprise's internal factors, but also by environmental factors. Considering the significant differences in the level of economic development, openness, market size, and marketization in various regions may have a particular impact on the growth of the green brand. Therefore, these factors are introduced as control variables. The regional economic development level (*EDL*) is measured by per capita GDP. The regional opening up level (*OUL*) is measured by the proportion of total imports and exports in local GDP. The market size (*MS*) of the region is measured by the total resident population of the region. The degree of marketization (*MD*) is measured by the proportion of the government's general public budget expenditure to the local GDP. If the proportion is high, the government has more intervention in the market, and the degree of marketization is low. See Table 2 for specific measurement indicators of each variable in this paper.

Table 2. Variable Description.

Variable Type	Index Name	Indicator Measurement
Interpreted variable	Green Brand Value (*BV*)	The total value of all brands in China's 500 Most Valuable Brands by region, taking the natural logarithm
Explanatory variable	R&D efficiency (*TRD*)	Calculated by super efficiency SBM model.
	Achievement transformation efficiency (*TAT*)	Calculated by super efficiency SBM model.
Threshold variable	Intellectual property protection level (*IPR*)	Technology market turnover divided by regional GDP
Control variable	Economic Development Level (*EDL*)	Per capita GDP of each region, taking natural logarithm
	Openness to the outside world (*OUL*)	Import and export volume divided by regional GDP
	Market size (*MS*)	The total number of permanent residents in each region, taking the natural logarithm
	Marketization degree (*MD*)	General public budget expenditure divided by regional GDP

3.3. Sample Selection and Data Source

The research sample of this paper is 25 provinces in China. Due to the lack of brand value data in some years in Tibet, Qinghai, Gansu, and other regions, these regions are not within the scope of the study, considering the continuity of data. There are 12 provinces in the east: Beijing, Fujian, Guangdong, Hebei, Heilongjiang, Jiangsu, Jilin, Liaoning, Shandong, Shanghai, Tianjin, and Zhejiang. There are 7 provinces in the central region: Anhui, Henan, Hubei, Hunan, Jiangxi, Inner Mongolia, and Shanxi; There are 6 provinces in the western region: Chongqing, Guangxi, Guizhou, Shaanxi, Sichuan, and Yunnan.

In calculating the total value of brands of enterprises listed in various regions, green brand screening is based on the Huazheng ESG index rating. Considering that the innovation characteristics of enterprises in the hotel, catering, jewelry, and other industries

are not obvious enough, the data of such enterprises are excluded. In addition, since the brand value released by the World Brand Experiment is calculated based on the relevant data of the previous year; that is, the brand value released in 2021 is the brand value in 2020, so the statistical year of the green brand value is one year ahead of schedule. The innovation data of each province and city come from the China Science and Technology Statistics Yearbook over the years, and other data come from the China Statistics Yearbook and the statistical yearbooks of each province and city. Some missing data are processed by interpolation. This paper uses panel data, and the research range is from 1 January 2009 to 31 December 2020.

4. Empirical Analysis Process and Results

4.1. Time Change Trend of Green Brand Value and Two-Stage Innovation Efficiency in Three Major Regions of China

Before the empirical analysis, the time trend of green brand value and two-stage innovation efficiency in the three regions over the years is statistically analyzed. Figure 4 shows the development trend of green brand value in three regions of China from 2009 to 2020. From the overall trend, the value of green brands in China is steadily rising, and the development trend of green brands is good. However, the value of green brands varies significantly among regions. The growth trend of green brand value in the eastern region is significantly higher than in the central and western regions. This is because the eastern region has a relatively high level of economic development and opening to the outside world and a good market environment and innovation environment, which can contribute to the development of enterprises and brand building in the region.

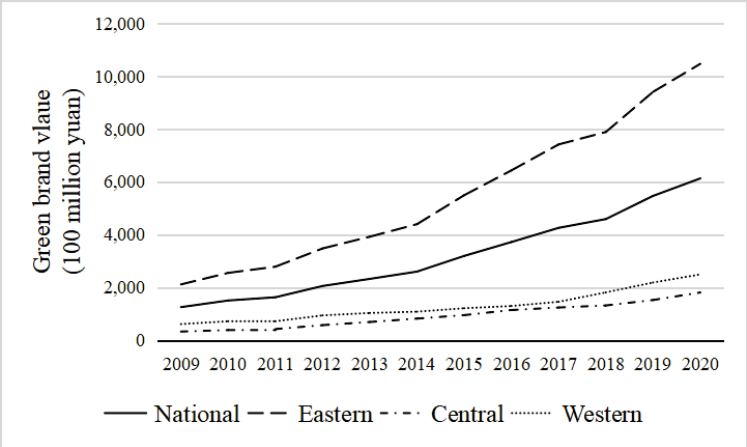

Figure 4. Change of average value of green brands in different regions of China from 2009 to 2020.

Figure 5 shows the trends of R&D efficiency and achievement transformation efficiency in China's regions from 2009 to 2020. From the overall trend, the efficiency of R&D and the efficiency of achievements transformation in China are rising. The trend of achievement transformation efficiency is greater than that of R&D efficiency. This shows that with the progress of science and technology and the deepening of market-oriented reform, China has made specific achievements in R&D and achievement transformation. Regarding R&D efficiency, the eastern region showed a steady growth trend, the central region showed an apparent upward trend after 2017, and the western region showed a downward trend after 2017. In terms of the efficiency of achievements transformation, the three regions are subject to volatile changes, and the fluctuation range is extensive. To a certain extent, the economic benefits of innovation will be affected by various factors, such as the regional economic environment, market changes, and policy changes. These factors vary significantly among different regions, leading to a volatile trend in the efficiency of innovation achievements transformation.

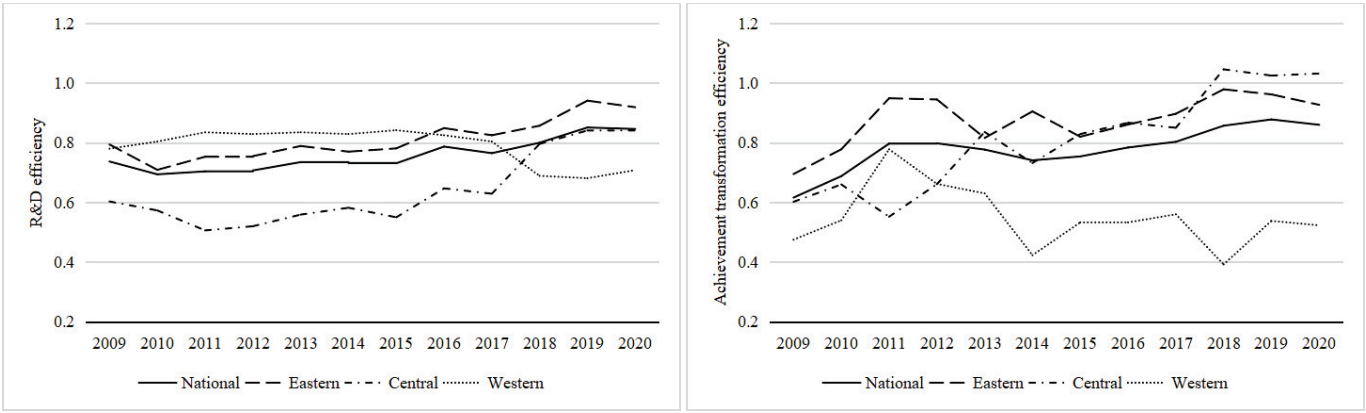

(**a**) (**b**)

Figure 5. Changes in average R&D and achievement transformation efficiency in different regions of China from 2009 to 2020. (**a**) Change in R&D efficiency. (**b**) Change in achievement transformation.

4.2. Impact of Two-Stage Innovation Efficiency on Green Brand Value

4.2.1. Time Series Stationarity Test

This paper uses Stata16.0 software to conduct statistical analysis on sample data. The correlation analysis results show that explanatory and control variables are significantly correlated with the explained variables at 1%, which preliminarily verifies the rationality of the empirical model construction in this paper. The factor independence test results show that each variable's variance inflation coefficient (VIF) is less than five, and the mean VIF is less than two, indicating that there are no multiple collinearities between variables and that the variable indicators are suitable.

Considering that this paper uses panel data to avoid the "pseudo regression" phenomenon, it is necessary to conduct a unit root test on panel data and judge the stability of the data. In this paper, the LLC test (in the case of the same unit root) and the Fisher ADF test (in the case of different unit roots) are used to test the stability of data. Table 3 shows that *BV*, *EDL*, and *MS* are unbalanced sequences under the horizontal sequence. However, under the first-order difference sequence, all variables reject the assumption that "there is a unit root". Hence, all first-order differences are stable, and each variable is at least cointegrated with first-order units I (1).

Table 3. Descriptive statistics and correlation analysis.

Variable	LLC Statistics		ADF Statistics		Test Result (If the Sequence is Stable)
	Statistics	*p* Value	Statistics	*p* Value	
BV	−11.4794 ***	0.0000	25.2830	0.9986	No
TRD	−16.3135 ***	0.0000	105.9524 ***	0.0000	Yes
TAT	−9.6603 ***	0.0000	183.8841 ***	0.0000	Yes
EDL	−11.7807 ***	0.0000	46.2625	0.6241	No
OUL	−14.2522 ***	0.0000	73.6434 **	0.0164	Yes
MS	−7.9454	0.9102	191.2413 ***	0.0000	No
MD	−10.2202 ***	0.0000	132.1372 ***	0.0000	Yes
L.BV	−14.2425 ***	0.0000	67.7333 **	0.0481	Yes
L.TRD	−14.9561 ***	0.0000	102.6958 ***	0.0000	Yes
L.TAT	−8.7227 ***	0.0003	160.5342 ***	0.0000	Yes
L.EDL	−20.1709 ***	0.0000	71.3872 **	0.0252	Yes
L.OUL	−14.7298 ***	0.0000	66.0949 *	0.0632	Yes
L.MS	−18.3309 ***	0.0000	153.4215 ***	0.0000	Yes
L.MD	−9.1084 ***	0.0002	118.0936 ***	0.0000	Yes

Note: *, **, and *** are significant at 10%, 5%, and 1% statistical levels, respectively.

4.2.2. Regression Results and Analysis of Two-Way Fixed Effect Model

Above all, this paper uses the Hausman test to judge whether to choose a fixed or random effect model. The test results show that all models pass the significance test at least at the 10% level, so we choose the fixed effect model. Secondly, the White and Wooldridge tests are used to test whether the sample data have heteroscedasticity and autocorrelation. The results show that there are heteroscedasticity and autocorrelation. Therefore, this paper uses a two-way fixed effect model to control the time variables, and the Driscoll Kraay standard is used for error estimation. See Table 4 for the specific regression results.

Table 4. Analysis of the impact of two-stage regional innovation efficiency on the value of green brands.

Variable	National			Eastern	Central	Western
	(1)	(2)	(3)	(3)	(3)	(3)
TRD	0.3696 ***		0.3209 ***	0.2036 **	−0.2288	0.9135 **
TAT		0.3286 ***	0.3057 ***	0.2500 ***	−0.0074	0.3188 **
EDL	−0.3564 *	−0.1698 *	−0.0873 *	0.9116 ***	−0.9127**	0.0268
OUL	0.3490 *	0.2055 *	0.2541 *	0.9955 ***	−0.3262	−0.9218
MS	0.4510	0.3007	0.6407	0.5371	0.9132	0.9811 ***
MD	−0.6199 **	−0.2212	−0.2017	0.7015 ***	−0.9166 **	−0.9217 **
C	5.9911 ***	5.3524 *	1.4011	−10.7175 ***	7.6209	−88.0073 ***
Time item	control	control	control	control	control	control
Sample size	300	300	300	144	84	72
R^2	0.7395	0.7474	0.7552	0.8805	0.9311	0.6478
Hausman test	17.02 ***	16.19 **	14.86 **	15.62 **	52.25 ***	9.36 *
Model	FE	FE	FE	FE	FE	FE

Note: *, **, and *** are significant at 10%, 5%, and 1% statistical levels, respectively.

From the national level, the impact coefficients of R&D efficiency and achievement transformation efficiency on the value of green brands are 0.3693 and 0.3286, respectively. Both have passed the significance test at the level of 1%, indicating that both can significantly promote the growth of green brand value. The regression results of national model (3) show that when the two innovation efficiency scores are simultaneously used as explanatory variables for regression analysis, the impact coefficients of R&D efficiency and achievement transformation efficiency are 0.3209 and 0.3057, respectively. Both pass the significance test at the 1% level, indicating that the R&D efficiency and achievement transformation efficiency positively impact the value of green brands together, which is synergistic.

In national Model (3), the impact coefficient of the economic development level is −0.0873, which is significant at the 10% level. Under normal circumstances, the higher the economic development level of a region, the better the brand development in the region. The negative impact may be that China's green brand development started late, and the development of green brands seriously lags behind economic construction. The impact coefficient of the degree of opening up is 0.2541, and the significance level test shows that the higher the degree of opening up, the better the development of green brands. Improving the level of opening up and expanding the international market can promote China's green brands from "China" to "the world". China's green brand value and influence can continuously improve through competition and cooperation with well-known international brands. The market size and the degree of marketization have positive and negative effects on the value of green brands, respectively. However, they need to pass the significance test, which the vast territory of China and the significant differences in resource endowments and market environments between different regions may cause.

At the regional level, the efficiency of R&D and the efficiency of achievements transformation in the eastern region positively impact the value of the green brand. The impact of the efficiency of achievements transformation is more significant than the efficiency of R&D due to the relatively developed market in the eastern region. In the developed market environment, once the new products enterprises develop successfully enter the market, the

economic benefits will be incredible, which is conducive to improving the brand value. The R&D efficiency and achievements transformation efficiency in central China have not significantly impacted the value of green brands in this region. The sci-tech innovation efficiency in central China needs to be further improved. Attention should be paid to strengthening the economic transformation of innovation achievements. The efficiency of R&D and the efficiency of achievement transformation in the western region positively affect the value of green brands. The impact of R&D efficiency is far more significant than the efficiency of achievement transformation. While improving the level of R&D, the western region should also pay attention to the economic benefits of sci-tech achievements transformation.

The economic development level of the eastern region will have a significant positive impact on the green brand value. In contrast, the economic development level of the central and western regions has yet to have a significant positive impact. The development of the economy and green brands in the eastern region is relatively balanced. Only the level of opening up in the eastern region has a significant positive impact on green brand value, while only the market size in the western region has a significant negative impact on green brand value. This shows that the green brand market in the western region is still mainly domestic, while the eastern region has opened the international market. The degree of marketization in the eastern region positively impacts the value of green brands because the public economy dominates China's primary economic system. The eastern region is the first to realize reform and opening up in China. Government market policies and economic support are an essential part of developing enterprises and brand building in this region. The degree of marketization in the central and western regions harms the value of green brands, indicating that improving marketization is conducive to developing green brands in the region.

In summation, improving the efficiency of regional R&D and the efficiency of achievements transformation can promote the growth of green brand value. The regional innovation efficiencies of the two stages have obvious synergy. However, due to the evident differences in the brand growth environment between regions, there are significant regional differences in the impact degree and effect of regional innovation efficiency of the two stages. The regional economic development level, the degree of opening up, the market size, and the degree of marketization also have significant regional differences in the impact of green brand value in different regions. Therefore, to speed up the construction and development of China's green brands, it is necessary to improve the R&D ability and innovation achievements transformation ability, adapt to local conditions, and formulate a targeted development path according to the regional brand growth environment.

4.3. Analysis of Spatial Spillover Effect of Regional Innovation Efficiency on Green Brand Value

Referring to Elhorst (2014)'s idea of spatial applicability test [67], before building the spatial Dubin model, we should first use Moran's I index to test the global spatial correlation of three core variables, namely, green brand value, R&D efficiency, and achievement transformation efficiency in 25 provinces. Furthermore, we depict the spatial aggregation of regional economic activities from the overall regional space. Moran's I index is calculated as follows:

$$\begin{gathered} \text{Moran's} \quad I = \frac{\sum_{i=1}^{n}\sum_{j=1}^{n} w_{ij}(X_i-\bar{X})(X_j-\bar{X})}{S^2\sum_{i=1}^{n}\sum_{j=1}^{n} w_{ij}} \\ S^2 = \sum_{i=1}^{n}\frac{(X_i-\bar{X})^2}{n}, \bar{X} = \frac{1}{n}\sum_{i=1}^{n} X_i \end{gathered} \tag{10}$$

where X_i represents the observation value of the ith region, w_{ij} represents the standardized spatial adjacency matrix, and Moran's I index is $[-1,1]$. If its value is greater than zero, this indicates that the data are positively correlated in space. If its value is equal to zero, this indicates that the data are spatially random. If the value is greater than zero, this indicates that the data are spatially negatively correlated. Next, we carry out the LM and robust Robust LM test on the residuals of nonspatial econometric models to further judge whether

a spatial econometric model should be established. Finally, the applicability of the Spatial Doberman Model (SDM) is tested. LR and Wald tests are used to determine whether the SDM needs to degenerate into SEM or SLM.

4.3.1. Spatial Correlation Test Results

Based on the spatial adjacency matrix (W), this paper uses Moran's I index to test the spatial autocorrelation of green brand value, R&D efficiency, and achievement transformation efficiency. The global Moran's I index and test results of core variables in each province and city from 2009 to 2020 are shown in Table 5. From 2009 to 2020, the overall Moran's I index of green brand value is significantly negative. Most of them are significant at the 1% level, indicating that there is a negative spatial correlation between the green brand values of each province and city. That is, the value of green brands between regions presents the characteristics of "high-low" adjacent or "low-high" adjacent clustering. Based on the above analysis of the development of green brands in various provinces in China, some provinces have a high value of green brands, while neighboring provinces have a low value of green brands. It is not difficult to determine that there is a "siphon effect" in the development of green brands in China. That is, regions with a high development of green brands will attract talent, capital, technology, and other production factors from nearby regions due to their better market environment and economical level to promote their own region's brand development while inhibiting the brand development of neighboring regions. However, this negative correlation is gradually weakening with the development of science and technology and more convenient transportation in recent years.

Table 5. The overall Moran's *I* test results of green brand value and two-stage regional innovation efficiency.

Year		2010	2012	2014	2016	2018	2020
BV	Moran's I	−0.211 ***	−0.203 ***	−0.208 ***	−0.202 **	−0.198 **	−0.164 **
	Z-statistic	−2.810	−2.919	−2.707	−2.283	−2.256	−1.680
	p value	0.002	0.002	0.003	0.011	0.012	0.046
TRD	Moran's I	0.288 ***	0.146 *	0.165 *	0.189 **	0.223 **	0.189 **
	Z-statistic	2.509	1.443	1.591	1.909	2.197	1.945
	p value	0.006	0.075	0.056	0.028	0.014	0.026
TAT	Moran's I	0.143 *	0.167 **	0.181 **	0.241 ***	0.296 ***	0.288 ***
	Z-statistic	1.535	1.720	2.418	3.084	2.802	2.737
	p value	0.062	0.043	0.018	0.001	0.003	0.003

Note: *, **, and *** are significant at 10%, 5%, and 1% statistical levels, respectively.

The overall Moran's I index of R&D efficiency and achievement transformation efficiency from 2009 to 2020 is significantly positive and at least passes the 10% significance test, indicating a "spatial diffusion" effect of regional innovation in China. There is a positive interaction between R&D efficiency and achievement transformation efficiency in each region. The core variables have spatial correlation, which preliminarily verifies the rationality of using the spatial econometric model to conduct empirical research.

4.3.2. Regression Results and Analysis of Spatial Dubin Model

According to the LM test and robust Robust LM test results, the panel data model has spatial autocorrelation, and a spatial panel regression model should be built. According to the LR and Wald test results, the SDM model is a better choice. Finally, according to the results of the Hausman test and the comparison of the goodness of fit, this paper uses the spatial Dubin model with fixed time effect as the benchmark return model. Regarding Elhorst (2010)'s practice [68], this paper uses the partial differential method to estimate the direct effect, indirect effect (spatial spillover effect), and total effect of two-stage innovation efficiency and other relevant influencing factors on green brand value. The direct effect represents the impact of local innovation efficiency on local green brand value. The indirect

effect indicates the impact of local innovation efficiency on neighboring regions. The total effect represents the overall impact of innovation efficiency on green brand value. See Table 6 for the regression results of the spatial Dubin model.

Table 6. Analysis of the spatial effect of two-stage regional innovation efficiency on the value of green brands.

	Variable	National			Eastern	Central	Western
		(4)	(5)	(6)	(6)	(6)	(6)
Direct effect	*TRD*	0.6025 ***		0.7767 ***	0.9179 ***	0.2497	0.5073 ***
	TAT		0.3111 **	0.3519 **	0.2563 **	0.0826	0.6742
	EDL	0.9144 ***	0.9188 ***	0.9197 ***	0.6074	0.9362 ***	−0.3645
	OUL	0.9123 ***	0.9104 ***	0.8205 **	0.1946	−0.5140	0.5933
	MS	0.8599 ***	0.9263 ***	0.9038 ***	0.8769 ***	0.8849 ***	0.9228 ***
	MD	−0.9110 **	−0.4710	−0.9842 **	0.9485 ***	0.9192 **	−0.9593 ***
Indirect effect	*TRD*	0.1239		0.0041	0.2135 *	0.7754 **	0.4614
	TAT		0.6369 ***	0.8021 ***	0.2543 **	0.0441	0.9184
	EDL	−0.9187 ***	−0.9191 ***	−0.9154 ***	−0.9107 **	−0.9255 ***	0.9261
	OUL	0.3715	0.4995	0.1159	0.9118 ***	0.9106 ***	0.9413 ***
	MS	−0.9152 ***	−0.9118 ***	−0.9104 ***	0.1772	0.1944	0.9490 ***
	MD	−0.9255 ***	−0.9126	−0.4261	−0.9573 ***	0.5581	0.9495 ***
Total effect	*TRD*	0.7275 ***		0.7809 ***	0.4446 ***	0.5258 **	0.9687 **
	TAT		0.7480 ***	0.9540 ***	0.5106 ***	0.1267	0.9117
	EDL	−0.4238	−0.0356	0.4269	−0.4617 ***	0.9111 **	0.9225 *
	OUL	0.9160 ***	0.9155 ***	0.9364 **	0.9137 ***	0.9101 ***	0.9100 ***
	MS	−0.6582 ***	−0.2545	−0.1319	0.9105 ***	0.9108 ***	0.9718 ***
	MD	−0.9365 ***	−0.9173 **	−0.9141 *	−0.8821	0.9248 ***	0.9492
	Sample size	300	300	300	144	84	72
	R^2	0.7041	0.6876	0.7160	0.9366	0.7933	0.7538

Note: *, **, and *** are significant at 10%, 5%, and 1% statistical levels, respectively.

From the national level, the direct effects of R&D efficiency and achievement transformation efficiency on green brand value are significantly positive, indicating that improving R&D and achievement transformation efficiency will significantly promote local green brand value. It can be seen from the national Model (6) that when the two stages of innovation efficiency are simultaneously used as explanatory variables for regression analysis, the influence coefficients of the direct effect and the total effect of R&D efficiency and achievement transformation efficiency are significantly increased. This shows that R&D efficiency and achievement transformation efficiency can jointly promote the increase of green brand value. They have the "1 + 1 > 2" effect. That is, the innovation value chain has a spillover effect.

The indirect effect coefficient of R&D efficiency on green brand value is 0.1239, which fails to pass the significance test, indicating that the positive impact of R&D efficiency on adjacent regions is insignificant. The indirect effect coefficient of achievement transformation efficiency is 0.6369, which passes the significance test. It shows that a spatial spillover effect on the impact of achievement transformation efficiency on the value of the green brand. The achievement transformation efficiency in this region has a significant role in promoting the value of the green brand in neighboring regions. The overall impact of R&D efficiency and achievement transformation efficiency on green brand value is significantly positive, and the total effect of achievement transformation efficiency is greater than that of R&D efficiency.

The regression results of national Model (6) show that the direct effect coefficient of economic development level on the value of the green brand is significantly positive at the level of 1%, the indirect effect is significantly negative, and the total effect is significantly positive. This indicates that if the value of the green brand is higher in regions with high economic development, the "siphon effect" will be generated to inhibit the development of

the green brand in adjacent regions. The direct and total effects of the degree of opening up and market size are significantly positive. In contrast, the indirect effects are not significant, indicating that improving the level of opening up and exaggerating the market size is only conducive to the promotion of the value of the local green brand. The direct and total effects of the degree of marketization are significantly negative. In contrast, the indirect effect is insignificant, indicating that improving the level of marketization is only conducive to developing local green brand value.

From the regional level, the direct, indirect, and total effects of the efficiency of R&D and achievement transformation in the eastern region are significantly positive, and the three effect coefficients of achievement transformation efficiency are more significant than R&D efficiency. This reveals that the two-stage innovation efficiency in economically developed regions will not only positively impact the development of the local green brand, but will also promote the development of the green brand in neighboring regions. The value of the green brand will be more affected by achievement transformation efficiency. The three effects of the achievement transformation efficiency in the central region are insignificant, indicating that the achievement transformation efficiency has not played a significant role in promoting the green brand value of the region and adjacent regions. The direct effect of R&D efficiency in the central region is not significant, but the indirect effect is significantly positive, indicating that there is a problem of uncoordinated development between sci-tech innovation and green brands in some provinces in the central region; that is, provinces with solid sci-tech innovation experience poor development of the green brand. For example, the efficiency of R&D in Anhui Province ranks seventh in the country, but the value of the province's green brand only ranks seventeenth. Therefore, the central region should focus on improving the ability to transform innovation achievements, improving the ability to coordinate the development of innovation and brand, and building a brand with innovation. The direct effect and total effect of R&D efficiency in the western region are significantly positive, indicating that R&D efficiency in the western region has a significant role in promoting the improvement of green brand value. However, the indirect effect is not significant, which may be caused by the low mobility of innovation factors among regions due to the limited geographical environment of the transportation industry in the western region. The three effect coefficients of achievement transformation efficiency in the western region are insignificant, indicating that the western region needs to improve the achievement transformation ability to develop its brand. This relies on innovation.

In summation, we can draw the following conclusions: improving the efficiency of regional R&D and the efficiency of achievements transformation will promote the improvement of the green brand value as a whole, and the innovation value chain has noticeable spillover effects. Regional innovation efficiency's spatial effect on the green brand's value in the two stages has noticeable regional differences. The spatial spillover effect of R&D efficiency in eastern and central regions is significantly positive, while the spatial spillover effect of achievement transformation efficiency is significantly positive only in eastern regions.

4.4. Analysis of Threshold Effect of Intellectual Property Protection

4.4.1. Threshold Inspection

For the threshold test of intellectual property protection, firstly, we estimate the number of regression model thresholds when there is one threshold, two thresholds, and three thresholds using STATA16.0 software in Model (8) and Model (9), respectively. The estimation results are shown in Table 7. It can be seen from Table 7 that the single threshold model with the explanatory variable of R&D efficiency and the single threshold model with the explanatory variable of achievement transformation efficiency has passed the 5% significance test, and it is preliminarily judged that there is only one threshold in Models (8) and (9).

Table 7. Threshold effect test and estimation results of intellectual property protection.

		Threshold Effect Test			Threshold Estimation Results		
Explanatory Variable	**Model**	**F Value**	***p* Value**	**BS Times**	**Threshold**	**Estimated Value**	**95% Confidence Interval**
TRD	Single threshold	34.57 **	0.0200	500	Single threshold	0.0109	[0.0104, 0.0110]
	Double threshold	12.09	0.1940	500	Double threshold	0.0017	[0.0015, 0.0018]
	Triple threshold	6.00	0.7400	500	Triple threshold	0.0036	[0.0035, 0.0037]
Conclusion	There is a single threshold						
TAT	Single threshold	25.42 **	0.0480	500	Single threshold	0.0064	[0.0062, 0.0065]
	Double threshold	5.90	0.4740	500	Double threshold	0.0104	[0.0102, 0.0106]
	Triple threshold	5.24	0.7180	500	Triple threshold	0.0016	[0.0015, 0.0016]
Conclusion	There is a single threshold						

Note: *, **, and *** are significant at 10%, 5%, and 1% statistical levels, respectively.

Secondly, we verify the authenticity of the threshold with the help of the likelihood ratio function graph, as shown in Figure 6. When LR = 0, the corresponding threshold parameter is the threshold estimate value. The confidence interval of the threshold estimate value is the threshold parameter interval corresponding to the LR value being less than the critical value under a specific significance level (when the significance is 5%, the critical value is 7.35) [69]. It can be seen from Figure 6 that the threshold estimate value of intellectual property protection in Model (8) (explanatory variable is *TRD*) is 0.0109, and the threshold estimate of intellectual property protection in the Model (9) (the explanatory variable is *TAT*) is 0.0064. The single threshold values of the two models are within their corresponding confidence zones, indicating that the single threshold estimates of the two models are consistent with the valid threshold values. It can be determined that there is only a single threshold for intellectual property protection in Models (8) and (9).

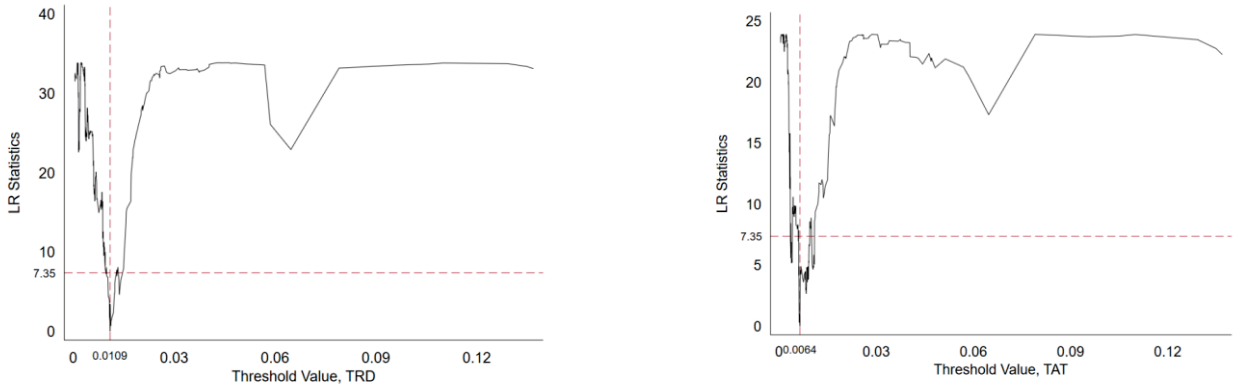

(**a**) (**b**)

Figure 6. IPR threshold likelihood ratio function with TRD and TAT as explanatory variables. (**a**) IPR threshold likelihood ratio function with TRD as explanatory variable. (**b**) IPR threshold likelihood ratio function with TAT as explanatory variable.

Therefore, this paper selects a single threshold model to analyze the threshold effect of intellectual property protection. The threshold value of intellectual property protection in the Model (8) is 0.0109, and its 95% confidence interval is [0.0104, 0.0110]. The threshold

value of intellectual property protection in the Model (9) is 0.0064, and its 95% confidence interval is [0.0062, 0.0065].

4.4.2. Regression Results and Analysis of Threshold Model

When the explanatory variable is R&D efficiency, the threshold model regression results are shown in Table 8, Model (8). When the explanatory variable is achievement transformation efficiency, the threshold model regression results are shown in Table 8, Model (9). According to the regression results of Model (8), the indirect impact of intellectual property protection on the value of the green brand through the efficiency of R&D shows a positive single threshold feature: When the level of intellectual property protection in a region does not exceed the threshold (0.0109), the regression coefficient of the impact of R&D efficiency on the value of the green brand is 0.3687, and it passes the 1% significance level test. When the level of intellectual property protection in a region crosses this threshold, the regression coefficient of the impact of R&D efficiency on the value of green brand increases to 0.7220 and passes the 1% significance level test. Eighteen provinces, including Beijing, Tianjin, Shaanxi, Shanghai, Hubei, and Jilin, have crossed the threshold of intellectual property protection (0.0109) by 2020. Compared to 2009, only Beijing, Shanghai, and Tianjin have crossed the threshold. It can be found that intellectual property protection in China has developed rapidly and achieved remarkable results over the past 12 years. However, the level of intellectual property protection in some regions is still low. It is still necessary to further strengthen the protection of intellectual property rights.

Table 8. Analysis of threshold effect of intellectual property protection.

Variable	(8)	(9)
$TRD \times \mathrm{I}(IPR < 0.0109)$	0.3686 ***	
$TRD \times \mathrm{I}(IPR \geq 0.0109)$	0.7220 ***	
$TAT \times \mathrm{I}(IPR < 0.0064)$		0.2607 ***
$TAT \times \mathrm{I}(IPR \geq 0.0064)$		0.5027 ***
EDL	−0.4106	−0.1166
OUL	0.3743 *	0.2364 *
MS	0.9844	0.2316
MD	−0.7061 *	−0.2550
C	2.0457	5.4149
Time item	control	control
Sample size	300	300
F statistic	77.22 ***	86.02 ***
R^2	0.7602	0.7622

Note: *, **, and *** are significant at 10%, 5%, and 1% statistical levels, respectively.

It can be seen from the regression results of Model (9) that the indirect impact of intellectual property protection on the value of the green brand through the efficiency of achievement transformation is also characterized by a single positive threshold: When the level of intellectual property protection in a region does not exceed the threshold (0.0064), the regression coefficient of the impact of achievement transformation efficiency on the value of the green brand is 0.2607, and it passes the 1% significance level test. When the level of intellectual property protection in a region crosses this threshold, the regression coefficient of the impact of achievements transformation efficiency on the value of green brand increases to 0.5027 and passes the 1% significance level test. By 2020, 20 provinces, including Beijing, Tianjin, Shaanxi, Shanghai, Hubei, and Jilin, have crossed the threshold of intellectual property protection (0.0064). Compared to 2009, only six provinces, including Beijing, Shanghai, Tianjin, Liaoning, Shaanxi, and Heilongjiang, have crossed this threshold, indicating that China's intellectual property protection has also made remarkable achievements in the field of innovation achievements transformation. Compared with the threshold value of intellectual property protection in the field of achievement transformation, its threshold value in the field of R&D is higher. The reason for this may be

that the innovation output in the stage of R&D usually takes the form of intangible assets such as knowledge and technology. Such intellectual property infringement is relatively secret, so the requirements for relevant legal systems and law enforcement are high.

To sum up, intellectual property protection has a significant threshold effect in the stage of R&D and the stage of achievement transformation. When intellectual property protection crosses the corresponding threshold, it will significantly improve the efficiency of R&D and the efficiency of achievement transformation on the positive effect of green brand value. Furthermore, because of the different innovation elements in each stage, the threshold effects of intellectual property protection on innovation efficiency in the two stages are quite different.

4.5. Robustness Test

Standard robustness testing methods include changing data sources, replacing variables, variable lag, model replacement, selecting subsamples, grouping regression, etc. Since the explained and explanatory variables in this paper are difficult to replace, grouping regression has been conducted according to regional division. Therefore, this paper tests the robustness of the benchmark model and the panel threshold model by lagging the explanatory variables by one period and tests the robustness of the spatial Dubin model by replacing the spatial adjacency matrix (W) with the spatial inverse distance matrix (W*).

The robustness test results show that R&D efficiency and achievement transformation efficiency lagging behind by one period have a significant positive impact on the green brand value on the overall level. The efficiency of R&D has a greater impact on the green brand value than the achievement transformation efficiency. At the national level, the direct, indirect, and total effects of the efficiency of R&D are significantly positive, while the direct and total effects of achievement transformation efficiency are significantly positive, but the indirect effects are not significant. The protection of intellectual property rights has a significant single threshold effect on the efficiency of R&D and the efficiency of achievements transformation that are lagging by one phase. The above conclusions are consistent with the empirical results of the experimental model. Therefore, the model settings are robust, and the results are reliable.

5. Conclusions and Suggestions

5.1. Research Conclusions

Firstly, this paper estimates the total value of the green brand in 25 provinces in China from 2009 to 2020 using the data released by the World Brand Lab. The regional R&D efficiency and achievement transformation efficiency of each province and city in 12 years are calculated by building the super-efficiency SBM model. The paper provides a descriptive statistical analysis of the time and space change trend of the green brand value and the two-stage regional innovation efficiency of each province and city over a 12-year period, according to the calculation and measurement results. Secondly, the paper explores the impact of two-stage regional innovation efficiency and other control variables on green brand value by building a two-way fixed effect model as the benchmark model. With the help of SDM, this paper analyzes the spatial spillover effects of the two stages of regional innovation efficiency and other influencing factors. The level of intellectual property protection is introduced as a threshold variable to study the difference in the impacts of R&D efficiency and achievement transformation efficiency on green brand value under different levels of intellectual property protection. Finally, the main conclusions of this paper are as follows:

(1) The development trend of the green brand in various regions of China is good, but the differences among regions are large. The development of the green brand in the eastern region is significantly better than that in the central and western regions. The upward trend of green brand value is also significantly greater than that in the central and western regions, which indicates that the development of the green brand is better in regions with better market economic conditions and policy systems. In some regions, there is a "siphon effect"

when developing the green brand. That is, regions with high brand development levels usually absorb brand resources and brand elements from surrounding regions, resulting in faster development in regions with a higher level of green brand development during slower development in regions with a low level of green brand development.

(2) The imbalance of innovation capability among regions in China is prominent, and there are differences among regions in different innovation stages. The eastern region is higher than the central and western regions in the efficiency of R&D and the efficiency of achievements transformation. This is due to the more developed economy and an advantage in the eastern region's input and output of sci-tech innovation. The efficiency of R&D in the central region is lower than that in the western region, but the efficiency of achievements transformation is higher than that in the western region. The central region must strengthen institutional innovation and improve management efficiency. Due to its limited market development potential, the western region will inhibit the enthusiasm of enterprises to develop new products and expand the scale of market operation. Therefore, it is necessary to speed up the construction of the market system to stimulate innovation with demand. From the perspective of time trends, the efficiency of R&D and the efficiency of achievement transformation in the eastern and central regions are rising. However, the efficiency of R&D and achievement transformation in the western regions have declined in recent years. This is because the brain drain in the western regions has been severe in recent years, and a large number of outstanding scientific researchers, professors, scholars, etc., are flowing to the eastern and central regions, making the innovation ability of the western regions increasingly weak.

(3) The efficiency of R&D and the efficiency of achievements transformation will significantly enhance the value of the green brand. The efficiency of R&D and the efficiency of achievements transformation will have a significant value chain spillover effect. However, at the regional level, the two-stage innovation efficiencies of the central region have no significant impact on the value of the green brand. Enterprises in the central region should emphasize transforming innovation into productivity and improving the innovative value of products and services. There are regional differences in the impact of economic development level, the degree of opening up, market size, and marketization on the value of the green brand. The level of economic development in the eastern region has a significant positive impact on the value of the green brand. In the central region, there is a phenomenon that the development of brands needs to catch up with economic development. This may be because the innovation ability of the central region needs to promote brand development. The western region has yet to have a significant positive impact on the value of green brands due to its low level of economic development. Only the degree of opening up in the eastern region has a significant positive impact on the value of the green brand, and only the market size in the western region has a significant positive impact. It can be found that brand development in economically developed regions has shifted from market scale orientation to market scope orientation. The higher the level of marketization in the central and western regions, the greater the value of the green brand. The situation in the east is the opposite. Considering that this article measures the level of marketization by the degree of government intervention, it shows that the eastern region is a demonstration area for reform in many fields, which will promote the development and growth of the green brand to a certain extent.

(4) There is a significant single threshold effect in the level of intellectual property protection. When the level of intellectual property protection crosses the corresponding threshold, the positive effects of two-stage innovation efficiency on the value of an green brand are significantly improved. It can be seen that speeding up the construction of intellectual property laws and regulations, improving the judicial system, and strengthening law enforcement are of great significance to the development of China's green brands.

(5) The two stages of regional innovation efficiency have spatial spillover effects on the value of the green brand, but there are significant regional differences. The spatial spillover effect of regional innovation efficiency in the two stages of the eastern region is significantly

positive. In contrast, only the R&D efficiency in the central region has a significant positive spatial spillover effect. In comparison, the spatial spillover effect of the two stages of regional innovation efficiency in the western region is insignificant. In addition, there is a significant negative spatial spillover effect at the national level and in the eastern and central regions. That is, regions with a high level of economic development will harm the value of the green brand in their adjacent regions, which also explains why the development of the green brand in China has a "siphon effect". This means that economically developed regions have better material living conditions, a market environment, policy support, and greater space for improvement, which will attract excellent talents, high-quality resources, and excellent brands from the surrounding regions, thus promoting the development of the local green brand. However, at the same time, this will have a certain inhibitory effect on the construction of green brands in the surrounding regions. The degree of opening up only produces positive spillover effects in the eastern and central regions. The market scale only produces a positive spillover effect in the western region. The degree of marketization has a positive spillover effect in the eastern region and a negative spillover effect in the western region, indicating that the policy support in the eastern region will radiate to the surrounding regions. In contrast, the marketization development in the western region will have a "crowding out effect" on the surrounding regions. In summary, the main reason for the existence of the "siphon effect" in China's green brand development is that the "radiation effect" of regional sci-tech innovation and other factors is far less significant than the "siphon effect" of economic development.

5.2. Policy Suggestion

The brand economy is the product of the development of the market economy to a particular stage and is also a high-level manifestation of regional economic development. In the international market, the brand is not only a symbol of an enterprise but also a symbol of the competitiveness of a region or even a country. Improving the value and influence of green brands is of great practical significance to China's green development. Therefore, based on the above research conclusions, this paper proposes the following suggestions:

(1) Improve the two stages of innovation efficiency and emphasize the effect of sci-tech innovation in promoting brand value. While continuing to increase R&D funds, personnel, and other innovative resources, all localities should also pay attention to improving innovation output capacity, optimizing the allocation of innovation resources, and improving innovation efficiency, so as to provide strong power for China's green brand building. The eastern region continues to produce a marked effect on R&D and achievement innovation in promoting the value of the green brand. The central region needs to strengthen institutional innovation, improve management efficiency, and formulate relevant policies to encourage enterprises to focus on products and quality, so as to produce a driving effect in innovation on brands. The western region needs to strengthen the construction of the market system, create a good market environment, shift the market competition from price and scale competition to product and service competition, and improve the corporate image and brand value with high-quality products and services. All regions should strengthen the degree of opening up to the outside world, improve marketization, and improve the construction of market mechanisms. Especially in the central and western regions, it should open up the international market, participate in competition and cooperation in the international market, take its essence, eliminate its dregs, and create a greener brand with international influence.

(2) According to each region's sci-tech innovation resource endowment, focus on superior resources and create a regional solid green brand. For example, the Jilin Province should encourage the development of green automobile brands (FAW, Hongqi, Jiefang, etc.); the Guangdong Province ought to promote the greening of household appliance brands (Gree, Midea, Skyworth, etc.); and the Jiangsu Province should vigorously

develop green machinery manufacturing brands (Xugong, Hengtong Optoelectronics, Tongding, etc.).

(3) Improve intellectual property laws and regulations and strengthen law enforcement and justice. The government should speed up the construction of laws and regulations system for intellectual property protection, implement the intellectual property protection law, strengthen the enforcement of intellectual property protection, and ensure the judicial fairness of intellectual property protection. Regional differences should be fully considered in policy formulation. Investment in sci-tech innovation should be increased for regions with a high level of intellectual property protection to promote the process of sci-tech innovation while improving the formulation of intellectual property protection for regions with a low level of intellectual property protection.

(4) Give full play to the spatial spillover effect of R&D and achievements transformation, and strengthen regional innovation cooperation and communication, including the communication of scientific researchers, technologies, patents, management systems, and other innovative resources. The central government should overall construct a coordinated regional development mechanism, and its planning and requirements for regional economic development should not be limited to the local region. At the same time, it should consider its contribution to the coordinated development in regions and achieve win–win or multi-win through market mechanisms and benefit compensation mechanisms. The eastern region should support the central and western regions with redundant innovation resources. On the one hand, it can improve the innovation efficiency of the eastern region, and on the other hand, it can promote the innovation ability of the central and western regions. The central region should strengthen the spillover effect of innovation achievements and pay attention to the communication of innovation achievement transformation ability between regions. The western region needs to speed up the construction of transportation infrastructures such as expressways and high-speed rail, promote the construction of the market system and mechanism, drive innovation with demand, and promote green brand development with innovation. In areas with low economic development levels, the government should formulate relevant policies to improve the treatment of talents and strengthen support for enterprises so as to prevent brain drain and outflow of enterprise resources. Areas with high economic development levels should provide counterpart support to areas with low economic development, strengthen the interaction between universities, enterprises, and governments in their regions, and achieve win–win cooperation between regions in areas with high economic development levels.

(5) Strengthen the spillover effect of the innovation value chain. In the market environment, the innovation competition is not only the competition for knowledge, technology, and other R&D capabilities but also the competition for research and development of new products, new markets, and other achievements and transformation capabilities. Therefore, all regions should promote the deep integration of IUR, improve the communication channels at all stages of the innovation value chain, and strengthen the effective interaction between the government, enterprises, universities, and research institutions, so that R&D and achievements transformation can form a benign interaction, producing "1 + 1 > 2" spillover effect.

5.3. Research Limitations and Future Research Directions

First of all, the sample selection could be better. Because of the availability and integrity of the data, this paper only studies 25 provinces in China. It excludes the sample data of nine provinces, such as Gansu, Xinjiang, and Tibet. Secondly, due to the need for more systematic and perfect evaluation methods for a regional green brand value in China, only the relevant data released by the World Brand Lab and Shanghai Huazheng are used. Although relatively authoritative, these data need more comprehensiveness and can only reflect a single region's total green brand value. In contrast, each region's green brand characteristics, influence, and structure are not considered. Finally, although this paper has

divided three regions, including the eastern, middle, and western regions, there are still some limitations in the study areas. Regional development has presented the characteristics of urban clustering in recent years. The trend of urban clustering development in "Beijing-Tianjin-Hebei", "YangtzeRiver Delta", "Pearl River Delta", and other cities is noticeable, and there are their regional development advantages. It impacts the region's green brand development strategy and direction, so the regions need to be further divided.

With the rapid development of China's market economy, developing the green brand economy is of great practical significance to realize the green transformation of economic development, improve China's sustainable development ability and enhance its international competitive position. In the future, scholars can conduct more extensive and in-depth research in the following aspects: study various main elements of innovation (enterprises, universities, research institutions, government, etc.), nonmain elements (material conditions required for innovation), and coordinate the impact of policies and systems that various elements on green brand development from the static (innovation environment) or dynamic (innovation system) perspective. Improve the evaluation system of regional green brand development. Explore the path of brand innovation and development of small and medium-sized enterprises. Innovation drives green brand development and provides a relevant theoretical and practical basis for realizing the development of the green economy.

Author Contributions: Conceptualization, X.Z. and Y.X.; methodology, X.Z. and L.W.; software, X.Z.; resources, Y.X.; writing—original draft preparation, X.Z.; writing—review and editing, L.W. All authors have read and agreed to the published version of the manuscript.

Funding: The research was funded by the Program of Shanghai Planning of Philosophy and Social Science of China (No. 2020BGL023) and the Natural Science Foundation of Zhejiang Province (No. LQ23G010001).

Institutional Review Board Statement: Not applicable.

Data Availability Statement: Not applicable.

Conflicts of Interest: The authors declare no conflict of interest.

References

1. Zhang, Q.Y.; Sun, X.X. Theory construction and measurement of green brand value based on the consumers' perspective. *J. Beijing Technol. Bus. Univ. (Soc. Sci.)* **2015**, *30*, 86–92. (In Chinese)
2. Hartmann, P.; Ibáñez, A.V.; Sainz, F.S.J. Green branding effects on attitude: Functional versus emotional positioning strategies. *Mark. Intell. Plan.* **2005**, *23*, 9–29. [CrossRef]
3. Chang, C.H.; Chen, Y.S. Managing green brand equity: The perspective of perceived risk theory. *Qual. Quant.* **2014**, *48*, 1753–1768. [CrossRef]
4. Lin, J.L.; Lobo, A.; Leckie, C. Green brand benefits and their influence on brand loyalty. *Mark. Intell. Plan.* **2017**, *35*, 425–440. [CrossRef]
5. Zhang, Q.Y.; Sun, X.X. The effect of benefit perception on consumers' green brand purchase intention—The moderating effect of self-concept clarity. *Enterp. Econ.* **2019**, *38*, 23–33. (In Chinese)
6. Lin, W.L.; Ho, J.A.; Sambasivan, M.; Yip, N.; Mohamed, A.B. Influence of green innovation strategy on brand value: The role of marketing capability and R&D intensity. *Technol. Forecast. Soc. Change* **2021**, *171*, 120946.
7. Gehani, R.R. Corporate brand value shifting from identity to innovation capability: From Coca-Cola to Apple. *J. Technol. Manag. Innov.* **2016**, *11*, 11–20. [CrossRef]
8. Clayton, T.; Turner, G. Brands, innovation and growth: A PIMS study of brand value. *Int. J. Innov. Manag.* **1998**, *2*, 455–468. [CrossRef]
9. Klink, R.R.; Athaide, G.A. Consumer innovativeness and the use of new versus extended brand names for new products. *J. Prod. Innov. Manag.* **2010**, *27*, 23–32. [CrossRef]
10. Royne, M.B.; Levy, M.; Martinez, J. The public health implications of consumers' environmental concern and their willingness to pay for an eco-friendly product. *J. Consum. Aff.* **2011**, *2*, 329–343. [CrossRef]
11. Hartmann, P.; Apaolaza-Ibáñez, V. Consumer attitude and purchase intention toward green energy brands: The roles of psychological benefits and environmental concern. *J. Bus. Res.* **2012**, *65*, 1254–1263. [CrossRef]
12. Suki, M.N. Green product purchase intention: Impact of green brands, attitude, and knowledge. *Br. Food J.* **2016**, *118*, 2893–2910. [CrossRef]

13. Smith, S.; Paladino, A. Eating clean and green? Investigating consumer motivations towards the purchase of organic food. *Australas. Mark. J.* **2010**, *18*, 93–104. [CrossRef]
14. Akehurst, G.; Afonso, C.; Gonçalves, H.M. Re-examining green purchase behaviour and the green consumer profile: New evidences. *Manag. Decis.* **2012**, *50*, 972–988. [CrossRef]
15. Weisstein, F.L.; Asgari, M.; Siew, S.W. Price presentation effects on green purchase intentions. *J. Prod. Brand Manag.* **2014**, *23*, 230–239. [CrossRef]
16. Wang, X. Brand value evaluation system and its method selection. *Price Theory Pract.* **2012**, 85–86. (In Chinese)
17. Qi, Y.Z.; Li, Y.Y.; Yan, Y. Research on the threshold effect of government subsidies and technological innovation on brand value. *Macroeconomics* **2020**, 60–70. (In Chinese)
18. Li, Y.Y.; Liu, J.H.; Duan, K.; Huang, L. Research on the threshold effect of corporate social responsibility, technological innovation and brand value. *Soft Sci.* **2020**, *34*, 1–7. (In Chinese)
19. Liu, J.; Li, Y.; Duan, S.; Meng, L. Characteristics of board of directors, innovation input and brand value—An empirical study based on endogenous perspective. *Manag. Rev.* **2019**, *31*, 136–145. (In Chinese)
20. Chen, Y.S. The drivers of green brand equity: Green brand image, green satisfaction, and green trust. *J. Bus. Ethics* **2010**, *93*, 307–319. [CrossRef]
21. Ng, P.F.; Butt, M.M.; Khong, K.W.; Ong, F.S. Antecedents of green brand equity: An integrated approach. *J. Bus. Ethics* **2014**, *121*, 203–215. [CrossRef]
22. Lowe, B.; Alpert, F. Forecasting consumer perception of innovativeness. *Technovation* **2015**, *45*, 1–14. [CrossRef]
23. Aaker, D.A. Measuring brand equity across products and markets. *Calif. Manag. Rev.* **1996**, *38*, 102–120. [CrossRef]
24. Zhang, H.; Ko, E.; Lee, E. Moderating effects of nationality and product category on the relationship between innovation and customer equity in Korea and China. *J. Prod. Innov. Manag.* **2013**, *30*, 110–122. [CrossRef]
25. Kliestikova, J.; Kovacova, M. Motion to innovation: Brand value sources have (not) changed over time. *SHS Web Conf.* **2017**, *39*, 01010. [CrossRef]
26. Kurt, S. Investigation of the relationship between brand value and R&D activities: Fortune 500 companies analysis. *Procedia Comput. Sci.* **2019**, *158*, 1019–1024.
27. Yao, Q.; Huang, L.; Li, M. The effects of tech and non-tech innovation on brand equity in China: The role of institutional environments. *PLoS ONE* **2019**, *14*, e215634. [CrossRef]
28. Gatignon, H.; Weitz, B.; Bansal, P. Brand introduction strategies and competitive environments. *J. Mark. Res.* **1990**, *27*, 390–410. [CrossRef]
29. Yli-Renko, H.; Autio, E.; Sapienza, H.J. Social capital, knowledge acquisition, and knowledge exploitation in young technology-based firms. *Strateg. Manag. J.* **2001**, *22*, 587–613. [CrossRef]
30. Li, W.X.; Liu, Y. Technology innovation, corporate social responsibility and corporate competence: An empirical analysis based on data from listed companies. *Sci. Sci. Manag. S. T.* **2017**, *38*, 154–165. (In Chinese)
31. M'Zungu, S.D.M.; Merrilees, B.; Miller, D. Brand management to protect brand equity: A conceptual model. *J. Brand Manag.* **2010**, *17*, 605–617. [CrossRef]
32. Han, R.E.; Zhao, F. Analysis on the advantages and disadvantages of the factors in China's development of processing trade. *HLJ Foreign Econ. Relat. Trade* **2008**, 50–51.
33. Zhu, S.Z.; Wang, Z.L. Analysis of the path to enhance brand competitiveness based on the perspective of intellectual property: Take new energy automobile enterprises as an example. *J. Chongqing Univ. Sci. Technol. (Soc. Sci. Ed.)* **2018**, 43–46. (In Chinese)
34. Huang, Q.H.; He, J. The core capability, function and strategy of chinese manufacturing industry—Comment on "Chinese manufacturing 2025". *China Ind. Econ.* **2015**, *6*, 5–17. (In Chinese)
35. Zhang, Z.Y.; Chen, J. The composition, characteristics and management of enterprises' innovation resource based on open innovation pattern. *Sci. Sci. Manag. S. T.* **2008**, *29*, 61–65.
36. Helm, C. From tech-led to brand-led—Has the internet portal business grown up? *J. Brand Manag.* **2007**, *14*, 368–379. [CrossRef]
37. Wang, Z.; Wang, C.R. The relationship between r&d innovation and brand growth of "Time-honored brand" Enterprises. *Manag. Rev.* **2020**, *32*, 156–167. (In Chinese)
38. Wang, Z.H.; Chen, J.G.; Huang, T.; Chen, Y. A field study on the dynamic evolution of the key influential factors for enterprises to create their own brands: A qualitative analysis based on the field interview data of 12 enterprises in guangzhou. *J. Manag. World* **2013**, 111–117. (In Chinese)
39. Wang, J.F.; Cheng, T.Y. Empirical research on the impact of technological innovation on brand value. *Soft Sci.* **2012**, *26*, 10–14. (In Chinese)
40. Wang, B.L.; Xie, X.J.; Lou, Y.L. Evaluation of regional scientific and technological innovation and its impact on brand value: Based on the data analysis of key provinces and cities along the "the Belt and Road". *Product. Res.* **2019**, 16–22. (In Chinese)
41. Zhou, C.H.; Qin, J.L.; Liu, C.J. The effect of technological innovation on brand values: An empirical study based on provincial panel data. *Sci. Technol. Manag. Res.* **2014**, *34*, 10–13. (In Chinese)
42. Qi, X.; Liu, J.S. Innovation synergistic degree, regional innovation performance and own-brand competitiveness. *Soft Sci.* **2015**, *29*, 56–59. (In Chinese)
43. De Vries, N.J.; Carlson, J. Examining the drivers and brand performance implications of customer engagement with brands in the social media environment. *J. Brand Manag.* **2014**, *21*, 495–515. [CrossRef]

44. Fang, G.G.; Cui, D.F. On organization, attribute the environmental restriction and development of enterprise brand of agricultural industrialization of bing-tuan in xinjiang. *Econ. Manag.* **2010**, *24*, 35–39. (In Chinese)
45. Sukarmijan, S.S.; Sapong, O.D.V. The importance of intellectual property for smes; challenges and moving forward. *UMK Procedia* **2014**, *1*, 74–81. [CrossRef]
46. Wang, F.M.; Cheng, L.R.; Wang, J.X. Intellectual property rights protection, technology innovation and brand growth: Based on threshold regression analysis of inter-provincial panel data. *J. Beijing Technol. Bus. Univ. (Soc. Sci.)* **2015**, *30*, 102–109. (In Chinese)
47. Yan, B.H. The development of the brand of agricultural products based on the protection of intellectual property: From the perspective of Hebei province. *Sci. Manag. Res.* **2018**, *36*, 84–87. (In Chinese)
48. Hansen, M.T.; Birkinshaw, J. The innovation value chain. *Harv. Bus. Rev.* **2007**, *85*, 121–135.
49. Yu, Y.Z.; Liu, D.Y. The study on the path of improvement in China's regional innovation efficiency from the perspective of innovation value chain. *Sci. Res. Manag.* **2014**, *35*, 27–37. (In Chinese)
50. Li, D.H. Study on the influence of industrial structure optimization on regional innovation efficiency: Based on the angle of innovation value chain. *Econ. Probl.* **2020**, *10*, 120–129. (In Chinese)
51. Chu, S.S.; Wang, T.; Xia, S.Y.; Yang, X.M.; Chen, J. Differences and influencing factors of enterprise innovation efficiency based on innovation value chain: A case study on enterprises of national high-tech zones in Jiangsu province. *Resour. Environ. Yangtze Basin* **2021**, *30*, 269–279. (In Chinese)
52. Perrings, C. Conservation of mass and instability in a dynamic economy-environment system. *J. Environ. Econ. Manag.* **1986**, *13*, 199–211. [CrossRef]
53. Chen, X.D.; Yang, X.X. The impact of digital economic development on the upgrading of industrial structure: Based on the research of grey relational entropy and dissipative Structure Theory. *Reform* **2021**, *3*, 26–39. (In Chinese)
54. Li, L.; Mao, G.; Zhang, S.Y. Research on regional economic development supported by sci-tech innovation based on dissipative structure under financial environment. *Inf. Sci.* **2012**, *30*, 1385–1388. (In Chinese)
55. Xu, H.; Xue, Z.C.; Deng, W.S. The empowerment mechanism study and growth path of local specially regional brand ecosytem—A case study based on Bohea Rock Tea. *Chin. J. Manag.* **2019**, *16*, 1204–1216. (In Chinese)
56. Wang, Q.W.; Zhu, H.; Wang, X.Y. Driving mechanism of cluster brand based on brand ecosystem. *Res. Econ. Manag.* **2015**, *36*, 132–138. (In Chinese)
57. Prigogine, I. Time, structure, and fluctuations. *Science* **1978**, *201*, 777–785. [CrossRef]
58. Wu, J.S.; Ruan, J.Q.; Xu, G.T. Economies agglomeration, economies distance, and farmer's income growth: A study on direct and spillover effects. *China Econ. Q.* **2017**, *16*, 297–320. (In Chinese)
59. Cao, X.; Zhang, L.P. The direct and spillover effects of financial support on technological innovation research: Based on spatial panel durbin model. *Manag. Rev.* **2017**, *29*, 36–45. (In Chinese)
60. Hansen, B.E. Threshold effects in non-dynamic panels: Estimation, testing and inference. *J. Econom.* **1999**, *93*, 345–368. [CrossRef]
61. Tone, K.A. Slacks-based measure of super-efficiency in data envelopment analysis. *Eur. J. Oper. Res.* **2002**, 32–41. [CrossRef]
62. Pittman, R.W. Multilateral productivity comparisons with undesirable outputs. *Econ. J.* **1983**, *93*, 883–891. [CrossRef]
63. Shang, H.J. Reestimatinq the capital stock of China: 1952~2006. *J. Quant. Technol. Econ.* **2008**, *25*, 17–31. (In Chinese)
64. Ginarte, J.C.; Park, W.G. Determinants of patent rights: A cross-national study. *Res. Policy* **1997**, *26*, 283–301. [CrossRef]
65. Han, Y.X.; Li, H.Z. Quantitative analysis for intellectual property protection level of China. *Stud. Sci. Sci.* **2005**, *23*, 377–382. (In Chinese)
66. Hu, K.; Wu, Q.; Hu, Y.M. The effects of intellectual property rights protection on technology innovation: Empirical analysis based on technology trading market and provincial panel data in China. *J. Financ. Econ.* **2012**, *38*, 15–25. (In Chinese)
67. Elhorst, J.P. Matlab software for spatial panels. *Int. Reg. Sci. Rev.* **2014**, *37*, 389–405. [CrossRef]
68. Elhorst, J.P. Applied spatial econometrics: Raising the bar. *Spat. Econ. Anal.* **2010**, *5*, 9–28. [CrossRef]
69. Su, Y.; An, X.L.; Lei, J.S. Impact of R & D investment on innovation performance of regional innovation system based on coupling degree threshold regression analysis. *J. Syst. Manag.* **2018**, *27*, 729–738. (In Chinese)

MDPI
St. Alban-Anlage 66
4052 Basel
Switzerland
www.mdpi.com

Entropy Editorial Office
E-mail: entropy@mdpi.com
www.mdpi.com/journal/entropy

Academic Open
Access Publishing

mdpi.com

ISBN 978-3-7258-1255-4